The Gulf of Carpentaria palaeoenvironments: OSL dating and nannofossil evidence

Martine Jeanine Josette Couapel
University of Wollongong

The Gulf of Carpentaria Palaeoenvironments:

OSL Dating and Nannofossil evidence

A thesis submitted in fulfilment of the requirements
for the award of the degree

Doctor of Philosophy

From the

University of Wollongong

By

Martine Jeanine Josette Couapel

School of Earth and Environmental Sciences

2005

Certification:

I, Martine J. J. Couapel, declare that this thesis, submitted in fulfilment of the requirements for the award of Doctor of Philosophy, in the School of Earth and Environmental Sciences, University of Wollongong, is wholly my own work unless otherwise referenced or acknowledged.

The document has not been submitted for qualifications at any other academic institution.

Martine J. J. Couapel

March 2005

Acknowledgements

A first thanks goes to my supervisor Allan Chivas, who gave me the opportunity to come to Australia to undertake this study on the Gulf of Carpentaria at the University of Wollongong, and to Adriana for making it feel not so far away.

This thesis was financially supported by OPRS and UPA scholarships, both granted by the University of Wollongong and administered through the Office of Research, which I acknowledge for its constant support.

Over the four years of this research, the work was often eased by the technical support of Atun Zawadski and Christopher Bowles from ANSTO, David Carrie, John Head, and the IT people from the School of Earth and Environmental Sciences, Nick Mackie from The Faculty of Engineering, and Steve and Peter from the University of Wollongong workshop, and the life was enjoyable due to my fellow postgrads, thanks to Ben Ackerman for his proofreading.

I owe a great debt of gratitude to Luc Beaufort and Noëlle Buchet without whom the work on coccoliths would not have been feasible, and for their logistic assistance during my working trips to CEREGE.

Keeping my head above the water during the last months would not have been possible without the help of Carol & Gerald, Sonia & Graeme, and Jenny & Ivars whom I also thank for their proofreading.

On every occasion, we could count on Sabine & Sunirmalya's support and I acknowledge them for their constant availability, with a special mention for Sabine's proofreading and other kindnesses.

Revitalising walks and talks to Mt Keira were as energizing as undergrad teaching; thanks to Nick Gill, Lesley Head, Laurie Chisholm and Colin Woodroffe for these opportunities.

I am indebted to Jessica Reeves for her constant support, constructive discussion, proofreading, friendship and dark chocolate blocks.

Gratefulness to Bert Roberts and Hiro Yoshida for long productive conversation on the endless OSL topic, to Jon Olley and Henk Heijnis for similar debate on dose rate and to Brian Jones for repetitive discussions on depositional scenarios should be expressed here. Thanks again to Bert and Brian for their prompt-advised availability for corrections and comments.

At last I would like to thank Yvon Balut, Elisabeth Michel and my family for their trust and support over the years, with an especial pensée to Mum who always believed it.

Nadir is the best position to gather the needed energy to reach the zenith, merci to Korigan for being the source of this energy.

Adversity is a boundless inspiration for the optimistic

Abstract:

The Gulf of Carpentaria is a near-equatorial region, a domain in which past environmental changes are not well understood, but in which much of the world's weather has its origin. Being situated adjacent to the Western Pacific Warm Pool, responsible for the largest transfer of heat and moisture between the surface and the atmosphere, the Gulf of Carpentaria is an epicontinental sea (maximum depth 70 m) bordered to the east by Torres Strait (12 m depth) and to the west by the deeper Arafura Sill (53 m depth), an area sensitive to the Asian monsoon and ENSO, which have a crucial importance on a worldwide scale. Furthermore, this region could be a key point to monitor the palaeocirculation between the Pacific and the Indian oceans that records the switching on and off of the global thermohaline circulation during glacial/interglacial alternations. The Gulf is tectonically stable, therefore no corrections are necessary when interpreting the palaeo-sea level curve. Throughout the Late Quaternary, during times of sea-level low-stands, the gulf was separated from the open waters of the Indian and Pacific oceans, forming Lake Carpentaria with outlet channels to the Arafura Sea.

In 1997, six sediment cores were collected from the Gulf of Carpentaria using a giant piston-corer deployed from the *Marion Dufresne*, as part of the International MArine Global changEs Study (IMAGES). This study provides an interpretation of the palaeoenvironments in the Gulf of Carpentaria over the last 180 ka by means of OSL dating and analysis of abundance and distribution of coccolith assemblages within this series of sediment cores. The usefulness of the OSL Dating technique on such sediment cores covering marine to lacustrine conditions has been demonstrated by establishing a time frame for the changing environments of the Gulf of Carpentaria since MIS 6.6. The shallowness of the Gulf of Carpentaria, as well as its restricted basin size, allow the use of Optically Stimulated Luminescence (OSL) to date the sediment. Indeed, these parameters mean that the quartz grains were bleached soon before deposition and thus that the event date is the real time of deposition. From the thirteen samples processed, twelve dates ranging from 7 ± 1 to 178 ± 18 ka, have been estimated over three cores from the Gulf of Carpentaria. These dates also allow the calculation of the sedimentation rate, which ranges from 4.3 cm ka^{-1} in the central area to 7.8 cm ka^{-1}on the western margin. These results are consistent with the modern sedimentation rate observed in the Gulf of Carpentaria. A clear reduction in the sedimentation rate starting about 90-100 ka

ago is noticed in the three cores, however this needs to be confirmed by further dating on other levels.

Coccolithophores are planktonic marine algae distributed from the open ocean to nearshore littoral and lagoonal environments. They secrete minute calcified plates, coccoliths, which are a major component of pelagic carbonates. Coccolith assemblages preserved in marine sediments are excellent proxies of palaeoceanographic conditions. The lack of coccoliths could be either due to bad preservation conditions or to a freshwater environment. In the Gulf of Carpentaria, coccolith assemblages confirm at least two non-marine/marine cycles, during the past 180 ka, as well as some short marine intervals, as minor incursions of seawater during a non-marine sequence.

These collated results are presented on a series of maps illustrating the discrete closure and breach sequences of the Arafura Sill and Torres Strait as related to Quaternary sea level fluctuations, and the corresponding alternations between the Gulf of Carpentaria and Lake Carpentaria. When viewed together, the compilation and interpretation of these data enables the development of a detailed spatial and temporal understanding of the palaeoenvironmental history of the Gulf of Carpentaria since MIS 6.6 (ca. 180 ka). From the sedimentary record of the Gulf evidence of dry and wetter episodes are observed and interpreted as intensification of the monsoon and cyclonic activity. These may be linked to ENSO events and global oceanic and atmospheric processes.

Table of Contents

Chapter 1: Background

Chapter 2: Core assessment and sampling

Chapter 3: Optically Stimulated Luminescence

Chapter 4: Nannofossils

Chapter 5: Synthesis and Conclusions

Table of Figures

Chapter 1

Chapter 2

Chapter 3

Chapter 4

Chapter 5

Table of Tables

Chapter 1

Chapter 2

Chapter 3

Chapter 4

Chapter 1:

Background

1.1 General Introduction

Throughout the Late Quaternary, during times of low sea-level, the Gulf of Carpentaria in northern Australia was separated by a land bridge from the open waters of the Indian and Pacific Oceans, forming Lake Carpentaria. This study investigates in detail the environments of the Gulf since the Last Interglacial. The knowledge of Late Quaternary palaeoenvironmental changes in this critical area between two major oceans is indispensable for a better understanding of palaeoclimatological and palaeooceanographic evolution on a worldwide scale. The establishment of a chronological framework for the Gulf of Carpentaria, and the recognition of successive palaeoenvironments using nannofossils, allow the determination of sea-level variation with time.

The Gulf of Carpentaria is a large shallow embayment with very gentle sea-floor slopes and a maximum depth of 70 m. The sediments collected and studied from the Gulf during the past 40 years have revealed palaeoenvironments that include marine, both fresh-water and hyper-saline lacustrine, and subaerial conditions. The Gulf is open to the Indian and Pacific oceans through the Sahul Shelf to the west and the Coral Sea to the east. The combination of low relief and the two sills of different height positions the Gulf of Carpentaria as a key area for the determination of sea-level fluctuations over time. The flooding of these two sills leads to the connection of the Indian and Pacific oceans during high sea-level stands. The continental nature of the Gulf through low sea-level stands allows for an easy correlation between marine and continental palaeoenvironments. In addition, the Gulf has potentially witnessed major atmospheric changes such as variable seasonality, monsoon intensification and migration of the Intertropical Convergence Zone over the Late Quaternary.

Optically Stimulated Luminescence (OSL) based on quartz grains is the geochronological tool chosen for this research because of its applicability to the range of ages encountered. The estimated OSL dates, combined with Accelerator Mass Spectrometry (AMS) ^{14}C, Amino Acid Racemisation (AAR) and Thermoluminescence (TL) dates, allow the definition of the time frame for sediment deposition in the Gulf of Carpentaria and thus for investigations of successive palaeoenvironmental changes over the past 180 ka.

Environmental changes through time are assessed using nannofossil *Coccolithophorid* assemblages. These planktonic marine algae secrete minute calcified plates, coccoliths, which are a major component of pelagic carbonates. Coccolith assemblages preserved in marine sediments are excellent proxies of palaeooceanographic conditions. This study demonstrates the supremacy of placolith-bearing species among coccolith assemblages in the Gulf of Carpentaria and defines two non-marine/marine cycles. The assemblage diversity, the degree of dissolution and the morphological variation of coccoliths are readily related to environmental changes and stresses.

The aim of this study is twofold:

1) to establish a time frame for the Gulf of Carpentaria within a series of sediment cores over at least the last Glacial/Interglacial cycle; and
2) to use this chronology to interpret palaeoenvironmental conditions deduced from nannofossil assemblages.

Thesis outline

The thesis is divided into 5 chapters as follows:

Chapter 1 introduces the research and presents an overview of modern physical geography, climate, hydrology and sedimentation processes operating in the Gulf of Carpentaria, establishing its regional importance from a palaeoclimatological point of view. An understanding of these modern conditions is necessary for any interpretation of past environment within the area. The current state of knowledge, outlining Quaternary climate characteristics and associated sea-level fluctuations is also summarised, thereby presenting the necessary framework for this research.

Chapter 2 deals with material and methods from core collection onboard the *Marion Dufresne* to slide preparation for nannofossil investigation and summarises the results of the previously reported and parallel analyses.

Chapter 3 outlines OSL history, principles, applications and requirements. It focuses on the luminescence of quartz, describes sample processing and analyses including equivalent-dose and dose-rate estimations, and ultimately, age calculations. The OSL dating undertaken for this thesis allows the establishment of a time frame for the Gulf of Carpentaria over the past 180 ka.

Chapter 4 investigates nannofossil abundance and distribution using both traditional microscope observation methods and a semi-automatic coccolith recognition software system (SYRACO), to define the succession of palaeoenvironments in the Gulf of Carpentaria.

Chapter 5 combines interpretation, discussion and syntheses of the palaeoenvironmental data from this research and previous work, integrating them in the chronological framework established in Chapter 3, thereby allowing the reconstruction of the palaeoenvironments of the Gulf of Carpentaria for the last 180 ka. This chapter also presents an integration of the deduced sea-level changes within a worldwide framework and outlines the major findings of the present research.

The remainder of this first chapter considers the contemporary characteristics of the Gulf of Carpentaria in terms of physical geography, climate, hydrology and sedimentation processes. An understanding of these modern conditions is necessary for any interpretation of past environment within the area. The Gulf of Carpentaria's regional position is assessed and integrated in the global circulation and climate scheme. Following this, an overview of earlier and parallel research on the Gulf. In concluding this chapter, the more important facets of the Gulf of Carpentaria are summarised.

1.2 The Gulf of Carpentaria today

1.2.1 Situation

The Gulf of Carpentaria is an epicontinental sea that partly covers the continental shelf extending between Australia and New Guinea. The Gulf is bordered to the north by the south coast of West Papua and Papua New Guinea, to the east by Torres Strait and the west coast of Cape York Peninsula, to the south by the coasts of Queensland and the Northern Territory, and to the west by the east coast of Arnhem Land and the Arafura Sill (Figure 1.1). This large, shallow asymmetrical basin has a very gentle sea-floor slope of the order of 1 in 18,000 in the central area below 45 to 50 m depth (Jones and Torgersen, 1988), and a deeper zone reaching a maximum depth of 70 m nearer its eastern side (Edgar et al., 2003). The Gulf of Carpentaria covers over 511,000 km^2 (Torgersen et al., 1983) between 8°S and 18°S and 135°E and 142°E, with a maximum extension of 690 km from west to east and 1070 km from north to south.

- Torres Strait

Torres Strait is a shallow shelf with abundant coral reefs and has a sill depth of 12 m (Haddon et al., 1894; Morrison and Delaney, 1996; Woodroffe et al., 2000). The area seems to have been stable since the Carboniferous and its drowning is most likely linked to the downfaulting of the Gulf of Carpentaria late in the Pleistocene (Phipps, 1970) to the west and to Pleistocene volcanism to the east (Willmott et al., 1969). The location of Torres Strait between the northernmost point of the Cape York Peninsula and Papua New Guinea makes it the only conduit for water flow between the Coral Sea and the Gulf of Carpentaria. The strong currents generated by the narrowness of channels between islands and the dissimilarity of tidal systems between the Coral Sea and the Gulf of Carpentaria (Jennings, 1972; Hemer et al., 2004) have exerted a strong control on the structure and morphology of reefs within the Strait, with many being elongated in a west-south orientation (Brander et al., 2004).

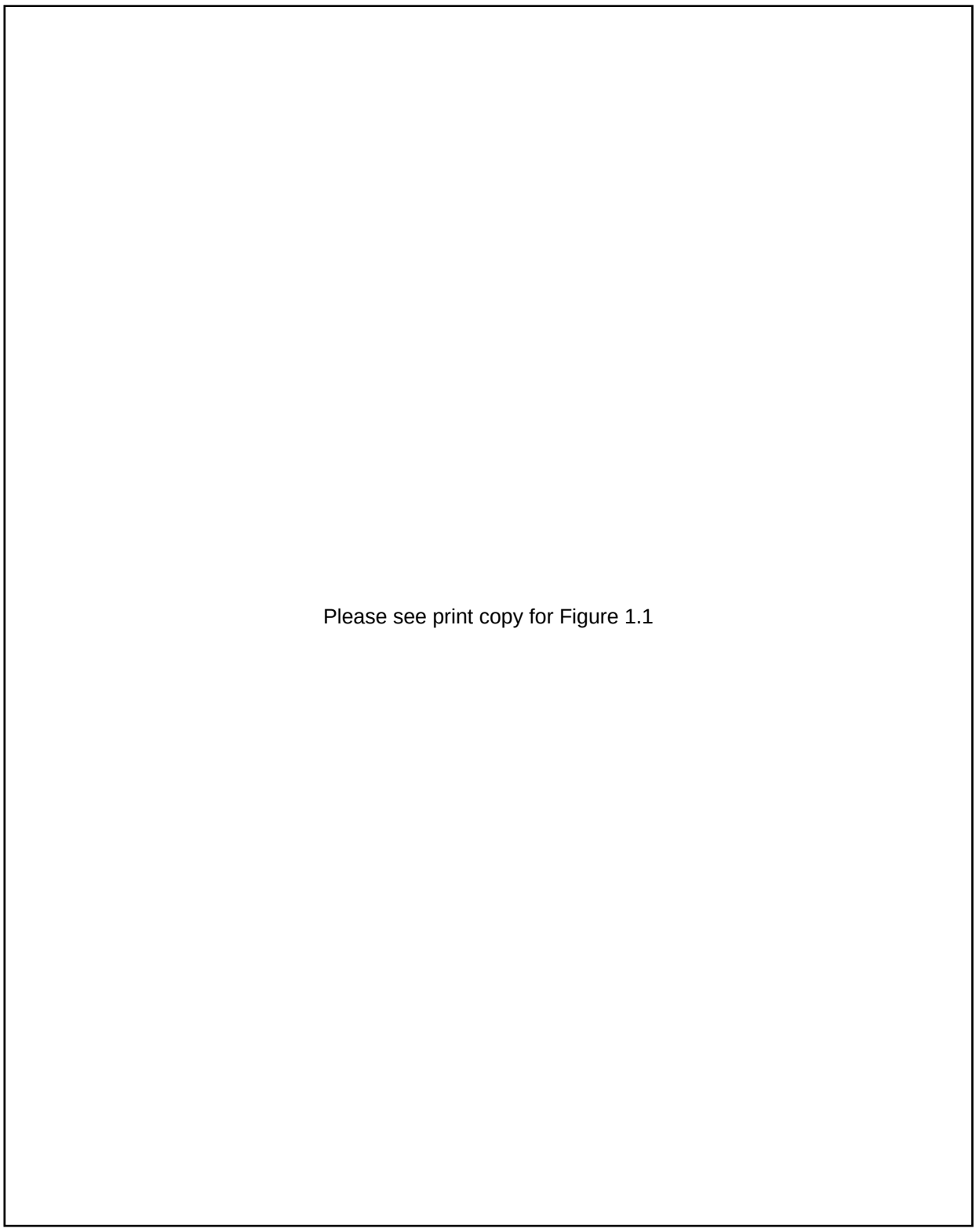

Figure 1.1: Map of the Gulf of Carpentaria, showing bathymetry (blue lines, from Grim and Edgar, 1998; Edgar et al., 2003 and Chivas et al., 2001 for the 53 m contour), core locations (red and dark-blue) and selected meteorological stations (brown).

Recent studies using moored current meters have shown that Torres Strait in its southern region is largely impervious, for oceanic budget calculations, to low-frequency currents (Wolanski et al., 1995). The prevailing winds in Torres Strait are southeasterly, although the northwest monsoon creates episodic calm and windy conditions from December to March (Hopley, 1982). The strait is an area of low wave energy (Jennings, 1972), the northern-most extension of the Great Barrier Reef serving to block long-period swell during the southeast trades (Hemer et al., 2004). Satellite data indicate that significant wave height rarely, if ever, exceeds 3.5 m in Torres Strait, and is nearly always less than 1.5 m during the northwest monsoon (McMillan, 1982).

- Arafura Sill

The Arafura Sill, which extends over 100 km in both north-south and west-east directions, is an almost flat feature with less than 2 m of local relief. This topography may have resulted from aeolian action when the sill was exposed during Pleistocene low sea level times (Tija, 1966; Doutch, 1972) and/or subsequent sea-level sediment infilling and bevelling (Torgersen et al., 1983). The sill is currently 53 m deep and floors the sole connection between the Gulf of Carpentaria and the Indian Ocean.

1.2.2 Climate

- Tropical climate

The climate of the Gulf of Carpentaria is governed by the position of the Intertropical Convergence Zone (ITCZ) and the migration of the Subtropical High Pressure belt (STHP). In summer, the STHP is sufficiently south (37-38°S) to displace the westerlies so that they do not influence the continental landmass, and to allow the southern movement of the ITCZ (8-10°S) and monsoonal flow into the Gulf of Carpentaria region (Figure 1.2a). During winter, the STHP is further north (29-32°S) and the Gulf area is dominated by south-easterly trade winds (Figure 1.2b). This seasonal change in atmospheric circulation results in distinctive seasonal patterns in temperature and rainfall distributions in the Gulf as shown in Figure 1.3. The average monthly ambient temperature in the Gulf from 1968 to 1991 ranged from 24.4°C in July to 31.6°C in November, and the average rainfall was about 1300 mm (Somers and Long, 1994).

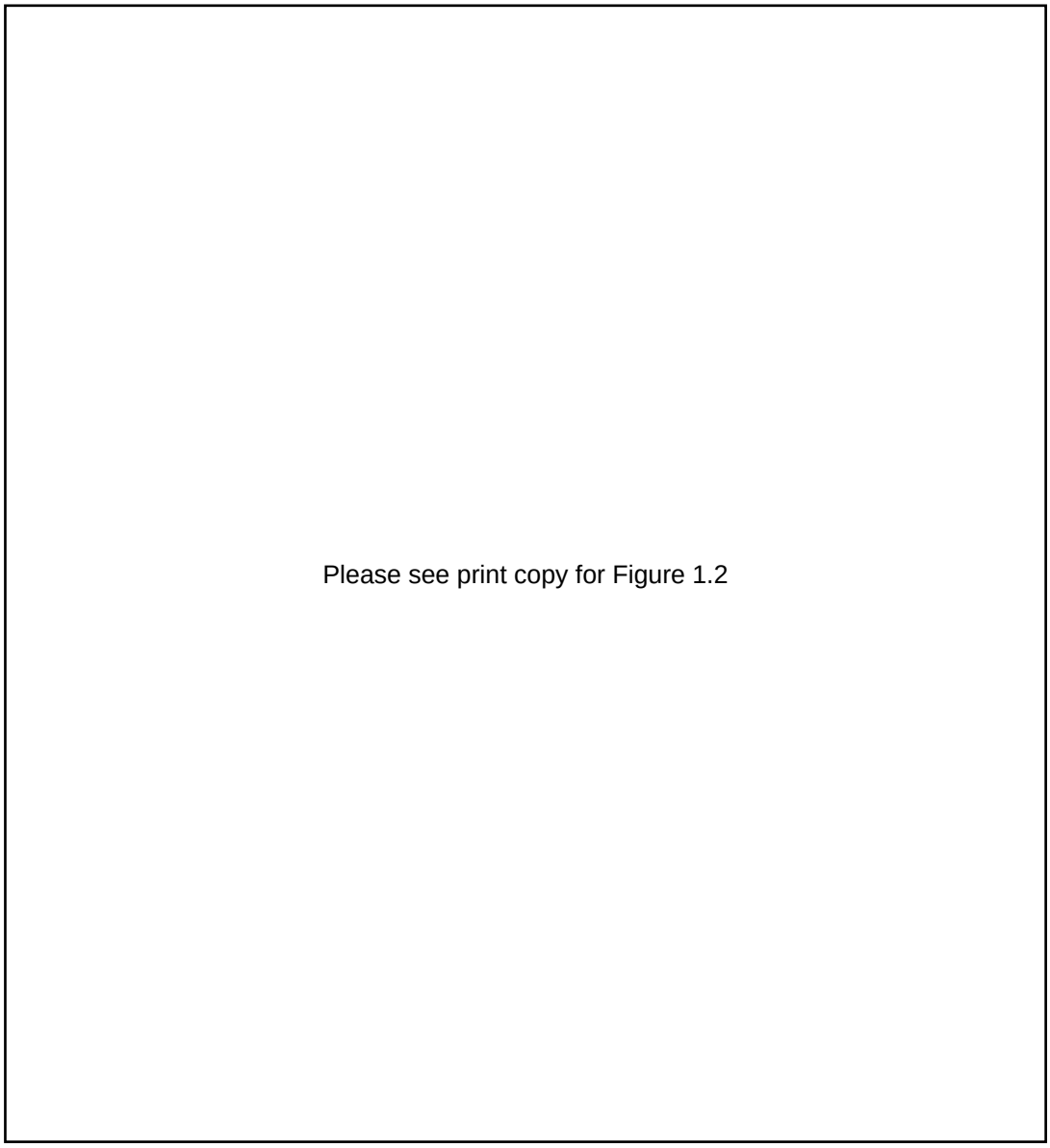

Figure 1.2: Seasonal circulation patterns over Australia and New Guinea. ITCZ refers to the Intertropical Convergence Zone (from Harrison and Dodson, 1993).

Six meteorological stations were selected to calculate more recent and long-term averages. These stations are distributed around the Gulf of Carpentaria (Figure 1.1), and have been operational for at least the past thirty-four years (Table 1.1). The annual daily averages are of similar order with minimum and maximum temperatures of 21.9°C and of 31.6°C, respectively and an annual rainfall of 1225 mm (Meteorology, 2004).

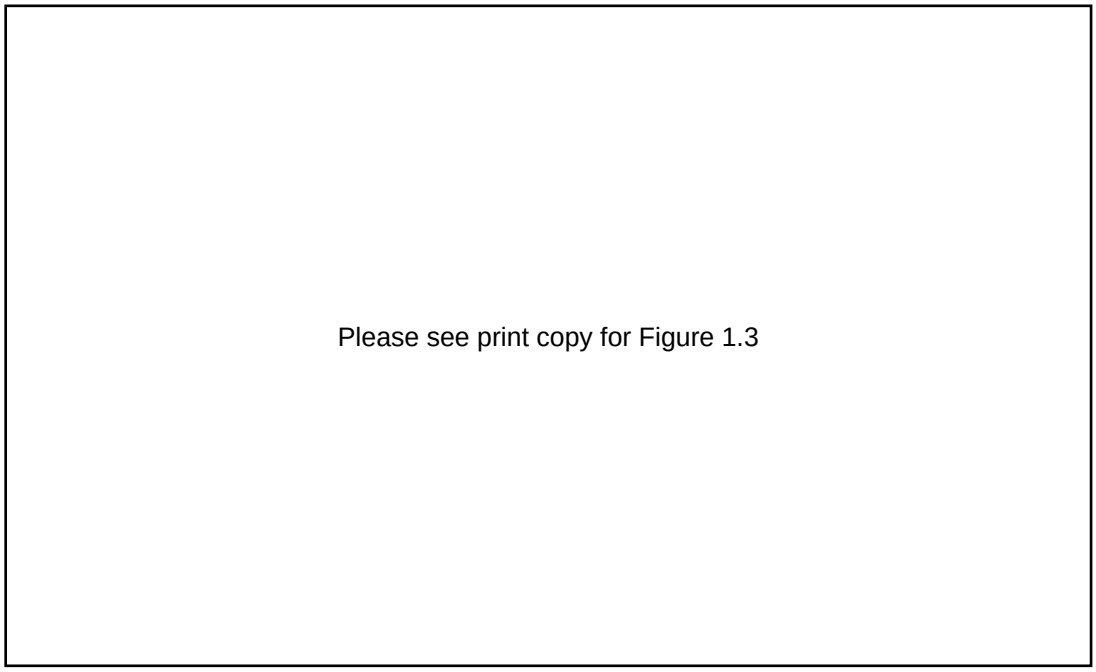

Figure 1.3: Mean monthly minimum and maximum temperatures, precipitation and maximum wind gust for six selected stations in the Gulf of Carpentaria region (Meteorology, 2004).

Table 1.1: Name and location and of the six stations used to estimate the average daily minimum and maximum temperature, and the monthly rainfall and maximum wind gust.

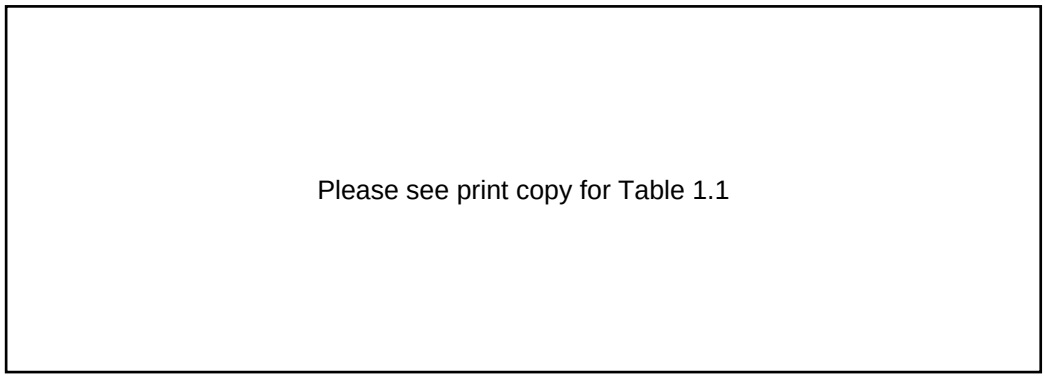

The climate of the Gulf of Carpentaria is typically tropical with heavy summer rains and dry mild to warm winters. Maximum wind gusts are highest during summer. This is could be due to the position within the Gulf of Carpentaria of the limit of the zone of the trade wind influence or to the intensification of tropical cyclone activity during this season. These tropical cyclones also bring additional but erratic rainfall to much of the northern part of the Australian continent (Harrison and Dodson, 1993).

- Importance of Walker Circulation or Southern Oscillation

Pittock noticed in the 1970s, that the variation in Australian rainfall on decadal time-scales has an amplitude correlated with the strength of the Walker Circulation (WC) and thus that climatic variation in eastern and northern Australia is associated with variations in the amplitude of the standing wave pattern of the general circulation of the atmosphere (Pittock, 1975, 1978). The WC is a circulation in the plane of the equator, involving ascent over the Indonesian sector and subsidence over the eastern Pacific (Figure 1.4b).

The Southern Oscillation Index (SOI), defined as the normalised difference in surface air pressure between Tahiti, French Polynesia and Darwin, Australia, corresponds to a quantification of the variation of the strength of the WC. This index with irregular periodicity is a measure of the strength of the trade winds, which have a component of flow from regions of high to low pressure. A low SOI is associated with weaker than normal trade winds and El Niño conditions (Figure 1.4c), whereas a high SOI corresponds to stronger trade winds and La Niña events (Figure 1.4a). The former condition is also referred to as ENSO (El Niño Southern Oscillation), and the latter as LNSO (La Niña Southern Oscillation). However ENSO is also used as a global term characterising all these variation patterns in the atmospheric and oceanic realms. In this thesis, El Niño and La Niña will be used where appropriate and ENSO will refer to the global phenomena.

La Niña conditions are characterised by low Sea Surface Temperature (SST), low rainfall and cloudiness in the equatorial eastern Pacific (Pittock, 1978). The strong WC leads to increased surface flow toward the south over northern and eastern Australia. This increases rainfall, particularly in the eastern interior of the continent but also over much of the north and east (Harrison and Dodson, 1993).

The variations in WC are independent of the position of the STHP (Pittock, 1975; 1978) and thus provide an additional mechanism to explain changes in effective moisture regimes on a regional scale (Harrison and Dodson, 1993). The changes in the structure of the monsoon are consistent with composite tropical cyclogenesis and cyclone track data (Evans and Allan, 1992).

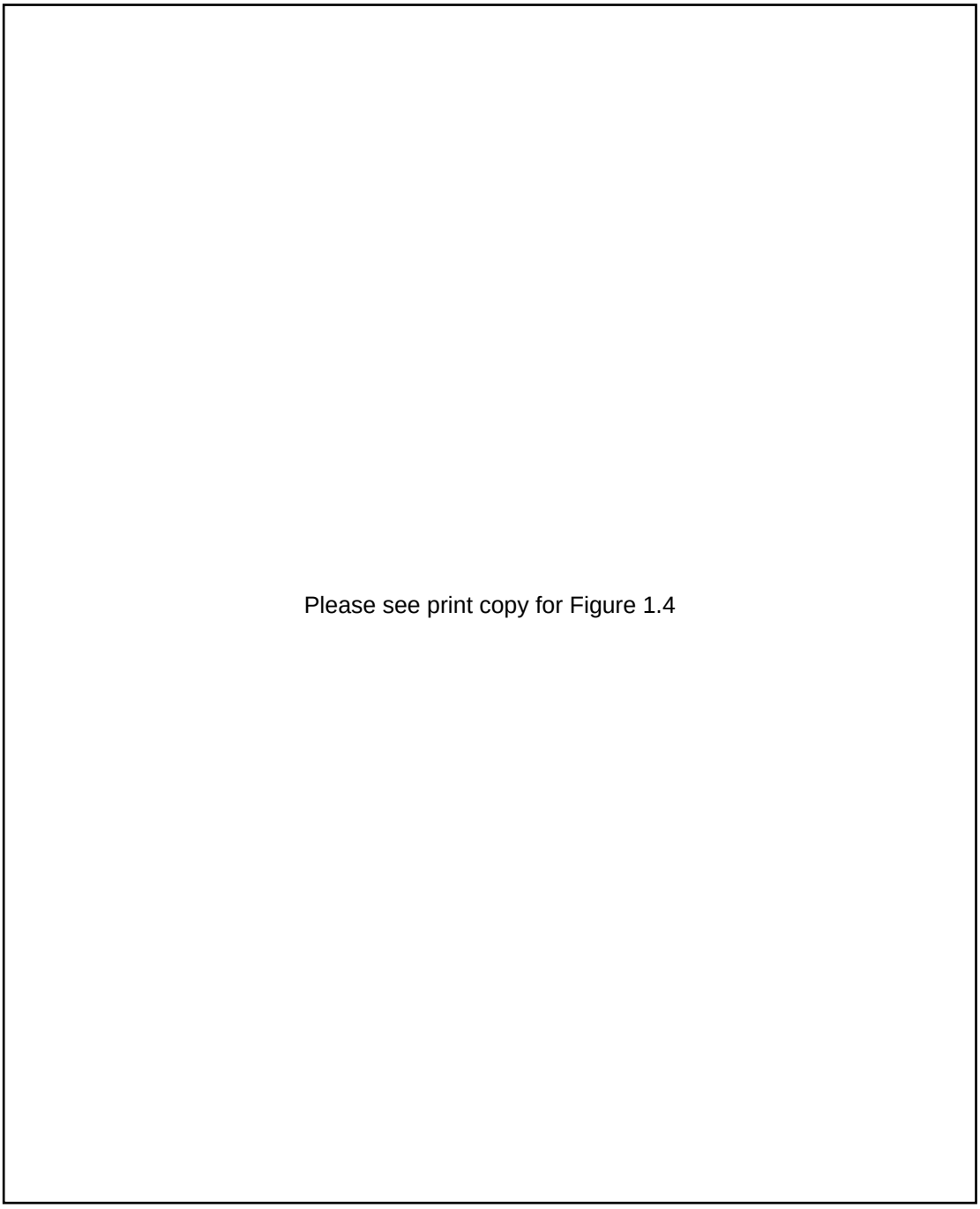

Figure 1.4: Walker circulation: La Niña, Normal and El Niño conditions (NOAA, 2005).

More tropical cyclones are evident in the North Australian region in El Niño years than in La Niña years, and could be related to the equatorward position of the monsoon trough, weaker vertical wind shear and warmer SST values (Evans and Allan, 1992).

The major convective zone, which is usually located over the Indonesian-North Australia region (Figure 1.4b), moves into the central equatorial Pacific during El Niño events (Figure 1.4c) (Rasmusson and Carpenter, 1982). This major convective zone is located over the Indonesian-Northern Australian region during La Niña years (Figure 1.4a) (Suppiah, 1993), allowing many parts of the Australian tropics to receive above-normal rainfall. In reverse, the Australian tropics receive below-normal rainfall during El Niño years (Suppiah, 1993). Nicholls and Wong (1990) also suggested ENSO phenomena amplify rainfall variability in the regions they affect.

1.2.3 Hydrological regime

- Water flow

Thirty-seven rivers flow into the Gulf of Carpentaria, of which twenty-seven are on the Queensland portion of the coast (Jones and Torgersen, 1988). The climate and the water balance of the Gulf of Carpentaria drainage basin is also sensitive to the effect of the ENSO phenomena in general (Torgersen et al., 1988). During 'El Niño' events, summer monsoon rainfall in northern Australia is decreased, as the trough is weak and displaced towards the equator and the tropical cyclone activity is low in the northeast of Australia. Both phenomena reduce the amount of river flow to the Gulf. During 'La Niña' events, the monsoon trough is stronger and heavier rainfall leads to greater river run-off to the Gulf (Evans and Allan, 1992; Suppiah, 1993, 2004; Simmonds and Hope, 1997). Most of the rivers are seasonally ephemeral, however a few permanent rivers flow into the Gulf.

- Stratification

Forbes (1984) considered that the hydrology of the Gulf is better correlated with local seasonal processes than with water masses originating from adjacent seas. In winter, temperatures are at a minimum, salinity at a maximum and the water column is well mixed, whereas during summer, central Gulf waters show a strong vertical temperature stratification and coastal zone salinity is affected by monsoonal runoff (Forbes, 1984).

Numerical models and cross-correlation with several mooring sites prove the existence during summer of a sharp thermocline supporting well mixed water for the duration of tropical cyclone activities (Wolanski, 1993). These observations were reviewed by Somers and Long (1994) who recognised a vertical stratification of the water in the south-eastern deep part of the Gulf whereas the waters of the top 20 m and those in the northern part of the Gulf were well mixed. They noted that waters below 50 m depth were 4 to 5°C cooler than surface waters during summer, and that salinity did not show vertical stratification, just a slight latitudinal increase southward (Somers and Long, 1994). Wolanski and Ridd (1990) also found evidence of a coastal boundary layer in the Gulf that would act as barrier between estuarine and offshore waters, trapping freshwater runoff. Wolanski (1993) confirmed the poor mixing between estuarine and offshore waters and established that the probably nutrient-enriched trapped freshwater is ejected during summer in the southernmost region of the Gulf, generating large-scale coastal outwelling.

Hallegraeff (2000) also observed in summer an invasion of tropical nutrient-rich waters in the North West Shelf region and that a variety of processes such as tidal currents, internal waves and cyclone mixing carry these nutrients into the bottom water of the shelf. This author proposed that nutrient enrichment in the eastern Arafura Sea and northern Gulf of Carpentaria originates in the Aru Island up-welling system (Hallegraeff, 2000).

- Currents

Church and Forbes (1981) found a clockwise residual current in the Gulf of Carpentaria that they later modelled (Forbes and Church, 1983). This hydrodynamic feature is the result of a combination of tides, northeasterly monsoon winds and density-induced currents. Diurnal tides enter through the north of the Arafura Sill and propagate clockwise (Church and Forbes, 1981). This circulation is accentuated by summer easterly monsoon winds and its associated density-induced currents, and weakened by winter south-easterly winds that can even create a weak counter clockwise circulation (Forbes and Church, 1983). Strong tidal currents (more than one metre per second) flow alternatively east and west in Torres Strait, but there is no evidence of net current flow through the strait (Poiner and Peterken, 2000). However, between April and November a westward trend caused by the southeasterly trade winds throughout the region is observed (Wolanski et al., 1988; Hemer et al., 2004). Tidal currents are also an important sand-transporting agent in mesotidal (two- to four-metre tidal range) areas and can even dominate sand transport in microtidal areas (tidal range less than two metres) where coastal geometry affords shelter from ocean swell and wind-driven currents (Harris, 2000).

However, despite the fact that the tidal range in the Gulf of Carpentaria varies from 3.2 to 1.5 metres, sediment transport in the Gulf is dominated by tropical cyclone generated currents. Tropical cyclones are the cause of storms events in northern Australia and induce currents that erode and transport sediment over a wide area (Harris, 2000). Near-bottom current measurements in the Gulf of Carpentaria during a tropical cyclone show hourly-averaged speeds up to six times larger than background current speeds (Church and Forbes, 1983).

1.2.4 Sedimentation

- Sediment origin

With the large number of rivers and heavy rainfall during tropical summer, fluvial sediments can be expected to contribute a major part of the regional sediment budget. Jones and Torgersen (1988) classified sediments of the Gulf of Carpentaria into two main zones: a nearshore zone of active sedimentation and an offshore zone of comparatively low sedimentation activity corresponding to the remainder of the Gulf floor. This classification is consistent with more recent extensive sampling and mapping of the Gulf surface sediments undertaken by Somers and Long (1994). The latter study confirms that the nearshore zone shallower than 20 m is mainly sandy, whereas the offshore zone is clay dominant. However, muddy sediments are also recognised in shallow coastal waters in sheltered embayments or near rivers. The mud content increases from southeast to northwest with the portion of mud ranging from 10% to 90%, respectively, and a clear deficit of offshore sediment exists in the eastern and southern Gulf, even in depths up to 40 m (Somers and Long, 1994).

- Sediment composition

The surficial sediments of the Gulf are highly heterogenous and consist of both young and relict mineral and carbonate components. The terrigenous fraction is fluvial in origin and consists mainly of quartz, minor feldspars and traces of siderite. In shallower parts of the Gulf of Carpentaria, the carbonated component of the sediment is biogenic and has a variable degree of alteration caused by sediment transport and/or diagenesis (Preda and Cox, 2005). Preda and Cox (2005) credited the eastern side as the origin of both terrigenous and carbonate sediment fractions. Thereafter, residual clockwise circulation in

the Gulf (Section 1.1.3) disperses these fractions sorting them by grain size and level of 'purity', with physicochemical and mineralogical changes occurring during transportation (Preda and Cox, 2005).

- Sediment distribution

Wolanski and Ridd (1990) found evidence of a coastal boundary layer in the Gulf that would act as barrier between estuarine and offshore waters, trapping suspended sediments. This is consistent with the coastal muddy zone previously defined. The sandy sediments derived from fluvial sources are distributed northward and segregate by size by waves and tides (Jones, 1987; Edgar et al., 2003). In addition, the combination of the clockwise circulation in the Gulf, the shape of the Gulf and the tidal mixing to the north may lead to higher sediment deposition in the deeper parts of the north-western Gulf (Somers and Long, 1994).

The combined effect of both sea current and wind patterns can determine the redistribution of sediments within shallow coastal waters, while the deeper waters of the central Gulf are less dynamic. The above factors have an important influence on the overall distribution of sedimentary material (Preda and Cox, 2005).

- Sediment transport

According to Harris (2000), sediment transport in the Gulf of Carpentaria is dominated by tropical cyclones with tidal transport prevailing in some coastal areas. At locations of high tidal energy, subtidal bedforms occur and in the central Gulf sediments have an increased carbonate mud content (Figure 1.5).

These conclusions are quite different from the more recent chemically and mineralogically based work of Preda and Cox (2005), who infer that the residual clockwise circulation is the main factor for sediment dispersion in the Gulf of Carpentaria. In fact, they found that the eastern side is the main source of terrigenous and carbonate material, which is then transported clockwise and dispersed throughout the Gulf. They noted that during this process physicochemical and mineralogical changes occur as well as a grain size sorting, with the sediment becoming finer and the carbonates more stable towards the centre (Preda and Cox, 2005).

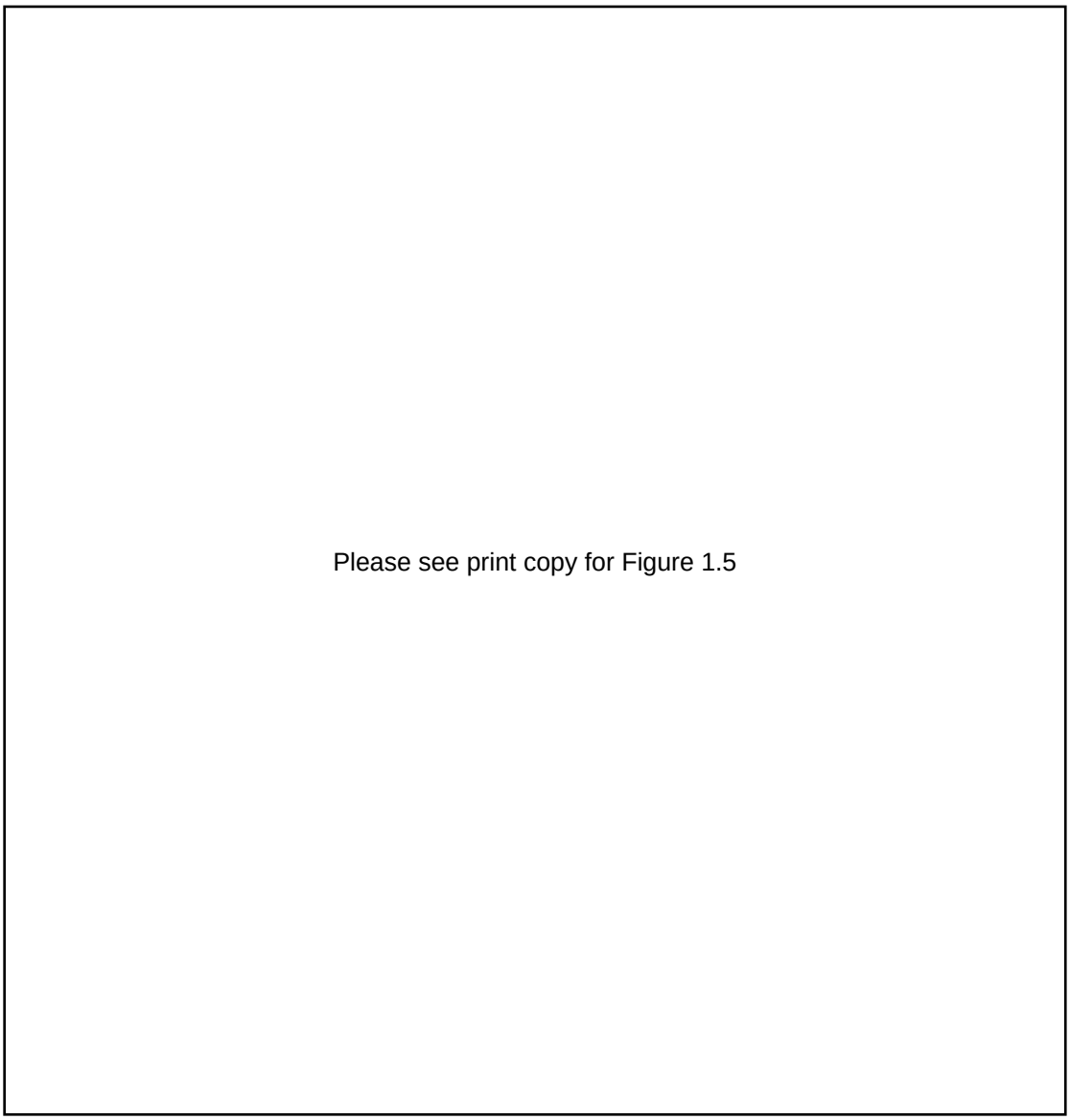

Figure 1.5: Sedimentary facies in the Gulf of Carpentaria and Torres Strait areas (Harris, 2000, from Harris 1988, 1994).

Nevertheless, it is more than likely that both clockwise residual circulation and the more episodic tropical cyclone generated circulation govern sediment distribution in the Gulf of Carpentaria.

1.3 Strategic location

1.3.1 Tectonic stability

The Gulf of Carpentaria is a near-equatorial region, located within a relatively tectonically stable portion of the Australian plate (Nakada and Lambeck, 1989; Harris, 2000). Since the Gulf is distant from areas of major ice-sheet accumulation and disintegration, it is not affected by isostatic adjustments (Woodroffe and Chappell, 1993). Therefore, the Gulf of Carpentaria has the potential of having recorded relatively easily deciphered sea-level fluctuations.

1.3.2 Link between the Indian and Pacific Oceans

The Gulf of Carpentaria, because of it special location, represents a link between the Indian and Pacific Oceans. During times of low sea-level, the Gulf has been separated from the open waters of the Indian and Pacific Oceans, forming Lake Carpentaria, perched above contemporaneous sea-level with outlet channels to the Arafura Sea (Chivas et al., 2001). The time frame of these connections between the Gulf and both oceans is of great importance to the understanding of global ocean circulation.

1.3.3 Proximity to the Indo-Pacific Warm Pool

The Gulf of Carpentaria is located near the Indo-Pacific Warm Pool (IPWP) that includes the Indonesian Archipelago, a 'marine continent' with a normal SST of at least 28°C (Figure 1.6). This region is responsible for the largest transfer of moisture and heat between the surface and the atmosphere on a global scale and forms an engine driving much of the world's climate (Yan et al., 1992).

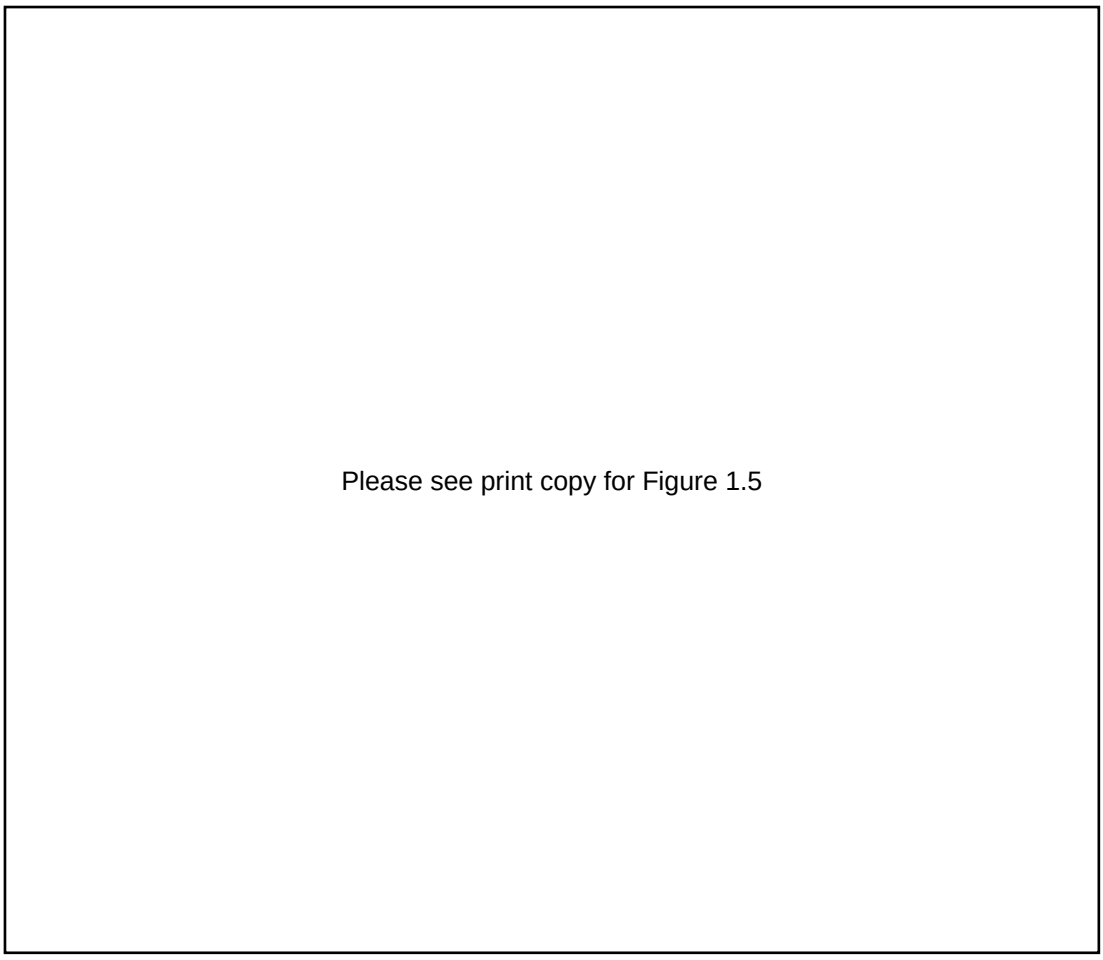

Figure 1.6: Map showing the limit of the Indo-Pacific Warm Pool (IPWP). The Kuroshio, Leeuwin and East Australian currents are also indicated as outflow from the IPWP (Martinez et al., 1997).

1.3.4 Monsoon influence and ENSO

As discussed previously (Section 1.1.2), the Gulf of Carpentaria experiences monsoonal rainfall during summer, with the intensity and duration of the monsoon being related to ENSO phenomena. The amount of freshwater inflowing to the Gulf is proportional to the monsoonal influence. The lacustrine sediments of the Gulf have recorded such influences, and their study will allow the tracing of the history of palaeomonsoon activity in northern Australia, and thus the frequency and intensity of ENSO related phenomena.

1.3.5 Link between marine and continental climatic records

The Gulf of Carpentaria has a complex environmental history; at various time it has been connected to the open waters of both the Indian and Pacific Oceans or isolated from them forming Lake Carpentaria during sea-level fluctuations since about the Miocene (Nix and Kalma, 1972; Smart, 1977; Torgersen et al., 1983, 1988; Jones and Torgersen, 1988; Chivas et al., 2001; Yokoyama et al., 2001). This background gives it the potential to form a link between marine and continental climatic records spanning the Quaternary and much of the Neogene. This correlation between continental and marine climatic records has tantalised researchers for a long time and will eventually allow a better understanding of the climatic system on a global scale, and has been already extensively considered for the Gulf region (De Deckker et al., 1988; McCulloch et al., 1989; Norman and De Deckker, 1990; De Deckker and Corrège, 1991).

1.4 Previous studies

1.4.1 Geological background

The Gulf of Carpentaria consists of three superimposed sedimentary basins beneath the actual topographic expression of the Gulf: the Palaeozoic Bamaga Basin, the Jurassic-Cretaceous Carpentaria Basin and the Cenozoic Karumba Basin (Figure 1.7) (Edgar et al., 2003). A high-resolution seismic survey undertaken by US Geological survey in 1993/94 in the Gulf of Carpentaria allowed the definition of at least 14, and possibly 17, basin-wide transgression/regression reflectors within the three hundred metres of sedimentary sequence in the Karumba Basin which is of probable Miocene to Pleistocene age (Edgar et al., 2003). These authors described two broad units: a lower unit of uniform sediments and an upper stratified unit marked by numerous sediment filled channels. The ten upper reflectors indicate abundant channels incising the floor of the Gulf, especially over the Arafura Sill, where the stratification is poorly preserved.

1.4.2 Physiographic, hydrodynamic and chemical studies

The Gulf of Carpentaria also hosts a large prawn fishery industry (based in Karumba) that has engendered many studies since the late 1960s. The need for a complete understanding of the modern marine environment and its biology has generated numerous physiographic (Munro, 1967, 1972, 1984; Jones, 1986), hydrodynamic (Church and Forbes, 1981, 1983; Forbes and Church, 1983; Wolanski, 1993); and chemical studies on the Gulf of Carpentaria (Cox and Preda, 2003; Preda and Cox, 2005). Most of the results of these studies that relate to the present research have already been presented in several previous sub-sections (Sections 1.2.3 and 1.2.4).

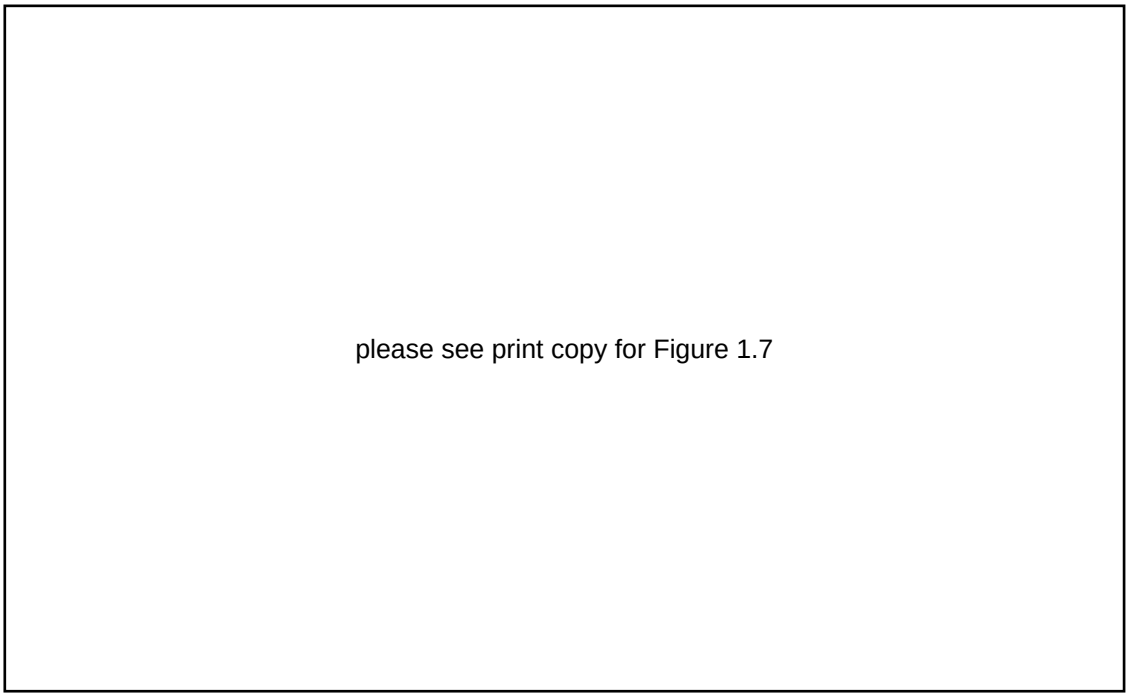

Figure 1.7: Location of basins within the Gulf of Carpentaria region (Passmore et al., 1993). The red stars represent core locations.

1.4.3 Studies related to Quaternary climate

- Lake Carpentaria

Beginning in 1966, Phipps mounted the first important geological investigation in the Gulf of Carpentaria. He collected short cores in the following years, and suggested in 1970, the presence of a former closed basin (Phipps, 1966, 1970, 1980). This hypothesis was supported by several later studies (Nix and Kalma, 1972; Jones, 1986; Jones and Torgersen, 1988).

The second major research project in the Gulf began in 1982 and was lead by Tom Torgersen (then at the Australian National University) and Mal Jones and others from the Queensland Geological Survey, and included more than 1600 km of seismic line and thirty-five shallow cores up to 2.2 metres long and covering the past 50 ka. This project

confirmed the presence of Lake Carpentaria and established that its maximum extent correlated with the –53 metres isobath (Torgersen et al., 1983, 1988; Jones and Torgersen, 1988). Thereafter many papers were published relating the palaeoenvironment and palaeoclimatology of the area (Chappell et al., 1982; Forbes and Church, 1983; Torgersen et al., 1983, 1988; Forbes, 1986; De Deckker et al., 1988; McCulloch et al., 1989; De Deckker and Corrège, 1991; Chivas et al., 2001; Reeves, 2004) and coastal environments (Ridd et al., 1988; Norman and De Deckker, 1990; Woodroffe and Chappell, 1993; Woodroffe et al., 2000).

The most recent campaign involved piston coring using the French scientific vessel *Marion Dufresne* and resulted in the collection of six cores up to 14.82 m long, and spanning at least the past 170 ka. The present thesis is a part of this large project including many other researchers in several disciplines (Chivas et al., 2001; Reeves, 2004). The PhD thesis of Jessica Reeves (2004) is particularly relevant to this study, and is referred to in subsequent discussions of Gulf palaeoenvironments. All other papers dealing with the palaeoclimate of the Gulf of Carpentaria are cited also where appropriate.

1.5 Sea-level history

1.5.1 Eustatic variations

Sea level is directly related to the expansion and contraction of the Earth's ice sheets, or eustatic variation, and thus to the changes in quantity and distribution of the solar radiation. When the solar radiation is greater, the ice melts and the sea level rises. Conversely when this radiation is less efficient, the ice sheets expand and the sea level falls. For the time frame of this study, restricted to the Late Quaternary, variations of sea-level and global climate are due to the distribution of solar radiation rather, than the change in the solar insolation (Imbrie et al., 1984).

1.5.2 Climatic cycles

Milankovitch (1941) presented an astronomical theory on the periodicity of three major components controlling the Earth's orbit around the sun. The eccentricity cycle lasts about 100 ka and is related to the Earth trajectory around (meaning distance from) the sun. The obliquity has a cycle of around 41 ka and depends on the tilt of the Earth's spin axis. The precession of the Earth's equinoxes (or wobble) produces a roughly 23 ka cycle. This theory implies a significant variation in the distribution of the solar radiation reaching Earth that can partly explain ice volumes and therefore sea-level fluctuations over time.

1.5.3 Marine Isotope Stages

The volume of the Earth's ice sheets, and thus the global sea level, has been assessed by measuring the $\delta^{18}O$ of fossil benthic foraminifers in marine sediments. This method allows the division of the Quaternary into Marine Isotope Stages (MIS) according to the difference between modern and estimated sea level (Martinson et al., 1987). The MIS are

commonly divided into substages, and are numbered from the present backward, with odd numbers referring to high sea level or interglacial stages and even numbers referring to low sea level stands or glacial stages (Figure 1.8).

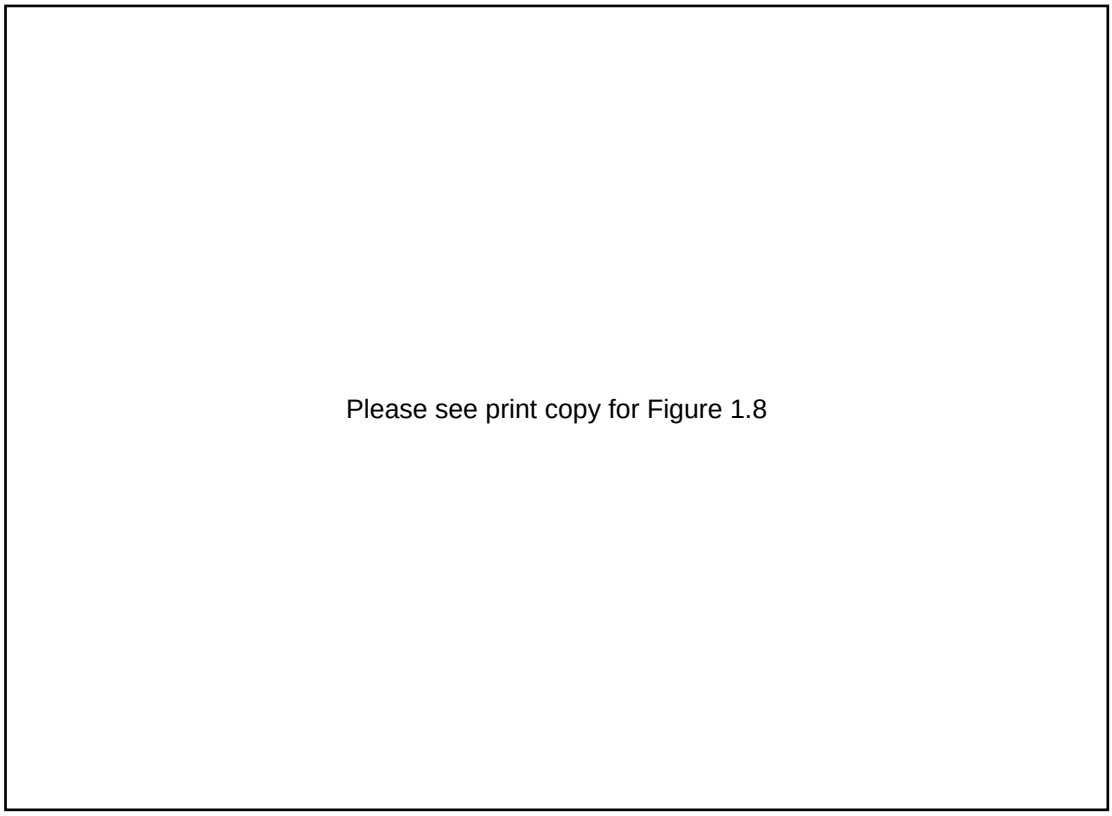

Figure 1.8: Sea level curve (dark blue line) and associated confidence interval (pale blue lines) showing the MIS. Interglacial stages are red and Glacial stages are blue (from Waelbroek et al., 2002).

1.5.4 Isostatic and tectonic variations

There are some other major parameters that modify, even if locally, sea level fluctuations, such as tectonic and isostatic factors. The constant movement of tectonic plates around the world generates collision or rifting, both acting usually on local, and at times wider scales, to complicate apparent sea levels. On a broader scale, the melting of ice sheets also causes uplift of the underlying continental plates when the ice is unloaded. Conversely ice sheet expansion, sediment deposition and water loading generate sinking of continental shelf areas and oceanic plates.

1.5.5 Sea-level curve

For the past thirty years, the production of sea-level curves as a function of time has occupied many researchers. Several curves have been established using benthic or planktonic foraminifera $\delta^{18}O$ values (Shackleton and Opdyke, 1973; Shackleton, 1977, 1987; Shackleton et al., 1983; Imbrie et al., 1984; Waelbroek et al., 2002), coral records (Chappell, 1983; Chappell and Shackleton, 1986; Chappell et al., 1996) or oxygen isotope records from Greenland ice cores (Grootes et al., 1993), with variable degrees of cross referencing (Chappell et al., 1996; Waelbroek et al., 2002).

The Waelbroek et al. (2002) sea-level curve (Figure 1.8) is a composite curve based on coral data and associated with benthic foraminifera $\delta^{18}O$ records that have been corrected from temperature (Shackleton, 1987), ice volume and local effects (Waelbroek et al., 2002). This curve will be utilised as a baseline for comparison with the present study.

1.6 Summary

Observation of modern climate indices indicates that the Gulf of Carpentaria is within an area sensitive to the Asian monsoon and ENSO. Knowledge of the fluctuation and rhythmicity of these phenomena is crucial for developing a better understanding of climate dynamics on a worldwide scale. The Gulf is tectonically stable, therefore no corrections are necessary when interpreting the palaeosea-level record. The presence of Lake Carpentaria during low sea level stands has been confirmed by historical investigations of Gulf sediments proving the quality of the latter for palaeoclimatic reconstructions. The understanding of the modern hydrodynamics of the basin provides a significant tool to help the interpretation of the Gulf sediment records in terms of their deposition, palaeoenvironments and sea level variations.

Chapter 2:

Core Assessment and Sampling

2.1 Introduction

As outlined in Chapter 1, this study aims to establish a detailed chronology for the Gulf of Carpentaria, using OSL dating on the quartz fraction of the collected core sediments, and investigates palaeoenvironments from nannofossil records. This Chapter presents an outline of the broader project being undertaken on the Gulf of Carpentaria and describes sampling techniques and protocols from the core collection to the individual samples that are used for OSL dating (Chapter 3) and nannofossil investigations (Chapter 4) central to this thesis.

2.2 The team

This study forms part of a large project on the Gulf of Carpentaria lead by Professor Allan Chivas and funded mainly by grants from the Australian Research Council. The Gulf project started with the collection of six sediment cores in the Gulf of Carpentaria during 1997 and continued with several studies on the collected material including pollen, ostracods, foraminifers, nannofossils and geochemistry. The team undertaking study on the cores are mainly based at the University of Wollongong and include Professor Allan Chivas (coordinator), Dr Jessica Reeves (ostracods), Dr Brian Jones (sedimentology), PhD student Sabine Holt (foraminifers), Dr Adriana Garcia (charophytes), Dr Dioni Cendon (trace element geochemistry) and Mr David Wheeler (geochemistry). Dr Sander van der Kaars from Monash University performed the pollen analysis on all six cores. Allan Chivas, Adriana Garcia and Martine Couapel (University of Wollongong), Drs N Terry Edgar and Frank Dulong (USGS) and Luc Beaufort (CEREGE) formed the scientific team during the coring aboard the *Marion Dufresne*.

This PhD, which forms a major component of this larger Gulf project, is principally concerned with the OSL dating and nannofossil aspect of the Gulf record. Relevant elements of other Gulf project components are, where relevant, referred to and discussed throughout this thesis.

2.3 The cores

2.3.1 Collection

In June 1997, six cores were collected in the Gulf of Carpentaria using a giant piston-corer deployed from the *Marion Dufresne*. This system allows the recovery of cores of variable length with a diameter of 98 mm. The core collection took place during a program operated by the Institut Francais pour la Recherche et la Technologie Polaire (IFRTP) IPHIS-IMAGES III (International MArine Global changE Study) campaign as a collaboration between Australian, American and French scientists. The labelling of the cores MD972128 to MD972133 refers to the ship that collected the cores (MD), the year of collection (97), the campaign number (21) and the core collecting rank (28 to 33 for the Gulf of Carpentaria area). For the remainder of this study, each core is designated by its shortened code: MD28; MD29; MD30; MD31; MD32 and MD33.

2.3.2 Coring sites

The sediment cores with recovered lengths ranging from 4.2 to 14.8 metres were collected in 59 to 68 metres water depth (corrected for tidal variation) (Table 2.1). These cores are much shorter than those usually collected in open marine oozes using the same piston-coring system that can often recover core lengths of over fifty metres. The reason for the shorter cores collected from the Gulf is undoubtedly due to the semi-lithified nature of the Gulf of Carpentaria sediments with their common calcretised and ferruginous intervals. The high-resolution bathymetry record available onboard and the simultaneous collection of high-resolution seismic data (800Hz) facilitated the selection of the core sites. The main aim was to core along a transect from within the limit of the past Lake of Carpentaria to its shallower outside rim, in order to obtain a succession of marine and lacustrine sediments together with sub-aerial exposure horizons. All cores terminated in indurated sediment and were bent, the deeper/older sediment collected being calcretised and/or ferruginised.

Table 2.1: Core locations, water depths at each core site and core lengths (cf. Figure 1.1).

Please see print copy for Table 2.1

2.3.3 Onboard processing

- Non-destructive analysis

After collection, the cores were processed using procedures typical to all IMAGES cores. After being brought onboard, the PVC core casing was removed from the steel coring tube, cut into 1.5 metre sections and numbered from top to bottom (i.e. recent to old). These sections were then passed through a Geotek® Multi-Sensor Core Logger (Geotek®, 2000) that allows the non-destructive measurement of physical parameters such as magnetic susceptibility, P-wave velocity and γ-ray attenuation densitometry. It has to be noticed that, during usual ^{137}Cs exposure from γ-ray attenuation densitometry, core sediment particles are exposed to a maximum of 1.45×10^{-6} Gy (Couapel and Bowles, in press; Appendix 3).

- Archived and work halves

Each core section was then split in half longitudinally, one half being stored as archive and the other half, labelled 'work', being further analysed. Throughout this thesis, the core section used is the work-half unless otherwise advised. Core splitting was achieved with a nylon wire stretched between two handles to slice through the sediments after the PVC casing tube had been cut on a special saw-bench with two opposing circular saws. The surface of work-half was then cleaned using a wet plaster knife applied from one edge to

the other, perpendicular to the length of the core. This bedding-parallel smoothing of the work-section surface minimises contamination from older or younger levels.

- Sedimentological observation

After cleaning, a preliminary sedimentological description of each core was completed with reference to the Munsell Colour Chart. Some smear slides (defined in Section 2.6.1) were prepared if further details were needed or to clarify a particular sedimentological structure/feature. This initial observation is essential to define the core quality (noting coring artefacts or disturbance, major reworking or slumping evidence) and thus to rank the cores for their potential level of interest/quality. None of the six cores exhibited signs of major structural deformation. MD31 and MD32 were ranked at the higher priority level because of their length and the recording of clear successions between more than one palaeoenvironment. This study primarily focuses on these two higher value cores, but also draws on the other shorter cores to develop a more complete understanding of the palaeoenvironments of the study area.

- Other analyses and storage

After the sedimentological analysis, each work-half was photographed using a digital camera and the colour variation was assessed using a Minolta Spectrophotometer CM-2002. Each work-half was then covered with plastic wrap, sealed in a thick plastic bag and stored in a stackable plastic tube. Both the archived and work-half cores for MD28, MD29, MD30, MD31, MD33 were kept in a cold room under 4°C on board and during their later transfer to the University of Wollongong where they have since been stored continuously in a cold room. MD32 (an IMAGES reference core) was initially transferred to CEREGE (Aix-en-Provence, France). The MD32 archived-half is still in CEREGE in a cold container whereas the work-half has been sampled (as individual 1-cm depth-increment slices) by Allan Chivas, Adriana Garcia, Martine Couapel (University of Wollongong) and Sophie Bieda (CEREGE) in early 2000 at CEREGE and brought back for further analysis to the cold room at the University of Wollongong School of Earth and Environmental Sciences.

2.4 Core sampling

Sampling of cores MD28, MD29, MD30, MD31 and MD33 was undertaken at the University of Wollongong in the 4°C cold room. The principal contestants to undertake this work, which spanned over two years (1998-99), were Sabine Holt, Jessica Reeves, Adriana Garcia and Martine Couapel. Grant Pearson and Sandrine Pendu were also involved for short sampling periods. Core MD32 (the IMAGES reference core stored in France) was sampled at ambient room temperature (approximately 15°C) at the CEREGE underground laboratory in January/February 2000.

2.4.1 Sampling method

About 53 metres of sediment half-cores (from 5 of the cores) were sliced in 1 cm-thick segments that were weighed and stored flat in sealed glass Petri dishes. The sampling campaign produced about 5300 core segments, with over 1040 of these being later sub-sampled for further analysis. The reference depth for each sample corresponds to the top depth of the sample. For example the 1 cm-thick segment sample from 5 to 6 cm depth in the core is labelled 5 cm. The outer 3 mm of each segment was discarded to minimise the risk of contamination due to the coring process or PVC casing.

Every fifth centimetre (0, 5, 10…) was further dissected for a variety of analyses, including micropalaeontology, palynology, diatoms and nannofossils, sedimentology and organic geochemistry (Figure 2.1). Approximately thirty percent of the volume of these slices was retained in the Petri dishes for later use and/or archiving. In this study, nannofossil samples every 5 cm in all six cores were investigated. Additional sampling for nannofossil analyses was also undertaken on several undissected samples to enable higher-resolution investigation. For this sampling, a minute amount of sediment was collected from the subsurface of the archived half-core with a spatula and stored in a small plastic vial. Five archive-portions from these 1 cm-thick segment (4 from MD32 and 1 from MD33) were also sampled for OSL analyses.

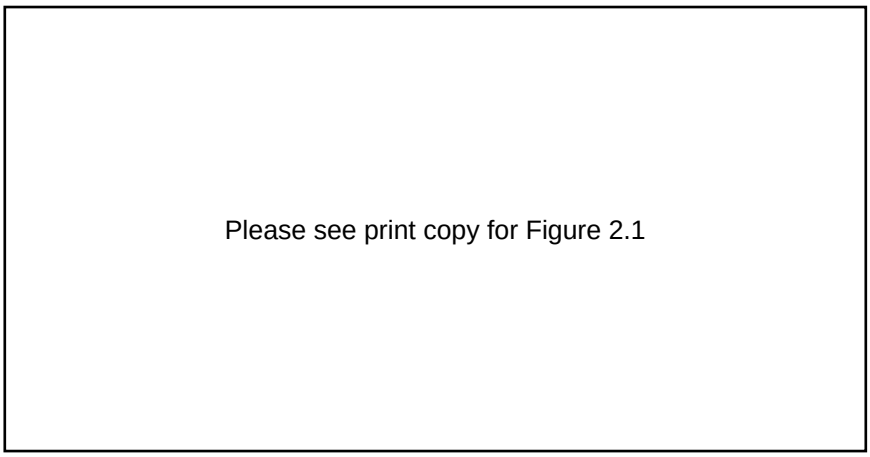

Figure 2.1: Pattern of sub-sampling of every fifth 1 cm-thick-segment of half core material from the Gulf of Carpentaria (modified from Chivas et al., 2001). The nannofossil samples from all six cores were analysed. Five archived portions were also sampled for OSL dating.

This sampling process also allowed better observation and description of the core as for each 1-cm depth-increment, the observable surface area increased from an initial 9 cm^2 (top of the slice) to about 64 cm^2 (sides of the slice). In all six cores, the presence of large concretions in some sections, prevented the 1 cm segment sampling protocol to be followed, and resulted in several large segment samples of up to 3 cm thick.

2.4.2 Water content analysis

The micropalaeontological samples previously defined (Figure 2.1) were used for ostracod, foraminifer and charophyte distribution and abundance investigations together with mineralogical analysis. These samples were initially weighed in grams to three decimal places, then oven-dried overnight at 60°C, and re-weighed. The difference in weight was used to determine the water content of the sample.

2.4.3 Nannofossil analysis

Nannofossil samples (Figure 2.1) were stored in a 0.5 ml plastic vial with an attached push-in lid. Two types of slides, smear slides and filter slides, were prepared. Details of

these two slide-preparations, the analysis of which forms a major component of the present study, are described in Section 2.6.

2.4.4 Other analyses processed on these cores

- Ostracod analysis

Jessica Reeves performed a systematic investigation of every 10 cm on cores MD31, MD32 and MD33 of the coarser than 63 µm fraction, assessing sedimentological and microfossil characteristics, prominent biota, lithic fragments and evidence of alteration (Reeves, 2004). Reeves also focussed on the ostracod assemblages of MD32, determining species presence and abundance for each 5 cm sample of core MD32. The results from this study are compared to those of Reeves (2004) in Chapter 5 of this thesis.

- Foraminifer analysis

Sabine Holt completed a systematic analysis of foraminifer assemblages every 5 cm on the top 1.5 metres of all six cores for the coarser than 63 µm fraction (Holt, 2005). Holt's study corresponds to a high-resolution investigation of the Gulf of Carpentaria palaeoenvironments from the Last Glacial Maximum (LGM).

All the following outlined analyses have been presented in a paper summarising the preliminary results of the Gulf of Carpentaria project that should be referred to for further details (Chivas et al., 2001).

- Pollen analysis

Sander van der Kaars performed the palynological investigation of the top 1.5 metres of five cores (MD28 to MD31 and MD33) with these findings been reported by Chivas et al. (2001). Van der Kaars also investigated core MD32 every 5 cm (unpublished results) and Reeves (2004) was able to draw clear correlations between his results and her own findings. In Chapter 5 of this thesis, Van der Kaars' palynological interpretation of the past

environments is also compared to the nannofossil palaeoenvironmental reconstruction of the Gulf of Carpentaria.

- Particle size analysis

Particles-size analysis (mean particle-size and clay/silt/sand percentages) was undertaken by Adam Switzer on 1030 samples using a Malvern Mastersizer 2600 in the Faculty of Engineering at the University of Wollongong (reported in Chivas et al., 2001). This instrument permits a rapid analysis of particle size and clay/silt/sand percentages, where clay is finer than 2 μm, silt is 2 to 63 μm and sand is coarser than 63 μm. The results from this analysis were used to ascertain which levels in MD31, MD32 and MD33 had an adequate amount of coarse material amenable to optically stimulated luminescence dating of the quartz fraction.

- Geochemistry analysis

The total carbonate content, organic carbon and nitrogen content, atomic C/N ratio and $\delta^{13}C$ of organic matter for the top first metre of 6 cores was measured by Grant Pearson (reported in Chivas et al., 2001) at the School of Earth and Environmental Sciences at the University of Wollongong. David Wheeler subsequently completed the analyses for all six cores to a depth of 1.5 metres (unpublished results).

- Diatom analysis

A detailed search for diatoms performed by the author on core MD32 was unsuccessful due to an almost complete lack of preserved material. An intended systematic study of diatoms could not be pursued.

2.4.5 Dating analyses

To support these investigations, a chronological time frame is required. Several dating techniques including Accelerator Mass Spectrometer (AMS) ^{14}C, Amino Acid Racemisation (AAR), thermoluminescence (TL) and Optically Stimulated Luminescence (OSL) were used in the early stages of the project to enable initial correlation with the $\delta^{18}O$-derived sea-level curve (Chivas et al., 2001). Sixteen initial dates, comprising eleven

^{14}C, three AAR, one TL and one OSL, demonstrated a high level of consistency among techniques.

These encouraging results and the need for a more precise time frame for the Gulf of Carpentaria beyond the traditional radiocarbon dating limit of 45 ka, partly initiated the current research into OSL techniques. This research direction also forms a logical consequence of the good agreement between ^{14}C, AAR, TL and OSL dates together with the establishment of the OSL laboratory at that time at the University of Wollongong.

The AMS ^{14}C method is outlined next as additional dates were acquired and corrections and calibrations for previously reported dates were updated. One new TL minimum age was estimated following the same protocol as detailed in Chivas et al. (2001). The OSL methods used in this study are described in Chapter 3 whereas the core sampling protocols, together with the sample selection, are described in Section 2.4.

- ^{14}C Dating methods

Fifty-three AMS ^{14}C analyses funded by the Australian Institute of Nuclear Science and Engineering (AINSE) grants 98/155R, 01/032 and 02/025 awarded to A. Chivas, were carried out at the Australian Nuclear Science and Technology Organisation (ANSTO), Lucas Heights, using methods described by (Lawson et al., 2000). The analyses were processed on well-preserved, clean mollusc and ostracod shells with no clear evidence of reworking.

The accepted half-life of ^{14}C, or Libby half-life, for calculating a conventional radiocarbon age is 5568 years (Stuiver and Polach, 1977). Conventional radiocarbon ages were corrected for isotopic fractionation when $\delta^{13}C$ was known. Calibrated ^{14}C ages were calculated with CALIB 5 (Stuiver and Reimer, 1993; Stuiver et al., 2005) for samples younger than 26 ka (Stuiver et al., 1998). This latter calculation was performed for marine samples using the Marine04.14C calibration dataset (Hughen et al., 2004) that incorporates a time-dependent global ocean reservoir correction of about 400 years, and applying a reservoir correction (ΔR) of 52 ± 31 years that is regarded as the average for northeast Australian waters (Reimer and Reimer, 2005). The South-Hemisphere calibration dataset SHCal04.14C (McCormac et al., 2004), which is limited to 0-11 ka BP and corresponds to the Southern Hemisphere, was applied to sufficiently young (< 11 ka) lacustrine samples. The IntCalo4.14C calibration dataset (Reimer et al., 2004) was

utilised for all other lacustrine samples and no reservoir correction was applied due to the lack of information regarding ^{14}C reservoir values for Lake Carpentaria. All conventional radiocarbon ages have been rounded according to Stuiver and Polach (Stuiver and Polach, 1977) and calibrated ages were also rounded (Stuiver et al., 1998). The results presented conform with the recommendations of Stuiver et al. (1998) in Appendix 1.

2.5 OSL sample selection and sampling

2.5.1 Sample selection

MD31 and MD32 are much longer than the other cores collected and were classified as highest priority. MD33 was collected in the modern deeper part of the Gulf and thus is also of critical interest. These three cores, therefore, form the focus for the OSL sample selection. In addition, estimated dates from more than one core also permit a spatial correlation. The first step of the selection was the designation of key sedimentological units or boundaries that needed to be dated. This designation was done after discussion with other researchers involved in the Gulf of Carpentaria project to agree on significant horizons, some of them being common across multiple cores to allow later correlation between similar stratigraphic sequences.

The aim in sample selection for this OSL dating was to select the nearest stratigraphic level(s) to these significant horizons that appeared to have a high quartz (63 to 150 µm) content. To process OSL dates on quartz grains, the minimum amount of sample required is in the order of a few grams (Duller, 1994b; Banerjee et al., 2001). All available information on sediment characteristics such as water content, percentage of sand, mean particle size, magnetic susceptibility and sedimentological description (Appendix 2) were taken into account to determine which was the nearest sample(s) to the significant unit that might be measurable by OSL dating. Because of the muddy quality of most of the sediment cores collected in the Gulf, the number of suitable stratigraphic levels for OSL dating on coarse-grained material was rather restricted.

For cores MD31 and MD33, OSL samples were chosen after viewing the whole archive-half core and considering the presence of concretions or evidence of elevated coarse quartz grain content in the vicinity of the preferred sampling level(s). In core MD32 OSL samples were taken from the already segmented core, which precluded such visual assessment.

The depths of the selected samples shown in Appendix 2 are:

Core MD31:

30 cm, 120 cm, 530 cm, 902 cm, 1040 cm and 1340 cm;

Core MD32:

38 cm, 629 cm, 921 cm, and 1397 cm;

Core MD33:

220 cm, 360 cm and 629 cm.

In addition, MD32 segment 1482 cm that was already OSL dated in the early stage of the Gulf of Carpentaria project by Debabrata Banerjee (reported in Chivas et al., 2001), was redated in this study to test for consistency. Furthermore, to test for possible differences resulting from sampling of the archive-half core versus the entirely segmented work-half, OSL samples from core MD33, segment 629 cm were extracted from both the archive-half core and the segmented work-half . A total of 15 samples were dated for this study using OSL techniques.

2.5.2 Sampling

Because the work-half cores had already been cut into 1 cm-thick segments, OSL sampling was performed on the archive-half for cores MD31 and MD33, in order to prevent mixing with light-contaminated samples. The sampling procedure was carried out in a photo-processing (i.e. dark) laboratory.

Several 3 cm-length pieces were cut from a 2 cm-diameter clean glass tube, these tube-segments were gently pushed into the sediment (Figure 2.2). Special wooden-handles were made at University of Wollongong workshop, one to insert the glass tube in the sediment (Figure 2.2a) and one with a longer dowel to extrude the sediment from the glass tube (Figure 2.2d). While in the sediment, the glass tube was rotated to help it detach from the surrounding sediment and core casing (Figure 2.2b and c).

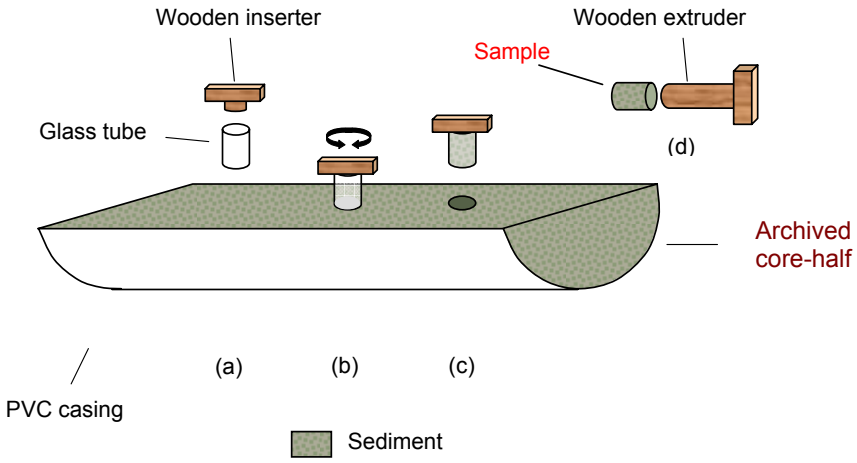

Figure 2.2: Illustration of the four steps of the OSL sampling procedure for archive-half cores undertaken under red light to prevent light contamination.

For core MD32, the archived core-half was unfortunately inaccessible (stored at CEREGE), and sampling was thus performed on the remnant archive portion of the work-half. Although these samples had been wrapped in aluminium foil (light-proof), the cleaning of the light-contaminated surface sediments was performed with particular attention. As with the sampling of cores MD31 and MD33, the entire procedure was undertaken in a photographic darkroom under red light.

All OSL samples where then processed as detailed in Chapter 3.

2.6 Slide preparation for nannofossil investigation

2.6.1 Smear slides

The aim of the technique outlined here is to rapidly obtain microscopic slides of bulk sediments that allow the qualitative study of calcareous nannofossil species. A minute amount of bulk sediment (as little as a pin's head) is mixed on a clean and dry glass slide with a drop of tap water, using a flat wooden toothpick. This mixture is smeared on the slide with a toothpick using force to obtain 'rib-pattern' features on the slide. The slide that should appear extremely light-transparent is heated on a hot plate and mounted with Canada balsam, appropriate for the calcite refraction index. The abundance ratio among calcareous nannofossil species of similar size is not affected by smearing, thus the relative abundance between species can be established. To eliminate the possible error arising from size fractionation due to the preparation process, four orthogonal transects were systematically examined.

Smear slides were prepared for each 10 cm depth-increment samples of core MD32 to investigate nannofossil abundance and assemblages. The smear-slide microscope investigation and its results are presented in Chapter 4, Section 4.

2.6.2 Filter slides

The preparation of filter slides took place at CEREGE, Aix-en-Provence during July/August 2001 under the supervision of Luc Beaufort and with the help of Noëlle Buchet and Shaun Ellis. This visit was supported by a collaboration/exchange grant (AMVSG30763) co-founded by the CNRS (Centre National de Recherche Scientifique, France) and the ARC (Australian Research Council) and managed by the French Embassy in Canberra, together with GeoQuEST from University of Wollongong.

The filter slide technique allows a quantitative investigation of nannofossil abundance expressed as the number of individuals per gram of wet sediment. Approximately 0.02 grams of sediment is precisely weighed to 4 decimal places in a 5 ml beaker and diluted with about 3 ml of water. To guarantee a total dispersion of the sample, the beaker is manually agitated, the sediment may be crushed if necessary and eventually the beaker is immersed in an ultrasonic bath for ten seconds. The solution is then poured into a 500 ml volumetric flask, and the water level is adjusted. Then 20 ml of this nannofossil-bearing solution is drawn up with a pipette and poured into the top part of the filtration unit. This filtration unit includes a leak-proof screw-closure and is used with 0.45 μm effective pore size, 47mm-diameter cellulose nitrate membranes. The entire solution is then pumped out up through the filter, which traps the nannofossils. The pumping is stopped when the filter membrane is dry. The filter is placed flat into a small aluminium container, and put in the oven to dry overnight (60°C for 12 hours). A piece of the filter is then cut and laid on a glass slide on a hot plate (110°C) with one drop of Canada balsam underneath and one drop on top. The whole filter needs to be translucent.

Filter slides were prepared for each 5 cm depth-increment sample of all six cores. Additional filter slides (up to single centimetre spacing) were prepared for core MD31 when particular features of interest were noted, in order to obtain a high-resolution investigation. These filter-slides were analysed using SYRACO, a semi-automatic analysis software, and the results are presented in Chapter 4, Section 5.

Chapter 3:

Optically Stimulated Luminescence

3.1 Introduction

Optically Stimulated Luminescence (OSL) dating is a relatively recent method, developed over the past 20 years, emanating from the more established Thermoluminescence (TL) research. The common principle of the two methods is to obtain dates based on the physical property of luminescence, which is exhibited by some minerals. This property is the ability of certain minerals to store energy and to emit a luminescence signal when excited. For TL, the stimulus is heat whereas for OSL it is light. In a method originally proposed by Huntley et al. (1985), it was found that the released luminescence signal is directly proportional to the time since the material was last heated or last exposed to daylight.

This chapter is broken into three parts: background, laboratory analysis and finally age calculation and application.

The first part of this chapter presents the background, applications and requirements of the OSL dating method. The OSL principle is outlined, with a focus on the luminescence characteristics of quartz, which is the mineral used in this study. Thereafter the environment of the Gulf of Carpentaria is assessed for its suitability for OSL dating.

The second part of this chapter begins with a presentation of the sample processing technique, and a detailed synopsis of protocols used to measure OSL signals in quartz. Following this, is a description of the analytical equipment and methods employed to calculate the Equivalent Dose (D_E) and the Dose Rate (D_R). The D_E is the laboratory dose necessary to produce the same luminescence signal as that which occurs in the natural sample, whereas D_R corresponds to the first derivative of environmental radiation dose with respect to time. Doses are defined as the energy absorbed per kilogram and the unit is the gray (Gy) which corresponds to 1 joule per kilogram. Therefore D_E is expressed in Gy and D_R in Gy ka^{-1}.

Finally, the D_E and D_R are used to establish the subsequent dating results using the simple relationship: Age = D_E / D_R. As a conclusion, the dates obtained using the OSL technique are compared to results from other independent dating methods employed on

core material from the Gulf of Carpentaria. This suite of dates is integrated to form a chronological framework for the Gulf through the past 180 ka.

3.2 History

This section provides an overview of the background, origin and development of the Optically Stimulated Luminescence technique up to the emergence of single grain analysis.

3.2.1 The origin of thermoluminescence

The property of thermoluminescence was first described by Sir Robert Boyle who reported to the Royal Society on the 28 October 1663 that “a remarkable diamond he took into his bed and held a good while upon a warm part of his naked body, gave off a weak glow” (Boyle, 1663). Farrington Daniels was one of the first to investigate TL systematically for dosimetry in the 1940s (McKeever and Moscovitch, 2003). However, it wasn’t until 1953 that he suggested the use of TL to determine how long ago pottery was fired (Daniels et al., 1953). In the 1970s TL was established as a numerical dating technique through the work of a broad international community including Martin Aitken (Oxford, UK), Vagn Mejdahl (Risø, Denmark) and Georges Valladas (Gif-sur-Yvette, France). These researchers applied the method to a diverse range of materials such as ceramics, hearthstones, lava, and burnt flint.

3.2.2 Early stages of TL dating applied to ocean sediments

Russian and Chinese researchers in the early 1970s recognised partial bleaching of the TL signal after exposure to sunlight; however, their work was not widely appreciated throughout the western scientific community. It was not until 1979 that Wintle and Huntley, described and published experimental evidence showing that exposure to sunlight could at least partially bleach the TL signal, and thus provide the possibility of dating ocean sediment cores (Wintle and Huntley, 1979). The difficulty in estimating the residual TL signal not bleached during transport (Figure 3.1) generated several research studies on various materials to address this problem (Wintle and Huntley, 1980; Wintle, 1981; Mejdahl, 1988).

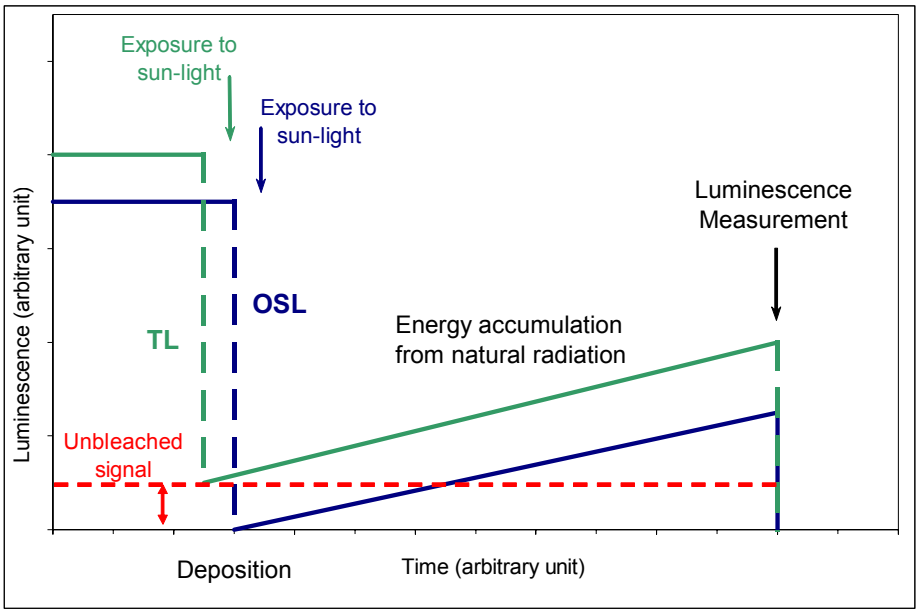

Figure 3.1: Schematic representation of the TL and OSL dating principle.

3.2.3 The emergence of optically stimulated luminescence

Some years later, Huntley et al. (1985) stimulated some previously irradiated quartz using the 514 nm (green light) ray of an argon laser. They obtained a signal proportional to the irradiation dose, similar to that of a TL signal. They determined that this optically stimulated signal could then be used to determine the effective dose absorbed by minerals. Because optical stimulation activates only light-sensitive traps, it is more appropriate for sediment dating than is thermal stimulation, which also activates traps not sensitive to light, hence at deposition there is liable to be a non-negligible latent thermoluminescence signal. For TL, heat is the excitatory agent, for OSL the stimulus is light, which means that a mineral exposed to sufficient daylight no longer retains an OSL signal, as it is bleached or 'zeroed' (Aitken, 1994, 1998; Rhodes and Pownall, 1994; Wintle, 1997).

3.2.4 Stimulation wavelengths

Hütt et al. (1988) proved the existence of a rather deep light-sensitive trap in K-feldspars, from which the content may be bleached by both visible (490 nm) and infrared (IR) wavelengths (860 nm, 930 nm). About the same time, while testing the bleaching by natural light of their brightest feldspar and quartz samples, Godfrey-Smith et al. (1988) also revealed that IR photons (753 nm and 799 nm) could also stimulate natural luminescence and that ultraviolet blockers, such as water, do not prevent bleaching. Further studies on stimulation as a function of wavelength have shown that there is an optimal incident light to be used for each material: feldspar will release luminescence under IR whereas quartz needs shorter, green to blue/green, wavelengths to free electrons from their traps (Aitken, 1994; Bøtter-Jensen et al., 1994; Bøtter-Jensen, 2000). The use of diverse wavelengths both increased the possibilities of the OSL method, and revealed the importance of the choice of the wavelength of the incident light. This excitation light has to be optimal in terms of stimulation spectra, but it also has to be distinct from the emitted light so as not to be confused with the luminescence being measured during excitation.

3.2.5 Stimulation techniques

Markey et al. (1997) and McKeever and Chen (1997) tested a new stimulation technique, in which the stimulation is pulsed and the OSL recorded only after the end of the pulse, to circumvent the problem of wavelength superimposition. These authors also demonstrated that the shorter the excitation pulse, the greater the amount of light emitted after the pulse, compared with that emitted during the pulse. While working on the different components of the OSL signal, Bulur (1996) developed the linear modulation technique, in which the excitation light intensity is increased linearly during stimulation. This allows the separation of the overlapping OSL components, assumed to originate from different traps (Bulur et al., 2000).

3.2.6 Towards single-grain analysis

Researchers using smaller samples for OSL measurement clearly demonstrated that the natural bleaching of quartz and feldspar was heterogeneous, contrary to what was previously assumed (Rhodes and Pownall, 1994; Murray et al., 1995; Olley et al., 1998). The next development in the OSL technique was the prospect of single-grain analysis.

Lamothe et al. (1994) first tested the method on feldspar, followed by Murray and Roberts (1997) who applied a similar technique to quartz. These single-grain analyses can now be processed routinely on the automated Risø luminescence reader (Bøtter-Jensen, 2000) and have stimulated successful research (Murray and Roberts, 1997; Roberts et al., 1998b, 1999; Galbraith et al., 1999; Olley et al., 1999, 2004a, 2004b; Bulur et al., 2002; Duller, 2003; Yoshida et al., 2003). These technological improvements have not only established OSL as a reliable dating tool, but also a key technique in various other radiation dosimetry fields.

3.3 Luminescence Principle

This subsection deals with the physical aspects of luminescence and the associated technology.

3.3.1 The origin of luminescence

Stored energy accumulates in minerals as a result of absorption from environmental radioactivity and cosmic ray doses. Indeed, constant bombardment of the Earth by cosmic rays, and environmental radioactivity from the decay of naturally occurring radioactive elements in rocks and soil, creates an ionising radiation that knocks electrons loose from the atoms it hits.

Natural crystalline materials usually have defects (such as impurity ions or stress dislocations) in their lattice, leading to areas where free electrons are attracted and trapped (Figure 3.2a). These 'electron-traps' can be deep, holding electrons tightly for many thousands of years (Figure 3.2b), or shallow, allowing easier release of electrons upon stimulation (Figure 3.2c).

3.3.2 Energy accumulation

The last exposure of the mineral to sunlight may, under suitable conditions, reset the latent OSL signal to zero, before burial by continuous sedimentation (and thus unexposed to daylight) whereby its absorbed dose accumulates again in response to ionising radiation (Figure 3.1). Later, optical stimulation of these minerals will give a natural luminescence signal, that rapidly decreases with the time of exposure, as shown in Figure 3.3.

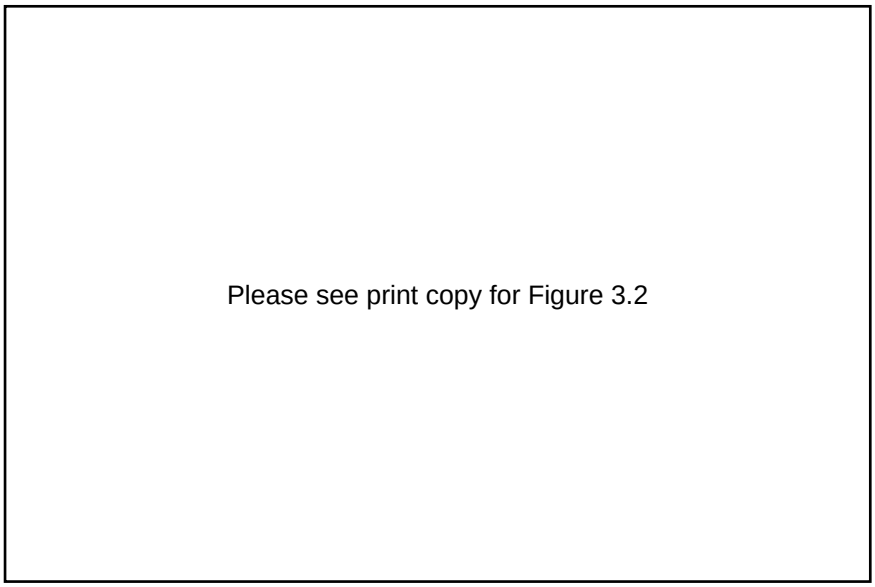

Figure 3.2: Energy-level representation of TL and OSL processes (from Bøtter-Jensen, 2000). (a) Ionisation due to exposure to ionising radiation with trapping of electrons and holes at defects T and L, respectively. (b) Storage of radiation energy during time; to be able to neglect leakage only traps with lifetimes much longer than the storage time of the sample are appropriate. This lifetime is dependent, besides other factors, on the energy depth E of the trap below the conduction band. (c) By heating or shining light onto the sample, electrons are evicted from the electron traps and some of these reach luminescence centres (L); if so, light (i.e. TL or OSL) is emitted as a result of the process of recombining into these centres.

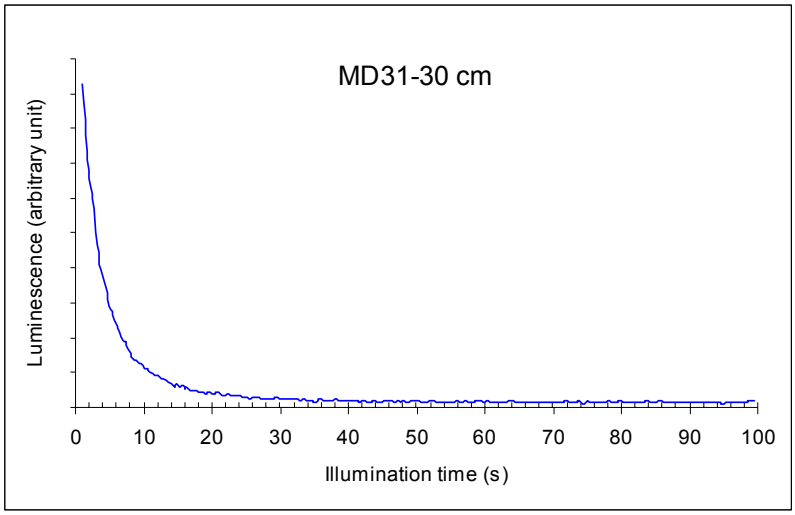

Figure 3.3: Typical OSL decay curve using blue light stimulation on a quartz sample from the Gulf of Carpentaria.

Luminescent minerals act like radiation dosimeters and are capable of storing energy for up to 1 Ma at the Earth's surface temperature. But with respect to quartz, dating is restricted by the degree of dose saturation of the grain, rather than by the poor stability of the OSL signal over time (Aitken, 1985b, 1994).

3.3.3 Luminescence measurement

The use of a highly sensitive light-detection device, such as a photomultiplier (Figure 3.4), is essential to enable the measurement of the commonly minute OSL signal corresponding to the energy accumulated by the mineral since its last exposure to sunlight.

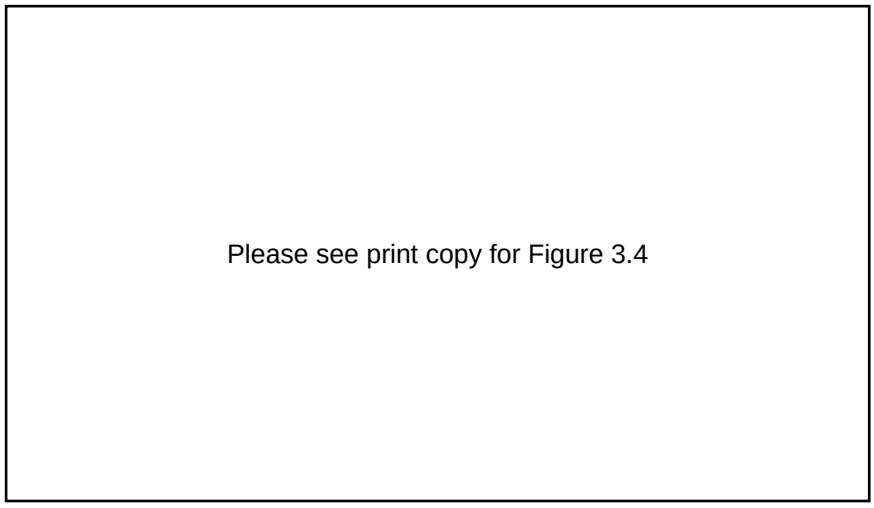

Figure 3.4: Basic experimental arrangement of the OSL system with stimulation light source, photomultiplier detector and readout electronics (from Bøtter-Jensen, 2000).

Measurements are processed on aliquots composed of grains of a given size range and mineral composition. Comparison of the intensity of the natural signal with artificial signals generated in the laboratory, after exposure to calibrated radioactive sources (usually $^{90}Sr/^{90}Y$ β source, ^{60}Co or ^{137}Cs γ source), allows the determination of the D_E. The D_E is the laboratory β or γ dose required to provoke the same luminescence signal as the past

environmental dose. The D_E is expressed in Gy and is always presented with a standard error (*se*). This final *se* corresponds to a combination of the *se* associated with the measurement of each aliquot's D_E, and the *se* associated with the inter-aliquot variation in D_E that is related to the inherent natural variability between aliquots that have received identical doses (see, for example, Galbraith et al., 2005). The sample *se* is commonly higher than five percent of the D_E.

There are two predominant techniques used to estimate D_E:

- An Additive procedure (e.g. MAA: Multi-Aliquots Additive-dose), in which different doses are added to several aliquots before measuring the resulting OSL signals. These are plotted as a growth-curve of luminescence versus dose (Figure 3.5). The D_E is then estimated by extrapolation back to the dose axis.

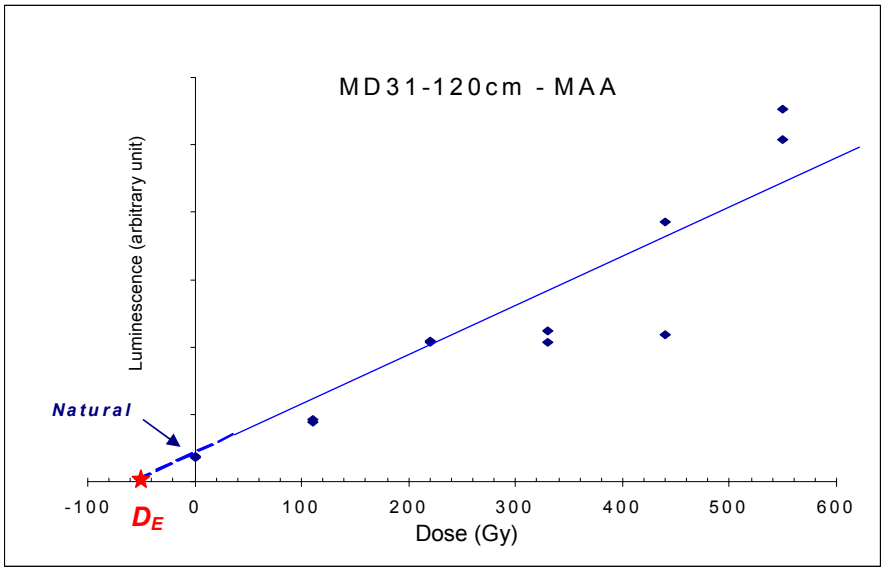

Figure 3.5: Typical additive procedure growth-curve and D_E extrapolation for a quartz sample from the Gulf of Carpentaria. Natural represents the original luminescence signal of the sample.

➢ A Regenerative procedure (e.g. SAR: Single-Aliquot Regenerative-dose) in which the total OSL signal is measured several times on the same aliquot after being regenerated using different doses. The sample is thus bleached prior to any laboratory dose. In this case, the growth curve permits an interpolation of the D_E (Figure 3.6). Because the samples were already exposed to bleaching/dose exposure cycles in the natural environment, the laboratory process only repeats this natural process and should not deteriorate the luminescence properties. However, regeneration commonly leads to sensitivity changes, and the SAR procedure is only successful if the sensitivity changes can be monitored and corrected for.

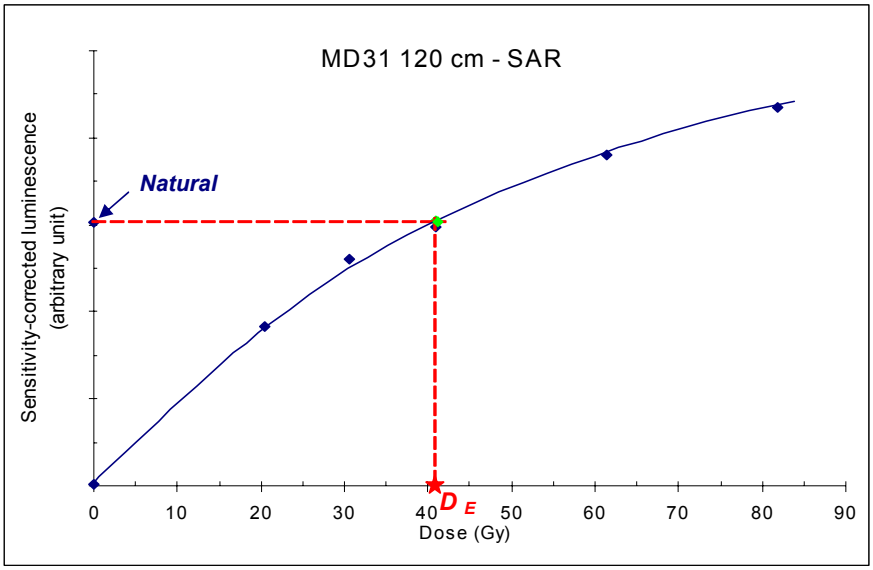

Figure 3.6: Typical regenerative procedure growth curve and D_E interpolation for a quartz sample from the Gulf of Carpentaria. Natural represents the original luminescence signal of the sample. Green diamond represents the last measurement, which corresponds to a repeated measurement.

It is possible to estimate the annual radiation dose or Dose Rate (D_R) from in situ measurements or calculations (Section 3.10). From this, the time elapsed since the sample was last exposed to daylight may be obtained by dividing the total amount of radiation the grains have absorbed by the D_R (Age = D_E/D_R).

3.4 Applications and requirements of the OSL dating technique

3.4.1 Applications

Luminescence dating methods (OSL and TL) are applicable not only over an age range from a few decades to several hundred thousand years, but also to a variety of minerals and litho-stratigraphic settings (Aitken, 1994, 1998; Berger, 1995). Furthermore, due to its optical non-destructive nature (compared to the heating cycle required for TL), OSL has several potential advantages over TL such as higher sensitivity, the possibility of repeated readouts whereas TL measurements involves total erasure of the signal, and focused beam stimulation of small samples which is not feasible with heating treatments (Bøtter-Jensen, 2000).

Terrestrial sediments such as loess and beach deposits, sand dunes and other sediments with a subaerial mode of deposition are highly suitable for OSL dating. The optical signal in subaerially deposited sediment is rapidly bleached by natural light, whereas underwater sediment will be bleached, although a longer period of exposure is required. The two most important minerals used for OSL dating are quartz and feldspar, but polymineral fine-grained sediments (Ditlefsen and Huntley, 1994; Lang, 1995, 1996), flint (Poolton et al., 1995), ceramics and fired clay (Krbetschek et al., 1996; Rieser et al., 1997), zircon (Godfrey-Smith et al., 1989) and volcanic glass have also been promisingly investigated (Berger and Huntley, 1994).

3.4.2 Requirements

Because of its nature, OSL dating requires some essential criteria to be met:

- Stability over time of the OSL signal

Since OSL is normally measured at or near room temperature, the common problem in TL of thermal quenching, in which the luminescence efficiency is decreased as the

temperature is increased, is avoided (Bøtter-Jensen, 2000). However, Rhodes (1990) observed a large increase of OSL beginning at 200°C on archaeological (fired) quartz, that he credited to charge transfer to deeper traps. Wintle and Murray (1997) made similar observations on unheated quartz using preheat temperatures up to 300°C to assess the impact of charge transfer, or sensitivity changes, due to heating. They suggested the OSL signal was stable over time, since 99% of the initial OSL signal measured using a broad-band blue/green-light stimulation source was derived from a single trap with a predicted lifetime at 20°C of about 850 Ma (Wintle and Murray, 1998). Later they concluded instead that the observed increase could be better explained by changes in luminescence recombination probability resulting from the preheating (Murray and Wintle, 1999; Wintle and Murray, 1999). The OSL signal stability is effective only after removing the unstable component of the signal with an adequate preheat treatment (Rhodes, 1988, 1990; Murray and Wintle, 1999).

- Minerals should not be saturated

When all electron traps are full, the mineral is not able to accumulate the ambient ionising radiation and the dose within its lattice will only reflect the time of collection up to saturation. To date old sediment (e.g. > 150 ka, Prescott and Robertson, 1997), the mineral's saturation needs to be tested. An easy test when measuring the OSL from an old sample is to give the sample a higher dose than that required to obtain the same luminescence from the natural signal, and to check if the resulting signal is greater. The observation of the shape of the growth curve drawn after a basic SAR analysis (Single Aliquot Regenerative-dose analysis defined in Section 3.7.2) also provides information regarding the sample saturation.

- Minerals should not be exposed to artificial radiation

If minerals are exposed to an artificial ionising radiation in the natural environment (e.g., gamma-ray scanning of cores for density determinations), their natural luminescence signal could be affected and the D_E will then be overestimated. Unless this additional exposure can be precisely estimated, such samples should not be used.

- High-quality bleaching (or knowledge of the partial bleaching risk)

Even if just a few seconds of daylight are needed to bleach most of the OSL signal (Figure 3.7) (Aitken and Smith, 1988; Godfrey-Smith et al., 1988; Hütt et al., 1988), it has been shown that the bleaching efficiency can drop drastically under certain conditions related to weather conditions (Godfrey-Smith et al., 1988; Murray and Olley, 2002),

transportation and flow regime (Stokes et al., 2001), water depth (Rendell et al., 1994) and turbidity (Clarke et al., 1999; Agersnap Larsen et al., 2000; Fuchs and Wagner, 2003), which change the light spectra and intensity that reaches the grains (Figure 3.8).

The use of single-grain analyses can prevent an over-estimation of the OSL signal from poorly bleached samples (Duller, 1996; Murray and Olley, 1999; Roberts et al., 2000). If this facility is not available, analysis of the scattering of all aliquots' results could also provide information about bleaching homogeneity (Duller, 1994a). When using the OSL dating technique on sediment, it is always important to investigate the extent of pre-depositional bleaching of the sample.

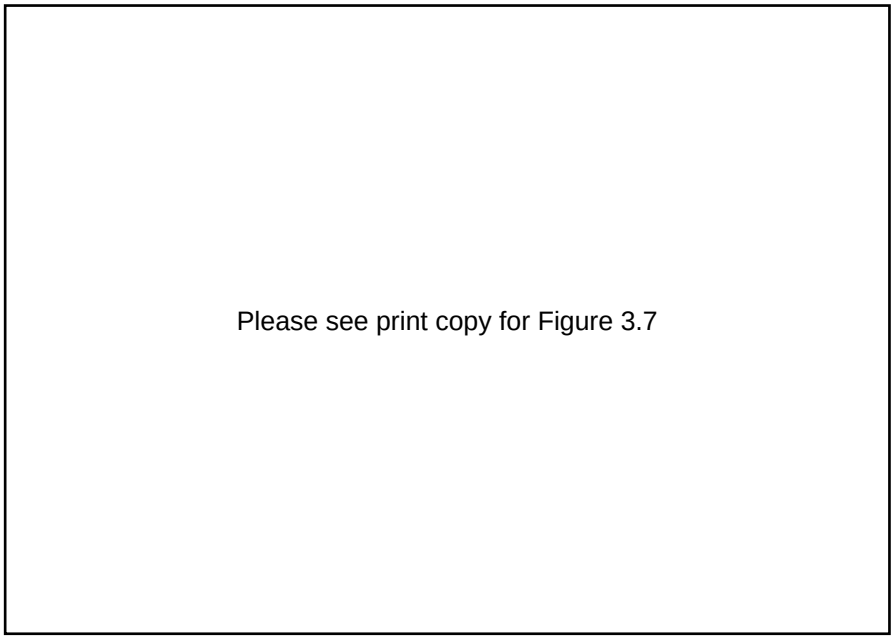

Figure 3.7: OSL and TL bleaching using 514 nm as the exciting wavelength (from Godfrey-Smith et al., 1988).

- Consistency over time of the related D_R

The OSL dating method is a two-step analysis, the D_E measurement being the first step and D_R estimation forming the second. The D_R is a combination of cosmic ray impact, which is related to burial depth, latitude and altitude, and environmental radioactivity,

mainly derived from the beta and gamma decay of lithogenic radionuclides (from ^{40}K, ^{232}Th, ^{235}U and ^{238}U decay chains) (Prescott and Hutton, 1994; Olley et al., 1996, 1997; Nathan et al., 2003). Moisture is of great importance for both the cosmic-ray contribution and the gamma and beta components of the D_R for sand-sized quartz grains.

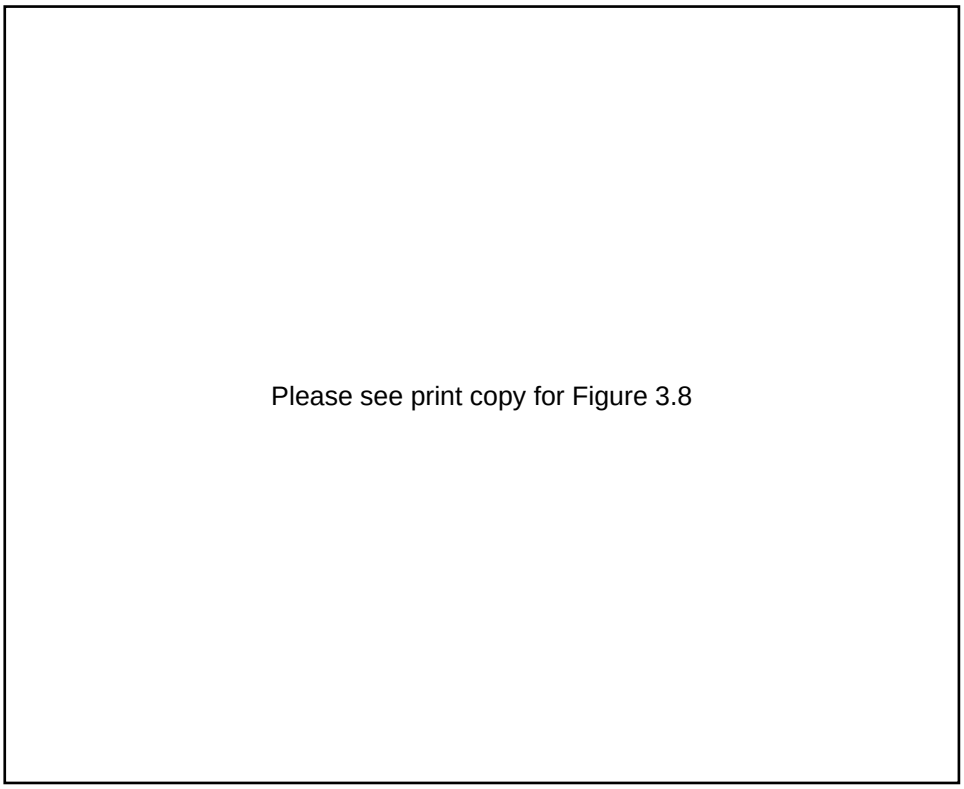

Figure 3.8: Example of a drastic change of the natural solar spectrum (orange) through 4 m of turbid water (blue), which can delay or obviate the sediment bleaching (from Berger and Luternauer, 1987).

At the time of collection, the sample's burial depth is known and it is important to be able to estimate the sample's burial history to calculate the cosmic ray impact. The water content also needs to be evaluated, and is commonly assumed to be similar to the modern moisture content. The environmental radioactivity is not necessarily constant in space or time, and thus should be measured for each sample. Where the environment is more likely to have changed significantly over time, it is also necessary to assess the

possible variation in the concentration of the main radioisotopes responsible for natural radioactivity. However, Olley et al. (1996) demonstrated that the disequilibrium in the ^{238}U decay chain observed in some sediment could have a minor impact (less than 3 percent) on the D_R value, less than or similar to the other uncertainties involved in the age calculation. But the importance of the disequilibrium in the ^{238}U decay chain on the environmental D_R can be significant in some environments (Aitken, 1985a).

3.5 Luminescence of Quartz

3.5.1 Quartz luminescence properties

Quartz is a “well-behaved” mineral and has been used in TL and OSL dating since the early stages (Huntley et al., 1985; Aitken, 1985b). Due to its robust physical and chemical characteristics, alteration processes do not easily affect quartz, and it is thus a ubiquitous mineral that has been concentrated over time. Godfrey-Smith et al. (1988) recognised that the optical signal in quartz is far more sensitive to light than the TL of quartz. The presence of electron traps that are extremely sensitive to sunlight give a large optical signal but make a negligible contribution to the TL. The authors also demonstrated that modern quartz does not possess any natural luminescence regardless of the wavelength of the incident light, and that the shape of the quartz luminescence versus dose curve changed as the photon energy of the incident beam was increased.

It has been shown that the quartz OSL signal arises from charges related to the 325°C TL peak (Smith et al., 1986; Spooner, 1994; Wintle and Murray, 1997; Bøtter-Jensen, 2000) and that there is an exponential relationship between OSL and the energy of the stimulation light (Bøtter-Jensen et al., 1994; Spooner, 1994). An excitation of 16 m W cm^{-2} is enough to bleach the OSL signal of quartz, with the half-value reached after 1.6 seconds (Bøtter-Jensen, 2000).

3.5.2 Quartz luminescence signal

These properties of omnipresence, preservation and luminescence define quartz as being a suitable mineral for OSL dating. The quartz luminescence signal is centred on 365 nm at room temperature (Huntley et al., 1991). In the present study, the wavelengths of incident (420–550 nm and 470 ± 30 nm) and emitted light (365 nm) were sufficiently different to be discriminated between using filters (Figure 3.9), and the wavelength band was narrow enough, in accordance with Rees-Jones et al. (1997). Furthermore, using the U-340 detection filter does not increase the photomultiplier background count rate on a blank sample disc at full light power (Bøtter-Jensen et al., 2003).

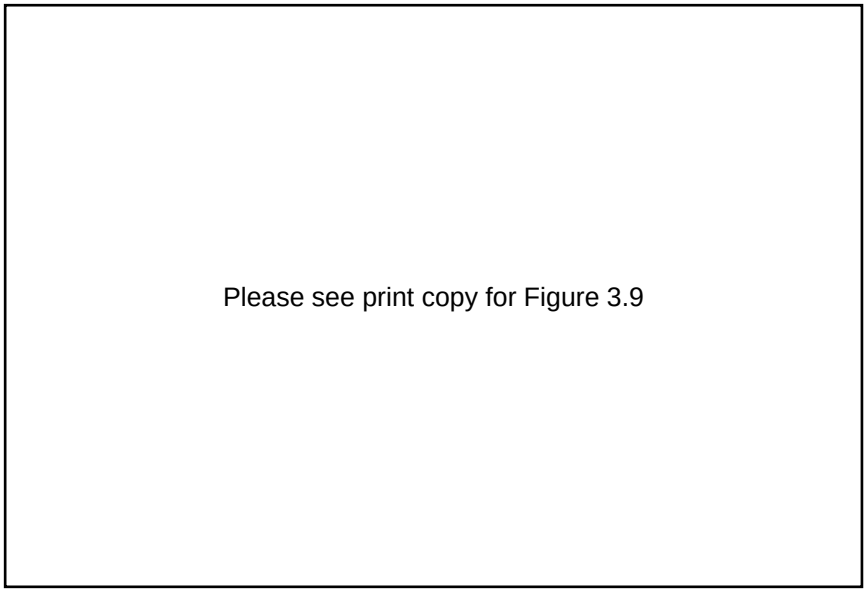

Figure 3.9: The observed stimulation (blue) and detection characteristics of the broadband blue/green OSL attachment. The dotted line (red) represents the published characteristic of the U-340 filter (from Bøtter-Jensen et al., 1999).

Quartz OSL is insensitive to near infrared (IR) at room temperature (Aitken, 1990; Bøtter-Jensen et al., 1994; Bøtter-Jensen, 1997). Dim red illumination was thus used in the laboratory for sample preparation. In addition, feldspar could be excited using IR or visible light. This difference in stimulation characteristics allows the use of IR to test the purity of quartz samples (Spooner and Questiaux, 1990; Bøtter-Jensen and Duller, 1992; Bøtter-Jensen et al., 2000).

3.5.3 Luminescence measurement

By studying the shape of the OSL decay curve of quartz in relation to stimulation temperature, Murray and Wintle (1998) deduced that a single trap must be responsible for the majority of the OSL signal measured at temperatures of between 150°C and 275°C. They recognised that shallow traps, especially those giving rise to the 110°C TL peak, do play a role in charge cycling, and thus the OSL measurement routine should be

performed at 125°C to keep the 110°C TL trap empty and to improve measurement sensitivity (Murray and Wintle, 2000b).

3.5.4 *Preheat treatment*

A limitation of quartz luminescence is that some of the quartz light-sensitive traps are thermally unstable (Li and Wintle, 1992). To circumvent this inconvenience, a preheat plateau test for OSL, in which an equivalent-dose experiment is repeated with different preheat temperatures (usually ranging from 160°C to 300°C) (Figure 3.10), allows determination of the necessary temperature to empty these thermally unstable traps that are populated by laboratory irradiations (Huntley et al., 1985; Aitken, 1992; Berger, 1995).

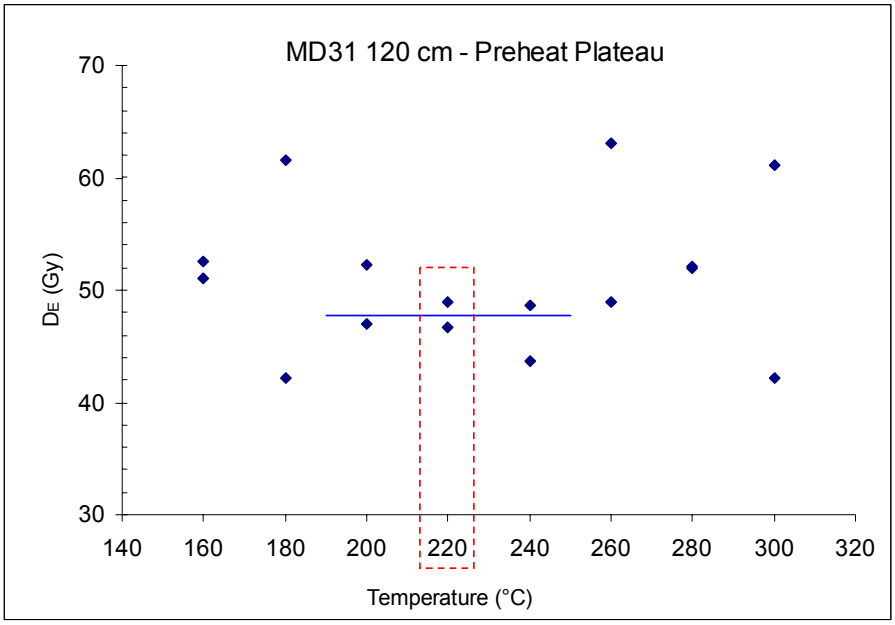

Figure 3.10: Typical preheat plateau test for a quartz sample from the Gulf of Carpentaria. The red box corresponds to the selected preheat temperature for this particular sample.

The choice of the preheat temperature is critical to not induce a sensitivity change in the OSL signal (Rhodes, 1990; Jungner and Bøtter-Jensen, 1994; Roberts et al., 1994; Wilkinson, 1997; Wintle and Murray, 1998; Vartanian et al., 2000; Roberts and Wintle,

2001). As the optimal preheat temperature is different for every quartz grain, the plateau test has thus to be processed for each different sample (Godfrey-Smith et al., 1988; Vartanian et al., 2000).

3.5.5 Establishing single aliquot protocols for quartz

Duller (1991) was the first to propose a single aliquot (SA) method. The main benefits of this method are smaller sample size requirements, improved precision (as there is no need for inter-aliquot normalisation) and improved accuracy (as the existence of contaminant grains is revealed by the inter-aliquot spread in D_E). The amount of labour involved in D_E determination is also drastically reduced. The principle is to make multiple luminescence measurements on one small aliquot instead of one measurement on multiple aliquots. Reviewing this SA protocol for feldspar, proposed by Duller (1991) and revised by Galloway (1996), Murray et al. (1997) proposed a Single-Aliquot Additive-Dose protocol (SA-AD) for quartz. This protocol included:

1) A 10 second (s) preheat between stimulations,
2) Measurement of the natural initial (first 0.1 s) OSL signal,
3) Several cycles of adding dose/preheat/initial OSL measurement,
4) And then a preheat/OSL measurement to define the OSL exponential decay rate that is used to correct previously measured OSL signals for variation arising from stimulation and preheating; and
5) The corrected data are plotted on a growth curve, which is extrapolated back to the dose axis to estimate the D_E.

The first attempt to apply the regeneration-based single-aliquot protocol to quartz, was unsuccessful due to sensitivity changes (Stokes, 1994; Mejdahl and Bøtter-Jensen, 1997). Following this, Mejdahl and Bøtter-Jensen (1997) developed a Single-Aliquot/Regenerative and Additive dose (SARA) protocol that required a minimum of two aliquots and took account of the sensitivity changes. This protocol was tested (Duller et al., 1999) and applied to archaeological and geological material (Mejdahl and Bøtter-Jensen, 1997).

Murray and Roberts (1998) tested a Single Aliquot Regenerative-dose (SAR) protocol on a sample of quartz, and showed a parallel between the sensitivity changes of the 110°C TL and the OSL signal peak and they proposed to use this correlation to correct both natural and regenerated OSL signals for the effects of sensitivity changes. The SAR protocol was thus tested (Stokes et al., 2000; Murray and Wintle, 2003) for doses ranging from 0.1 Gy to 100 Gy (Murray and Roberts, 1998) and extensively applied successfully on various material such as loess deposits (Roberts and Wintle, 2001; Stokes et al., 2003a), dunes and beach deposits (Jungner and Bøtter-Jensen, 1994; Folz and Mercier, 1999a, 1999b; Shulmeister et al., 2001; Murray-Wallace et al., 2002; Banerjee et al., 2003; Regnauld et al., 2003), sediments from rock shelters (Smith et al., 1997; Roberts et al., 1998a, 1998b, 1999; Turney et al., 2001), and to sedimentation rate determination (Murray and Olley, 1999).

3.5.6 Instituting a test-dose normalisation

Murray and Wintle (2000b) proposed that a test dose should be included in each normal dose/preheat/OSL cycle. The test dose consists of a small identical dose given to the sample after each Natural or Regenerative dose luminescence measurement, followed by a preheat to 160°C at a 5°C per second rate before a “shine down” at 125°C. The measurement of the test-dose luminescence is then used to monitor sensitivity changes while applying a SAR protocol (Murray and Wintle, 2000b; McKeever et al., 1997). The authors also determined to use the first part of the OSL signal to be sure that only the rapidly bleachable OSL traps are considered. The SAR protocol results in improvement of precision per unit instrument time, without the need for normalisation or correction for low-dose supralinearity, and requirement of smaller sample, as all measurements are made on the same aliquot (Banerjee et al., 2000). Furthermore SAR results can be analysed for the extent of resetting (Olley et al., 1999; Stokes et al., 2001).

3.6 Suitability of the Gulf of Carpentaria sediments for OSL dating

3.6.1 Potential of the Gulf sediments for OSL dating

The shallowness of the Gulf of Carpentaria (never deeper than 100 m) means that sediment minerals should have been bleached just before the time of their deposition and burial, if the process was sufficiently slow. The use of the OSL technique was thus chosen to date the accumulated sediment in the Gulf. Quartz was preferred because of its ubiquitous presence and its higher reliability than feldspar in such an environment (Lamothe et al., 1994; Wallinga et al., 2001). Indeed the Gulf of Carpentaria environment means that the quartz grains present in the sediment were likely bleached soon before deposition, and thus the dated event is representative of the true time of deposition. These quartz grains are characterised by their size, colour and lustre, texture and shape that inform on the mode of transportation and depositional environment. The sorting of the various grain types is also an important indicator of the energy of the system (Reeves, 2004). Major sedimentary parameters for the core levels selected for OSL dating are summarised in Table 3.1.

3.6.2 Similar studies

Agreement among OSL dates and other independent dating techniques, such as ^{14}C, tephrostratigraphy or U-Th disequilibrium, in floodplains (Lang and Nolte, 1999), fluvial and estuarine channels (Wallinga et al., 2001), coastal, shallow marine, fluvial and lacustrine environments (Prasad and Gupta, 1999; Thomas et al., 2003), or deep-sea (Stokes et al., 2003b; Olley et al., 2004a) sediment studies prove the potential for OSL dating in such milieu. For OSL, the clock is reset or zeroed when the sediment is exposed to daylight, thus caution has to be taken about which event is dated (Wintle, 1997; Aitken, 1998). However, incomplete or non-uniform exposure, which is commonplace in many depositional environments, may result in a heterogeneous luminescence signal from different aliquots of the same sample (Olley et al., 1998, 1999; Murray and Olley, 2002).

Changes in the stratigraphy relating to, for instance, breaks in the depositional history, will show up as discontinuities in the apparent radiation dose in the sediment either as a result of different ages or different bleaching histories (Bøtter-Jensen et al., 1995).

Table 3.1: Major sedimentary parameters from Reeves (2004) for OSL dating samples in this study.

OSL samples	>2%>63 µm	Quartz	subangular	subrounded	glassy	frosted	Pyrite	Iron-oxide	Concretions	Gypsum	Organic matter	Microfauna	Comments
													+ present ++ common +++ abundant + reworked + coated quartz
MD31-30		++	+	+	+	+						+	well-preserved marine material
MD31-120		+++	+	+	+				+			+	well preserved non-marine material, essentially fine-grained with concretions, broken shell material and abundant quartz
MD31-530		+++	+	+		+		+					periodic input of quartz-rich material
MD31-1040		++		+	+	+	+					+++	fine dark grey clays with scattered shell material
MD31-1340		++	+		+				+		+	+	very dark grey, sticky with abundant well-sorted and rounded quartz and calcareous concretions
MD32-38	+	+	+		+		++		+			+++	fine grained, pale greenish-grey, bioclastic ooze
MD32-629		+++	+	+	+			+	+++		+	+	dark grey silty clays with orange mottling, fine-grained, pinkish concretions, and quartz grains commonly yellow-stained
MD32-921		+	+	+	+	+	+++				+++	+++	shell layer with many broken shell and fish fragments black and shiny corresponding to organic-rich, anoxic substrate
MD32-1397	+	+++	+	+	+	+		+++	+				greenish-grey silty-clay and fine sand yellow stained containing well sorted abundant quartz, some coated, and other minor rock fragments including pumice, periodic increase in coarser material
MD32-1482	+	+++	+	+	+	+		+++					
MD33-220	+	++	+	+	+	+	+	+	+			+	shell layer
MD33-360	+	+++	+	+	+	+		+				++	Iron oxide on both the fine fraction and coating quartz grains
MD33-629	+	+++	+	+	+	+			+	+			grey with some iron oxide stained quartz grains, gypsum and large concretions

3.6.3 Cesium-137 exposure (Appendix 3)

After collection on-board the research vessel *Marion Dufresne*, the marine sediment cores used in this study were processed using a Multi-Sensor-Core-Logger (MSCL). Via this system, the density of the sediment cores is estimated using the γ-ray attenuation of a ^{137}Cs source. It is thus important to evaluate if this ^{137}Cs exposure increased the existing luminescence signal in the quartz grains within the cores. Such estimation will allow determination of the validity of OSL dating to be applied to sediments from cores treated in such a way. Because of its importance this question has been addressed in a separate paper (Couapel and Bowles, in press; Appendix 3) and it is concluded that the ^{137}Cs exposure from such γ-ray attenuation densitometry has a negligible impact on the luminescence signal of quartz grains in sediment cores. This result thus permits the OSL dating technique to be applied to the marine cores collected from the Gulf of Carpentaria and processed by MSCL.

3.7 Sample processing

This section presents each of the preparation steps in the OSL process, from the sediment sample to the aliquot discs. Thirteen depth-levels from MD31, MD32 and MD33 were selected and sampled for OSL dating (Chapter 2, Section 2.4 for details). One level was duplicated using two different sampling techniques and another sample from a previous study (Chivas et al., 2001) was also re-analysed. Altogether 15 samples wrapped in several layers of thick black plastic were brought to the OSL laboratory to process further.

3.7.1 Laboratory conditions

The OSL laboratory is equipped with filtered red light that has previously been tested (Debabrata Banerjee, personal communication, 2000) and does not affect the quartz OSL signal. Firstly, the bench was thoroughly cleaned to remove any grains from other samples and a new A3 paper sheet was spread over the working area. Plastic beakers (polyurethane or polypropylene) were utilised, avoiding glass which would not resist hydrofluoric acid etching. A small and a large beaker were rinsed with tap water and labelled with a sticker big enough to write further information. A plastic bag used to hold sediment for the D_R measurement was also labelled.

3.7.2 Physical preparation, sieving

The outermost 3 mm of the sediment was removed to avoid contamination with light-exposed material. A sieve-stack was prepared using at least the 63 µm, 90 µm, 106 µm, 125 µm and 150 µm sieves, depending on how coarse the material was. Each sieve's cleanliness was verified out of the dark room and rinsed with tap water. Samples were chosen from the part of the sediment that had not been exposed to sunlight, and a further 4 mm (at least) of sediment that was kept for D_R measurement, was removed on each side of the sample to avoid all possibility of exposure to light. Samples were then sieved using tap water after being broken up with a spatula on the paper sheet on the bench or using a clean mortar and pestle. The mortar and pestle are made of agate to avoid possible radiation contamination that occurs with porcelain.

3.7.3 Choice of the fraction

When the sieving was finished, the largest fraction, or a combination of two fractions in the case of small sample sizes, was transferred to the smaller beaker, using a wash-bottle filled with distilled water. The size of the fraction was then written on the sticker and all other fractions were transferred to the large beaker. Most of the water used to transfer the sieved sediment in the beaker was gently discarded into a sink after a short decantation time to allow the grains to settle at the bottom of the beakers. These two beakers were then kept in an oven to dry overnight at a temperature not exceeding 50°C. When dried, the selected fraction (usually 90–150 µm) was then ready to be loaded onto the discs. The remaining fractions were kept in vials in case further experimentation was needed.

3.7.4 Purification and etching

All the following steps were done in a fume hood, under red light. The selected fraction was purified with 8% HCl to remove carbonates and 35% H_2O_2 to eliminate organic matter. This fraction was then etched in 40% HF for 45 minutes to dissolve feldspars (Prasad, 2000), providing a quartz-rich extract and etching the surfaces of the quartz grains, to remove the α-irradiated layer. Hydrofluoric acid etching was processed on a magnetic stirrer plate to enable a more homogeneous reaction and to minimise the preferential erosion along cleavage planes (Bell and Zimmerman, 1978; Wintle, 1997). Then a brief rinse with 8% HCl was used to stop the HF reaction and remove the acid-soluble fluorides. No heavy mineral separation was undertaken as no dark-coloured grains were noticed in the samples (Huntley et al., 1993; Roberts et al., 1994; Lang et al., 1996).

3.7.5 Disc preparation, cleaning and loading

As with the other material, the discs needed to be perfectly clean. They were soaked, rinsed and dried in the oven before being checked outside the dark room. Stainless steel discs were used to prevent the “spurious” luminescence phenomenon recognised by Godfrey-Smith et al. (1988) when using aluminium discs. Discs were then loaded on a special support tray (Figure 3.11) that allows the use of spray-masks to spray the silicone oil (Silkospray) on which the quartz grain will adhere. Different mask sizes, from 0.5 to 5 mm, were used depending on the analysis to de done. A typical process starts with a

large disc size to have a good representation of the sample luminescence. Then the disc size decreases, since smaller aliquots have to be used to obtain better quality results, particularly when there is some partial bleaching (Olley et al., 1999; Stokes et al., 2001).

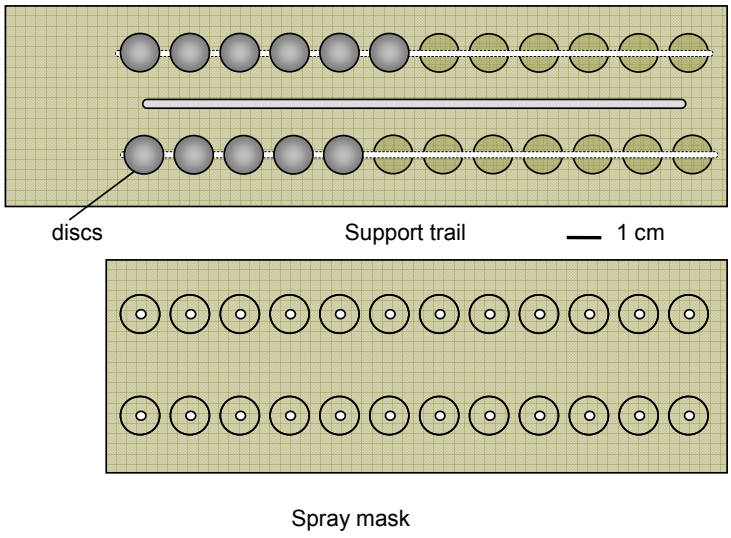

Figure 3.11: Support trail and spray mask.

3.8 Sample analysis

This section presents the apparatus used at the University of Wollongong OSL facilities, a detailed explanation of how the luminescence signal is measured and eventually how the D_E is calculated for a quartz sample.

3.8.1 Risø readers, TL-DA12 & TL-DA15

For the measurement of the OSL signal, two generations of Risø automatic apparatus were used: a TL-DA12 and a TL-DA15 (Figure 3.12). These two devices are similar, however their differences are outlined below. These devices can be used for both TL and OSL measurements (GSL and IRSL, green light and infrared stimulation luminescence, respectively), and constitutes 2 main parts: excitation and detection units.

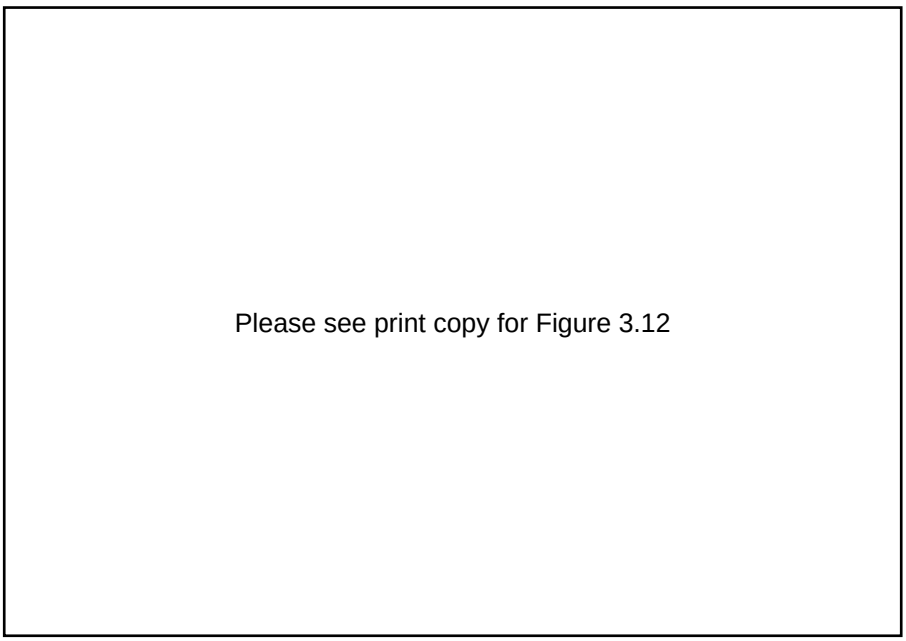

Figure 3.12: Photograph of the TL-DA15 reader showing the carousel (from Bøtter-Jensen, 2000).

- The excitation unit

The excitation unit is where the disc samples are loaded and stimulated. This unit includes heating, lighting as well as ionising radiation devices. The heater plate is used for TL measurement but also to heat the sample for OSL measurement. The TL-DA12 reader illumination device consists of a 75 Watt tungsten halogen lamp filtered to produce a stimulation band from 420 to 550 nm delivering a power of 16 $mW.cm^{-2}$ to the sample whereas the TL-DA15 apparatus includes a blue (λ = 470 ± 30 nm) diode array arranged to focus through GG420 filters and delivers a changeable 18 $mW.cm^{-2}$ onto the sample (Bøtter-Jensen, 2000; Banerjee, 2001). Both pieces of apparatus have a $^{90}Sr/^{90}Y$ β source, which were calibrated using ANUcalib (2.85Gy), ARL20Gy (18.6Gy) and Risø (4.6Gy) samples on 10 October 2001, delivering a dose of 2.452 $Gy.min^{-1}$ for TL-DA12 and 6.420 $Gy.min^{-1}$ for TL-DA15 at that time. TL-DA12 was supplied with a 24-disc carousel, whilst the TL-DA15 has a 48-disc carousel.

- The detection unit

The detection unit consists of a photomultiplier (PM) that counts the emitted photons, which is associated with filters and an amplifier. The counting device consists of a Thorn-EMI 9235QA photomultiplier coupled to one heat-rejecting HA-3 (Pilkington) and 7 mm U-340 (Hoya) detection filters. The TL-DA12 PM tube count rate is 2:1 (two pulses are needed to increment the counter by one) while the PM coupled with TL-DA15 count rate is 1:1. That means that the photo-electrodes will produce, through a photoelectric effect, one electron for each 2 or 1 received (incident) photon(s), respectively. The carousel that carries samples is motorised and a computing system allows the user to define all parameters such as temperature and length of measurement or excitation, the light to be used as well as the extent of the irradiation. Elise Folz demonstrated in her PhD thesis that the leakage of irradiation between two following discs for the TL-DA15 carousel that carries 48 discs is negligible (~0.045%), but that the impact of a long illumination (2000s) induced a 20–30% signal loss on the nearest discs (Folz, 2000).

- The acquisition software

Two generations of software were used. The older one, 'Risø TL-OSL' software for DOS, version 4.65, was only used coupled with TL-DA12 (Olley et al., 1999) and produced '.DAT' files, whereas the second 'Mini-Sys for PC' used on both readers after April 2001, is Windows compatible and generates '.BIN' files (Bøtter-Jensen, 2000).

3.8.2 Sequence

All samples were preheated to remove charge from the shallow unstable traps prior to light stimulation (Huntley et al., 1996; Bøtter-Jensen, 1997, 2000; Wintle and Murray, 1997, 1998). This treatment ensures that the trapped electrons distribution resulting from any laboratory dose is similar to that resulting from the natural dose (Murray and Roberts, 1998). The preheat temperature was chosen after running a preheat test (from 160°C to 300°C) to check which temperature gave the best reproducibility. OSL measurements were processed with continuous stimulation for 100 s at 125°C to remove interaction with the 110°C TL peak (Bøtter-Jensen, 1997; Wintle, 1997). This total OSL signal was recorded on 250 channels and the integration of the first 5 channels (corresponding to the first 2 s) were used as the OSL signal in this study to achieve the smallest statistical uncertainties in the OSL signal. It has been demonstrated that from both physical and statistical viewpoints that it is more appropriate to use the fast component of the signal (Murray and Wintle, 2003), which corresponds to the first second or so of the total OSL signal (Banerjee et al., 2000). The background count rate was estimated using the last 50 channels corresponding to the final 20 s of shine-down.

3.8.3 Protocols

These protocols define systematic procedures already tested; to date quartz samples using the OSL dating technique. Each modus operandi is important to obtain reliable reproducible results. In the following paragraphs, N stands for the estimated Natural luminescence signal after first running the initial sequence.

In this study all OSL measurements, except when applying MAA protocol (Multiple Aliquot Additive-dose protocol defined below), were sensitivity corrected. This means that the OSL signal from either the natural (L_0) or regenerative dose (L_n) was divided by the appropriate test dose (T_0, T_n) OSL signal to obtain sensitivity-corrected natural (N) and regenerative (R_n) signals, respectively ($N = L_0 / T_0$, $R_n = L_n / T_n$). Repeating the first regenerative dose and measurement cycle after the principal regeneration measurements had been completed allowed testing of the reliability of the sensitivity correction. Measurement of the OSL signal without giving any dose after preheating, and of the OSL response from the test dose again to obtain a sensitivity-corrected zero-dose signal, confirmed that the sensitivity-corrected regenerated dose-response curve passed through the origin (Banerjee et al., 2000). While processing a MAA protocol, a Short Shine (SS),

which consists of a 0.1 s illumination and OSL measurements on the natural sample, was given before further analyses to normalise results.

The four typical sequences used in this study (Figures 3.13 and 3.14) and their aims are described individually in the following section and summarised in Table 3.2.

Table 3.2: The several different steps of typical sequences used in this study. N corresponds to the Natural luminescence signal as defined after running the Initial sequence.

Sequence	Natural	Test dose	Doses		Aliquots		Disc size
			type	Value (Gy)	per batch	total	(mm)
INIT	*Yes*	*Yes*	*2 (3) Regeneratives*	N, 5, 25 (125)	*3*	3	5 or 3
PPT	*Yes*	*Yes*	*2 Regeneratives*	N	*2*	16	3 or 1
MAA	*Yes*	*No*	*4 Additives*	N, 2N, 3N, 4N, 5N	*4*	24	3
SAR	*Yes*	*Yes*	*5-7 Regeneratives*	N, N/2, 0.9N, 1.1N, (2N, 0) N	*12-24*	*12-24*	0.5 or 1

- Initial (INIT):

This sequence was usually run on three 3 or 5 mm discs and consists of a measurement of the natural luminescence signal (N), then two or three different regenerative doses are given thereafter, to obtain an idea about the range of N that will be closely bracketed further in the sample processing (Figure 3.13).

- Preheat Plateau Test (PPT):

This sequence usually runs on eight batches of two 1 or 3 mm discs, allowing the determination for each sample of the preheat temperature needed for the best reproducibility of results. This test consists of a natural luminescence measurement followed by two equivalent regenerative doses, which were chosen as close as possible to N estimated after running the Initial sequence (Figure 3.13).

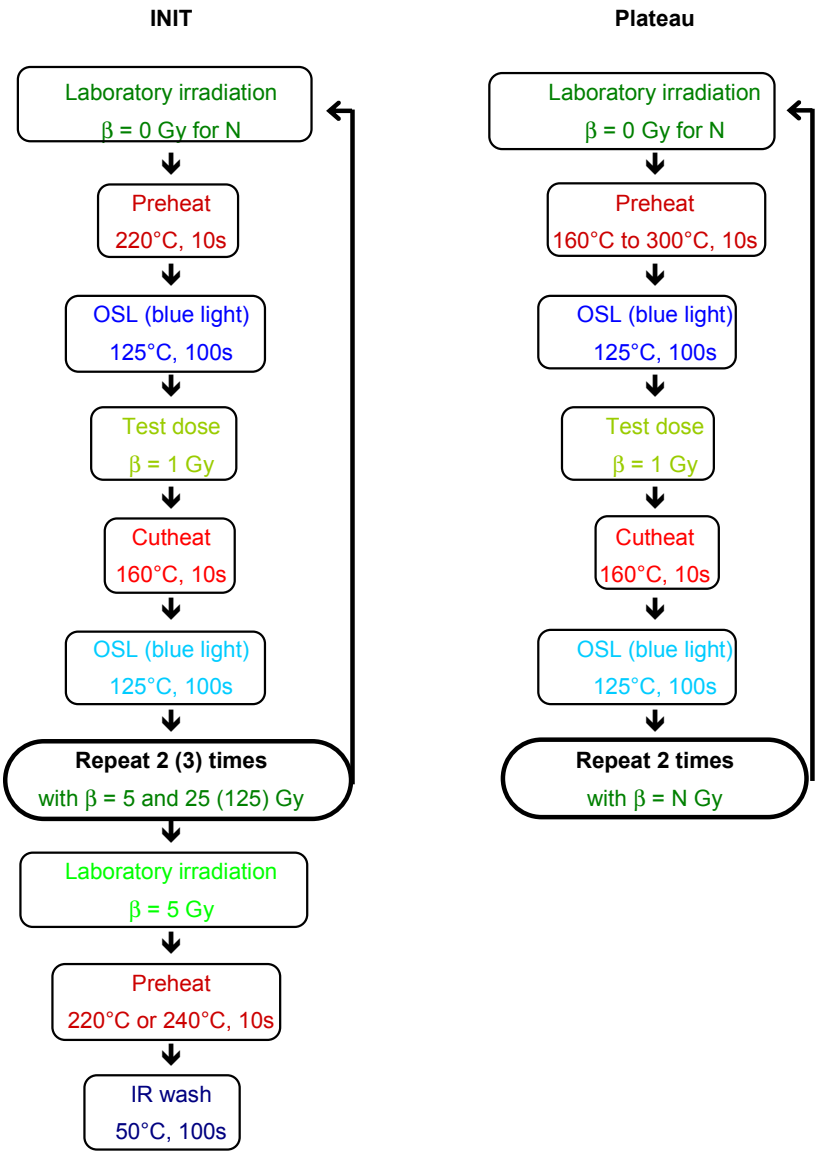

Figure 3.13: INIT and PPT protocols used in this study (N stands for the estimated natural luminescence signal). Laboratory irradiations are in greens, heating phases, in reds and luminescence measurements in blues.

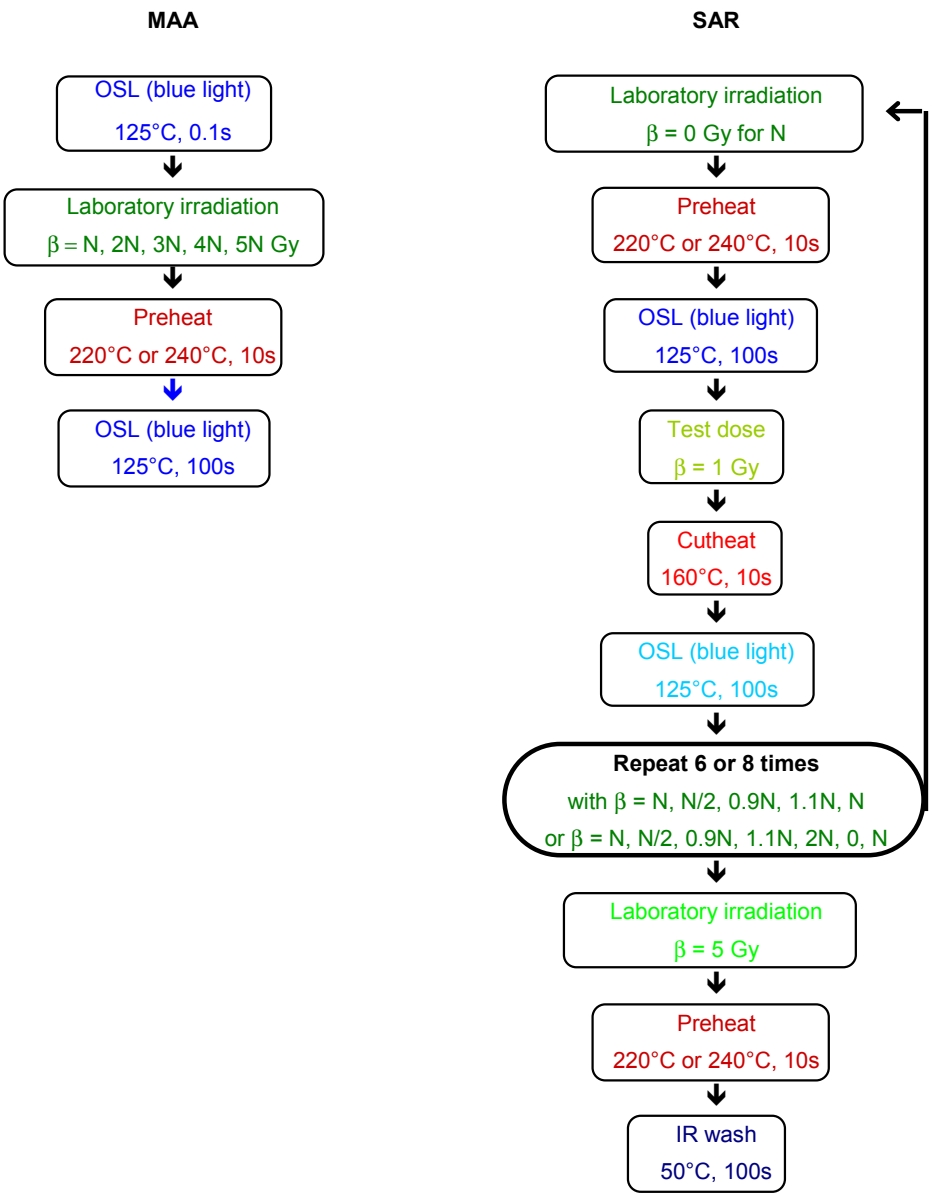

Figure 3.14: MAA and SAR protocols used in this study (N stands for the estimated natural luminescence signal).

- Multiple Aliquot Additive-dose (MAA):

This sequence was usually run on six batches of four 3 mm discs. This sequence consisted of a 0.1s SS, followed by preheating at a temperature defined during the Plateau test. Each batch of aliquots received different doses as a function of N previously estimated: N, 2N, 3N, 4N and 5N prior to OSL measurement (Figure 3.14). Problems were encountered with this protocol, resulting in very scattered growth curves that were hard to interpret. The small amounts of sample available for analysis prevented additional measurements, so none of the MAA results was used to determine the D_E.

- Single Aliquot Regenerative-dose (SAR):

This sequence was usually run on twelve to twenty-four 0.5 or 1 mm discs, as a function of sample availability, and generated the set of data ('.DAT' or '.BIN' depending on the date it was processed and, thus, the program used) that was used to estimate the D_E. This sequence consists of five to seven regenerative dose measurements to bracket the Natural luminescence signal. The choice of the regenerative doses was linked to the previous estimation of N and the succession was: N, N/2, 0.9N, 1.1N, (2N, 0) N. Furthermore an IR check or IR wash to detect any feldspar OSL signal contamination (Wallinga et al., 2002), was applied after giving a final regenerative dose before the OSL measurement (Figure 3.14).

3.8.4 Data processing

The OSL signal may be expressed as the total number of counts or only a defined part of the signal obtained in a fixed time (Wintle, 1997) minus an average 'background' count for each series. In this study, only the first 2 seconds of the OSL signal were integrated as suggested by Banerjee et al. (2000) and Murray and Wintle (2003), and the mean of 10 bins of 2 seconds was used for the background. All calculations were done using the Monte Carlo Fit (MCF) program (Nathan et al., 2003; Yoshida et al., 2003). The relative standard error (*se*) is calculated from variations of photon counts within each series, and curve-fitting certainties. Thus *se* does not reflect the variation in D_E between the aliquots of a sample, such over-dispersion is discussed in Section 3.8.6.

3.8.5 Monte Carlo Fit (MCF)

Depending on the date of the measurement – prior to or after April 2001 – and hence TLDA-12 reader with 'Risø TL-OSL' or 'Mini-Sys for PC' software, data were recorded in '.DAT' or '.BIN' files. To be able to process data in the same way, the '.DAT' files were converted to '.BIN' files, using a conversion program built by Hiro Yoshida (personal communication, 2004). All '.DAT' files were thus transformed to '.BIN' format that is compatible with the MCF. The MCF program consists of a two-step analysis:

1. The MCF program fits a growth curve to the sensitivity-corrected regenerated OSL signals from the '.BIN' file and interpolates the sensitivity-corrected Natural to estimate the equivalent dose (D_E);

2. MCF runs a finite number of simulations, defined by the user, to estimate the *se*. Each iteration was done following the procedure outlined by Yoshida et al. (2003).

The MCF program allows the determination of reliable results with a realistic standard error. In this study, 50 iterations were run for each aliquot. The resulting D_E and *se* data were thus analysed using a Common-Age-Model (COM), a Central-Age-Model (CAM) or a Minimum-Age-Model (MAM) that are defined in Section 3.8.7. The choice of one or the other method was discussed with Richard Roberts, and Hiro Yoshida processed the MAM.

3.8.6 Overdispersion

The *se* obtained after running the MCF program corresponds to photon count variation within aliquots and growth-curve fitting errors, and does not provide information about the variation in D_E between aliquots. This inter-aliquot variation is important to consider the quality and reliability of a sample along with the possibility of partial bleaching. Galbraith et al. (2005) define the 'overdispersion' as the dispersion remaining after photon-counting statistics have been taken into account. This over-dispersion could be explained by a combination of both experimental and natural variations. The latter is intrinsic to the studied quartz and its extent varies from sample to sample (Galbraith et al., 2005). Additional overdispersion could result from partial bleaching or recuperation as shown by Roberts et al. (2000).

3.8.7 Common-Age, Central-Age and Minimum-Age Models

The COM, CAM and MAM models (Galbraith and Laslett, 1993; Galbraith et al., 1999) determine and can take into account the over-dispersion when estimating the mean and minimum D_E and their precisions (Galbraith et al., 2005). The dose dispersion (σ) corresponds to the relative standard deviation of aliquot doses after having allowed for statistical estimation error (Roberts et al., 2000).

The COM is a weighted mean that is only applicable to a population consistent with a common value. This implies that all aliquots (or grains in the case of Single Grain analyses) in the population have absorbed similar radiation doses, have been evenly bleached before deposition, and have the same burial history.

The CAM approximates the geometric mean of the true D_E, independent of the measurement errors. The CAM is appropriate for a single-dose population of aliquots (or grains) with similar bleaching and burial histories, but allows for situations in which the measurement uncertainties do not account for the observed spread in values. A normal natural dispersion is usually less than twenty percent (Galbraith et al., 2005; Olley et al., 2004a). The CAM mathematically reduces to the COM when the overdispersion is zero.

The MAM presumes the existence of multiple-dose populations whereby the population with the lowest D_E value potentially corresponds to the most fully bleached aliquots. This model, used when the natural over-dispersion is higher than about 20%, corresponds to samples composed of multiple D_E populations, but it should be borne in mind that the population of aliquots/grains with the smallest D_E need not necessarily be the population of interest; for example, the MAM may pick out intrusive, younger grains that have infiltrated the host deposit after burial.

For each sample, the D_E was first calculated using the COM, then the CAM and when the dose dispersion was greater than 20 percent, the D_E was recalculated using the MAM.

3.9 Equivalent Dose, D_E

3.9.1 Definition and validity criteria

The D_E corresponds to the laboratory irradiation necessary to produce the same luminescence signal as the natural dose. The D_E is expressed in grays (Gy) with a standard error (*se*). Depending on the availability of sediment, and analytical performance, each measurement was made on 15 to 92 discs for each sample over the 3 typical sequences, INIT, PPT and SAR (Section 3.7.3).

Even if all measurements are important, only the SAR results are used for the D_E calculation because these were processed using adequate regenerative doses, at the right preheat temperature and on smaller-sized discs. Indeed, there was a clear overestimation of the D_E using the 3 mm discs compared to the 1 mm discs, and the latter estimates are also commonly greater than those obtained using the 0.5 mm discs; these findings are consistent with the observations of Galbraith et al. (2005). The number and size of discs utilised to calculate the D_E for each sample are listed in Table 3.3, and all first-fit curves of these selected discs are plotted in Appendix 4. Whenever possible (i.e., when enough discs were available), the D_E values were calculated using the 0.5 mm discs only.

The CAM mean D_E estimations for the archive-half and working-half samples of MD33-629 are similar, as shown in Table 3.3; they are also similar to the CAM mean D_E calculated on the population formed by both sub-samples of MD33-629. Thus the D_E assumed for this level is estimated using all aliquots (combination) of MD33-629 (Table 3.3).

This consistency between the D_E estimates for the level sampled in two different ways validates the use of sediment sampled from the segmented core. This is probably due to the muddy nature of the dense sediments from the Gulf of Carpentaria. The enclosing mud forms a compact lightproof cover that prevents the quartz from being bleached. However, caution concerning light contamination must be applied when sampling already-

segmented cores and, where possible, it is preferable to gather samples for OSL dating from larger blocks of sediment.

Table 3.3: Summary table showing the number of discs (total processed per sample in dark red text and available for final D_E estimation in red text) measured to calculate the D_E, the model (CAM in green, COM in orange and MAM in blue) used for this calculation, and their D_E and *se* values. Sample labels correspond to the short core number and the depth in the core in cm, separated with a hyphen. For example the sample at 921 cm depth in core MD972132 is labelled MD32-921. MD33-629 was sampled in duplicate. The sample from the archive-half is labelled MD33-629a, the sample from the segmented working-half MD33-629s, and the combination as MD33-629. No CAM values were estimated for MD31-1340 and MD32-38 because these populations are not overdispersed and are, thus, consistent with a common (COM) D_E value. Bold D_E values correspond to selected values for age determination.

	Discs		Number of discs for D_E calculation			Over-dispersion (%)	Model	mean D_E (Gy)	*Se* (Gy)
	total	SAR	used	0.5 mm	1 mm				
MD31-30	45	41	16	16	3	16.2	**CAM**	**4.46**	**0.25**
MD31-120	92	66	14	14	9	13.2	**CAM**	**42.7**	**2.1**
MD31-530	44	18	5	-	5	12.1	**CAM**	**171**	**11**
MD31-902	15	2	0	-	0	-	-	-	-
MD31-1040	27	27	6	-	6	8.9	**CAM**	**210**	**18**
MD31-1340	16	9	4	-	4	0	**COM**	**229**	**10**
MD32-38	56	50	6	-	6	0	**COM**	**5.49**	**0.60**
MD32-629	54	50	9	9	13	10.4	**CAM**	**233**	**12**
MD32-921	30	26	10	-	10	16.5	**CAM**	**284**	**16**
MD32-1397	41	34	18	-	18	40.4	CAM	194	19
							MAM	**126**	**4**
MD32-1482	24	17	8	-	8	28.7	CAM	176	19
			4		4	16.4	**CAM**	**233**	**24**
MD33-220	76	74	19	19	17	18.4	**CAM**	**83.7**	**3.9**
MD33-360	30	28	14	-	14	11.1	**CAM**	**194**	**6**
MD33-629a	22	20	4	-	4	6.0	**CAM**	**170**	**8**
MD33-629s	10	10	3	-	3	11.1	**CAM**	**160**	**14**
MD33-629	32	30	7	-	7	7.3	**CAM**	**168**	**7**

For quality and precision purposes, a drastic sorting of the data was undertaken. A disc result was not accepted if:

- The *se* on the D_E was greater than 30% (Feathers, 2003);

- The recycling ratio, that reflects the difference between the luminescence signal generated by identical regenerative doses given to the sample at the beginning and end of the measuring process (Murray and Wintle, 2000b), differs from unity at the 2 σ level (Richard Roberts, personal communication, 2004);

- The difference between the test dose OSL signal following the Natural and the last regenerative luminescence measurements was greater than 20% (Feathers, 2003).

These criteria substantially decrease the number of discs used to calculate the final D_E and age (Table 3.3), but it is considered that all discs accepted (red text in Table 3.3) are fully reliable. No disc from sample MD31-902 met all these criteria, thus no D_E or age has been estimated for this sample.

3.9.2 Results

For each core, the disc results used to calculate the D_E are plotted on a Radial Plot diagram (Galbraith, 1988, 1990) which allows a straightforward visualisation of data with *se* (Figures 3.15, 3.16 and 3.17). For an easier visualisation, the Radial Plots are centred on the CAM D_E value (Table 3.3) for each sample. The charts were drawn using Radial Plot software Version 1.3, provided by Jon Olley (CSIRO, Canberra).

In the following figures, the measured dose for each disc can be read by tracing a line from the y-axis origin through the point until the line intersects the radial axis (log scale) on the right side. The corresponding standard error for this estimate can be read by extending a vertical line to intersect the x-axis. This axis has two-scales: one plots the relative standard error of the dose estimate (in %) and the other plots the reciprocal standard error ('precision'). Therefore, values with highest precision, and thus smallest relative errors, plot closest to the radial axis on the right of the diagram.

A brief explanation for the choice of the final D_E estimation regarding the overdispersion of D_E values, the laboratory preparation and observations and environmental conditions at the time of deposition is given on the pages opposite the radial plots. The shaded area corresponds to a 2 σ error from the centre value (the CAM D_E value), except for MD31-1340 and MD32-38 where the centre value is the COM, and the red line represents the final COM, CAM or MAM D_E value that is preferred for the age calculation. The triangle symbols represent the 1 mm size samples whereas the round symbols represent the 0.5 mm size samples.

- Core MD972131 (MD31)

MD31-30 has a CAM D_E of 4.46 ± 0.25 Gy (overdispersion of 16.2%), which was calculated on sixteen 0.5 mm discs. The overdispersion being lower than 20%, this CAM value is selected for the age calculation.

MD31-120 has a CAM D_E of 42.7 ± 2.1 Gy (overdispersion of 13.2%), which was calculated on fourteen 0.5 mm discs. The overdispersion being lower than 20%, this CAM value is selected for the age calculation.

MD31-530 has a CAM D_E of 171 ± 11 Gy (overdispersion of 12.1%). which was calculated on five 1 mm discs. The overdispersion being lower than 20%, this CAM value is selected for the age calculation.

MD31-902 did not have any aliquots that met all criteria, thus no D_E was modelled.

MD31-1040 has a CAM D_E of 210 ± 18 Gy (overdispersion of 8.9%). All six 1 mm aliquots processed have a D_E within 2 σ, thus this CAM value is selected for the age calculation.

MD31-1340 has a D_E of 229 ± 10 Gy, which is a common value for all four 1 mm discs. This COM value is thus accepted for the age calculation.

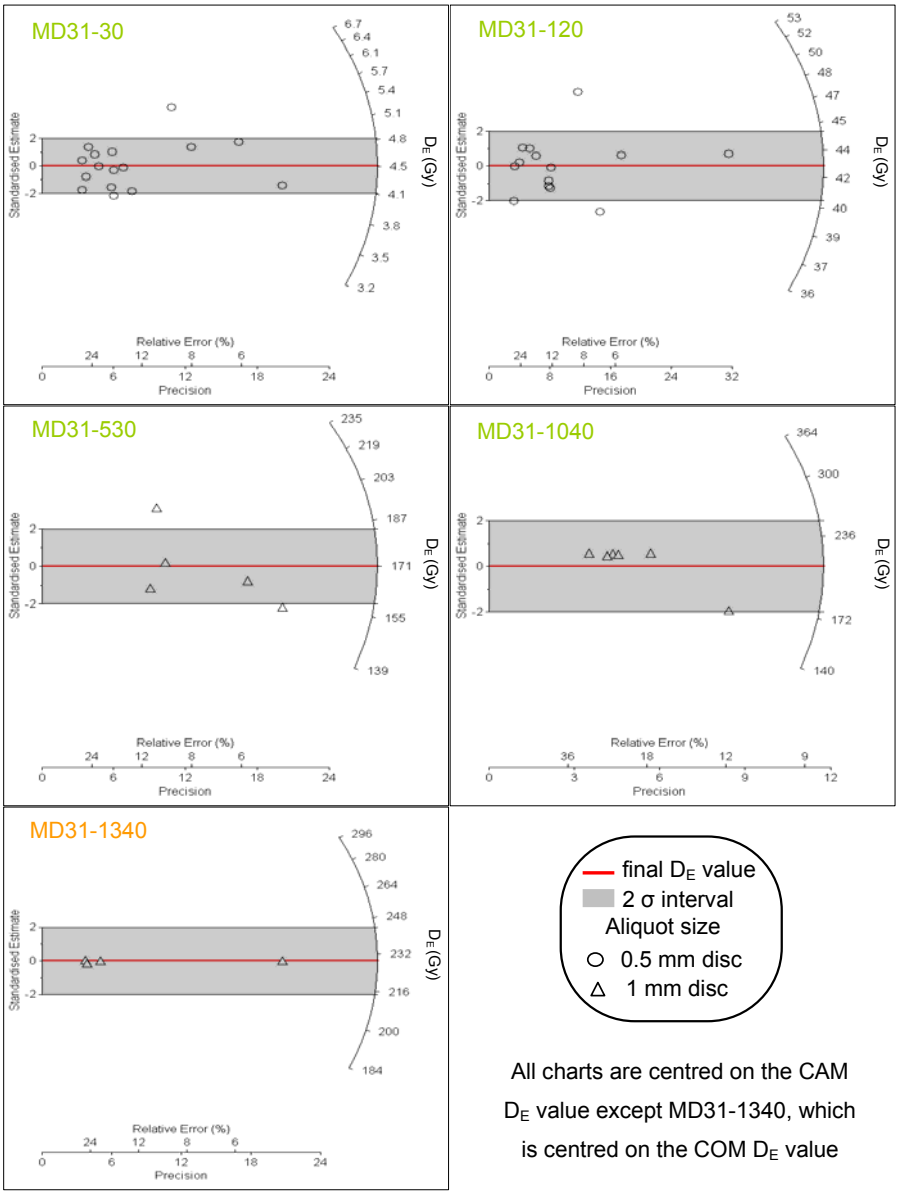

Figure 3.15: Radial Plots for MD31. The colour of the sample label, orange and green, indicates the model, COM and CAM, respectively, used for the final D_E estimation.

- Core MD972132 (MD32)

MD32-38 has a D_E of 5.49 ± 0.60 Gy, which is a common value for all six 1 mm discs. This COM value is thus accepted for the age calculation.

MD32-629 has a CAM D_E of 233 ± 12 Gy (overdispersion of 10.4%), which was calculated on nine 0.5 mm discs. The overdispersion being lower than 20%, this CAM value is selected for the age calculation.

MD32-921 has a CAM D_E of 284 ± 16 Gy (overdispersion of 16.5%), which was calculated on ten 1 mm discs. The overdispersion being lower than 20%, this CAM value is selected for the age calculation.

MD32-1397 has a CAM D_E of 194 ± 19 Gy (overdispersion of 40.4%), which was calculated on eighteen 1 mm discs. This level belongs to a unit that contains some iron-coated quartz (Reeves, 2004, p.83). This coating would clearly impede bleaching, producing a mix of more or less well bleached quartz grains and a large distribution of estimated D_E. The MAM D_E of 126 ± 15 Gy is thus preferred for the age calculation.

MD32-1482 has a CAM D_E of 176 ± 19 Gy (overdispersion of 28.7%) when calculated using eight 1 mm discs. This estimate, however, is considered of questionable accuracy owing to the high overdispersion value, which is probably due to a laboratory artefact. This tiny sample had a rough surface topography, so cleaning was very difficult and it is likely that some light-contaminated grains were also sampled during this process. To obtain an overdispersion value of less than 20% (a value used by Olley et al. (2004a) to distinguish between well-bleached and partially bleached samples), the four aliquots with the lowest D_E values (orange symbols in Figure 3.16) were discarded. For the four remaining aliquots, the CAM D_E was recalculated as 233 ± 24 Gy (overdispersion of 16.4%), which is the value used subsequently for the age calculation.

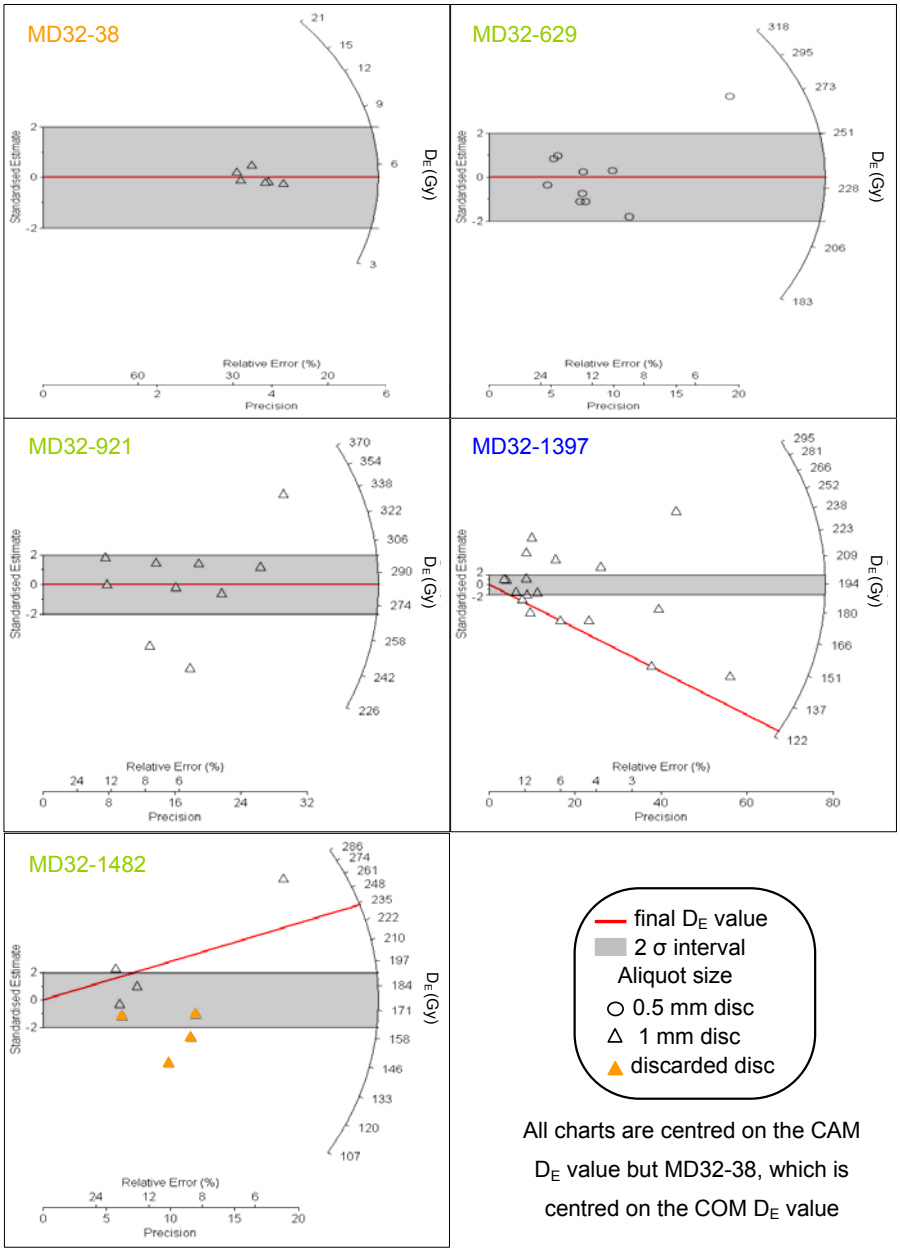

Figure 3.16: Radial Plots for MD32. The colour of the sample label, orange, green, and blue, indicates the model, COM, CAM, and MAM, respectively, used for the final D_E estimation.

- Core MD972133 (MD33)

All quartz samples from this core were noted as greyish (possibly due to iron content) after their physical preparation, with MD33-629 being somewhat paler.

MD33-220 has a CAM D_E of 83.7 ± 3.9 Gy (overdispersion of 18.4%), which was calculated on nineteen 0.5 mm discs. The overdispersion being lower than 20%, this CAM value is selected for the age calculation.

MD33-360 has a CAM D_E of 194 ± 6 Gy (overdispersion of 11.1%), which was calculated on fourteen 1 mm discs. The overdispersion being lower than 20%, this CAM value is selected for the age calculation.

MD33-629 has a CAM D_E of 168 ± 7 Gy (overdispersion of 7.3%), which was calculated on seven 1 mm discs. This sample presents a very low dispersion of D_E results and no distinction between MD33-629a and MD33-629s. All seven aliquots processed have a D_E within 2 σ, thus this CAM value is selected for the age calculation.

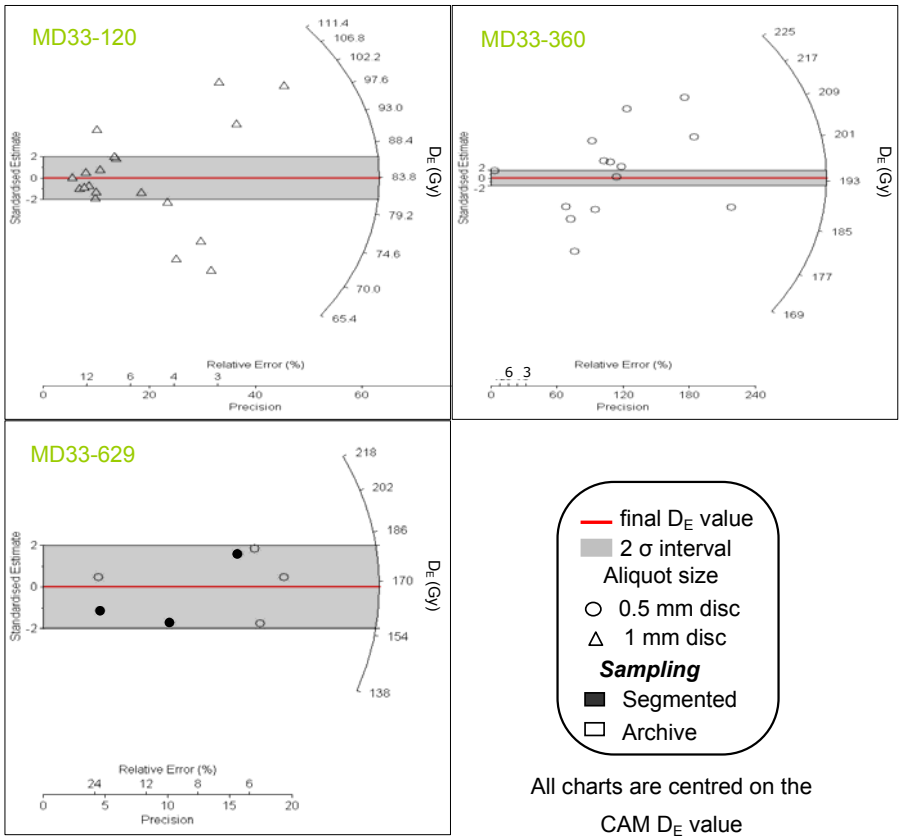

Figure 3.17: Radial Plots for MD33. The colour of the sample label (green) indicates that the CAM model was used for the final D_E estimation.

3.10 Dose Rate, D_R

3.10.1 Definition

The D_R results from the constant bombardment of the Earth by cosmic rays, and from the environmental radioactivity from the decay of naturally occurring radioactive elements, mainly from the Uranium-238, Uranium-235 (^{238}U and ^{235}U, 99.29% and 0.71%, respectively), and Thorium (^{232}Th) decay chains (Figure 3.18), and Potassium (^{40}K) that decays to a stable element (^{40}Ca by γ emission or ^{40}Ar by electron capture) and to a minor (negligible) extent Rubidium (^{87}Rb) (Aitken, 1998; Folz, 2000). The water content is also important in estimating the D_R because of the absorption of energy by water that would otherwise be absorbed in the mineral to produce a higher signal (Wintle, 1981). The D_R contribution of each radionuclide depends on the nature and energy of the ionising radiation produced by the radioactive decay (Nambi and Aitken, 1986; Adamiec and Aitken, 1998).

The D_R, commonly called 'annual dose', is quoted as an average annual dose and expressed in grays per thousand years ($Gy.ka^{-1}$) or milligrays per year ($mGy.a^{-1}$). A correct estimation of the D_R, is essential as a slight variation in the D_R value induces a large error in the age determination ($Age = D_E/D_R$). The D_R is commonly assumed to be constant for the duration of the sample burial.

3.10.2 Internal and external dose rates

For a grain, the D_R has two components: the inner D_{Ri} that is generated by radionuclides within the grain, and the external D_{Re} due to radionuclides in the surroundings and from cosmic rays. The internal dose rate due to the radionuclides present within the mineral is usually considered negligible for quartz, which is the mineral used in this study, compared with typical levels in sediment (Aitken, 1998). However, the D_{Ri} for 100 µm quartz grains using the parameters described in the following paragraphs, and an average content of 0.15 ± 0.03 ppm of uranium and 0.35 ± 0.07 ppm of thorium which is typical for Australian quartz has a value of 0.032 ± 0.011 $Gy.ka^{-1}$(Roberts et al., 1997, 1999; Bowler et al.,

2003). This D_{Ri} will be taken into consideration in the total D_R as it reaches up to 3 percent of the $D_{Re,}$ and it is thus not negligible.

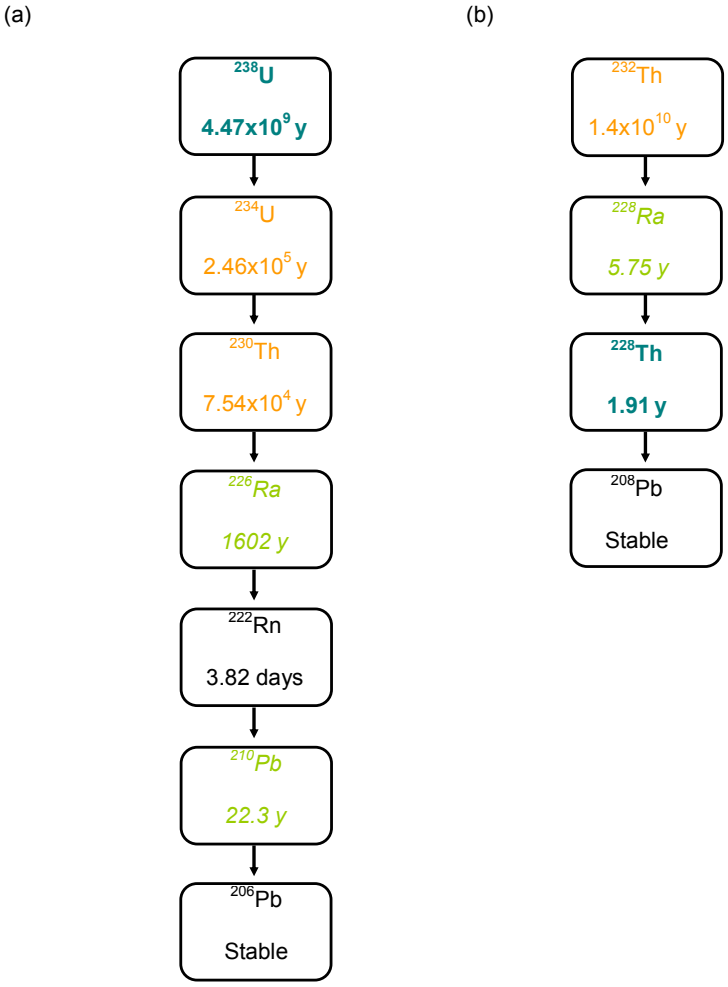

Figure 3.18: Simplified (a) ^{238}U and (b) ^{232}Th decay chains, showing nuclides contributing to the D_R and indicating their half-lives. The nuclides in orange, italic-green and bold-blue were measured through α-spectrometry, γ-spectrometry or both techniques, respectively.

3.10.3 Estimation

The D_{Re} estimation is a three-step process, each related to required parameters such as water content, cosmic ray component and lithogenic radioactivity estimation.

3.10.4 Water content

The sediment water content was measured while sampling the core, but the water content history of the samples is unknown. For the D_{Re} calculation, the modern water content is believed to have prevailed over time, as a first approximation. However, Mejdahl and Christiansen (1994) indicated that an incomplete knowledge of the variation of past water content of the sediment can noticeably change the estimate and uncertainty of D_{Re}.

- Water content estimation

The water content (% of dry sediment, Table 3.4) of each 1 cm-thick segment was assessed just after sampling the cores on a small amount of sediment oven-dried overnight at 60°C (weighed to 3 decimal places) (Chapter 2, Section 2.3.2). The error on the water content estimation is the difference between the water content at the sample depth and the average of the water content for the sample used to measure the D_R (Section 3.10.11) (i.e. 20 cm either side of the sample within the core).

There is clear evidence for pedogenesis (subaerial exposure) in the studied cores (Chivas et al., 2001). During these low sea-level phases the sediment was dry, or at least drier than at the time of collection. Since the water content is critical to the final D_R estimation as discussed in Appendix 5.1, a later correction of the water content (Section 3.11.3) is necessary to take into account these dry episodes.

An overestimation of the water content would lead to an underestimation of the D_{Re} and thus an overestimation of the age of the sample.

➢ Water correction factors

The water absorbs more radiation than air such that in a sediment deposit of 30% porosity held at 80% saturation, the annual dose is typically reduced by ~15 % (Aitken, 1985a; Roberts, 1991). The correction factor, the water content of the sediment and the equation to calculate the moisture correction factor (Readhead, 1987) for each sample for cosmic-ray, β- and γ- dose rates are presented in Table 3.4. All uncertainties are calculated using Gaussian error propagation.

Table 3.4: Water content (% dry weight; blue shading), correction factors (orange shading) and equation (red, from Readhead 1987) to calculate moisture correction factors for each cosmic-ray, β and γ dose rates.

			Moisture correction factor					
			cosmic-ray	*se*	β dose	*se*	γ dose	*se*
	Correction factors (Cf)		1.176		1.14		1.25	
Sample	Water %	*se*	*Readhead equation: 1/(1+(Cf x (W% / 100)))*					
MD31-30	71.6	10.9	0.543	0.041	0.551	0.040	0.528	0.041
MD31-120	22.9	2.8	0.788	0.021	0.793	0.021	0.778	0.022
MD31-530	15.9	1.2	0.728	0.008	0.734	0.007	0.716	0.008
MD31-902	28.0	0.3	0.602	0.001	0.610	0.001	0.588	0.001
MD31-1040	27.3	4.1	0.609	0.018	0.617	0.018	0.595	0.019
MD31-1340	19.3	4.7	0.688	0.027	0.694	0.027	0.675	0.028
MD32-38	55.0	12.3	0.607	0.058	0.615	0.058	0.593	0.059
MD32-629	20.2	0.4	0.678	0.002	0.685	0.002	0.665	0.002
MD32-921	31.2	6.1	0.577	0.025	0.585	0.025	0.562	0.025
MD32-1397	13.3	4.4	0.762	0.031	0.767	0.031	0.750	0.032
MD32-1482	12.1	2.6	0.778	0.019	0.784	0.019	0.768	0.020
MD33-220	21.4	4.2	0.665	0.023	0.672	0.022	0.651	0.023
MD33-360	20.5	1.6	0.675	0.009	0.681	0.009	0.661	0.009
MD33-629	7.0	2.0	0.859	0.018	0.863	0.017	0.851	0.019

The *se* of the moisture correction factor for each component of the D_{Re} is the greater of the two errors found when using the Readhead equation (Table 3.4) for minimum (water % – *se*) and maximum (water % + *se*) water content. The D_{Re} is inversely proportional to the water content of the sediment.

3.10.5 Cosmic-ray dose rate

The D_{Re} caused by cosmic rays (D_{Rc}) is about 0.3 $Gy.ka^{-1}$ at sea level, due to ionisation by electrons and muons, with a small contribution from heavier particles (Prescott and Hutton, 1988). The 'soft' component (mostly electrons) is rapidly absorbed by sediments and almost disappears below 150 $g.cm^{-2}$ of absorber; about 60 cm of standard rock (Figure 3.19). The penetrating muon is thus the primary component of cosmic rays which contributes a small dose to the sample (Aitken, 1985a; Roberts, 1991).

Please see print copy for Figure 3.19

Figure 3.19: Cosmic-ray D_R variation with burial depth, from Prescott and Hutton (1988) (blue set of points). The orange square and the solid line through it represents independent measurement of cosmic-ray muons. The red triangle is an independent measurement of the total cosmic-ray dose.

The cosmic ray flux varies with:

- Depth of burial

The depth of burial (Figure 3.19) is important due to absorption of electrons in the material and attenuation of muons in the ground beneath the surface (Roberts, 1991). The latter, which is more important than the former, is related to the density of the ground

through which the cosmic rays travel (Prescott and Stephan, 1982; Prescott and Hutton, 1988, 1994).

Prescott and Hutton (1994) define the dry D_{Rc} at sea level (D_0) at a geomagnetic latitude of 55° for any depth from the surface to 10^6 g.cm^{-2} of standard rock as:

$$D_0 = \frac{6072}{((x + 11.6)^{1.68} + 75)\,(x + 212)} \exp(0.00055x) \qquad \text{Equation (1)}$$

Where x, the depth-density, is the product of the depth and the density, in 10^2 g.cm^{-2},

D_0 is in Gy.ka^{-1} and the uncertainty is $\pm$ 5%.

In this study, two depths need to be considered: the first is the depth of the sampled level in the core and the second being the water depth at the core site.

a) Depth in core

The sediment thickness above each sampled level varies from zero at the time of deposition to the modern sediment thickness that equals the depth level in the core. For all D_{Rc} calculations, the depth is approximated to half of the modern-depth, assuming a mean constant sedimentation rate over time.

b) Water depth

Even if the water depth at the core site at the time of collection is known (Chapter 2, Table 2.1), sea-level fluctuations over time imply variations in the depth of the water column above the sample. During low sea-level stands much of the Gulf of Carpentaria was dry or nearly dry as witnessed by pedogenic evidence (Chivas et al., 2001), although the existence of Lake Carpentaria implies there would have been a small column of water above some samples. During the last interglacial the sea level was up to ten metres above the modern sea level (Waelbroek et al., 2002). Hence, the water depth for each core could have potentially reached the modern water depth at the core site plus ten metres. The D_0 is thus calculated, for each sample, for zero metre (W_0) and for the water depth at the core site plus ten meters (W_M).

A later correction of the probable water depth at the time of deposition has been made after the estimation of sample ages and a comparison to contemporaneous sea level (Section 3.11.2). This water depth was not constant over time at the core site, but because the cosmic-ray dose rate was greatest at the time of deposition (no overlying-sediment protection) the sea level at the time of deposition may be used as a proxy for each sample to calculate the D_R. The sample depth in the core, the maximum possible height of the water-column above the sample, the density, the depth-density and D_0 for W_0 and W_M, are given in Table 3.5. The product of the depth in core of the sample and the density of the overlying sediment, plus the product of the water depth and the seawater density (1.04 $g.cm^{-3}$), equals the depth-density.

Table 3.5: Sample depth in the core, water depth at the core site, average density of sedimentary overburden, depth-density and D_0 (dry D_{RC} at sea level at a geomagnetic latitude of 55°) for each sample and for both water depths (0 m in orange and maximum depth in blue).

Sample	Depth in core (cm)	Water depth (m)	Density ($g.cm^{-3}$)	Depth-density ($g.cm^{-2}$)		D_0 ($Gy.ka^{-1}$)	
				W_0	W_M	W_0	W_M
MD31-30	30	59	1.33	20	7196	0.207	0.012
MD31-120	120	59	1.46	88	7264	0.197	0.011
MD31-530	530	59	1.63	432	7608	0.156	0.011
MD31-902	902	59	1.61	726	7902	0.129	0.010
MD31-1040	1040	59	1.6	832	8008	0.121	0.010
MD31-1340	1340	59	1.59	1065	8241	0.105	0.009
MD32-38	38	64	1.32	25	7721	0.206	0.010
MD32-629	629	64	1.51	475	8171	0.152	0.009
MD32-921	921	64	1.54	709	8405	0.130	0.009
MD32-1397	1397	64	1.57	1097	8793	0.103	0.008
MD32-1482	1482	64	1.57	1100	8796	0.099	0.008
MD33-220	220	68	1.53	168	8280	0.187	0.009
MD33-360	360	68	1.56	281	8393	0.173	0.009
MD33-629	629	68	1.63	513	8625	0.148	0.009

To define the density of the overlying sediment, the density of each centimetre of the core above the sample was averaged. These densities were calculated from γ-ray attenuation, measured onboard the *Marion Dufresne* vessel (Chivas et al., 2001), just after the core collection (Chapter 2, Section 2.2.3) and are reported in Appendix 5.2. Then to calculate

the depth density, only half of the total sediment thickness above the sample was used. This is to take into account that each sample was first exposed and then sediment progressively accumulates on top. Assuming a constant sedimentation rate, the half depth over time is a good approximation of the integration of the real depth through time.

- Latitude and altitude

The latitude and altitude control on the cosmic-ray dose rate is due to the Earth's magnetic field variation. The cosmic-ray dose rate variations due to geomagnetic dipole variation do not exceed $\pm$ 3% and are absent above 35° of geomagnetic latitude for a period back to 80 ka and are not likely to be larger for earlier times (Prescott and Hutton, 1994). All latitudes share a possible common systematic error of 10% due to changes in the primary cosmic ray intensity for any time during the last 500 ka (Prescott and Hutton, 1994).

The value of the dry D_{Rc} at the geomagnetic latitude and altitude of the sampling site can be calculated from D_0 using the following equation:

$$\text{Dry } D_{Rc} = D_0 [F + J \exp(h / H)] \qquad \text{Equation (2)}$$

Where h is the altitude of the site in kilometres, H is in kilometres, F and J are dimensionless and all are given in Figure 3.20.

The geomagnetic latitude and the altitude are needed to find the value of the empiric parameters F, J and H on Figure 3.20. For each sample, the altitude used is the core depth. The conversion from geographic latitude θ and longitude φ (Chapter 1, Table 1.1), to geomagnetic latitude λ can be obtained with the expression (Prescott and Hutton, 1988):

$$\sin \lambda = 0.203 \cos \theta . \cos (\varphi - 291) + 0.979 \sin \theta \qquad \text{Equation (3)}$$

Where all angles are in radians, and east is positive and south is negative.

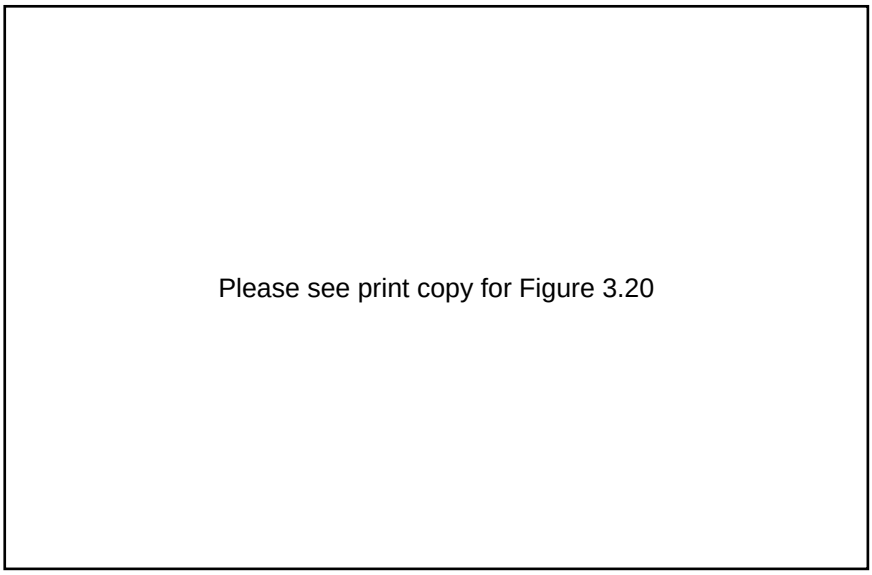

Figure 3.20: Parameters in Equation (2) for finding the cosmic-ray dose rate as a function of altitude and geomagnetic latitude; from Prescott and Hutton (1994).

The dry D_{Rc} is calculated for each sample and for minimal (W_0) and maximal (W_M) water depths at the core site using D_0 that was calculated in the previous paragraph, equations (1) and (2) and the core depth. The geomagnetic latitude, the core depth, and F, J, H parameters for the three cores from which sampling has been done, are presented in Table 3.6.

The D_{Rc} is then calculated from the dry D_{Rc} and the moisture-correction factor defined in section 3.10.4, for each sample and for both minimal (W_0) and maximal (W_M) water depths at the core site. The *se* of the D_{Rc} is the square root of the sum of squares of the moisture-correction factor *se* for the cosmic-ray dose rate and the five percent error that is the uncertainty on D_o. These results are presented in Table 3.6.

3.10.6 Water content and water depth estimation

An overestimation of the water content and/or water depth would lead to an underestimation of the D_{Re} and thus an overestimation of the age of the sample.

Table 3.6: Latitude (brown), longitude (khaki), water depth at the core site (purple), geomagnetic latitude (dark blue), Prescott and Hutton parameters (greens), dry D_{Rc} and D_{Rc} for all samples and for both water depths (0 m in orange and maximum depth in blue).

Sample	Core parameters	Geomagnetic latitude F; G; H	dry D_R (Gy.ka^{-1})		D_{Rc} (Gy.ka^{-1})		
			W_0	W_M	W_0	W_M	*se*
MD31-30	Latitude 12.0660°S Longitude 138.7497°E Water depth 59 m	-22.35 0.327; 0.609; 4.227	0.193	0.011	0.105	0.006	0.064
MD31-120			0.184	0.011	0.145	0.008	0.054
MD31-530			0.145	0.010	0.106	0.007	0.051
MD31-902			0.120	0.009	0.072	0.006	0.050
MD31-1040			0.112	0.009	0.069	0.005	0.053
MD31-1340			0.098	0.009	0.067	0.006	0.057
MD32-38	12.3132°S 139.9788°E 64 m	-22.47 0.332; 0.614; 4.236	0.194	0.010	0.118	0.006	0.077
MD32-629			0.143	0.009	0.097	0.006	0.050
MD32-921			0.123	0.008	0.071	0.005	0.056
MD32-1397			0.097	0.008	0.074	0.006	0.059
MD32-1482			0.093	0.008	0.072	0.006	0.053
MD33-220	12.3923°S 140.3720°E 68 m	-22.51 0.336; 0.618; 4.245	0.177	0.009	0.118	0.006	0.055
MD33-360			0.164	0.008	0.111	0.006	0.051
MD33-629			0.140	0.008	0.121	0.007	0.053

To thwart such overestimation, the D_{Re} was estimated in a three-step process.

1) The first step consisted of a rough estimation of the D_{Re} assuming a minimum and a maximum water depth that are defined in Section 3.9.5. Then, an approximate age was calculated, using the more appropriate D_{Re} according to all other available information on the sample.

2) In the second step, a comparison of the approximate age to a sea-level curve provided a more realistic water depth, and informed on the environment (marine/lacustrine) at the time of deposition (Section 3.11.2). This more accurate value for the water depth was thus used to recalculate a sea-level-corrected D_{Re} for marine samples.

3) In the final and third step, a more realistic estimation of the water content in the light of the estimated water depth, and using all available environmental information permitted a better estimation of the real D_R and thus a more accurate age.

3.10.7 ^{238}U, ^{232}Th and ^{40}K contents

Determining the concentration of the relevant lithogenic radionuclides allows the quantification of the environmental radioactivity. When a radioactive "particle" enters a mineral from an external source, it loses some energy to the mineral and, hence, the average external dose decreases with depth until all energy is absorbed at the maximum range for the given particles. A mineral's attenuation characteristics are defined by its ability to stop α-, β-particles and γ-rays (Blackwell, 1995). Gamma rays are more penetrating than either α- or β-particles, but less ionising. Because of the difference between α-, β-particles, and γ-rays penetration of the material (Figure 3.21), their contribution to the D_{Re} is separately assessed.

To estimate the contribution of α-, β-particles and γ-rays to the total D_{Re}, the concentrations of ^{238}U, ^{232}Th and ^{40}K were measured using both α and γ-spectrometry. The aim was to use two methods to correlate results and to assess the equilibrium status of both ^{238}U and ^{232}Th decay chains. The concentrations of the relevant nuclides were then converted to D_R using the formulae subsequently devised (Olley et al., 1996). The α- and γ-spectrometry analyses were processed at the Australian Nuclear Science and Technology Organisation (ANSTO), Menai, NSW 2234, and supported by an Australian Institute of Nuclear Science and Engineering (AINSE) Special Grant (01/182S).

- Description of the α-spectrometry analysis

This analysis was made using a α-spectrometry system containing thirty-one spectrometers. This technique allows the determination of the concentrations of nuclides in the ^{238}U and ^{232}Th decay chains, and can be applied after partial or total dissolution of the sediment. Two types of sample preparation were undertaken: leaching that consists of a partial dissolution and total dissolution.

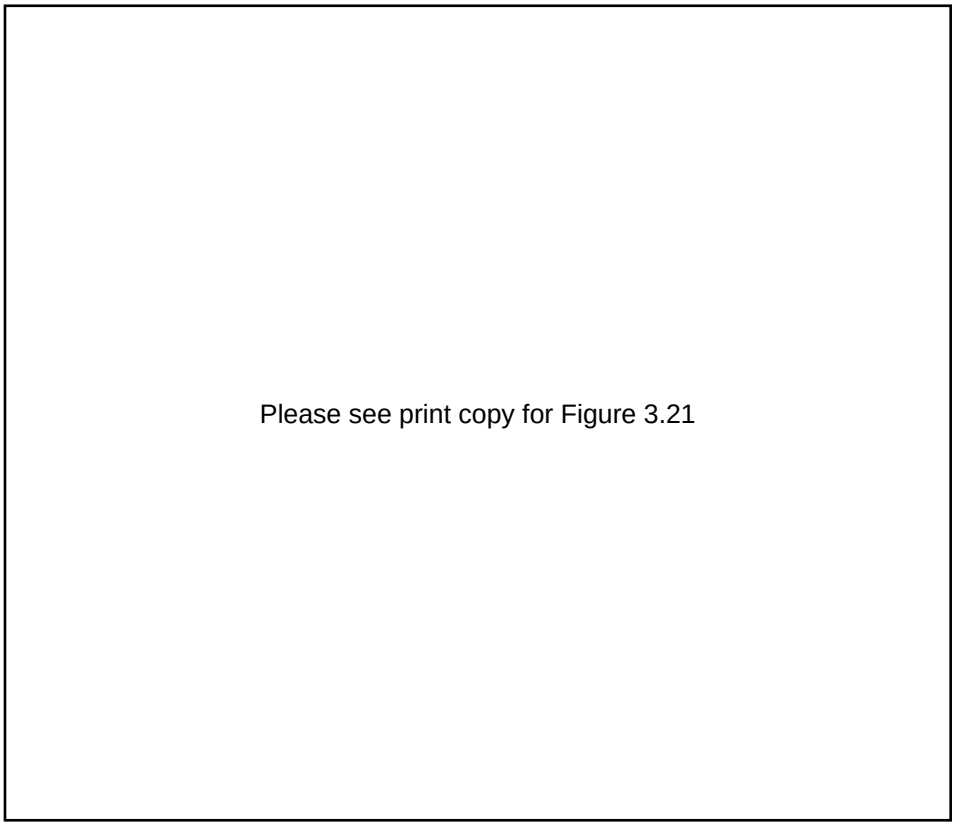

Figure 3.21: α-, β-particles and γ-rays spheres of influence (logarithmic scale, modified from Aitken, 1998). Each dashed circle represents the sphere surrounding a silt-sized grain (red) in sediment from within which radiation of a particular type is received. The radius shown for each is an approximate maximum value, dependent on the energy of the emitted particle or ray.

A standard sediment sample (IAEA-300 Baltic Sea) was analysed simultaneously to confirm the validity of the process and the reliability of the system, together with a blank to define the background level of the counter.

After addition of tracers to the sample (^{236}U for uranium or ^{229}Th for thorium), the sediment was digested, dissolved in acids and co-precipitated (see ANSTO protocol for partial and total dissolution for thorium and uranium analyses; Appendix 6.1). Then uranium was separated and purified by anion-exchange column, whereas thorium required an additional cation-exchange column. Both elements were then electroplated onto a stainless steel disc and assayed by α-spectrometry. The ^{234}U, ^{238}U, ^{232}Th, ^{230}Th

and ^{228}Th activities of samples and certified standards were measured on a semi-conductor counter (results in Appendix 6.2).

- Description of the γ-Spectrometry analysis

This analysis was processed on a Compton Suppression Gamma Spectrometer. This apparatus comprised an N-type high-purity germanium (HPGe) detector surrounded by a 75 mm thick sodium iodide annulus and 75 x 75 mm sodium iodide "plug" (Appendix 6.3).

An aliquot of the whole sample was dried in an oven and crushed using an agate mortar and a pestle. The resulting coarse powder was poured into a small Petri dish that was then sealed. Because the crushing could result in the loss of volatile radon (Ra), the box was set aside for 3 weeks to allow the Ra and its daughters to reach equilibrium.

The box was then placed on top of the HPGe and counted for a minimum of 160,000 seconds (~44 hours) and a maximum of 600,000 seconds (~168 hours) (results in Appendix 6.4). The duration of the counting was according to the sample activity. Both suppressed and unsuppressed spectra were recorded. Spectra were acquired and analysed with Canberra Genie 2000 Version 2.1 (Chris Bowles, personal communication, 2004).

The ^{40}K, ^{238}U, ^{226}Ra, ^{210}Pb, ^{228}Th, and ^{228}Ra activity evaluation was done by comparison of the intensity of sample rays with the spectra from standards. The standard sources for uranium series, thorium series and potassium were prepared from the following IAEA reference materials: RGU-1, RGTh-1, and RGK-1, respectively. These standards with a chemical composition as close as possible to the measured sample were also sealed in Petri dishes and counted. The gamma ray energies used to determine the activities of the corresponding radionuclides are summarised in Table 3.7.

- Comparison of the estimation methods and results

The α-spectrometry was initially performed on leached samples. A comparison with γ-spectrometry results showed a noticeable discrepancy. Thus, after discussion with Henk Heijnis (ANSTO) a total dissolution preparation was completed prior to another α-

spectrometry measurement to test the validity of the leaching process; the results are discussed in the following subsection.

Table 3.7: Gamma ray energies used to determine the radionuclide activities.

Suppressed spectrum

Radionuclides	Energy (keV)
^{210}Pb	46.5
^{234}Th	63.3
^{214}Pb	351.9
^{212}Bi	727.2
^{228}Ac	911.1
^{234m}Pa	1001
^{40}K	1460.5

Unsuppressed spectrum

Radionuclides	Energy (keV)
^{208}Ti	583.1
^{214}Bi	609.3

a) Leaching versus total digestion results (α-spectrometry)

A test was applied to three samples, from which remnant material was sufficient. The α-spectrometry results for both digestion methods are presented in Figure 3.22 (Appendix 6.5 lists results of both methods and calculation of their percentage of discrepancy) and show that the leaching results give significantly lower values than the total digestion results for uranium and thorium. Total digestion results are slightly lower and higher than the certified values of the uranium and thorium standards, respectively, analysed at the same time as the sample (Table 3.8).

Table 3.8: Percentage discrepancy between leaching and total digestion for α-spectrometry analyses of uranium and thorium isotopes on sediment samples from the Gulf of Carpentaria (orange) and on measured Certified samples (blue) analysed simultaneously. For these reference samples, the ratios of the leaching and total digestion measures to the certified values are also shown in the table (green).

	Total-Leach/Total		Total-Leach/Total		
	^{238}U	^{234}U	^{228}Th	^{230}Th	^{232}Th
MD32-629	22 ± 5%	16 ± 5%	45 ± 8%	45 ± 8%	54 ± 7%
MD33-360	44 ± 4%	40 ± 4%	32 ± 6%	62 ± 5%	48 ± 5%
MD33-629 (1)	32 ± 4%	29 ± 4%	49 ± 5%	44 ± 5%	52 ± 6%
MD33-629 (2)	34 ± 4%	33 ± 4%			
measured (M) Certified	10 ± 9%	19 ± 9%	9± 10%	35 ± 8%	29 ± 9%
Certified/Leach M	1.23±0.11	1.34±0.12	0.98±0.09	1.11±0.10	1.26±0.12
Certified/Total M	**1.11±0.05**	**1.08±0.05**	**0.89±0.05**	**0.72±0.03**	**0.89±0.05**

The test proves that the α-spectrometry results on leached samples are significantly underestimated, from 16 ± 5% to 44 ± 4% for uranium and from 32 ± 6% to 62 ± 5% for thorium, compared to the total digestion results (Figure 3.22 and Table 3.8).

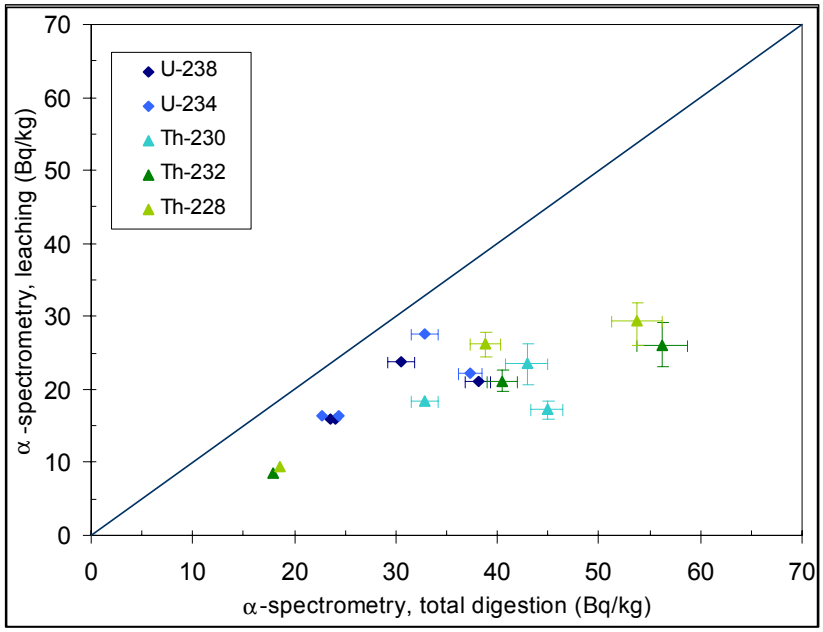

Figure 3.22: Comparison of leaching versus total digestion for α-spectrometry analyses of sediment samples from the Gulf of Carpentaria. The solid line represents a 1/1 ratio. Error bars are plotted only for errors greater than 1 $Bq.kg^{-1}$.

This investigation also demonstrates that the certified sample content was underestimated by both digestion procedures for uranium, whereas thorium concentration was underestimated by leaching and overestimated by total digestion (Table 3.8). This test proves the inappropriateness of the leaching digestion technique for this type of sample, which contains a non-negligible amount of resistant material. The underestimation of the total digestion values for the certified sample for uranium is probably due to the deficiency of the total dissolution experiment, which left a small amount of residue. The total digestion protocol employed is similar to that of Olley et al. (1997). The main difference is the significantly larger amount of sample processed, which probably prevents the complete dissolution of the whole sample (Gary Hancock, CSIRO Canberra, personal communication, 2002). There is apt to be some degree of cancelling of errors involved with the total digestion results, as the measured uranium and thorium

concentrations appear to be in error by a similar amount (about 10%) but of opposite sign. We attribute the discrepancy between the measured and certified thorium concentrations to problems of normalisation. There was insufficient material remaining, however, to reprocess all of the samples and resolve this discrepancy.

b) Comparison of α-spectrometry versus γ-spectrometry

- Leaching α-spectrometry versus γ-spectrometry

The γ-spectrometry estimations are noticeably higher than the leaching α-spectrometry values (Figure 3.23 and Appendix 6.6), the difference being greater for ^{238}U than for ^{228}Th. This result agrees with the underestimation of the α-spectrometry leaching versus total digestion (subsection a); that is, that thorium was more underestimated than uranium.

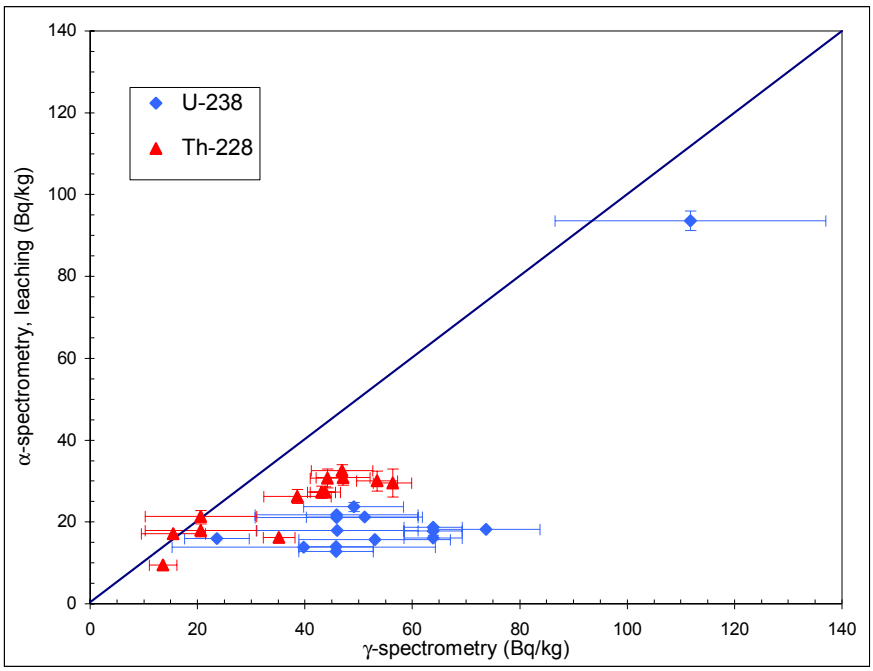

Figure 3.23: Comparison between the results of leaching-α-spectrometry and γ-spectrometry analyses of sediment samples from the Gulf of Carpentaria. The solid line represents a 1/1 ratio. Error bars are plotted only for errors greater than 1 Bq.kg^{-1}.

- Total digestion α-spectrometry versus γ-spectrometry

Comparison between total digestion α-spectrometry and γ-spectrometry results still shows a discrepancy (open symbols in Figure 3.24). However this discrepancy is smaller than 20% for ^{228}Th and smaller than 50% for ^{238}U. This has to be related to the conclusion of the previous subsection (a), which stated that total digestion α-spectrometry substantially underestimates uranium concentration and overestimates thorium contents.

Multiplying a total digestion α-spectrometry result by the efficiency of the corresponding Certified measurement (i.e. 'Certified/Total M' values, Table 3.8) produces a corrected value for each radionuclide. These corrected values are plotted on Figure 3.24 as filled symbols, and are listed in Table 3.9.

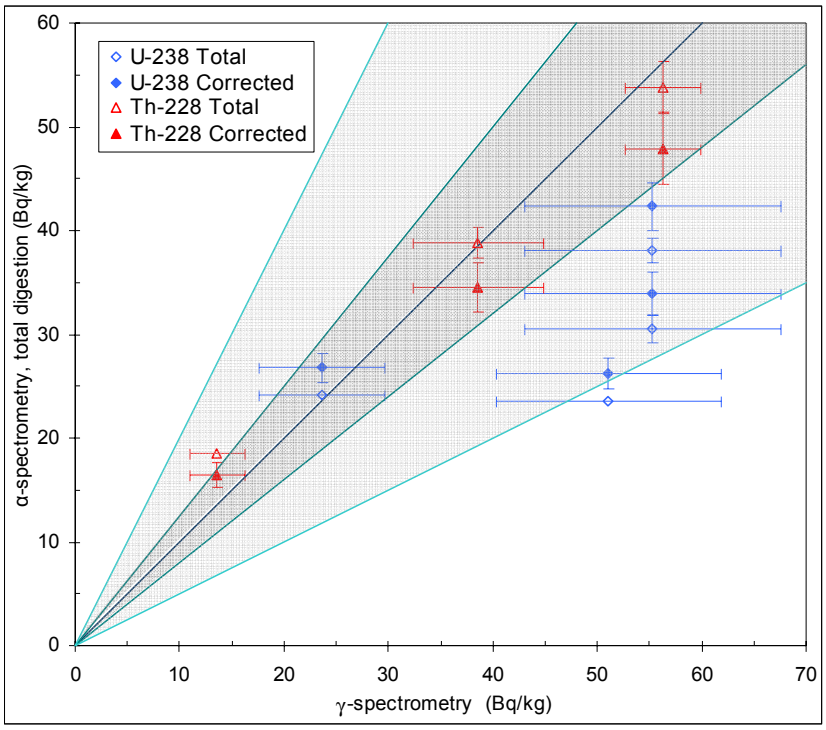

Figure 3.24: Comparison between results from total-digestion α-spectrometry and γ-spectrometry analyses of sediment samples from the Gulf of Carpentaria. The solid line represents a 1/1 ratio. The dark-shaded areas represent a 0–20% discrepancy whereas the light-shading indicates a 20–50% difference. Error bars are plotted only for errors greater than 1 Bq.kg^{-1}.

Table 3.9: Total digestion α-spectrometry, corrected values (blue) and γ-spectrometry (green) results and discrepancies for (a) ^{238}U and (b) ^{228}Th.

(a) ^{238}U	total α-spectrometry (Bq.kg^{-1})				γ-spectrometry (Bq.kg^{-1})		α total-γ / γ	cor. α total-γ / γ
	^{238}U	*error*	corrected (cor.) ^{238}U	*error*	^{238}U	*error*		
MD32-629	30.5	1.3	33.9	2.1	55.3	12.3	-45±25%	-39±24%
MD32-629	38.1	1.2	42.4	2.3			-31±23%	-23±23%
MD33-360	23.6	0.8	26.2	1.5	51.1	10.8	-54±24%	-49±24%
MD33-629	24.1	0.7	26.8	1.4	23.6	6.0	2±26%	14±26%

(b) ^{228}Th	total α-spectrometry (Bq.kg^{-1})				γ-spectrometry (Bq.kg^{-1})		α total-γ / γ	cor. α total-γ / γ
	^{228}Th	*error*	corrected (cor) ^{228}Th	*error*	^{228}Th	*error*		
MD32-629	53.8	2.5	47.9	3.5	56.3	3.6	-4±7%	-15±9%
MD33-360	38.8	1.5	34.5	2.4	38.6	6.3	1±17%	-11±18%
MD33-629	18.5	0.8	16.5	1.2	13.6	2.6	15±11%	21±21%

The total digestion α-spectrometry and γ-spectrometry estimations for the corrected ^{228}Th concentrations are indistinguishable at 1σ for two samples and at 2σ for the third. The corrected total-digestion α-spectrometry and γ-spectrometry estimations for ^{238}U are consistent at 1σ for two samples and at 2σ for a third, but in each case the ^{238}U content is underestimated by α-spectrometry.

Conclusion

There is some discrepancy between the α-spectrometry (Appendix 6.2) and γ-spectrometry (Appendix 6.4) results. The analysis conducted in the two previous paragraphs shows that the α-spectrometry results (a) are not internally consistent, (b) are not consistent with the concentrations of the calibration standards, and (c) do not match exactly the concentrations obtained by γ-spectrometry. However, the discrepancies between γ-spectrometry and corrected total-digestion α-spectrometry are not significant at the 2σ level for all three thorium comparisons and for three out of four uranium comparisons. In light of these findings, we consider the γ-spectrometry results to reflect more accurately the true concentrations of uranium and thorium in these samples. In this

study, therefore, the activities of nuclides in the ^{238}U and ^{232}Th chains, and ^{40}K, as measured by γ-bspectrometry were used to calculate the D_{re}. The divergence from a condition of secular equilibrium of nuclides in the ^{238}U and ^{232}Th decay chains is discussed in the next section.α

3.10.8 Equilibrium within the ^{238}U and ^{232}Th decay chains

The α- and γ-spectrometry analyses allow examination of the equilibrium condition of both the ^{238}U and ^{232}Th decay chains (Figure 3.18). Despite the systematic underestimation of the leaching α-spectrometry results, they are used to test the equilibrium status of the ^{238}U and ^{232}Th chains by comparing only the ratios of measured nuclides.

- Secular equilibrium

For the ^{238}U and ^{232}Th decay chains, the daughters' half-lives are commonly much shorter than that of the parent nuclide (Figure 3.18) and thus the activity of the parent does not decrease markedly over many daughter half-lives (Olley et al., 1996). That implies, assuming a closed system, that parent and daughters have the same activity concentration. This condition, when the parent sustains the activity concentration of each of its daughters, is called secular equilibrium. A condition of secular equilibrium is important for OSL dating because it simplifies the calculation of the modern (measurable) environmental dose rate, although it does not rule out the possibility of some forms of disequilibrium having existed during the burial time.

- Nature of the studied sediment

Because of the location of the Gulf of Carpentaria, the sediment cores have recorded various environmental conditions such as shallow marine, estuarine and lacustrine. This implies that some sediment of the Gulf is allochthonous and ultimately derived from the erosion of soil. Such erosion is the result of rock weathering, which corresponds to chemical and mechanical breakdown of the rock mass. These processes cause a sorting of elements in soils, the more soluble being lost and the less soluble concentrated, and the production of usually finer-grained secondary minerals (Olley et al., 1996).

- Causes of disequilibrium

Due to the high reactivity of Ra and the high volatility of Rn, disequilibria commonly occur within the ^{238}U decay chain (Blackwell, 1995) and are well documented for Quaternary samples (Wintle and Huntley, 1979; Michel, 1984; Greeman et al., 1990; Blackwell, 1995), whereas reports on the equilibrium conditions of the ^{232}Th decay chain are sparse. However, given the short half-lives of the longer-lived daughters in the ^{232}Th decay chain, ^{228}Ra (5.75 years) and ^{228}Th (1.91 years), secular equilibrium might be expected in most natural materials (Murray et al., 1991).

Soil erosion and sediment transport either by wind or water result in particle sorting. These processes are highly likely to increase the level of disequilibrium in transported sediments. Thus it is not surprising that disequilibrium has been reported in various sedimentary depositional environments (Murray et al., 1992; Olley et al., 1997). Furthermore, ^{230}Th is continuously precipitated from the ocean, and because its half-life is 75 ka, it is necessary to include its impact, known as ^{230}Th-excess, on D_R variation over time (Wintle and Huntley, 1979). As a consequence, disequilibria in sediments from the Gulf of Carpentaria should be expected.

- Quantification of the disequilibrium

To quantify these disequilibria, all 17 samples were analysed by both α- and γ-spectrometry, for the activities of ^{238}U, ^{234}U, ^{230}Th, ^{226}Ra, ^{210}Pb and ^{232}Th, ^{228}Ra, ^{228}Th (Appendices 6.2, 6.4). The ratios of daughter versus parent activity, measured by each technique, are shown in Table 3.10.

The relevant parent-daughter concentration pairs are plotted in Figure 3.25 for the ^{238}U decay chain and in Figure 3.26 for the ^{232}Th decay chain. Each daughter is plotted against its immediate longer-lived measured parent. In both plots, the filled symbols correspond to the α-spectrometry results whereas the unfilled symbols are γ-spectrometry measurements; each core is plotted in a specific colour range; and each ratio is represented with a particular symbol.

a) ^{238}U decay chain

Most of the disequilibria in the ^{238}U decay chain are smaller than 20% in all three core samples (Figure 3.25). The general trends are: ^{234}U is in excess with respect to ^{238}U, and to ^{230}Th, whereas ^{226}Ra is in deficit with respect to ^{238}U and in excess with respect to

^{210}Pb. These results are consistent with existing literature (Ivanovich and Harmon, 1992; Krbetschek et al., 1994; Olley et al., 2004a). Stokes et al. (2003b) reported activities for the nuclides of the ^{238}U decay chain that are comparable, but present an excess of ^{230}Th with respect to ^{234}U, which is consistent with the deep-sea nature of their sediments.

Table 3.10: The α- and γ-spectrometry results, for several nuclides of the ^{238}U and ^{232}Th decay chains. The italic red values are within 10% and the bold blue values between 10 and 20% of equilibrium. The black values are between 20 and 50% of equilibrium. The underlined green values represent data that are more than 50% from equilibrium.

	α-spectrometry			γ-spectrometry		
	^{238}U chain		^{232}Th chain	^{238}U chain		^{232}Th chain
	U-234 / U-238	*Th-230 / U-234*	*Th-228 / Th-232*	*Ra-226 / U-238*	*Pb-210 / Ra-226*	*Ra-228 / Th-228*
MD31-30	**1.14±0.05**	**0.82±0.04**	*1.04±0.06*	0.27±0.05	*0.94±0.45*	2.39±0.97
MD31-120	**1.17±0.05**	1.52±0.10	*1.01±0.08*	0.63±0.17	0.77±0.15	*1.08±0.08*
MD31-530	**1.15±0.06**	1.42±0.13	1.30±0.14	0.53±0.05	*0.96±0.14*	*1.08±0.09*
MD31-530 (1)	**1.18±0.05**	**1.19±0.10**				
MD31-530 (2)	1.27±0.11	**1.16±0.11**				
MD31-902	**1.18±0.08**	**0.84±0.08**	1.39±0.16	0.75±0.14	*0.90±0.22*	**1.14±0.09**
MD31-1040	1.27±0.08	**1.11±0.07**	**1.15±0.07**	0.67±0.10	*1.07±0.20*	*1.10±0.09*
MD31-1040	**1.16±0.11**	*1.10±0.09*				
MD32-38	1.23±0.05	0.77±0.07	0.84±0.10	0.53±0.18	**0.81±0.50**	1.84±0.98
MD32-38 (1)	**1.15±0.08**	0.72±0.06	*1.02±0.09*			
MD32-629	**1.17±0.06**	**0.85±0.11**	**1.13±0.18**	0.66±0.15	*0.98±0.15*	*0.97±0.08*
MD32-629 (1)		*1.02±0.06*	1.31±0.08			
MD32-921	*1.08±0.04*	*0.91±0.05*	1.45±0.12	*0.93±0.21*	*0.91±0.09*	*1.01±0.13*
MD32-1397	**1.11±0.05**	*1.06±0.05*	*0.99±0.05*	0.76±0.25	0.77±0.19	*1.07±0.12*
MD33-220	**1.12±0.05**	2.02±0.11	1.20±0.07	0.72±0.45	*0.93±0.30*	*1.03±0.15*
MD33-360	*1.05±0.04*	0.77±0.06	1.24±0.11	0.72±0.16	0.53±0.23	**1.15±0.22**
MD33-629 (1)	*1.02±0.04*	**1.13±0.06**	*1.11±0.08*	**1.11±0.28**	*0.97±0.14*	1.39±0.29

Three samples (MD31-120, MD31-530 and MD33-220) show disequilibrium of between 20% and 50%, and one sample (MD31-30) shows about 75% disequilibrium. MD31-120 and MD33-220 are the only samples presenting a ^{230}Th-excess whereas MD31-30 and MD31-530 present a clear depletion of ^{226}Ra with respect to ^{238}U. The higher disequilibrium observed in the MD31 samples might be a sampling artefact or may reflect a highly reactive environment relating to the core location, which is on a channel flooded by river waters and episodically draining the Gulf waters to the Indian Ocean.

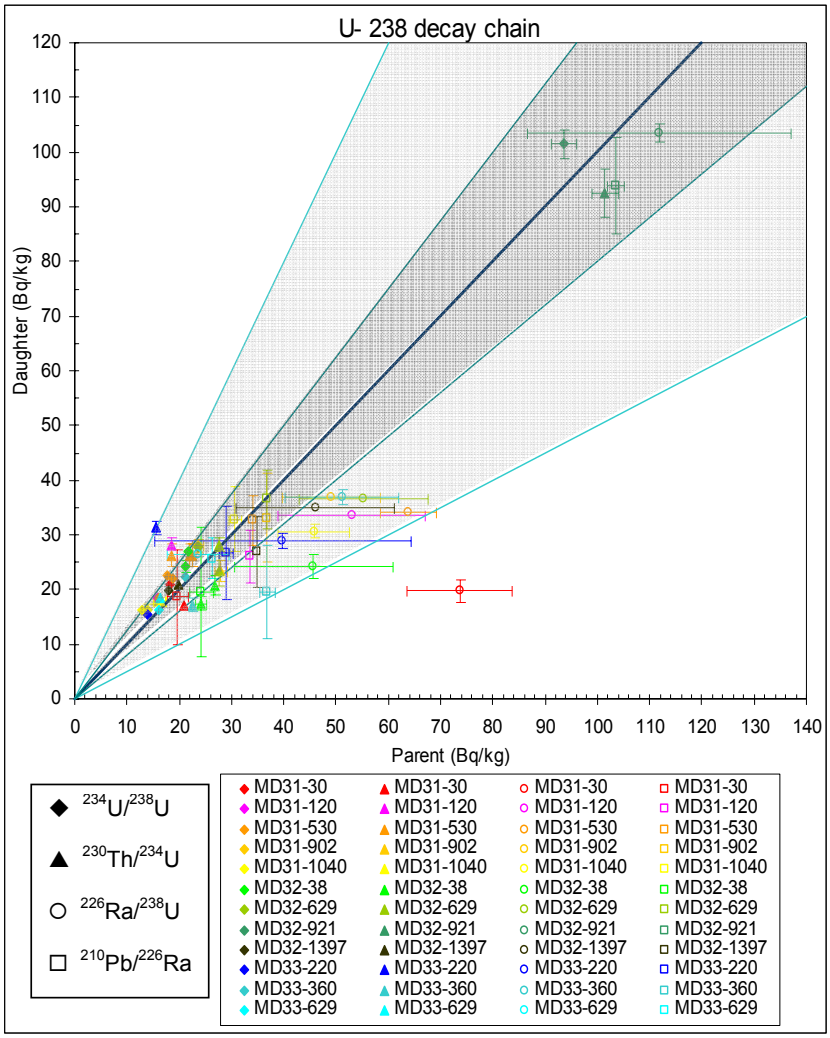

Figure 3.25: The α- and γ-spectrometry results for ^{238}U decay chain nuclides. Filled and unfilled symbols correspond to α- and γ-spectrometry results, respectively. The dark blue solid line represents secular equilibrium. The dark-shaded area represents a 0–20% discrepancy whereas the light-shaded area indicates a 20–50% difference. Error bars are plotted only for errors greater than 1 Bq.kg^{-1}.

One sample, MD32-921, has a ^{238}U concentration activity value five times higher than the other samples, which vary from 13 to 24 Bq.kg^{-1}. This sample shows consistency in its high concentration, with less than 10% variation between all nuclide concentrations (Table 3.10). This high concentration of ^{238}U decay chain nuclides may be associated with

the presence of abundant biogenic material together with pyrite in the sediment that corresponds to an organic-rich, anoxic substrate (Table 3.1). The typical activity of ^{238}U is in equilibrium with ^{226}Ra, which is in equilibrium with ^{210}Pb (within analytical uncertainties). ^{238}U present a deficit smaller than 10% with respect to ^{234}U, which is less than 10% in excess with respect to ^{230}Th.

b) ^{232}Th decay chain

Disequilibrium is less marked in the ^{232}Th decay chain. Most results are within error of equilibrium and the others never exceed 20% of disequilibrium (Figure 3.26). The general trends are: ^{228}Th is in excess with regard to ^{232}Th, which is itself in shortage with regard to ^{228}Ra. These findings are consistent with existing literature (Krbetschek et al., 1984; Olley et al., 1996, 2004a).

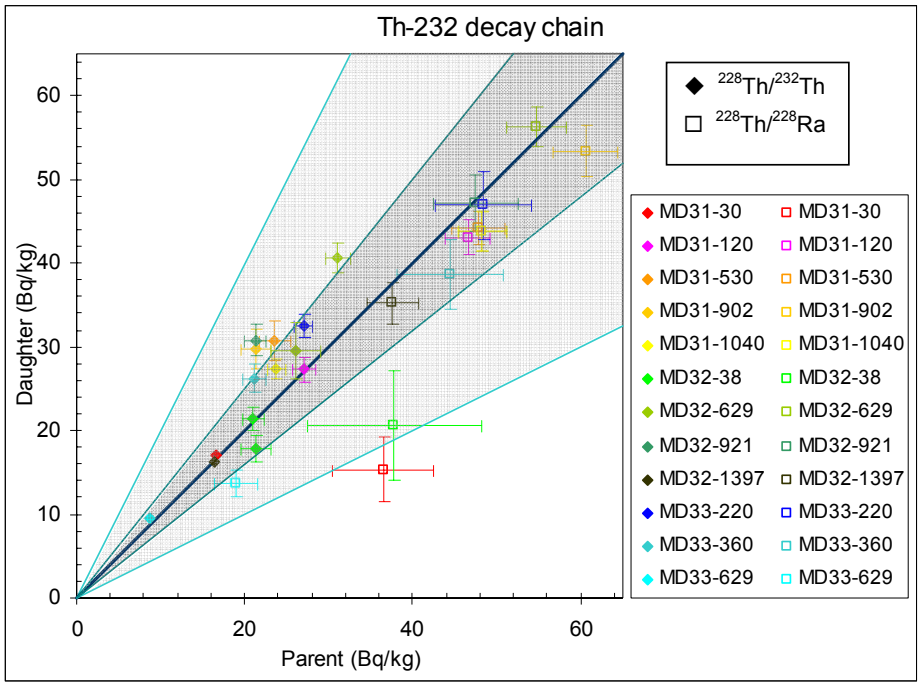

Figure 3.26: The α- and γ-spectrometry results for the ^{232}Th decay chain nuclides. Filled and unfilled symbols correspond to α and γ-spectrometry results, respectively. The dark blue solid line represents secular equilibrium. The dark-shaded area represents a 0–20% discrepancy whereas the light-shaded area indicates a 20–50% difference. Error bars are plotted only for errors greater than 1 $Bq.kg^{-1}$.

One sample (MD31-30) shows a clear excess of ^{228}Ra with respect to ^{228}Th. Similar ^{228}Ra excesses have already been reported in fluvial and lacustrine depositional environments by Olley et al. (1996), and are thought unlikely to be of direct importance to the D_R because of the short half-live of ^{228}Ra (5.75 years). This disequilibrium indicates that significant radium redistribution can occur and it could affect the migration of the much longer lived ^{226}Ra (1602 years) in the ^{238}U decay chain. However MD31-30 is a recently deposited sample at only 30 cm depth in the core, and a deficit of ^{226}Ra compared to ^{238}U was noticed. The excess of ^{228}Ra should thus not substantially affect the D_R estimation.

c) Results

The ^{232}Th decay chain is at or near equilibrium over the three cores of the Gulf of Carpentaria, except for one near-surface sample, MD31-30, that presents an excess of ^{228}Ra with respect to ^{228}Th. However this excess should not affect significantly the D_R due to the short half-life of ^{228}Ra. Consequently, it is assumed that the D_R measured at the time of collection prevailed throughout the period of sample burial, and that the depositional environment was chemically closed after deposition.

Disequilibrium is present in the ^{238}U chain but rarely exceeds 20% over the three cores of the Gulf of Carpentaria. According to Olley et al. (2004a), disequilibrium of this amplitude in the ^{238}U decay chain will induce a deviation of the calculated from the true D_R smaller than 3% (depending on the method of measurement and the relative contributions of U, Th and K to D_R), which is less than that associated with the D_E determination, as shown in Section 3.9.3. Because of the magnitude of the error associated with γ-spectrometry results, it would be unrealistic to try to obtain a more precise D_R using an iterative procedure as suggested by Stokes et al. (2003b).

3.10.9 Nuclide activities used to calculate the D_{Re}

Because of the underestimation of leaching α-spectrometry measurements (Section 3.10.7), only γ-spectrometry nuclide activities were used in D_R estimation.

In order to obtain an estimate heavily weighted to the lower part of the ^{238}U decay chain (i.e. ^{226}Ra and daughters, from where most of the γ and β D_R originates), the activities of all measured nuclides, ^{238}U, ^{226}Ra and ^{210}Pb for the ^{238}U chain, ^{228}Ra and ^{228}Th for the

^{232}Th chain, were averaged utilising a CSIRO program. This program, called AVVAR, combines readings and their errors, weighted according to their inverse variance, and favours the most precise measurements of activity, i.e. activities with the smallest error. For the uranium series, the error on ^{226}Ra activities ranged from 0.6 to 2.2 Bq.kg^{-1}, whereas the error on the other nuclide activities ranged from 3.7 to 25.2 Bq.kg^{-1}, so the final result is weighted towards the ^{226}Ra value, which is advantageous in the present context because the disequilibria occurring above ^{226}Ra in the decay chain have little influence on the final result. The calculated values in Bq.kg^{-1} are presented in Table 3.11.

For MD32-1482 cm (bold in Table 3.11), the uranium and thorium contents were obtained by thick alpha-counting, and the potassium content was acquired by Atomic Absorption Spectrophotometry (Chivas et al., 2001).

Table 3.11: Nuclide activities used to calculate the D_{Re}. MD33-1482 values are from Chivas et al. (2001).

Activity / Sample	^{238}U Chain (mean) (Bq.kg^{-1})	1 σ (Bq.kg^{-1})	^{232}Th Chain (mean) (Bq.kg^{-1})	1 σ (Bq.kg^{-1})	^{40}K (Bq.kg^{-1})	1 σ (Bq.kg^{-1})
MD31-30	21.4	1.8	30.2	3.3	62.7	3.0
MD31-120	33.5	0.7	45.2	1.6	106.2	2.0
MD31-530	34.4	0.6	46.8	1.7	98.1	1.9
MD31-902	36.9	1.0	57.7	2.4	127.1	2.8
MD31-1040	31.2	1.2	46.5	1.8	109.8	2.1
MD31-1340	*31.2*	*1.2*	*46.5*	*1.8*	*109.8*	*2.1*
MD32-38	24.5	2.0	33.0	5.5	82.4	5.5
MD32-629	36.7	0.8	55.2	2.0	136.8	2.7
MD32-921	103.1	1.6	47.4	2.8	90.3	2.9
MD32-1397	34.8	1.0	36.6	1.9	73.0	1.8
MD32-1482	**38.3**	**0.7**	**40.7**	**2.0**	**284.4**	**6.3**
MD33-220	28.8	1.4	47.9	3.3	134.0	4.0
MD33-360	36.6	1.5	42.7	3.5	105.4	3.7
MD33-629	26.3	0.6	17.4	1.4	44.1	1.5

No measurement was made for sample MD31-1340 (in grey italics in Table 3.11) because the residue from the OSL sample was too small for γ-spectrometry analyses. The dark grey clays with concretions present at 1340 cm depth can be related to those

found at 1040 cm depth in the same core (Reeves, 2004). The nuclide activities are thus assumed to be the same for both the 1040 cm and 1340 cm levels.

3.10.10 The α-particle contribution:

Because α-particles interact strongly with crystalline materials, they rapidly lose their energy. Their effect on material such as sediments is highly localised to within 25 μm of the emitting nucleus. Thus the quartz grain-size used in this study (90 to 150 μm) is coarse enough compared to the α-particle penetration distance (~20 μm) to receive α radiation from their external environment only in the outer part of the grain (Wintle, 1997). This contribution is thus eliminated by the 45-minute HF etching of the sample, which eliminates the outer irradiated layer of the quartz grains (Aitken, 1998). Therefore the α-particle contribution has been ignored for the remainder of the D_{Re} estimation.

3.10.11 The β-particle and γ-ray contribution:

Compared to α-particles, β-particles and γ-rays are less highly charged. Thus, their effects in sediments penetrate much further. The sphere of influence of β-particles is 3 mm (in radius), while the sphere of influence of γ-rays is 30 cm (Figure 3.21), which means, for the latter, that radionuclides up to 30 cm away from the studied grain will increase its dose. The sampling procedure for the D_R estimation, which is done by α- and γ-spectrometry measurement of the concentration of nuclides from ^{238}U and ^{232}Th decay chains, and ^{40}K, should take into account this latter characteristic and the fact that most sediment is inhomogeneous. In order to provide a relatively reliable sample for D_R determination, a bulk sample was assembled from sub-samples at the required sampling depth in the core, together with aliquots of sediment from 20 cm above and below the central sample (Figure 3.27). The amount of sediment collected vertically from the central sample-level decreased with distance from it. This sampling process is appropriate for the determination of the γ-ray contribution, and we have also used the composite sample to determine the β-particle contribution. The latter is considered satisfactory in the present context, as 50% of the composite sample is composed of sediment collected from within 5 cm either side of the OSL sample level and the sediments are homogeneous over this 10 cm vertical distance. Thus, the total dose rate is dominated by the radionuclide content of the sediments located closest to the OSL sample, and is relatively insensitive to the radioactivity of materials located further away. Combined samples were homogenised

before processing. Because of the small amount of sediment available, samples were first analysed by γ-spectrometry and then processed for the α-spectrometry analysis.

- Conversion and moisture-correction factors

Each radionuclide has a conversion factor that allows the transformation of the radioactive decay energy into absorbed dose per unit mass, presupposing the hypothesis of infinite matrix. These factors are commonly updated and in this study the values from Adamiec and Aitken (1998) shown in Table 3.11 were used. The D_{Re} is then the sum of the products of specific activity by absorbed dose for each radionuclide. The conversion factors have been established for dry sediments, thus a correction related to the water content or moisture-correction factor (Section 3.10.4) has to be included.

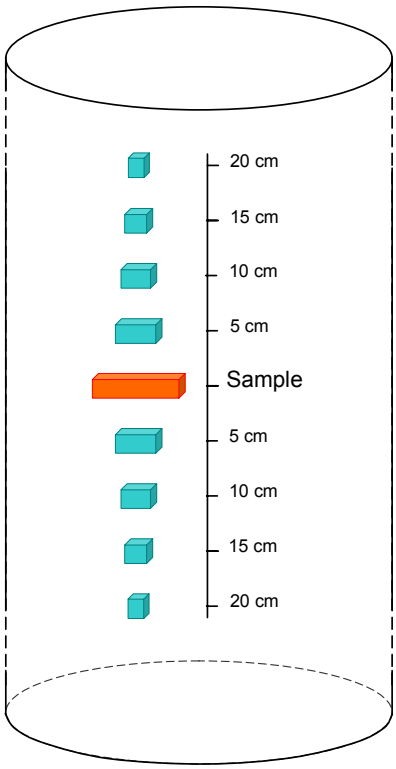

Figure 3.27: Spatial distribution of sub-samples for the D_{Re} measurement. The amount of sediment collected every 5 cm apart vertically (green) decreases with the distance from the central sample. These sub-samples are then mixed with the remaining sediment (orange) from the preparation of the OSL sample.

➢ Attenuation factors

The β dose suffers from significant attenuation by etching and when passing through coarse quartz grains (Aitken, 1985a; Mejdahl, 1979, Nathan et al., 2003), whereas the attenuation of γ rays is negligible for both aspects due to their larger penetration power. The β dose attenuation factors, specific to each radionuclides, for 100 μm-diameter grains, corresponding to the size of the quartz used in this study, are shown in Table 3.12 (Mejdahl, 1979).

Table 3.12: Values of β attenuation (green), dose rate conversion factors (blue), β D_{Re} for U, Th, K and total (dark red) and their *se* for each sample.

β dose rate (Gy.ka^{-1})	U		Th		K		Total	
β attenuation	0.904		0.857		0.965			
Conversion factors	0.146		0.0273		0.782			
Sample	Dose rate	*se*	Dose rate	*se*	Dose rate	*se*	Dose rate	*se*
MD31-30	0.126	0.019	0.096	0.019	0.082	0.007	0.304	0.028
MD31-120	0.284	0.007	0.206	0.009	0.201	0.005	0.691	0.012
MD31-530	0.270	0.006	0.197	0.010	0.172	0.005	0.639	0.013
MD31-902	0.240	0.011	0.202	0.014	0.185	0.007	0.627	0.019
MD31-1040	0.206	0.012	0.165	0.010	0.162	0.005	0.532	0.016
MD31-1340	0.231	0.012	0.185	0.010	0.182	0.005	0.599	0.016
MD32-38	0.161	0.022	0.116	0.032	0.121	0.013	0.398	0.041
MD32-629	0.268	0.008	0.217	0.011	0.224	0.006	0.709	0.015
MD32-921	0.644	0.017	0.159	0.016	0.126	0.007	0.929	0.024
MD32-1397	0.285	0.011	0.161	0.011	0.134	0.004	0.580	0.016
MD32-1482	0.321	0.008	0.183	0.012	0.532	0.021	1.036	0.025
MD33-220	0.206	0.015	0.185	0.019	0.215	0.010	0.606	0.026
MD33-360	0.267	0.016	0.167	0.020	0.171	0.009	0.605	0.027
MD33-629	0.242	0.006	0.086	0.008	0.091	0.004	0.419	0.011

The γ-spectrometry measurements of the ^{238}U, ^{232}Th and ^{40}K activities (in Bq.kg^{-1}) for each sample are divided by 12.357, 4.0721, and 316.04 respectively (Richard Roberts, personal communication, 2004), to convert into concentrations expressed as ppm, ppm

and percent, respectively. Subsequently for each sample these concentrations are multiplied by the appropriate moisture correction factors (Table 3.4), dose rate conversion factors (Tables 3.12 and 3.13) and β attenuation factors (Table 3.12) to obtain the γ dose rates (Table 3.13) and β dose rates (Table 3.12), respectively. Both dose rates are presented together with their standard errors (*se*).

Table 3.13: Values of γ dose rate conversion factors (blue), γ D_{Re} or U, Th, K and total (dark red) and their *se* for each sample.

γ dose rate ($Gy.ka^{-1}$)	U		Th		K		Total	
Conversion factors	0.113		0.0476		0.243			
Sample	Dose rate	*se*	Dose rate	*se*	Dose rate	*se*	Dose rate	*se*
MD31-30	0.103	0.017	0.186	0.038	0.025	0.002	0.315	0.042
MD31-120	0.238	0.006	0.411	0.019	0.064	0.002	0.713	0.020
MD31-530	0.225	0.005	0.392	0.020	0.054	0.001	0.671	0.021
MD31-902	0.198	0.009	0.396	0.028	0.057	0.002	0.651	0.029
MD31-1040	0.170	0.011	0.323	0.021	0.050	0.002	0.543	0.024
MD31-1340	0.192	0.011	0.367	0.021	0.057	0.002	0.616	0.024
MD32-38	0.133	0.019	0.228	0.064	0.038	0.004	0.398	0.067
MD32-629	0.223	0.007	0.429	0.023	0.070	0.002	0.722	0.024
MD32-921	0.530	0.014	0.311	0.032	0.039	0.002	0.880	0.035
MD32-1397	0.239	0.009	0.321	0.022	0.042	0.001	0.602	0.024
MD32-1482	0.269	0.007	0.365	0.024	0.168	0.007	0.802	0.026
MD33-220	0.171	0.013	0.365	0.038	0.067	0.003	0.603	0.040
MD33-360	0.222	0.013	0.330	0.041	0.054	0.003	0.605	0.043
MD33-629	0.204	0.005	0.174	0.016	0.029	0.001	0.407	0.017

3.10.12 Results

The total D_{Re} that is the sum of the D_{RC}, $D_{R\beta}$ and $D_{R\gamma}$, is shown in Table 3.14 with its *se*. The final D_R that corresponds to the sum of the D_{Ri} and the D_{Re} is also presented in this table with its *se*. Because of the uncertainty in the D_{RC}, two D_{Re} values and thus two D_R values are calculated for each sample, corresponding to the minimum (W_0) and maximum (W_M) extension of the water column above the sample.

Table 3.14: D_{Re} and D_R for each sample and for both minimum and maximum water depth (in orange and blue, respectively). The D_{Ri} used for the calculation is 0.032 ± 0.011 Gy.ka^{-1} (Section 3.10.2).

Sample	D_{Re} (Gy.ka^{-1})			D_R (Gy.ka^{-1})		
	W_0	W_M	*se*	W_0	W_M	*se*
MD31-30	0.724	0.625	0.082	0.756	0.657	0.082
MD31-120	1.549	1.412	0.059	1.581	1.444	0.060
MD31-530	1.416	1.318	0.056	1.448	1.350	0.057
MD31-902	1.352	1.285	0.061	1.384	1.317	0.062
MD31-1040	1.144	1.081	0.061	1.176	1.113	0.062
MD31-1340	1.282	1.221	0.064	1.314	1.253	0.065
MD32-38	0.914	0.802	0.110	0.946	0.834	0.111
MD32-629	1.528	1.437	0.058	1.560	1.469	0.059
MD32-921	1.880	1.814	0.070	1.912	1.846	0.071
MD32-1397	1.256	1.188	0.066	1.288	1.220	0.067
MD32-1482	1.911	1.845	0.062	1.943	1.877	0.063
MD33-220	1.327	1.215	0.073	1.359	1.247	0.074
MD33-360	1.321	1.216	0.072	1.353	1.248	0.073
MD33-629	0.947	0.833	0.057	0.979	0.865	0.058

3.11 Age estimations

3.11.1 Approximate ages

As discussed previously, an approximate age can be calculated using the basic equation Age = D_E/D_R for minimum or maximum water level (Section 3.10.5) for each sample, with the D_E and D_R previously estimated in Sections 3.9 and 3.10, respectively (Table 3.15). The Age *se* equals the square root of the sum of squared D_E and D_R *se* values.

Table 3.15: Approximate ages, given by Age = D_E/D_R and Age $se = \sqrt{D_E se^2 + D_R se^2}$, for both water depths (0 m in orange and maximum depth in blue).

	Water depth = 0 metre		Maximum water depth	
	Age		Age	
Sample	Age (ka)	*se* (ka)	Age (ka)	*se* (ka)
MD31-30	5.90	0.73	6.79	0.94
MD31-120	27.0	1.7	29.6	1.9
MD31-530	118	9	127	10
MD31-902	*No estimation*			
MD31-1040	179	18	189	19
MD31-1340	174	12	183	13
MD32-38	5.80	0.92	6.58	1.13
MD32-629	149	9	158	10
MD32-921	148	10	154	11
MD32-1397	97.9	5.9	103	6
MD32-1482	120	13	124	14
MD33-220	61.6	4.4	67.1	5.0
MD33-360	143	9	155	10
MD33-629	172	12	194	15

3.11.2 Correction for contemporaneous sea level

All approximate ages previously calculated were plotted on a sea-level curve for the last 200 ka (Figure 3.28). The intersection between the sea-level curve (red) and the shaded area between + 10 and - 53 m (wavy blue) corresponds to times when the Gulf of Carpentaria was connected to the open ocean. Thus, samples intercepting the sea-level curve on a clear-background, MD31-120, MD31-1040, MD31-1340, MD32-629, MD32-921, MD33-220 and MD33-360, were deposited in Lake Carpentaria. As there is no Lake Carpentaria lake-level curve, the water depth at the time of deposition for these lacustrine samples is difficult to assess. The only available information is a maximum water depth of about 15 m and some evidence of pedogenesis (at 0 m water depth).

The contemporaneous approximate sea-level and its error may be defined for each marine sample from Figure 3.28. These levels are given in metres; the negative values indicate values lower than modern sea level (Table 3.16). Subtracting these sea levels from the modern water depth gives a more realistic water depth at the time of deposition (Table 3.16). This latter value is then used to recalculate a water-depth-corrected D_{Rc}.

Table 3.16: Contemporaneous sea level and height of the water column at the time of deposition.

Sample	Modern water column height (m)	Contemporaneous sea level (m)	Water column height at the time of deposition (m)
MD31-30	59	-12 ± 7	47 ± 7
MD31-530	59	0 ± 5	59 ± 5
MD31-1040	59	-45±15	14 ± 15
MD32-38	64	-10 ± 5	54 ± 5
MD32-1397	64	-28 ±7	36 ± 7
MD32-1482	64	2 ± 2	66 ± 2
MD33-629	68	-40 ± 25	28 ± 25

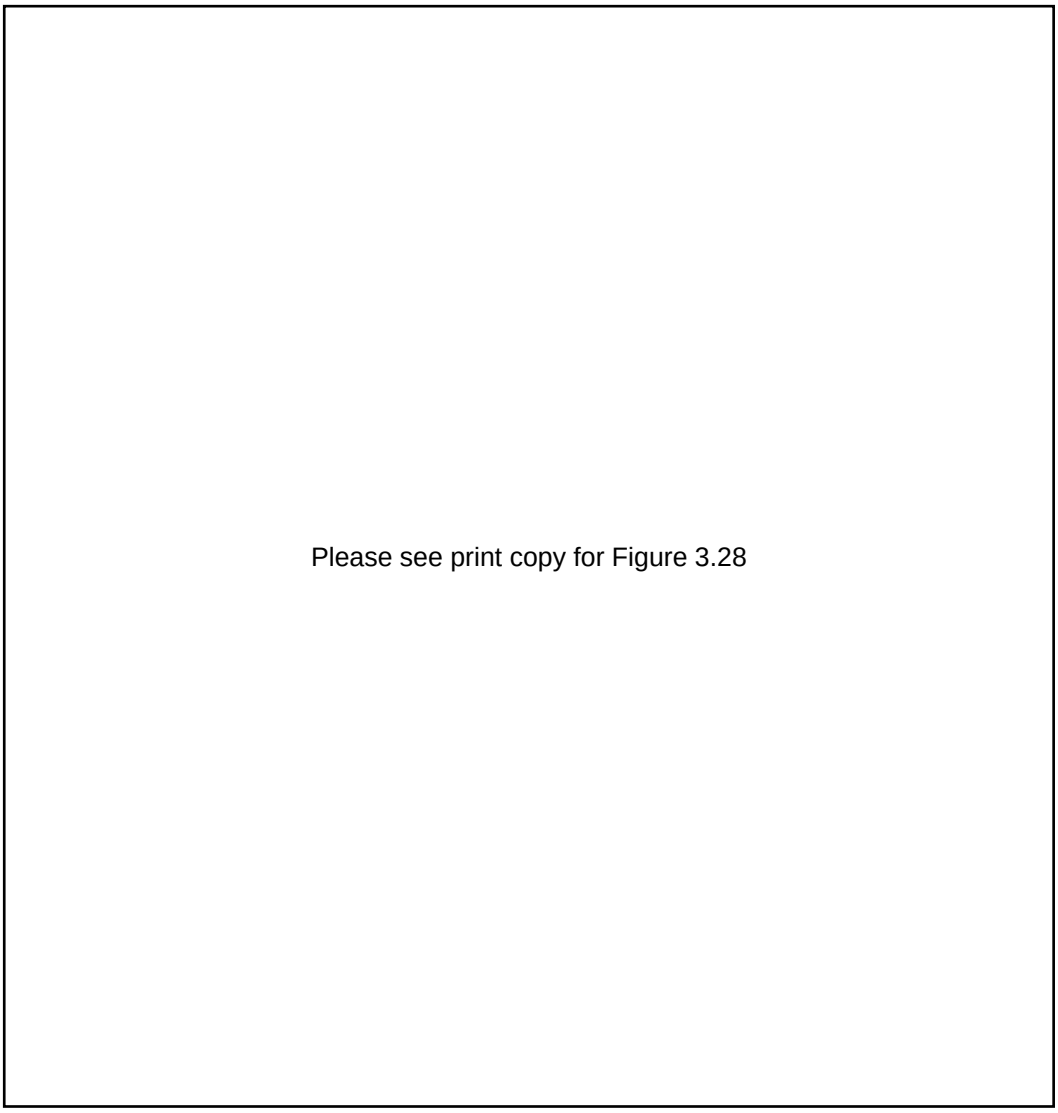
Please see print copy for Figure 3.28

3.11.3 Correction of the water content

The sediment analyses performed by Reeves (2004) was extensively referred to in this section. Each sedimentary log for MD31, MD32 and MD33 established by Reeves (2004) was scrutinised to estimate water depth at the time of deposition for the lacustrine OSL samples and their water contents (Appendix 7).

In fact, if the samples were deposited at the bottom of a water body, and remained under water, there would be little reason to question their modern water contents. However, periods of subaerial exposure of the core sites after deposition for some of the samples could affect their water contents. During these subaerial exposures, sediments are weathered and soils develop. In the low-slope-environment Gulf of Carpentaria, the soil development is principally controlled by climate (rainfall, temperature, and wind), time, and the presence/absence of organisms. The water content was reconsidered for each sample, and a 15% error was assigned to each value to reflect the genuine degree of uncertainty involved in estimating the long-term moisture content.

- Core MD31

6 m deeper than the Arafura Sill

MD31-30 was deposited in a shallow marine environment, no pedogenic intervals were recognised since deposition, thus the water depth previously defined, **47 ± 7 m**, and modern water content, **72 ± 15%**, were used for the age estimation.

MD31-120 was deposited in a lacustrine waterbody with permanent water, probably near the lake margin. There is evidence of reworking probably linked to high energy but no indication of exposure is noticed. An approximate water depth of **3 ± 2 m** is considered appropriate and the modern water content of **23 ± 15%** seems realistic, as there is no evidence for subaerial exposure.

MD31-530 belongs to a unit characterised as a non-marine waterbody, with desiccation and pedogenic features. Furthermore, this sample is within a 5.4 m-thick pedogenic

interval in the core (Figure 3.29), extending above the sample position in the core for more than 60% of the core length. This pedogenic interval is indicative of a significant subaerial exposure of the core site. This condition undoubtedly affected the water content of the sediment. The percentage of the core length not affected by pedogenesis after deposition has been arbitrarily applied to the modern water content to estimate the water content for the D_R calculation. For this level, a water content of **13 ± 15%** (40% of the modern 31.8 ± 1.2%) was used, to take into account this environmental characteristic, and the water depth is estimated to have been closer to **45 ± 5 m** than to the value of 59 ± 5 m listed in Table 3.16.

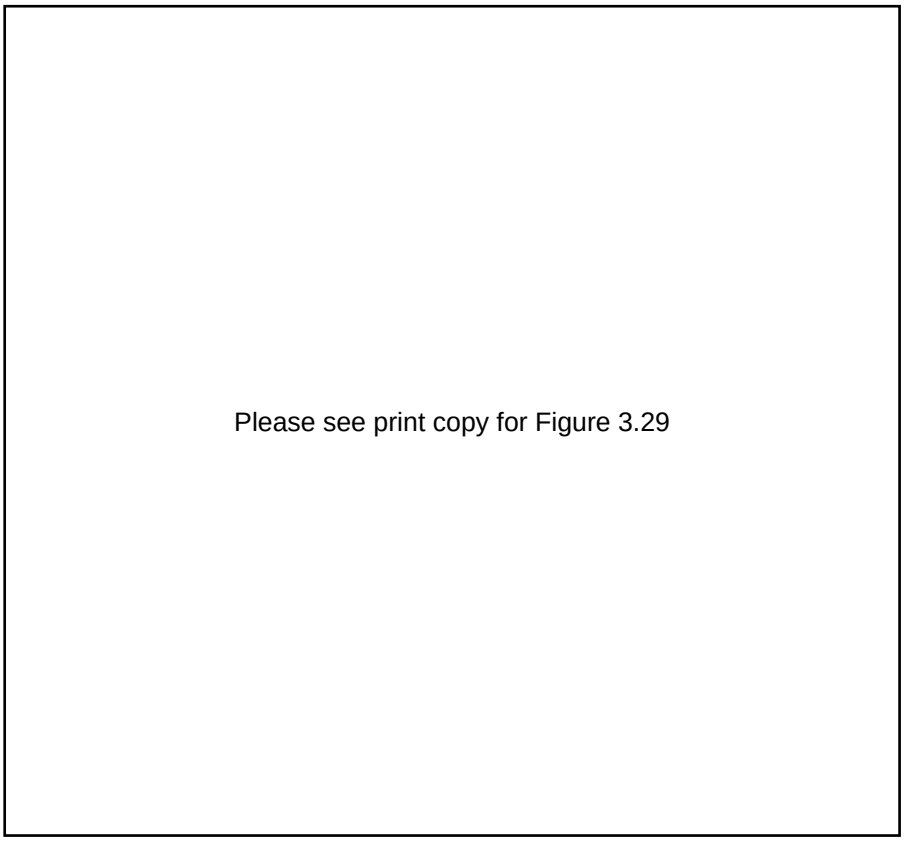

Figure 3.29: West-east cross section within the Gulf of Carpentaria showing the core locations. The wide black bars on each core indicate the positions of pedogenic intervals, and arrows point to data points dated by TL and AAR (from Chivas et al., 2001). Horizontal red bars represent the sample levels used for OSL dating, with the numbers referring to the depths in the core in cm.

MD31-1040 was deposited in an open shallow marginal marine environment, thus the water depth at the time of deposition is estimated to be **14 ± 15 m**. A long-term pedogenic interval spanning about 60% of the post-depositional length of the core is evident. Thus, a water content of **22 ± 15%** (40% of the modern 54.5 ± 4.1%) was used for the D_R estimation to take this environmental characteristic into account.

MD31-1340 is within a unit characterised by sticky dark grey clays and large carbonate concretions, which was interpreted as an evaporative mudflat. The water depth at the time of deposition was evidently shallow and is approximated to be **2 ± 2 m**. A long pedogenic interval exists on the more recent part of the core. The pedogenesis is mainly in the upper half of the core above the sample and it should not have significantly affected the water content of the sample, which was deeply buried at the time of the subaerial exposure of the core site. Thus the modern water content of the sample, **39 ± 15%**, was accepted as an estimation of the water content at the time of deposition.

- Core MD32

11 m deeper than the Arafura Sill

MD32-38 was deposited in a shallow marine environment, no evidence of pedogenesis was recognised since deposition, thus the water depth previously defined, **54 ± 5 m**, and the modern water content, **55 ± 15%**, were used for the age estimation.

MD32-629 was deposited in a mudflat environment by ephemeral waters, with evidence of contraction of the waterbody with exposed lake margins. The water depth at the time of deposition was evidently shallow and is estimated to be **2 ± 2 m.** This sample is also within a 4.3 m-thick pedogenic interval that continued after sample deposition for more than 40% of the core length, indicating a post-depositional subaerial exposure of the core site (Figure 3.29). This condition undeniably affected the water content of the sediment therefore an approximate value of **24 ± 15%** (60% of the modern 40.3 ± 0.4%) was used for the D_R calculation.

MD32-921 was deposited in a brackish lagoon and the water depth at the time of deposition is estimated as **19 ± 10 m**. A long-term pedogenic interval spanning over 50% of the post-depositional length of the core is recorded above the sample position in the

core. Thus, a water content of **31 ± 15%** (50% of 62.3 ± 6.1%) was used for the D_R estimation to take this environmental characteristic into account.

MD32-1397 is within a unit deposited in a fluctuating environment, the water depth at the time of deposition was thus approximated by the value previously defined: **36 ± 7 m** (Table 3.16). The orange stained material present in this unit that was recognised originally as pedogenic evidence (Chivas et al., 2001) is now attributed to transport of iron oxide as part of the sediment, rather than autochthonous production (Reeves, 2004). No weathering condition affected the sample following deposition, thus the modern water content, **27 ± 15%**, was used to approximate the water content at the time of deposition.

MD32-1482 was deposited in the same unit as MD31-1397, the only difference being the more pronounced orange staining, fewer mica, higher quartz content and absence of microfauna that indicate a more dynamic environment. The water depth at the time of deposition was thus estimated to be **66 ± 2 m** (Table 3.16). For similar reasons as applied to the previous sample, the modern water content, **24 ± 15%**, was used to approximate the water content at the time of deposition.

- Core MD33

15 m deeper than the Arafura Sill

MD33-220 was deposited in a non-marine shallow environment with permanent water, after a brief renewed influx of marine water. The water depth at the time of deposition for this sample has been estimated at **13 ± 2 m**. No pedogenic intervals were recognised since deposition, thus the modern water content of **43 ± 15%** was used for the D_R calculation.

MD33-360 is within a unit deposited in an enclosed embayment with slight marine influence and is characterised by later drier conditions and indications of pedogenesis (Figure 3.29). Pedogenic beds recognised in this core, collected in the deepest part of the Gulf of Carpentaria, indicate the dryness of the entire basin for certain periods. During these phases, the Gulf environment might have been similar to the modern Lake Eyre, with episodic filling, salt flats and gypsum deposition. The estimated water depth at the time of deposition is **10 ± 2 m**. The 2.6 m-thick pedogenic interval continues above the sample position in the core for about 35% of the core length. This condition would have

affected the water content of the sediment. For this level, a water content at the time of deposition of **27 ± 15%** (65% of the modern 41 ± 1.6%) has been used for the D_R estimation.

MD33-629 was deposited in a contracted non-marine environment with evidence of exposed margins, prior to a 2.6 m-thick pedogenic interval (Figure 3.29). The latter represents about 50% of the above-core length and has undeniably affected the water content of the sediment. For this level, a water content at the time of deposition of **7 ± 15%** (50% of 14 ± 2%) has been used to take into account this environmental characteristic. The water depth at the time of deposition is estimated to have been **28 ± 25 m.**

3.11.4 Corrected ages

The D_R (green) and age (red) values were recalculated for each sample using the corrected water depth and content (blue) for each sample and the formula previously devised in Sections 3.10.5 and 3.3.3 (Table 3.17).

Table 3.17: The final D_R (green) and ages (red) with their respective *se* values, and the water depths (dark blue) and contents (light blue) used for the calculations. In bold are the contentious levels MD32-629 and MD32-921, which do not follow a normal age-depth progression.

	Water depth (m)	*se*	Water content (%)	*se*	D_R (Gy.ka^{-1})	*se*	Age (ka)	*se*
MD31-30	47	7	72	15	0.659	0.092	6.77	1.02
MD31-120	3	2	23	15	1.499	0.139	28.5	3.0
MD31-530	59	5	13	15	1.610	0.168	106	13
MD31-902	*no estimation*							
MD31-1040	14	15	22	15	1.467	0.143	143	19
MD31-1340	2	2	39	15	1.282	0.112	178	18
MD32-38	54	5	55	15	0.836	0.119	6.56	1.17
MD32-629	**2**	**2**	**24**	**15**	**1.731**	**0.137**	**134**	**13**
MD32-921	**19**	**10**	**31**	**15**	**2.354**	**0.127**	**121**	**9**
MD32-1397	36	7	27	15	1.225	0.132	103	11
MD32-1482	66	2	24	15	1.876	0.138	124	16
MD33-220	13	2	43	15	1.272	0.113	65.8	6.6
MD33-360	10	2	27	15	1.438	0.138	135	14
MD33-629	28	25	7	15	0.943	0.188	178	36

For cores MD31 and MD33, the corrected ages increase with depth as expected for a normal sedimentation sequence. However, core MD32 has two samples (at 629 and 921 cm) that are 'out of sequence' with respect to their calculated ages.

3.11.5 Discussion

All OSL results, except for MD32-629 and MD32-921, are compatible with the ages estimated previously for all three cores by ^{14}C (Appendix 1.1) for the younger levels (Figure 3.30) and are within the error margins of Amino Acid Racemisation (AAR) and Thermoluminescence (TL) ages (Appendix 1.2) for the deeper levels of MD32 (Figure 3.31). The AAR dates are somewhat older than the OSL results suggest. This difference may be due to the lack of calibration samples from the Gulf of Carpentaria for AAR dating. A Holocene radiocarbon-calibrated specimen from Princess Charlotte Bay (Queensland) was utilised instead. This area, situated in the Coral Sea, experiences different climatic and oceanic regimes to the Gulf of Carpentaria.

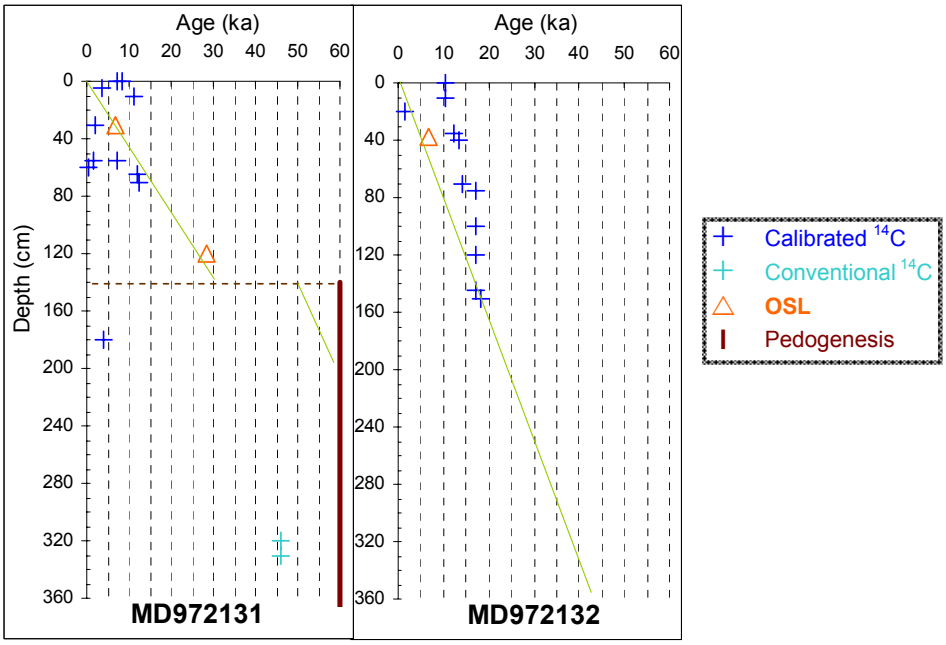

Figure 3.30: Diagram showing the OSL and ^{14}C ages (orange and blue, respectively) from the top of two cores from the Gulf of Carpentaria: MD31 and MD32. Error bars are plotted only when larger than the size of the symbols. The green lines symbolise mean sedimentation rate. The horizontal brown dotted line represents a time of subaerial exposure.

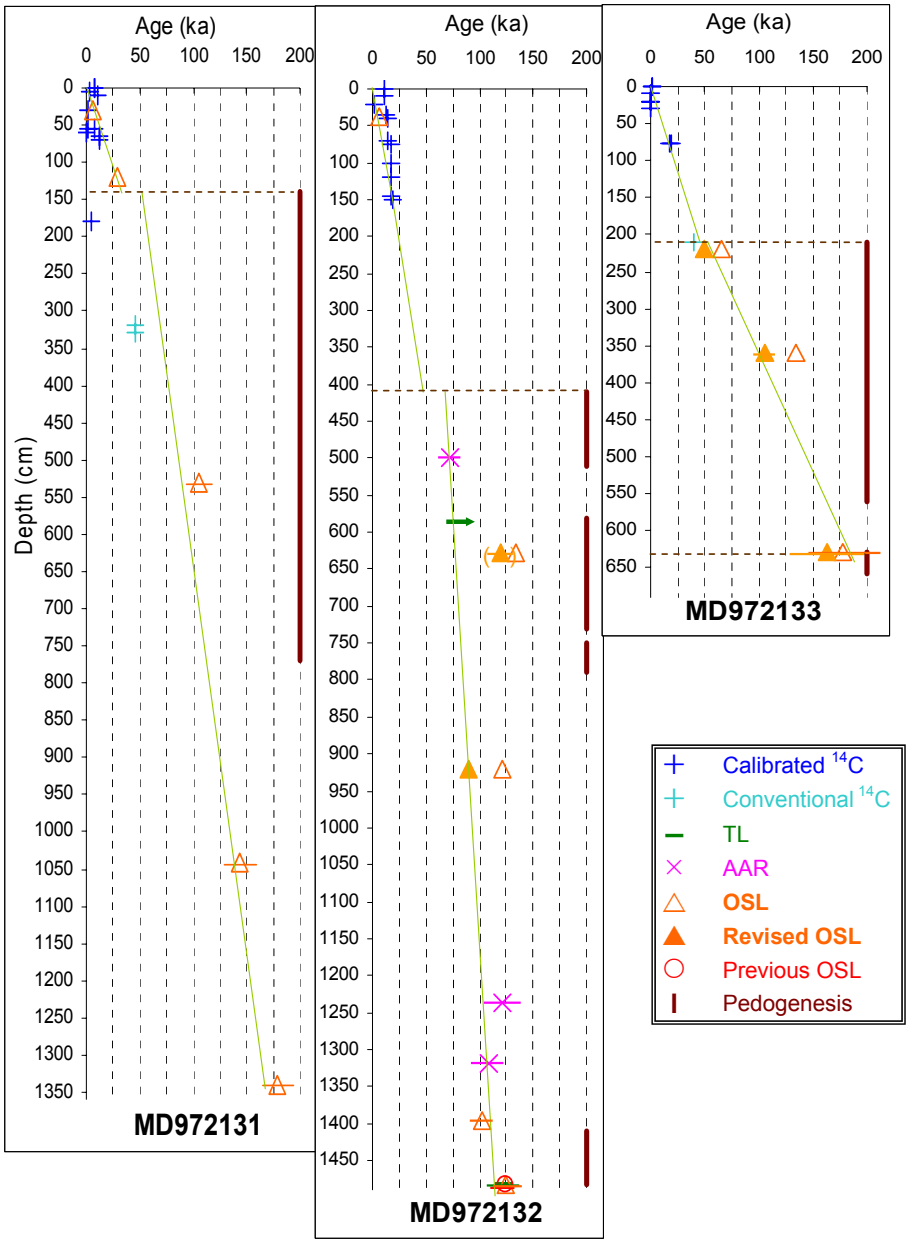

Figure 3.31: Diagram showing the OSL ages (orange and red) and all independently measured ages using other techniques (^{14}C, blue; AAR, pink and TL, green) from three cores from the Gulf of Carpentaria: MD31, MD32 and MD33. Error bars are plotted only when larger than the size of the symbols. The green arrow indicates a TL result in MD32 at 5.82 m depth in the core that was older than 64 ± 7 ka. The green lines symbolise mean sedimentation rate. The horizontal brown dotted lines represent times of subaerial exposure. Revised OSL ages are explained in the following section.

The OSL ages are directly proportional to the D_E and inversely proportional to the D_R. All D_E values were measured and analysed in the same way, so there is no reason to doubt the D_E estimates for MD32-629 and MD32-921. The overestimation by OSL of the age of samples MD32-629 and MD32-921 is of the order of 100% and 50%, respectively, assuming a constant sedimentation rate (Figure 3.31). Because the D_R estimation depends on several variables with large uncertainties, such as radionuclide activities, equilibrium conditions, water contents and water depths at deposition, the D_R calculation is now reassessed to ensure that all parameters were correctly gauged.

- Radioactivity

All uncertainties regarding the environmental radioactivity have been assessed already and taken into account for the D_R calculation, and there is no reason to consider that only samples MD32-629 and MD32-921 were incorrectly estimated. Nuclides from both the U and Th decay chains are in secular equilibrium, within analytical uncertainty (Table 3.10). Furthermore, U, Th and K activities for the MD32-629 level (36.7 ± 0.8, 55.2 ± 2 and 136.8 ± 2.7 $Bq.kg^{-1}$, respectively) and the MD32-921 level (103.1 ± 1.6, 47.4 ± 2.8 and 90.3 ± 2.9 $Bq.kg^{-1}$, respectively) are higher than the average nuclide activities for all samples (34.5 ± 1.1, 40.2 ± 2.4 and 91.5 ± 2.6 $Bq.kg^{-1}$, respectively), so an overestimation of the activities for MD32-629 and MD32-921 would result in an underestimation of the age, rather than an overestimation.

- Water

The water depths at the time of deposition of samples MD32-629 and MD32-921 were estimated to be 2 ± 2 and 19 ± 10 m, respectively (see above), and the water content was lowered by 40% and 50%, respectively, compared to the modern water contents. Both corrections were applied so as not to underestimate the environmental and cosmic-ray dose rates during the pedogenic interval that occurs in the core. These corrections tend to increase the D_R and thus decrease the age. Furthermore, a simulation with a water depth of 0 m (Table 3.14) and water content equal to zero gives an age of 104 ± 12 ka for MD32-629 and 87 ± 8 ka for MD32-921, which are still overestimated compared to the ages of other levels in core MD32. It is concluded that the D_R has been appropriately estimated and that the age overestimations of MD32-629 and MD32-921 are due to some other parameters.

From the general logging of the cores (Chivas et al., 2001), it is clear that the contentious sample MD32-629 is within a 4.3 m-thick pedogenic interval (Figure 3.29). However,

MD31-530 and MD33-360 are also found in 5.4 and 2.6 m-thick intervals, respectively, although their ages are seemingly not overestimated.

The sedimentary unit from which MD32-629 was sampled is characterised by reworking and transportation of sediment around the exposed margins of the basin (Reeves, 2004, p. 90). This unit is composed of dark-grey silty clays with orange mottling and includes abundant subangular and subrounded quartz grains, pinkish concretions, and reworked microfauna. The quartz grains are commonly yellow-stained (Table 3.1), which could explain the incomplete bleaching of this population. The low overdispersion (10.4%) of the D_E estimates is not inconsistent with the uniformly incomplete bleaching of a single population of stained quartz grains, whereas a mixture of populations of different ages would be expected to produce a higher overdispersion.

MD32-921 was sampled from a shell layer deposited in a brackish organic-rich and anoxic environment (Reeves, 2004, p.88). Such an environment is likely to be characterised by turbid water that allows only partial bleaching of the quartz grains. Once again, because of the low level of overdispersion of the D_E estimates (16.5%), uniformly incomplete bleaching of a single population is considered the most likely explanation for the unrealistically high D_E values.

These explanations are offered as the most probable reasons for the D_E over estimations for MD32-921 and MD32-629. The flaw is not in the measurement itself, but in the intrinsic quality of the samples, which were poorly bleached. For this reason, the OSL ages estimated for MD32-629 and MD32-921 using the CAM for D_E estimation represent maximum ages. Reassessing the D_E values for each of these samples using the MAM (Table 3.18) allows the definition of the lowest D_E value, which potentially corresponds to the most fully bleached aliquots. These should give more realistic ages, which are plotted as revised OSL ages (filled symbols) in Figure 3.31.

Other samples from core MD33 selected for OSL dating were deposited in similar environmental conditions to MD32-921 (MD33-220) or display similar staining of the quartz grains to MD32-629 (MD33-360 and MD33-629). The quartz grains of these samples were noted as greyish after physical preparation. The D_E values are also reassessed for these three levels of MD33 using the MAM (Table 3.18) and the resulting ages are plotting as revised OSL ages (filled symbols) in Figure 3.31. For MD32-1482, which is also characterised by iron-stained quartz grains, the MAM is not appropriate for

determining a more accurate D_E value, because of the probable contamination of the sample by laboratory-bleached grains.

Table 3.18: Summary table showing CAM (green) and MAM (blue) D_E values, and revised OSL ages (red) for five samples from two cores, MD32 and MD33, from the Gulf of Carpentaria, which were deposited in fluctuating environments. The two levels in bold were sampled from a shell layer, whereas the other samples contain iron-stained quartz.

	Over-dispersion (%)	Model	mean D_E (Gy)	se (Gy)	Model	mean D_E (Gy)	se (Gy)	Age (ka)	se (ka)
MD32-629	10.4	CAM	233	12	MAM	208	19	120	15
MD32-921	**16.5**	**CAM**	**284**	**16**	**MAM**	**209**	**15**	**89**	**8**
MD33-220	**18.4**	**CAM**	**83.7**	**3.9**	**MAM**	**63.2**	**2.7**	**49.7**	**4.9**
MD33-360	11.1	CAM	194	6	MAM	151	3	105	10
MD33-629	7.3	CAM	168	7	MAM	153	13	163	35

The revised OSL age for MD32-921 is compatible with other ages estimated for core MD32, whereas the revised OSL age for MD32-629 is still overestimated (Figure 3.31). This is probably due to the drying conditions that occurred at the MD32 site after deposition of the MD32-629 level, which may have induced weathering and mobilisation of lithogenic radionuclides responsible for the environmental dose rate. Accordingly, the age calculated for sample MD32-629 is deemed unreliable and will not be used in the interpretation of the Gulf of Carpentaria history. This analysis will be completed in Chapter 5 in light of the environmental changes recorded by the nannofossil assemblages. However, other information can be drawn from this chronological framework set up for the Gulf of Carpentaria sediments.

A model of mean sedimentation rate at each core site is drawn in Figure 3.31, taking into account periods of non-continuous deposition during subaerial exposures. This model gives mean sedimentation rates of about 8 $cm.ka^{-1}$, 12 $cm.ka^{-1}$, and 4 $cm.ka^{-1}$ at the MD31, MD32 and MD33 locations, respectively. The mean sedimentation rate for each site allows an estimation of the time during which subaerial exposure prevailed. These periods lasted about 20 ka at the MD31 site after deposition of the 140 cm level, about 25 ka at the MD32 site after deposition of the 410 cm level, and about 5 ka at the MD33 site after deposition of the 210 cm level. All of these aerial exposures began at about 70–50 ka and are at least partially contemporaneous.

3.12 Conclusions:

This chapter has shown the usefulness of the OSL dating technique for sediment cores. Because the Gulf of Carpentaria was exposed during low sea level, the water content history of each sample and the height of the water column on top of the sediment at the time of deposition were assessed individually. These precautions prevented the underestimation of the D_R which would result in an overestimation of the sample age. Particular attention was given to the determination of the relevant radionuclide activities for D_R estimation, including an evaluation of secular equilibrium in the ^{238}U and ^{232}Th chains.

From the thirteen samples processed, twelve ages ranging from 7 ± 1 to 178 ± 18 ka have been estimated over three cores from the Gulf of Carpentaria. These ages allow the establishment of a time frame for the Gulf of Carpentaria that is used later in this study to help with the interpretation of the palaeoenvironments reconstructed by means of nannofossil assemblages. The ages increase with depth in each core.

Core MD33 was collected in the deepest part of the Gulf and has an average sedimentation rate of about 4 $cm.ka^{-1}$, whereas cores MD32 and MD31 show higher average rates of around 12 $cm.ka^{-1}$ and 8 $cm.ka^{-1}$, respectively. These results are consistent with the modern sedimentation rate observed in the Gulf of Carpentaria, which shows the centre of the basin being depleted of sediment relative to shallower areas. The partly contemporaneous subaerial exposures of 5, 20 and 25 ka duration at the MD33, MD31 and MD32 sites, respectively, are consistent with an increase of exposure time proportional to the distance from the depocenter of the basin and/or to the modern depth of the site. A reduction in the sedimentation rate starting after these exposure episodes, which began about 70–50 ka ago, is noted in the MD31 and MD32 cores, but this needs to be confirmed by further dating of other levels.

Chapter 4:

Nannofossils

4.1 Introduction

Nannoplankton (from the Greek nanno = dwarf) is a collective term that includes the microscopic unicellular algae belonging to Class Prymnesiosphyceae, and co-occurring, but morphologically dissimilar, forms of uncertain affinity, that have left a fossil record at least since early Jurassic through to Recent marine sediments (Haq, 1984). The minutely sized ubiquitous calcareous nannofossils have been intensively studied since the early 1930's and have come to be heavily relied upon, in the past 40 years, for determining the age of marine sequences. In this study concerned with the Late Quaternary, nannofossil assemblages and distribution are used as an environmental proxy rather than for their biostratigraphic potential.

Coccolithophorids are simple algae that secrete minute calcified plates called coccoliths, with sizes ranging from 1 to 20 µm. This nannoplankton inhabits the euphotic zone in marine water and together with diatoms and dinoflagellates, comprises the bulk of the marine phytoplankton. Over 53 metres of core sediment were collected in the Gulf of Carpentaria, with part of this sedimentary record being of marine origin (Chivas et al., 2001). It was thus natural and logical to investigate coccolith assemblages to gain information on the marine palaeoenvironments in the Gulf over the past 180 ka. Because of the length of marine sediment core that needed to be analysed, and because of the domination of the coccolith assemblages by one or two species, two investigation methods where chosen: a high-resolution optical analysis of one of the cores (MD32) and an automated exploration over all six cores.

This chapter is divided into three parts: background, optical, and automated optical investigations, and provides a comparison of the optical and software-based results and interpretation of the results in terms of palaeoenvironmental changes recorded in the Gulf sedimentary records.

The first part of this chapter presents an historical review of calcareous nannoplankton, and the modern state of knowledge in terms of biology, ecology and modern distribution. Then the definition of the four typical nannofossil ecological groups from Young (1994) is presented and their importance for the reconstruction of the palaeoenvironments of the Gulf of Carpentaria is discussed.

The second section deals with the investigation of coccolith assemblages. The optical high-resolution investigation on core MD32 is described, together with an explanation about core selection and presentation of the materials and methods. Although core MD32 is dominated by 1-2 coccolith species, a full list of the 34 species is provided and SEM images are used to illustrate representative species found in a typical high-diversity sample. The up-core distribution of taxa found in MD32 is summarised diagrammatically. Following this is a description of SYRACO, the automatic coccolith recognition software used for this investigation, and the selection of the samples processed using this technique is discussed. Procedures that include data reprocessing to obtain more accurate results are detailed, together with the optical correction to validate the method. Finally, the results of the automated optical investigation are presented for all six cores. This section is concluded with a comparison between the traditional optical observation and the modern automated optical investigation for core MD32. This comparison is undertaken to validate the automated coccolith investigation procedure for sedimentary materials recovered from the Gulf of Carpentaria.

In the final part, the palaeoenvironmental succession in the Gulf of Carpentaria as deduced from the variation of coccolithophorid assemblages, is established.

4.2 Historical background

This section presents a brief history of coccolith research from their first sighting to modern multidisciplinary studies using coccoliths.

- Discovery

Coccoliths were first recognised by the eminent microbiologist Ehrenberg, who reported to the Berlin Academy of Sciences on 18 August 1836 his observation in chalk samples from the Island of Rügen of some elliptical, flattened discs, having one or several concentric rings on their surface (Ehrenberg, 1836). He described and illustrated them and considered that they had an inorganic origin similar to crystalline concretions. He tried unsuccessfully to produce them in his laboratory (Ehrenberg, 1854). It was not until the late 1850's that Huxley reported the discovery of Ehrenberg's "inorganic crystalloids" in deep-sea oozes collected during soundings taken by H.M.S. *Cyclops* in preparation for laying the first transatlantic telegraph cable, and called them coccoliths (Huxley, 1858).

- Nature

In 1861 Wallich, after being aboard H.M.S *Bulldog,* which was taking soundings for another transatlantic cable, reported to the Annals of Natural History (London) that coccoliths not only occur in the free state but as adjuncts to minute spherical cells that he named coccospheres (Figure 4.1). He suggested them to be a larval condition of some of the Foraminifera because of their abundant co-variation, the existence of coccoliths attached to foraminifer shells and the similarity between the coccospheres and the cells of juvenile globigerinids (Wallich, 1961). A few months latter, Sorby argued that coccoliths have a shape entirely unlike anything that could result from inorganic crystallisation. He found that coccoliths were not flat discs, but concave on one side and convex on the other side, and originated from small hollow spheres (Sorby, 1861). This author regarded them as an independent organism based on the differences in the optical character of the calcite of their skeleton, compared to those of the foraminiferal test. Sorby also pointed out that coccoliths represented a large part of the chalk that should thus be thought to have an organic origin as well.

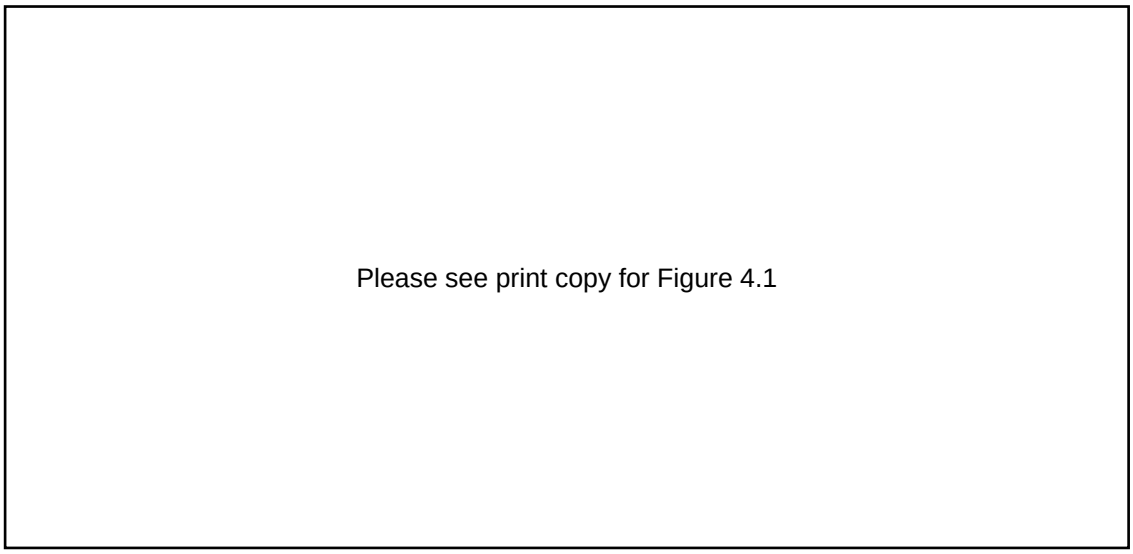

Figure 4.1: First illustration of a coccosphere showing coccoliths arranged at nearly regular intervals upon its outer surface and its defined outer wall (Wallich, 1961).

- Description

A few years later, Huxley (Huxley, 1868) presented a clear description of coccoliths and coccospheres and suggested that they constituted the microskeletal element of a sea-floor hugging, worldwide gelatinous protoplasm genus, *Bathybius*. This idea was accepted by most biologists but, for example, Thompson, who accepted the existence of *Bathybius*, but believed that coccoliths were the joints of minute one-celled planktonic algae that were used as food for the protoplasm (Thompson, 1874). During the expedition of H.M.S. *Challenger* (1872-76) to seek *Bathybius* on the sea floor, Murray and his colleagues onboard realised that the jelly-like layer on the surface of the mud in the bottle-stored samples preserved with alcohol, was a precipitate of calcium sulfate (Murray, 1876). He also credited minor amounts of organic matter in the sediment itself for the staining of the solution that mislead Huxley to define *Bathybius* as protoplasm. Wallich, who had been one of the few detractors of the *Bathybius* theory, published a paper in 1875 effectively annulling the concept (Wallich, 1875).

- Origin and role

Wallich in a further paper restated that coccoliths derive from their parent coccospheres, and have none of the characters of true 'cells' (Wallich, 1877). This author also noted that the attachment to a coccosphere is the normal state for a coccolith, and that the relative abundance of coccospheres indicates the degree of preservation of the assemblage. In this paper he gave a formal description of the two different species he had found:

Coccosphaera pelagicus and *carterii*, together with their distribution so far observed (Figure 4.2).

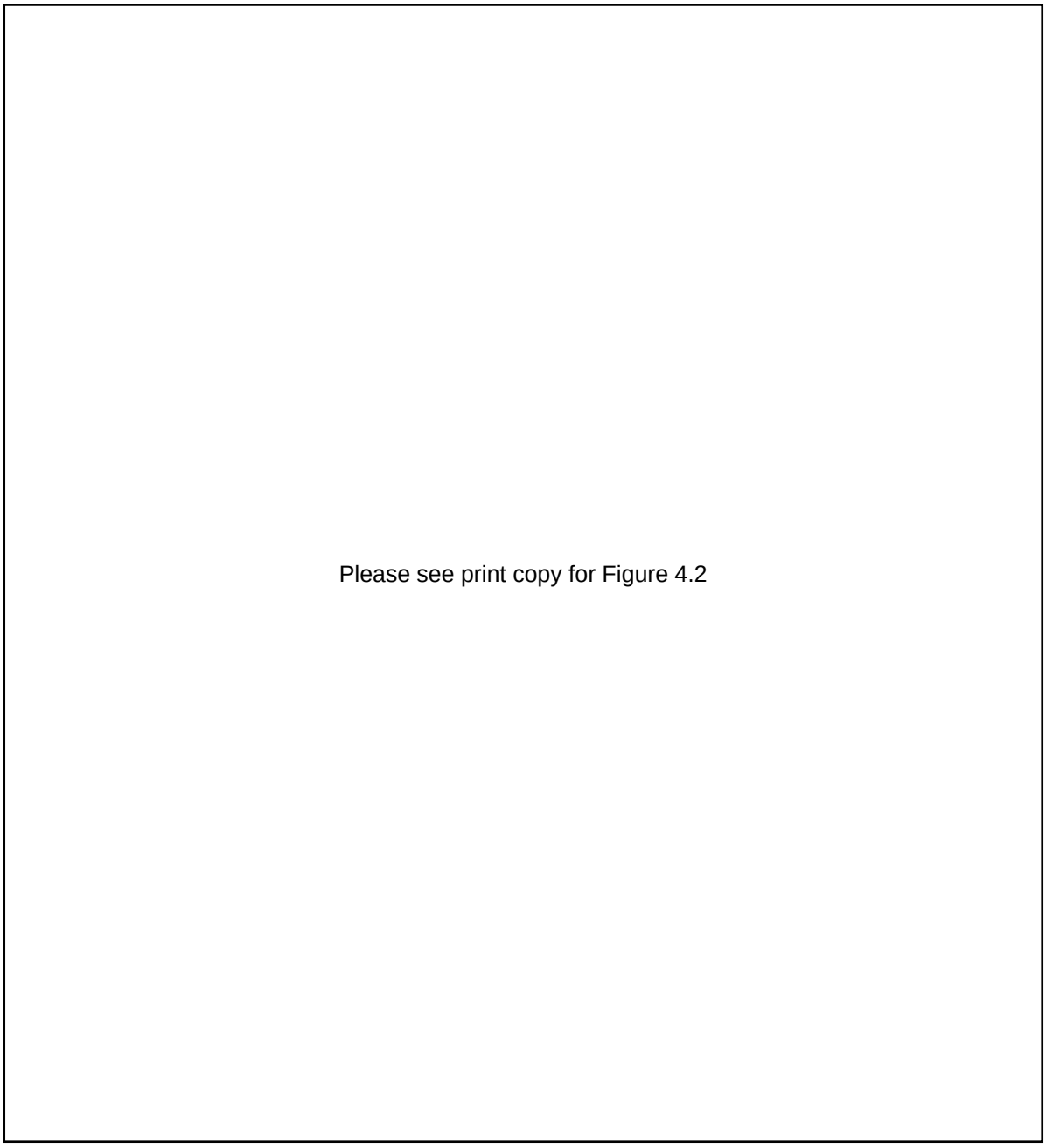

Figure 4.2: Coccospheres and coccoliths of *Coccosphaera pelagica* (1-7) and *carterii* (8-11) (Wallich, 1877)

The debate on the origin of coccoliths was largely settled in 1891 after the publication of the *Challenger* expedition report where Murray and his co-workers resolutely stated that coccospheres were the skeletons of minute algae (Tizard et al., 1885; Murray and

Renard, 1891). They also noted that the coccospheres were larger in size and more numerous in colder waters than in warmer waters. Finally they reported a variety of nannoflora in deep-sea oozes and supplied a basic biographic zonation of living algae (Murray and Renard, 1891).

Subsequently in 1898, Murray and Blackman were the first to suggest that the interlocking arrangement of coccoliths (Figure 4.3) would be a very efficient means of protection for the organism. They observed the protoplasmic body but could not see a nucleus. Coccolith nuclei were eventually observed and described by Ostenfeld in 1900.

Please see print copy for Figure 4.3

Figure 4.3: Plate clearly showing how coccoliths lock together to form a coccosphere (Murray and Blackman, 1898).

- Inventory

Lohman (1902 et seq.) and Ostenfeld (1899 et seq.) were the initiators of the fascinating work of describing living and fossil coccolithophorids, and were followed by Arkehangelsky (1913 et seq.) and Schiller (1913). Schiller, also collected living coccolithophorids, and his collection remains useful to the present day (Schiller, 1930). The cataloguing really began in the late 1920's and 1930's led by Kamptner (Austria), Deflandre and Barnard (France) and Braarud and his colleagues (Norway) (Haq, 1984;

Winter and Siesser, 1994b). Winter and Siesser produced a major book in 1994, including a classification (Jordan and Kleijne, 1994) system for living coccolithophorids together with an atlas (Winter and Siesser, 1994a) and their biogeography (Winter et al., 1994) in ocean waters (Winter and Siesser, 1994b).

- Imagery

Deflandres and Fert were the first to produce images of coccoliths using an electron microscope, 100 years after their first description (Deflandre and Fert, 1954). The use of a TEM (Transmission Electron Microscope) allowed Black a decade later to describe the fine structure of the mineral parts of coccolithophorids (Black, 1963) and to produce several electron micrographs of coccoliths (Black, 1965, 1972) that were among the best available till recently (Haq, 1984). The introduction of the SEM (Scanning Electron Microscope) a few years later gave another dimension to the observation of the ultra-fine structure of coccoliths (Hay and Sandberg, 1967). In 1994, Winter and Siesser published a remarkable book on modern coccolithophorids including 140 SEM images of species in the taxonomic and atlas chapters (Winter and Siesser, 1994b). In 2002, Young created a guide to calcareous nannopankton taxonomy and he established a website with all the provisionally selected images of coccoliths and coccospheres (Young, 2002).

- Taxonomy

Coccolithophorid taxonomy history is complex and has continually evolved with knowledge of their biology and phylogeny whereas the first classifications were based on morphological characters. Because of the uncertainty about the origin of coccoliths, it was not before 1902 that Lohman included them in the Mastigophoren superclass, alongside the chrysomonads (Lohman 1902). Sixty years later, a new class was created: Haptophyceae (Christensen, 1962) for this unique species with a smooth third flagella (Parke et al., 1955). In 1976, Hibbert changed this latter name to Prymnesiophyceae after the genus *Prymnesium*, in accordance with the revision of the International Code of Botanical Nomenclature (Jordan and Green, 1994). In his review of the Prymnesiophyceae, Hibbert (1980) divided the class into four orders: Isochrysdales, Prymnesiales, Pavlovales and Coccosphaerales (Jordan and Kleijne, 1994). Edvardsen (2000) proposed a taxonomic revision of the division Haptophyta; resulting in coccolithophorids now belonging to the class Prymnesiophyceae that also feature non-calcifying organisms. The subsequent demonstration that holococcolithophorids represent stages in the life cycle of oceanic heterococcolithophorids creates a real necessity for a

global revision of coccolithophorid taxonomy (Cortés, 2000; Cros et al., 2000). Sáez et al. (2004) by means of a major phylogenetic study that compares the gene sequences from 125 haptophytes to those of over 300 published and unpublished algae, started reviewing the phylogeny of the Haptophyta. These latter studies revealed the existence of coccolithophorid pseudo-cryptic species, where individuals belonging to morphologically recognised species are found to be genetically distinct (Sáez and Lozano, 2005).

- Diversification of interest

Systematic descriptions over the years engendered many other studies on aspects of coccolithophorids such as their biology (Dixon, 1900; Weber Van Bosse, 1901; Lohman 1902); physiology and ecology, with the first culturing of coccolithophorids in the laboratory revealing the two different phases of their life cycle (Parke and Adams, 1960); and the influence of environmental factors such as salinity, temperature, and nutrient availability on the growth of coccoliths (Watabe and Wilbur, 1966).

The importance of nannoplankton as a biostratigraphic tool was pointed out in the mid 20th century by Bramlette and Riedel (1954), and there followed numerous studies. Today nannoplankton are well established in the scientific community as a broad biostratigraphic tool spanning from Jurassic to recent. One of the most significant publications on their biostratigraphic potential is the book *Nannofossil Biostratigraphy* by Haq (1983).

- Multidisciplinary project

In the early 1990's, Westbroek initiated the first important multidisciplinary research project that focussed on *Emiliania huxleyi.* Many other similar projects flourished in the following years, such as GEM (Global *Emiliania* Modeling) and CODENET (COccolithophorid Evoluntionary BioDiversity and Ecology NETwork, 1998-2001). The latter focussed on six species (*Gephyrocapsa oceanica*, *Coccolithus pelagicus*, *Calcidiscus leptoporus*, *Umbilicosphaera foliosa*, *Helicosphaera carterii* and *Syracosphera pulchra*) that were cultured for the purpose (CODENET, 2002). This project generated about 100 papers on various themes such as biology, physiology, molecular phylogeny, taxonomy, evolutionary diversity and development, biochemistry, bloom fluxes and palaeoproxy studies (refer to Thierstein and Young, 2004a, for more details). Both ecological and palaeoproxy aspects of coccoliths are detailed in the following section.

- Application

By way of a summary statement, coccolithophorids are, for biologists, the main open ocean marine producer, with a distinctive role in the plankton ecosystem; and for geochemists, a key in the global carbon, carbonate and sulfur cycles. The coccoliths they produce constitute, for marine geologists, the single most important component of the deep-sea oozes and chalks and provide key flora, isotopic and biomarker signals for interpreting global change in the geological record. For palaeontologists, their exceptional fossil record makes them an outstanding biostratigraphic group, with unusual potential for testing evolutionary hypotheses (Thierstein and Young, 2004*a*).

4.3 Modern understanding

This section gives a broad view of modern knowledge about coccolith biology and ecology. Four main coccolith groups are herein defined.

4.3.1 Coccolith biology

Coccolithophorids include all haptophyte algae possessing calcified scales at some stage of their life. Among the approximately 300 haptophytes worldwide, 200 are indeed coccolithophorids (Jordan and Chamberlain, 1997). Recent technological methodologies and the establishment of multidisciplinary projects have considerably increased our understanding of coccolithophorids. Their biology is better understood even if for Brownlee and Taylor (2004) coccolithophorid cell biology is still in its infancy. A diagrammatic representation of the cell structure of a coccolithophorid showing morphological features and coccolith types from various species is presented in Figure 4.4.

Intensive recent cultures and meticulous observations of coccospheres in natural samples have confirmed in recent years that holococcolithophorids and other "anomalous" coccolithophorids are not autonomous but haploid stages in the life cycle of heterococcolithophorids (Cros et al., 2000; Laguna et al., 2001; Billard and Inouye, 2004; Noel et al., 2004; Geisen et al., 2004; Houdan, 2004). An example of the complexity of the life cycle of a coccosphere is shown in Figure 4.5.

4.3.2 Coccolithophorid ecology

- <u>Coccolith function</u>

Soon after the understanding of the relation between coccoliths and coccospheres was gained, specialists speculated on the function of coccoliths. Protection against predation (Murray and Blackman, 1898; Manton, 1986) and floating-regulation/nutrient absorption by forced-convection (Munk and Riley, 1952; Hutchinson, 1967; Walsby and Reynolds, 1980) were for a long time the most commonly suggested roles.

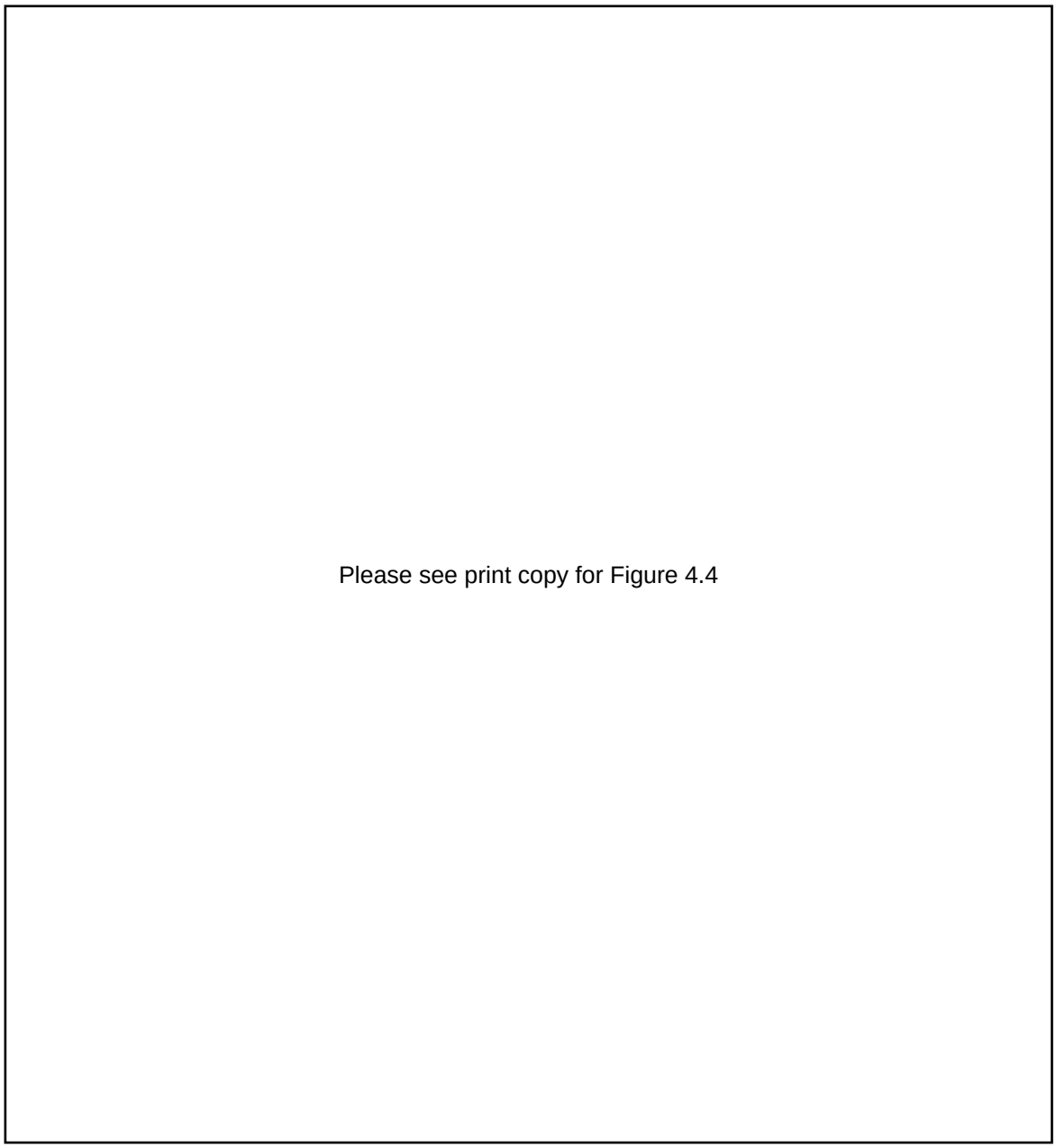

Figure 4.4: Diagrammatic representation of the cell structure of a coccolithophorid. Morphological features seen in various coccolithophorids have been combined in a single figure. Various types of coccoliths are drawn as silhouettes. Two types of coccolith-forming vesicles found in *Pleurochyris* (blue) and *Emiliania* (green) are illustrated. Pyrenoid (P1) is typical in the coccolithophorids and pyrenoid (P2) is seen in *Emiliania* and *Gephyrocapsa*. Heterococcoliths are shaded black and holococcoliths are shaded by a lattice pattern (Billard and Inouye, 2004).

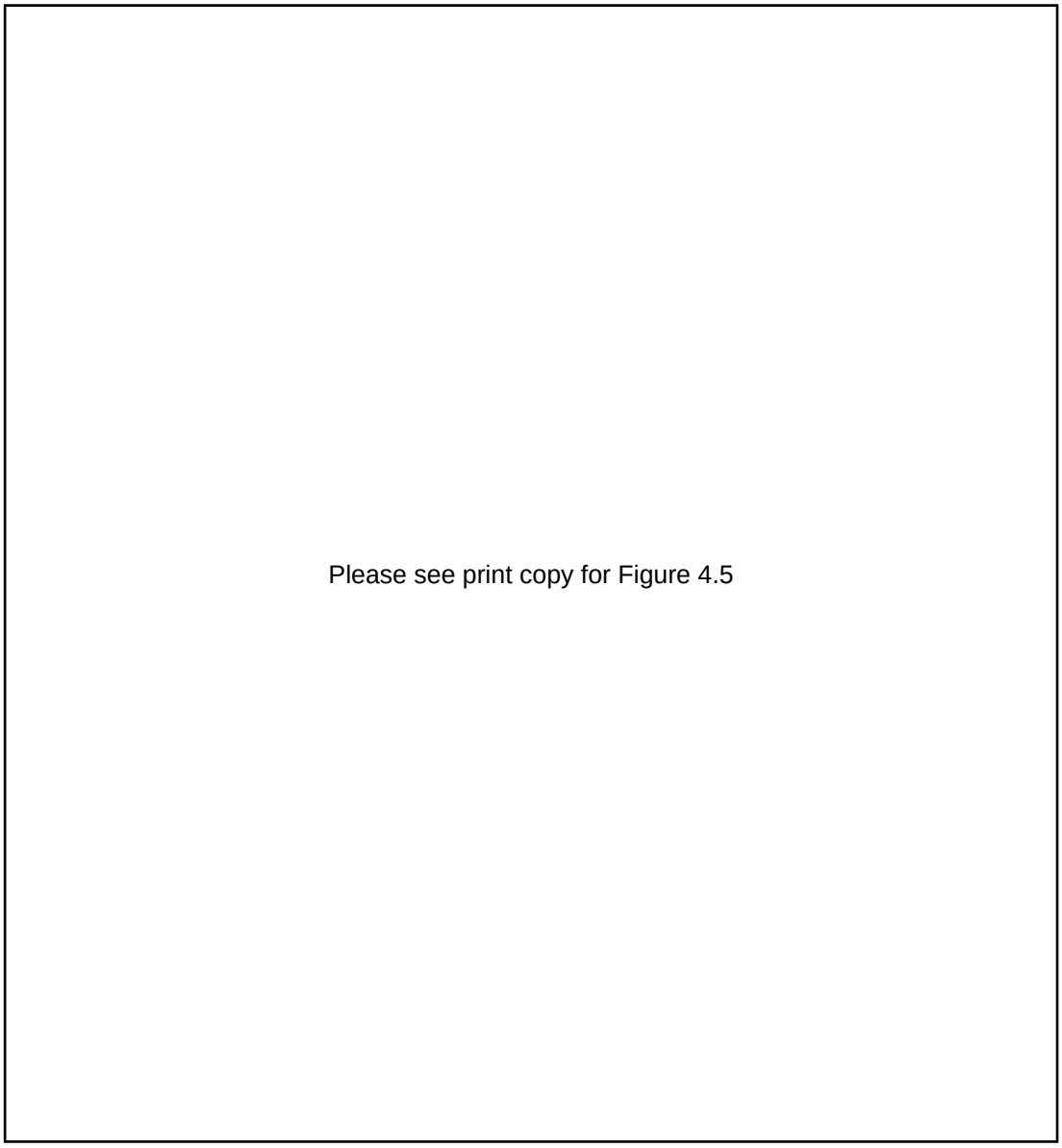

Figure 4.5: Schematic representation of the life cycle of *Pleurochrysis pseudoroscoffensis* (Gayral and Fresnel, 1983).

More recently some other functions have been proposed, such as a boost to photosynthesis, because calcification and photosynthesis rates show a close stoichiometric correspondence (Paasche, 1962; Klaveness and Paasche, 1979; Sikes et al., 1980) or protection from osmotic, chemical or physical shocks (Young, 1994). Light is also commonly mentioned, some authors claiming that coccoliths protect the cell from ultraviolet light (Braarud et al., 1952; Holligan et al., 1983), others stating that coccoliths

refract light towards the cell thus permitting life in light-depleted zones (Gartner and Bukry, 1969). All these potential functions of coccoliths are summarised in Figure 4.6.

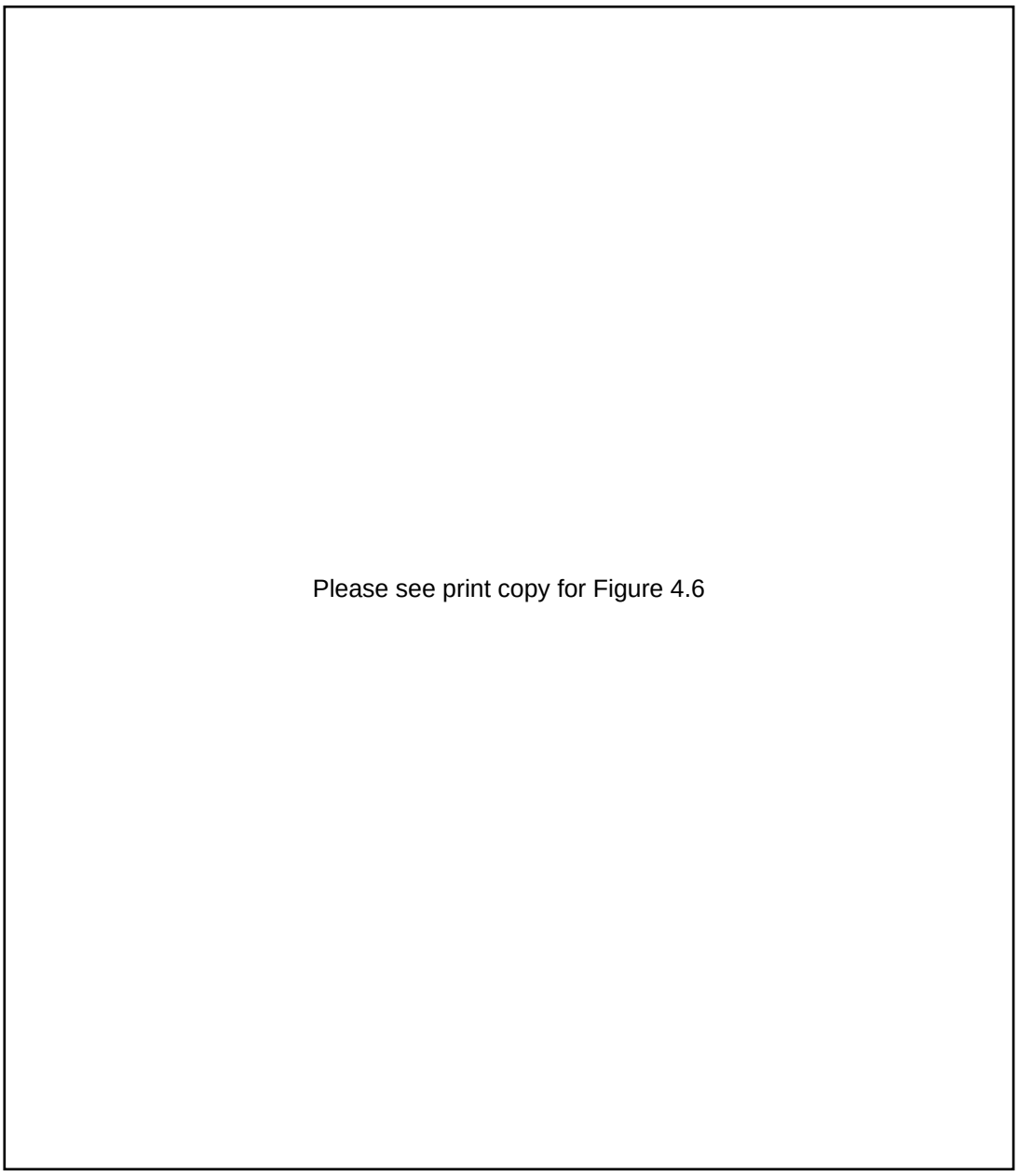

Figure 4.6: Cartoon summary of putative functions of coccoliths (from Young, 1994)

- Relation between biocoenosis and thanatocenosis

Coccolithophorids are immensely important in their role as a carbon pump on a global scale (approximately two-thirds of the total calcium carbonate flux; Takahashi, 1994) and

of primary production in the vast areas where oligotrophic conditions prevail. The secretion of coccoliths and their further sinking to the bottom of the oceans brings large amount of carbon from sea surface to sea-floor (Figure 4.7). Because their transportation occurs within aggregates (marine “snow” and faecal pellets) that act as a protective organic membrane, intact coccolithophorids can be recovered from deep sediment traps below the calcium carbonate compensation depth (Takahashi, 1994). This mode of transportation explains why the distribution of coccoliths in the upper ocean and in surficial sediment coincides reasonably well (McIntyre and Bé, 1967) without obvious wide lateral dispersion, indicating rather rapid transport of these fine particles.

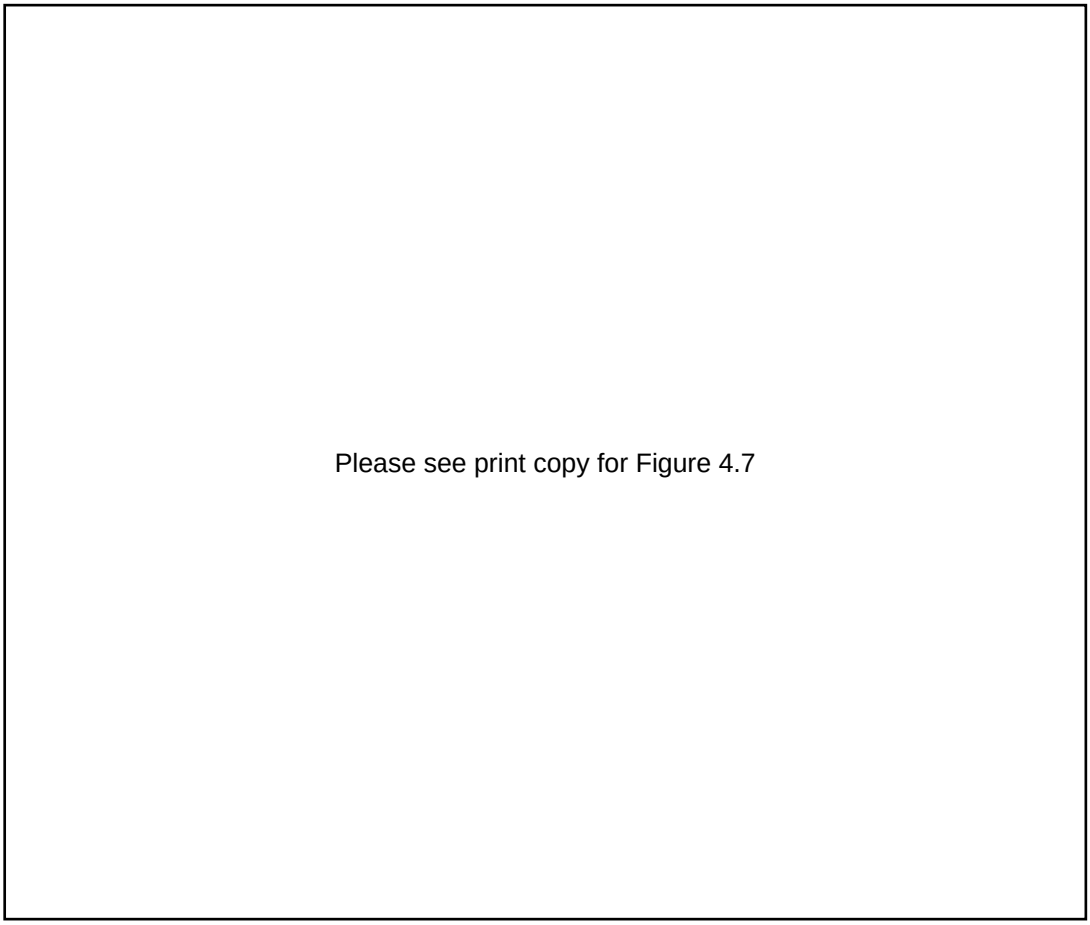

Figure 4.7: Conceptual model for coccolithophorid production in the upper ocean and coccolith faecal pellet transport to the deep sea (Honjo, 1976).

4.3.3 Coccolith distribution

A significant number of filtered sea-water, core-top sediments and sediment-trap samples have been collected on a world wide scale in the past 40 years (McIntyre and Bé, 1967; Okada and Honjo, 1973, 1975; Roth and Berger, 1975; Nishida, 1979; Okada and McIntyre, 1979; Kleijne et al., 1989; Winter and Siesser, 1994b; Boeckel and Baumann, 2004; Sato et al., 2004; Schiebel et al., 2004). This important database, which is still expanding, permits a reasonable knowledge of the distribution of modern living assemblages. Using these biogeographies and species idiosyncratic morphologies, Young (1994) defined four distinctive groups of coccolithophorids. Three of these groups dominate coccolithophorid assemblages in particular environments (Figure 4.8).

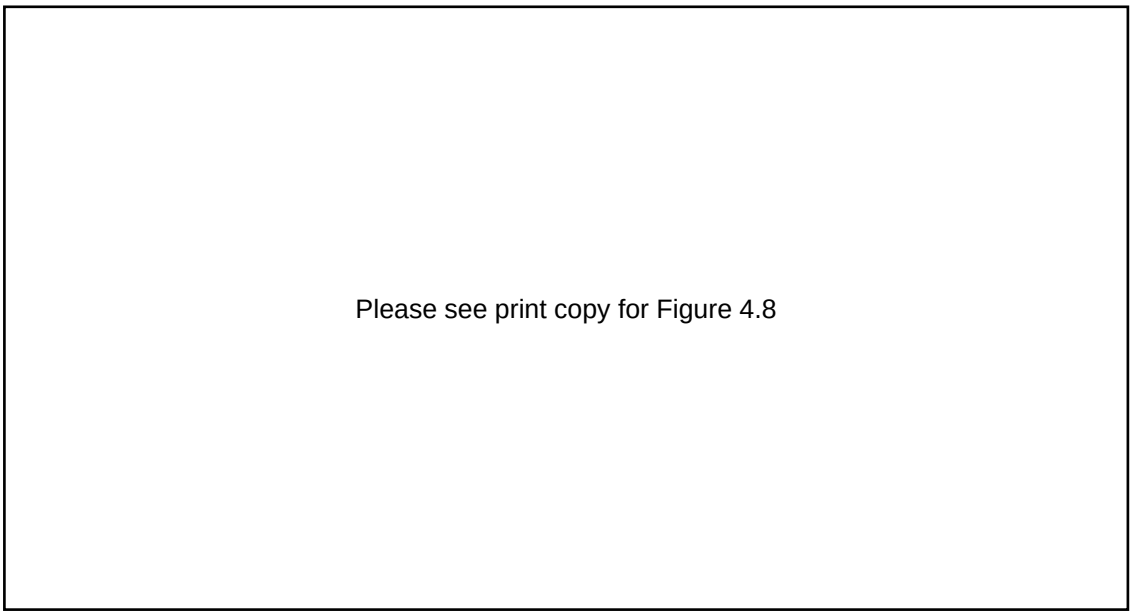

Figure 4.8: Ecological distribution of coccolithophorid types. *Above*: Schematic diagram illustrating the three main nannoplankton assemblage types (Placolith-bearing, Umbelliform, Floriform) representing a transect from continental shelf to mid-ocean at low latitude. Arrows indicate nutrient flux. *Below:* Typical representatives of each of the ecological groups. The scale bar is 1 µm (from Young, 1994).

- Placolith-dominated assemblages are present in coastal and up-welling environments. These environments correspond to the eutrophic ecological niche (Kilham and Kilham, 1980). *Emiliania huxleyi*, *Gephyrocapsa ericsonii*, *G. oceanica*, *Calcidiscus leptoporus*, *Umbilicosphaera sibogae*, *U. hulbertiana* and *Oolithus fragilis* (all placolith-bearing) represent more than 90 % of the total assemblage. The species are mainly

bloom-forming species and their relative proportions vary with latitude (Okada and Honjo, 1973, 1975; Nishida, 1979; Okada, 1983; Kleijne et al., 1989; Young, 1994).

- Umbelliform-dominated assemblages are found in oligotrophic nutrient-depleted mid-ocean environments. *Umbellosphaera tenius*, *U. irregularis* and *Discophera tubifera* characterise these assemblages, representing between 10 and 30 % of the total population (Okada and Honjo, 1973; Nishida, 1979; Okada and McIntyre, 1979; Kleijne et al., 1989; Young, 1994). These coccoliths are less abundantly preserved in the sediments than is their representation in surface waters (Roth and Coulborne, 1982).

- Floriform-dominated assemblages correspond to the deep-water assemblage that includes *Florisphaera profunda*, *Thorosphaera flabellate* and *Algiosphaera quadricornu* (Okada and Honjo, 1973; Honjo, 1977; Reid, 1980; Okada, 1983). These species occur extremely rarely in surface-water assemblages suggesting that they live below the mixed layer, in or under the thermocline (Young, 1994). Their ecological niche is typified by low-light and nutrient-rich levels.

- Miscellaneous assemblages comprise all less common species that do not fit into the three major groups previously defined. They represent probably more than 80% of the species diversity but less than 20% of the individual coccoliths abundance. Young (1994) includes most species of the Syracosphaeraceae, Helicosphaeraceae, Calyptrosphaeraceae, Rhabdosphaeraceae, and Pontosphaeraceae families in this group. These species that rarely dominate assemblages are more common in intermediate environments than in extreme eutrophic or oligotrophic conditions (Okada and Honjo, 1973; Reid, 1980; Young, 1994).

The partial restriction of these four different assemblages to specific ecological niches means coccolithophorids have a high potential for palaeoenvironmental reconstruction.

4.3.4 Palaeoenvironmental proxies

Coccolithophorids are unicellular planktonic marine algae, distributed from the open ocean to nearshore littoral and lagoonal environments. They secrete minute calcified plate coccoliths, which are preserved in marine sediments and are excellent proxies of

palaeoceanographic conditions. The lack of coccoliths within sediments could be either due to poor preservation conditions or to a non-marine environment. Since the 1970's, mapping of the geographic distribution of modern coccoliths in oceans has helped the interpretation of past environmental conditions (McIntyre et al., 1970; Okada and Honjo, 1973). Thereafter, nannoplankton have been commonly used as proxies for palaeooceanographic and palaeoclimatic conditions (McIntyre, 1967; Geitzenauer, 1969; McIntyre et al., 1970, 1972; Ruddiman and McIntyre, 1976; Aizawa et al., 2004; Baumann and Freitag, 2004).

Coccolith species diversity is related to the environmental constraints that are reflected in the fossil assemblages. Furthermore, environmental stress is indicated by the degree of dissolution and the morphological variations of coccoliths. The recent authentication of the haplo-diploid, typically heteromorphic life cycle of coccolithophorids (Cros et al., 2000) is revolutionising the interpretation of coccolith distribution in terms of ecological conditions. The determination of the environmental factors that trigger intra-species phase changes (Noël et al., 2004) is a key to better understanding the modern and palaeodistribution of coccolithophorids. However, very few holoccocolithophores are non-motile (Sym and Kawashi, 2000) and Billard and Inouye (2004) suggests that such rare cases may indicate that their heterococcolithophorid stage could be restricted to coastal areas. Further investigation will permit the verification of this hypothesis.

The use of satellite image analysis is becoming very popular to study modern coccolithophorid and coccolith distributions within bloom areas, coccoliths having a higher light-scattering power than coccolithophorids. As an example, Balch (2004) shows that the abundance of coccolithophorids and coccoliths increases up to 20% during the more stratified intermonsoon periods in the Indian Ocean.

4.4 Optical analysis of MD32

4.4.1 Why MD32?

Core MD32 was chosen for the optical systematic investigation because, apart from being the longest available core from the current sampling campaign, this core was collected close to the deepest part of the Gulf. MD32 is thus potentially the core with the longest and more complete record of the palaeoenvironmental history of the Gulf of Carpentaria that has been collected to date. Furthermore, detailed parallel pollen, foraminifer and ostracod studies (Chivas et al., 2001; van der Kaars, unpublished; Reeves, 2004; Holt, 2005) were already underway at the time that this thesis was commenced and several dates had been previously estimated for the deeper part of this core (Chivas et al., 2001).

4.4.2 The qualitative optical observation

Coccolith assemblages in core MD32 were assessed via qualitative systematic observation by the author, using a Leitz Orthoplan microscope, of smear slides, of every 10 cm increment (i.e. 149 samples for the 14.82 m core MD32). For each slide, four orthogonal optical transects were performed at a 1000x magnification under cross-polarised light. From this study, 34 species from 17 genera were identified. The species determination up to at least the genus level was done mainly with the training the author acquired from Luc Beaufort during two missions to CEREGE (France)[†].

Species level determination was facilitated by the atlas of living coccolithophorids of Winter and Siesser (1994b) and the online site created by Young (2002). The taxonomy used in this study derives from the recent 'Review of the phylogeny of the Haptophyta' by Sáez et al. (2004). This classification is based on DNA analysis. However, Sáez et al. (2004) did not analyse all the coccolithophorid species found in the Gulf, therefore a more classical approach based on morphology is also used (Jordan and Kleijne, 1994; Jordan et al., 1995, 2000; Young et al., 1997; Edvardsen, 2000; Kleijne, 2001; Billard and

[†] *The second trip was supported by CNRS (Centre National pour la Recherche Scientifique) / ARC (Australian Research Council) collaboration grant (AMVSG30763) and GeoQuEST (University of Wollongong).*

Inouye, 2004). A detailed systematic list of the taxa found in MD32 with their appropriate bibliography together with a short morphological description is given in Appendix 8.

4.4.3 SEM photos

The author captured SEM images for a single level (MD32-15) using the Leica Cambridge 440 SEM (Scanning Electron Microscope) at the Faculty of Engineering, University of Wollongong. This level was chosen because it contains the assemblage with the highest diversity and is thus representative of the Gulf of Carpentaria coccolith population. Twenty-two species are illustrated (Figure 4.9 and 4.10), some of them by several specimens to show the morphological variations or dissolution features that are common throughout the core. A tiny smear slide of this sample was prepared on a cover slip. David Carry (School of Earth and Environmental Sciences) coated this sample with gold by the mean of an Argon Gas Sputter Coater.

4.4.4 General characteristic of the coccolith population

The species assemblage found in the Gulf of Carpentaria is similar to those of modern assemblages recorded by earlier studies in the area (Okada and Honjo, 1973, 1975; Honjo, 1975; Conley, 1979; Okada, 1983; Hallegraeff, 1984; Biekart, 1989; Cheng and Wang, 1997; Takahashi and Okada, 2000*a*; Hagino et al., 2000) (Table 4.1), with a high number of unusual species such as *Reticulofenestra parvula, R. minuta* and *R. sessilis*, which are not usually abundant in Quaternary sediments. This difference between neritic marginal seas and open-ocean ooze associations has already been reported, and associated with a dissimilar spatial distribution within the water column, with the neritic population being more sporadic (Okada and Honjo, 1975; Cheng and Wang, 1997). Furthermore, these marginal inland and/or shallow-sea assemblages are always characterised by dissolution features (McIntyre and McIntyre, 1971; Okada and Honjo, 1975; Roth and Berger, 1975; Burns, 1977; Kleijne, 1990, Cheng and Wang, 1997), and often show high level of malformation. This malformation usually affects all coccoliths regardless of the species, and can take several forms, with malformed coccoliths displaying angular twisted shapes with fused or no elements in the central openings (Okada and Honjo, 1975; Kleijne, 1990). These observations are consistent with Watabe and Wilbur (1966) who observed that abnormal coccoliths resulted if crystal growth does not begin simultaneously in all centres in the basal region. They also noted that all coccoliths were normal at 18°C and that a variation of the temperature increased the proportion of abnormality.

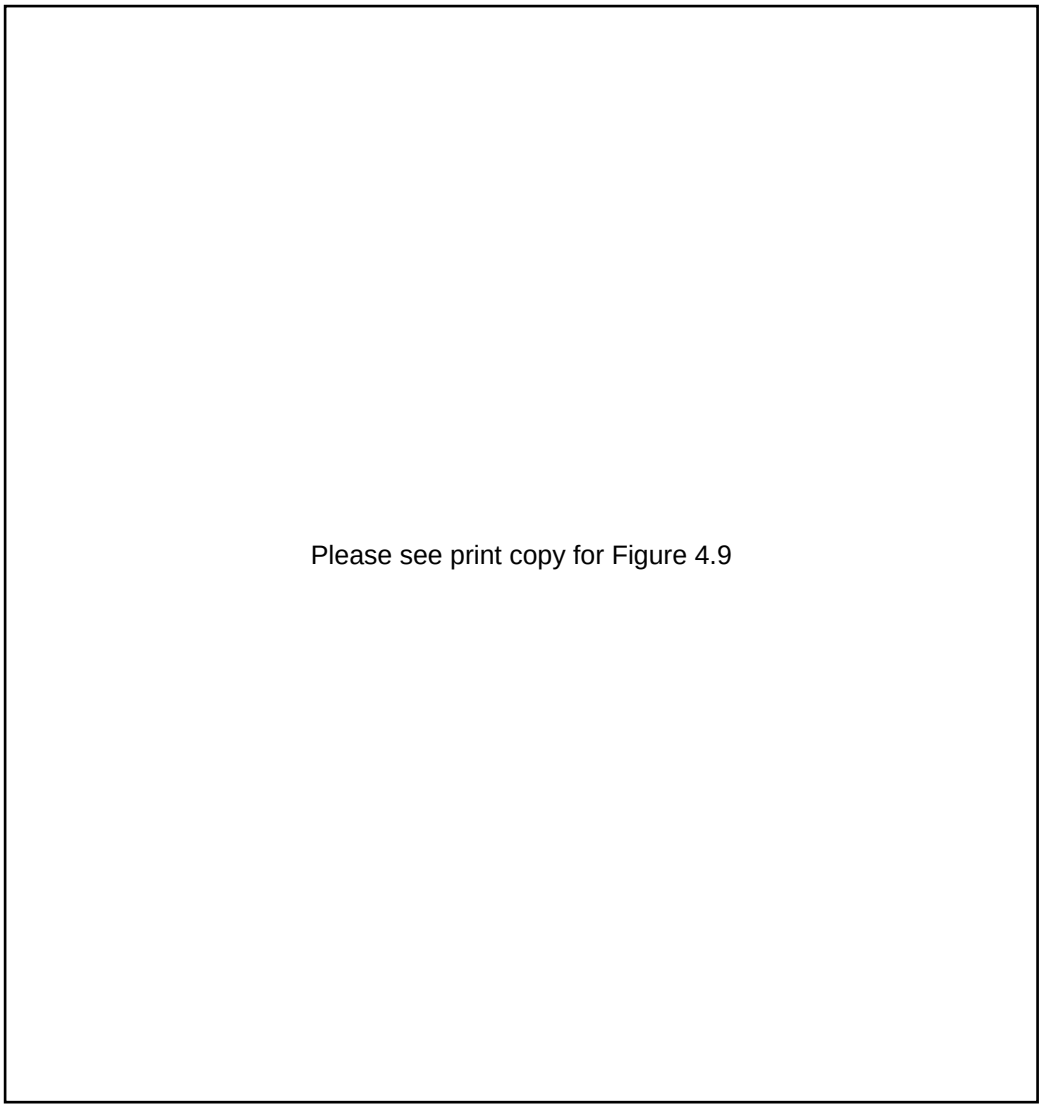
Please see print copy for Figure 4.9

Table 4.10: Comparison of the 34 coccolith species found in core MD32 with other studies in the area. Not all species determined in the other studies are presented. Because the numerous changes in coccolithophorid taxonomy for the past 30 years, this table may lack several species that were not determined using the same classification as this study.

1- Compilation from Hallegraeff (1984) with data from Okada and Honjo (1975) and Conley (1979) for the Coral Sea (CS), Gulf of Carpentaria (GoC), North West Shelf (NWS) and East Australian Current (EAC) areas

2- Kleijne et al. (1989) North Indian Ocean (NIO)

3- Bierkart (1989) Southeast Indonesian basins (SI)

4- Hagino et al. (2000) West Equatorial Pacific (WEP)

5- Takahashi and Okada (2000a) East Indian Ocean (EIO)

Present Study	1				2	3	4	5
Gulf of Carpentaria	CS	GoC	NWS	EAC	NIO	SI	WEP	EIO
Umbellosphaera tenius	x	x		x	x	x	c	c
Pontosphaera discopora				x			x	x
Emiliania huxleyi	x	x	x	x	x	x	c	c
Gephyrocapsa omega								
Gephyrocapsa ericsonii	x	x	x	x			x	c
Gephyrocapsa oceanica	x	x	x	x	x	x	c	c
Gephyrocapsa (small)						x		
Reticulofenestra parvula						x		x
Syracosphaera pulchra	x	x	x	x	x	x	x	x
Reticulofenestra sessilis	x	x	x	x		x	x	x
Helicosphaera carterii	x	x		x	x	x	x	x
Gephyrocapsa (large)								
Umbilicosphaera hulburtiana	x	x	x	x	x	x	c	c
Um bilicospharea sibogae	x	x	x	x	x	x	x	x
Umbilicospharea foliosa			x	x	x		c	x
Syracosphaera nana							x	x
Pseudoemiliania lacunosa								
Syracosphaera lamina					x	x	x	x
Helicosphaera hyalina						x	x	x
Syracosphaera anthos							x	x
Discosphaera tubifera	x	x	x	x		x	c	c
Calcidiscus leptoporus	x	x		x	x	x	x	x
Reticulosphaera minuta						x		
Rhabdosphaera clavigera		x	x	x		x	x	x
Calciosolenia murrayi	x		x			x		x
Anoplosolenia brasiliensis		x			x		x	
Oolithotus fragilis	x		x	x	x	x	x	x
Braarudosphaera bigelowii								x
Helicosphaera walchii	x			x				
Ceratolithus cristatus					x		x	x
Florisphaera profunda					x	x	c	c
Umbilicosphaera annulus								
Helicosphaera sp.							x	x
Emiliania corona							x	x

NB: *Calciosolenia murrayi* and *Anoplosolenia brasiliensis* were only differentiated with the SEM. Thus in the remainder of this chapter, *Calciosolenia murrayi* represents both species.

The highest degree of similarity in terms of assemblages with this study corresponds to the assemblages described in the two more recent papers (Hagino et al., 2000 and Takahashi and Okada, 2000a). That may be partly the result of the recent tendency for a homogenisation of coccolithophorid taxonomy (Table 4.1).

4.1.1 Systematic observation

The coccolith concentrations in the sediment from the Gulf of Carpentaria are very low compared to those of open-ocean oozes from the Atlantic, Pacific and Indian Oceans. Only a few specimens of coccoliths (if any) were observed in each microscopic field instead of the usual hundreds or thousands seen in open-ocean smear slides. This character reflects a low production or low preservation rate or, and more likely, a high dilution of the coccolith signature in the abundantly represented lithic and detrital fractions. Recent observations in the southeastern Indian Ocean offshore of western Australia reported standing crops varying form less than several hundreds to 85,000 cells per litre with a significant decrease of the abundance at all nearshore sites (Takahashi and Okada, 2000a). Kleijne et al. (1989) reported concentrations up to 110,000 cells per litres in the North Indian Ocean sea surface.

On the other hand, typical densities of coccolithophorids in marginal seas are much lower. Okada and Honjo (1975) reported a concentration as low as 1 cell per litre in the South China Sea and Red Sea surface-waters, and a maximum of 18,000 and 66,000 cells per litre, respectively. Okada and Honjo (1975) also found that the concentration of coccoliths in the surface-waters of the Gulf of Carpentaria ranged from 2,400 to 9,200 cells per litre. These observations plus the fact that there is a dilution of the coccolith signal that is incorporated into the abundant lithic and detrital sediment fractions, explains the very low density of coccoliths found in the Gulf of Carpentaria sediment. The sedimentation rates estimated for the three cores dated by OSL, MD31, MD32 and MD33, range from 4.3 to 14.2 $cm.ka^{-1}$ (Chapter 3, Section 3.12) whereas a typical sedimentation rate for open ocean is 1 $cm.ka^{-1}$.

Coccoliths were absent, or at least not preserved, in non-marine sediment from the cores. Furthermore their preservation is very variable throughout the core and in some intervals the preservation level is so poor that it precludes clear identification of any coccoliths present. For these taxa the genera are given.

To minimise the loss of important information given by the marginal species, a weighted representation was preferred (Figure 4.11). The subsequent figure summarises both coccolith abundance (= length of each species symbol) and distribution (= number of colours per sample level), and shows the species and depth clusters (Section 4.1.2) together with the four major units (Section 4.1.3). The attribution of the coefficients was done as specified in Table 4.12, and the raw
data are presented in Appendix 9.

Table 4.2: Definition of the rank (abundance key on Figure 4.9)
used for coccoltih abundance representation.

Number of individuals Counted per sample	1	2 to 10	11 to50	51 to100	101 to 500	>500
Coefficient	1	2	3	4	5	6

4.1.2 Results

Overall, there is a domination of the placolith-bearing species (especially *Gephyrocapsa* spp and *Emiliania huxleyi*) that represents more than 95% of the total counted individuals. This domination in the thanatocenose is probably due to their better resistance to deep-water dissolution. These results are consistent with those of the above-cited studies on the modern living assemblages in this area (Table 4.1),
particularly with Okada and Honjo (1975) who reported 94% to 98% of
Gephyrocapsa oceanica in the Gulf of Carpentaria sediment. Okada (1975) also noted that surface and bottom assemblages of coccoliths were rather similar in the Gulf although *Umbellosphaera irregularis* and *Discosphaera tubifera* were found only in the surface layer.

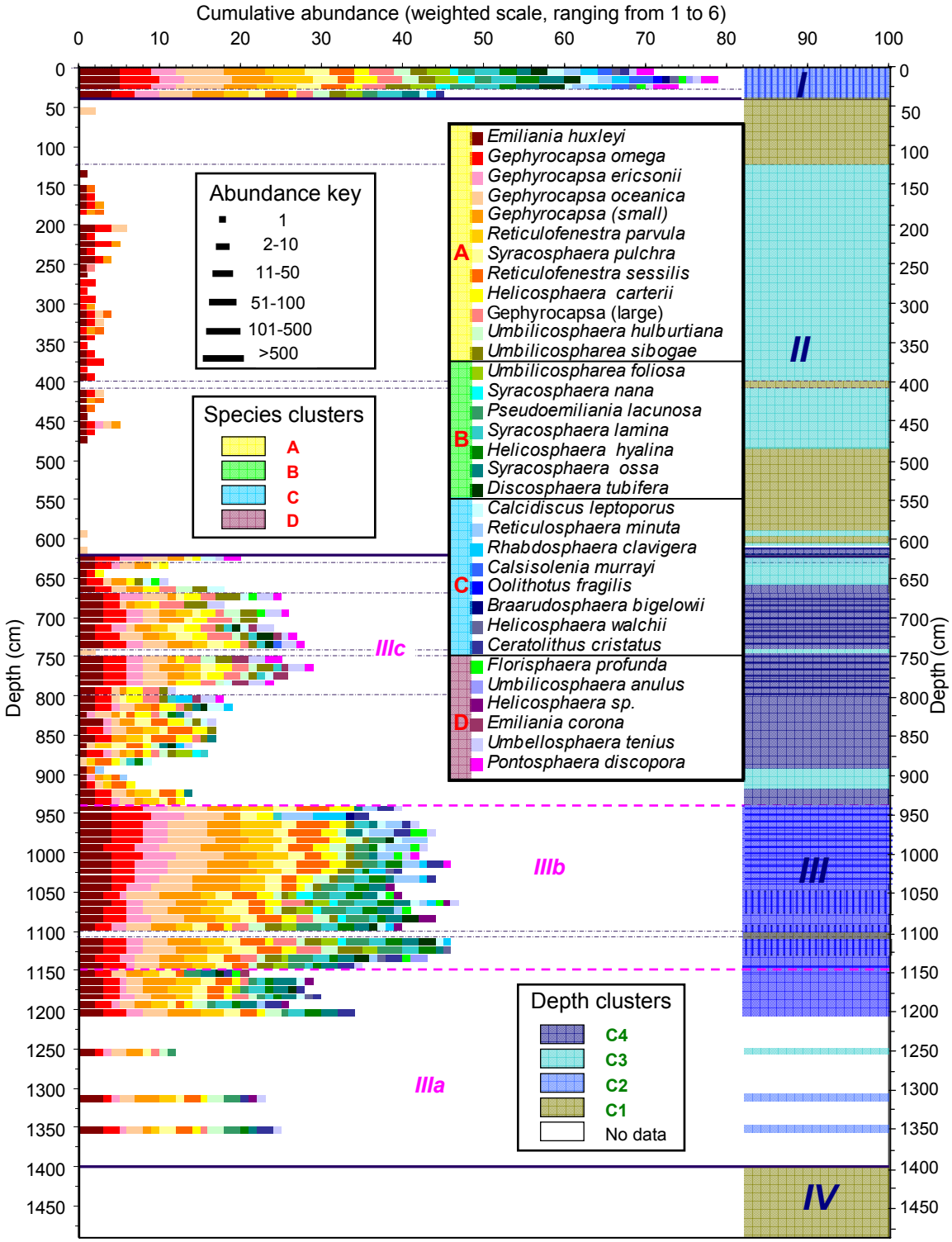

Figure 4.11: Coccolith weighted abundances (length of each symbol), assemblages distribution (colour of each symbol) in the core MD32, species clusters (A, B, C, D), depth clusters (C1, C2, C3, C4, sub-groups being represented per horizontal and vertical lines on top of the

cluster colour), and the four major units (I, II, III, IV) with sub-units (IIIa, IIIb, IIIc). From 12 to 14 m the lack of coccoliths is due to no samples been analysed.

- Cluster analysis

The results of this optical investigation of MD32 has been analysed by CORRMAT/PROG cluster analysis program (Jones and Facer, 1982) to compare the composition (R-mode) and distribution (Q-mode) of coccolith assemblages through the core. This analysis was performed on a matrix including the weighted number of individuals for each species recognised for each sample.

- R-mode

For this cluster analysis, the similarity matrix based on relative species abundance for each sample is obtained with a Pearson product moment correlation coefficient. This classification allows the definition of four assemblages **A**, **B**, **C** and **D** of species preferentially occurring together (Figure 4.12).

(A) consists of ten placolith-bearing species (Figure 4.12) plus *Syracosphaera pulchra* and *Helicosphaera carterii* that are relatively common species known to prefer oligotrophic warm water (Ziveri et al., 2004). *Umbilicosphaera sibogae* is also referred to as an oligotrophic dweller. Emilinia huxleyi is a ubiquitous species, its abundance increasing towards high latitudes (Okada and Honjo, 1973; Hiramitsu and De Deckker, 1997). Gephyrocapsa is recognised as the dominant species in marginal seas, and coastal areas (Okada, 1992; Cheng and Wang, 1997; Hiramitsu and De Deckker, 1997; Tanaka, 1997). The small placoliths (< 2.5 µm) have often been used for monitoring past nutrient conditions (Takahashi and Okada, 2000b, 2001; Okada 2000), and more recently were correlated with the carbonate dissolution index (Aizawa et al., 2004).

(B) is dominated by *Syracosphaera* species (*S. nana*, *S. lamina* and *S. anthos*) associated with two placoliths-bearing species, *Umbilicosphaera foliosa* and *Pseudoemiliania lacunosa*, together with *Helicosphaera hyalina* and *Discosphaera tubifera*. These species are commonly represented in the upper part of the photic zone in modern assemblages.

(C) is represented by *Calcidiscus leptoporus*, *Reticulofenestra minuta*, *Rhabdosphaera clavigera*, *Calciosolenioa murrayi*, *Olitithus fragilis*, *Braarudosphaera bigelowii*, *Helicosphaera walchii* and *Ceratolithus cristatus*.

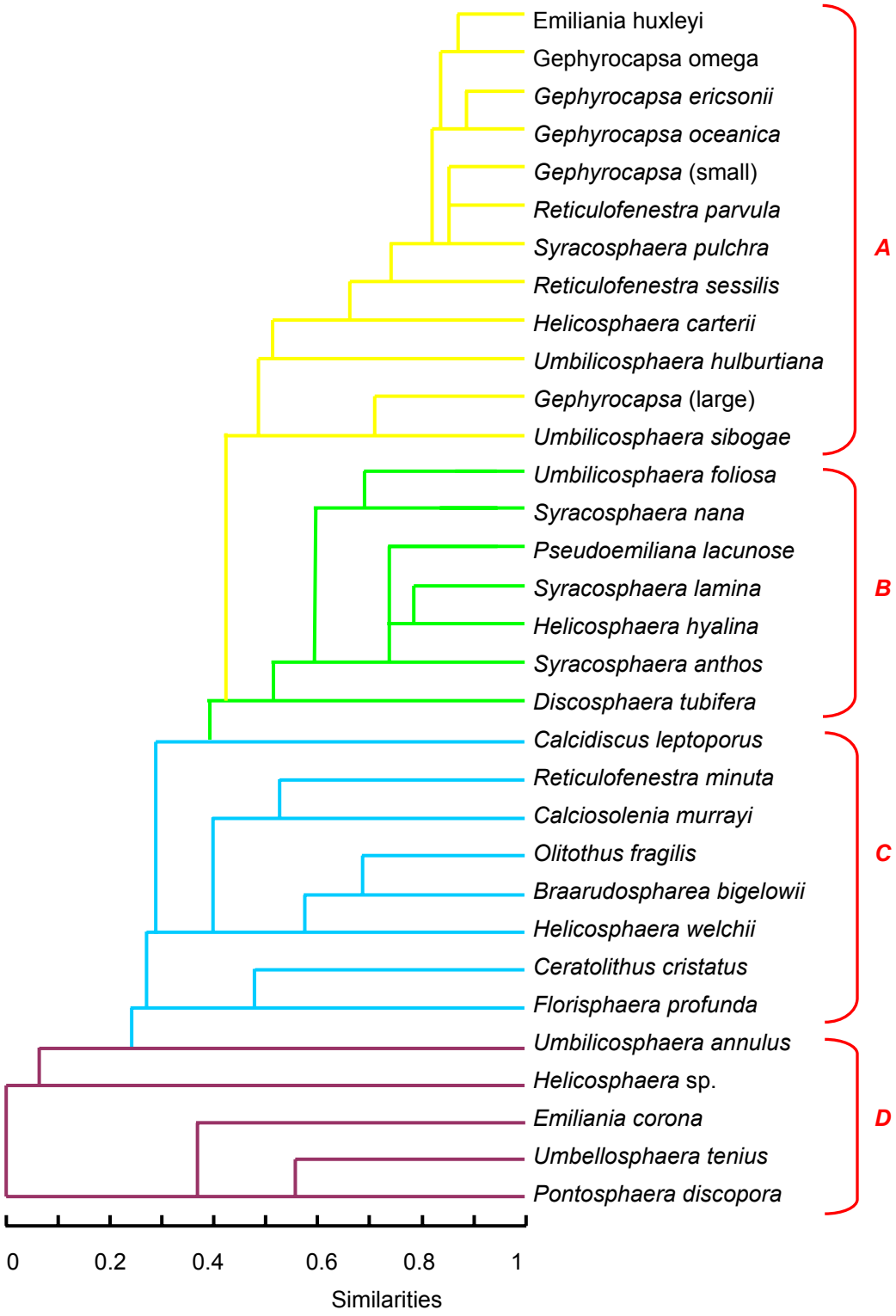

Figure 4.12: R-mode cluster analysis of coccoliths from core the core MD32 from the Gulf of Carpentaria.

R. clavigera and *C. leptoporus* are reported as sub-tropical dissolution-resistant species (Baumann et al., 2004), and the latter being correlated to decreased sea surface temperature (Hiramatsu and De Dekker, 1997; Kinkel, 2000) or high productivity (Flores and Sierro, 1997; Flores et al., 2003). *B.Bigelowi* is commonly used as a neritic environment index species (Tanaka, 1991; Okada, 1992; Aizawa et al., 2004).

(D) includes *Florisphaera profunda*, *Umbilicosphaera anulus*, *Helicosphaera* sp., *Emiliania corona*, *Umbellosphaera tenius* and *Pontosphaera discopora*. *F. profunda* is generally related to low-light (Okada and Honjo, 1973), low-temperature and high-nutrient levels, but it also has been associated with sea-water transparency and/or turdidity (Ahagon et al., 1993), lower euphotic zone temperature (Okada and Wells, 1997) or productivity (Beaufort et al., 2001). Whereas *U. tenius* is usually associated with warm (above 27°C) oligotrophic water (Nishida, 1979; Okada and McIntyre, 1979; Kleijne et al., 1989; Tanaka, 1991). In fact, this assemblage is characterised by a low level of similarity between species (<0.55) and corresponds to the 'left-over' species from the three previous assemblages.

These assemblages are shown in Figure 4.11, together with species distribution, versus depth in the core. Levels without coccoliths are associated with non-marine conditions and thus the Lake Carpentaria phases.

- Q-mode

For this cluster analysis, the similarity matrix based on relative species abundance for each sample (i.e. depth) is obtained using the cosine-theta similarity coefficient. This classification allows the definition of four clusters **C1, C2, C3, C4**, which were deposited under similar environmental conditions (Figure 4.13).

These groups are named in the order they appear in the core from the base, and their distribution along the core is shown in Figure 4.11.

(C1) Includes all thirty-one levels barren of coccoliths from the base of the core to 14 m, at 11.0 m, then from 6.0 m to 4.8 m, at 4.0 m depth and then from 1.2 m to 0.4 m. The lack of coccoliths indicates non-marine conditions for this cluster named "Lake Carpentaria".

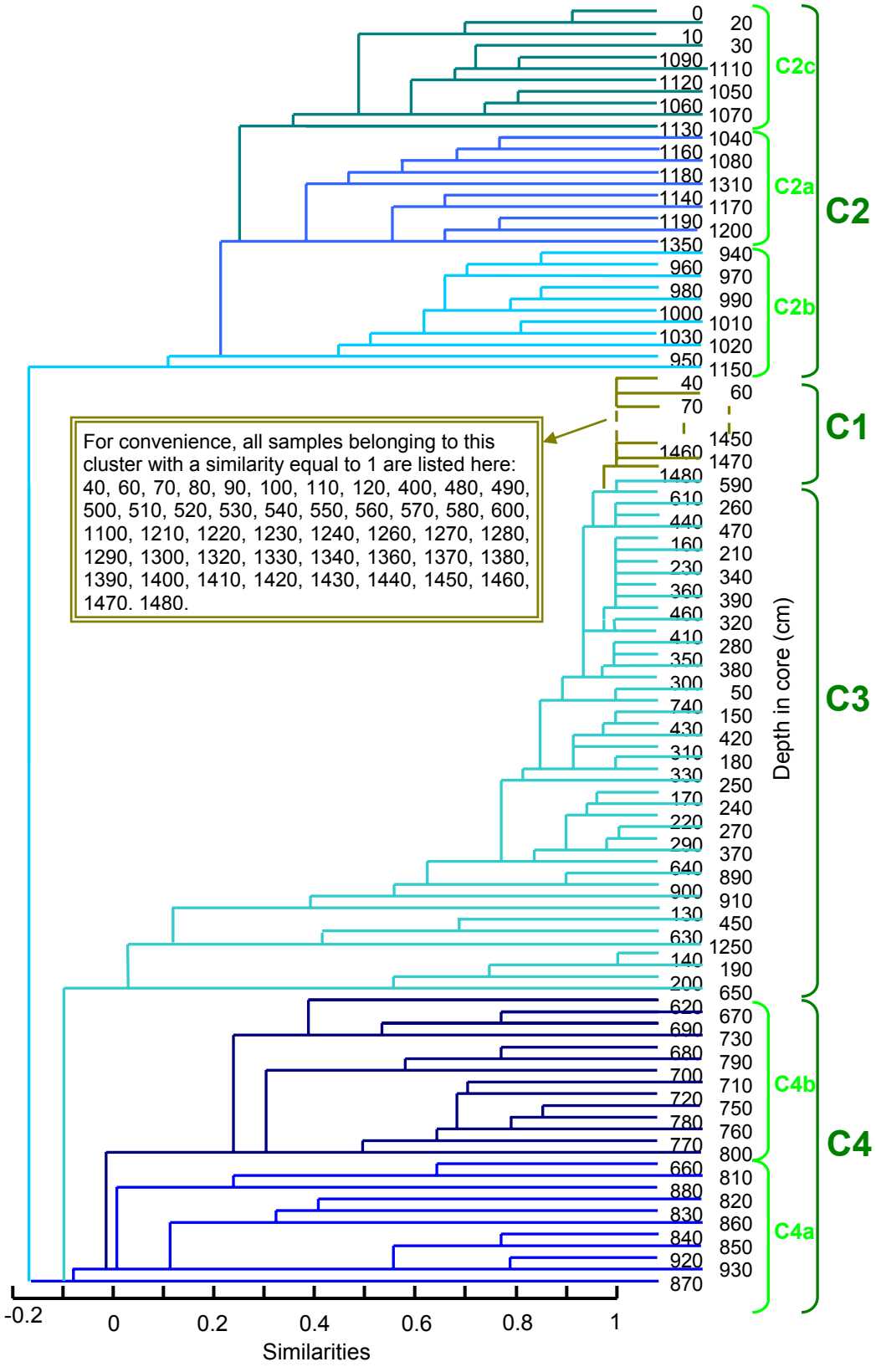

Figure 4.13: Q-mode cluster analysis of coccoliths from core the core MD32 from the Gulf of Carpentaria.

(C2) comprises thirty-two levels from 13.5 m to 13.1 m, from 12.0 m to 9.4 m (minus 11.0 m that is barren) and from 0.3 m to 0 m. This group corresponds to high-abundance and high-diversity assemblages including the modern levels, and which is here referred to as “open-ocean”. This cluster can be sub-divided into three sub-groups, **C2a**, **C2b** and **C2c** (Figure 4.12)
with higher affinity consisting of similar size clusters and likely
due to limited changes in the environmental conditions. The sub-units **C2c** corresponds to the modern environment, **C2a** represents transitional and **C2b** stable environmental conditions.

(C3) contains forty-five levels, 12.5 m, from 9.1 m to 8.9 m, 7.4 m, from 6.5 m to 6.3 m, 6.1 m and 5.9 m, from 4.7 m to 4.1 m and to 3.9 m to 1.3 m. The very low abundance and diversity of the coccolith community observed in these levels indicates a high degree of stress, a confinement with probably sporadic marine influence. Therefore, this cluster is termed “confined”.

(C4) Includes 9.3 m and 9.2 m, from 8.8 m to 6.6 m plus 6.2 m. Abundance and diversity are moderate in these levels, significantly lower than in C2**,** but, the marine influence is clear. Subsequently, this cluster is referred to as “marginal sea”. As with C2, this group can be divided into two sub-groups **C4a** and **C4b** (Figure 4.13), the former is
transitional whereas the latter represents a more stable environment.

These groups and sub-groups and their distribution along the core are shown on Figure 4.11. The ‘b’ and ‘c’ sub-units are represented by horizontal and vertical lines on top of the plain colour of the unit, respectively.

4.1.3 Palaeoenvironmental conditions

Four major units are recognised on Figure 4.11, they are marked by continuous dark blue lines. The units are numbered from top to bottom in the core to facilitate correlation with the other cores.

- **Unit IV**

Spanning from the base of the core to 14.0 m, this unit is characterised by the absence of coccoliths and corresponds to the Lake Carpentaria phase, and thus the closure of both sills or to very poor preservation conditions.

- **Unit III**

Covering from 13.9 m to 6.2 m, this unit corresponds to the longest quasi-continuous coccolith record in core MD32. This unit comprises three clear sub-units, **IIIa** from 13.9 m to 11.5 m, **IIIb** from 11.4 m to 9.4 m, and **IIIc** from 9.3 m to 6.2 m, separated with dashed pink lines on Figure 4.11.

Sub-unit IIIa: The first interval from the base (13.9 m) to 12.6 m consists of a high-diversity, relatively low-abundance assemblage. Placolith-bearing species are dominant with *Emiliania huxleyi* being the most abundant. This part of the unit corresponds to the transitional phase (C2a) of the open ocean environment previously defined. The transitional environment encompasses slight fluctuations of environmental conditions such as salinity, temperature, nutrients concentration or energy level, which affect the coccolith community. At 12.5 m the assemblage is less diverse or abundant and corresponds to the confined environment.

From 12.5 m to 11.6 m, the abundance of placolith-bearing species increases with a relative decrease of *E. huxleyi*. This assemblage is similar to those of the beginning of this unit and reflects transitional marine conditions. At 11.5 m, the lower abundance of coccoliths indicates a higher level of stress in the environment. This stress could be a drop in the temperature as indicated by the disappearance of warm water species, *Helicosphaera carterii* and *Calcidiscus leptoporus* and presence of the colder dweller *Florisphaera profunda*.

Sub-unit IIIb: begins at 11.6 m with rapidly increasing abundance that remains relatively stable from 11.7 m to 10.5 m, while the diversity is more fluctuating. This interval, as for those observed from 13.9 m to 12.6 m represents a transitional phase of the open marine conditions.

At 11.0 m, no coccoliths were preserved. This level is within a laminated interval of gypseous laminae alternating with dark organic and pyrite-rich laminae, from 11.2 m to 10.7 m (Reeves, 2004). But coccoliths were recognised in other samples within this interval (11.1 m, 10.9 m and 10.8 m), and on both sides of this atypical sample, the assemblages are similar. The minute amount of sample collected to prepare the smear slide for the barren 11.0 m sample must have been taken from a clear lamina and thus been mainly composed of gypsum.

The interval between 11 m and 10.5 m is similar to modern assemblages (Figure 4.13) and is thus equivalent to modern open ocean
environmental conditions. This assemblage is dominated by small placoliths.

From 10.6 m to 9.4 m the main trend is near constancy in both diversity and abundance that is interpreted as stability in the environmental conditions. This interval corresponds to the stable open marine environment (C2b) previously defined. This interpretation is confirmed by the fact that the abundance of *Gephyrocapsa oceanica* exceeds that of *E. huxleyi*. The ratio *E. huxleyi* versus *G. oceanica* is an important indicator for palaeoenvironmental studies as it expresses trophic conditions. *G. oceanica* dominates/monopolises nutrient-rich near-shore warm water, whereas *E. huxleyi* is more a eurytrophic form and is most abundant in cooler and oligotrophic stratified water (Hulburt, 1968; Gaarder, 1971). This specific distribution relates to West Pacific low-latitude shallow and semi-confined seas, *Emiliania huxleyi* being the dominant species in marginal seas at higher latitude (Okada, 1983; Houghton, 1993). This interval consists almost exclusively of species from A and C assemblages.

Sub-unit IIIc: starts with a substantial decrease in diversity and abundance indicating a radical change in the environmental conditions, which become more stressful. The declining trend persists to 8.9 m. The stress-increasing interval corresponds to two different environmental conditions: transitional marginal from 9.3 m to 9.2 m, and confined from 9.1 m to 8.9 m.

From 8.8 m, abundance and diversity increase, with a lower rate later, up to 7.9 m. A large variability is noticed in the assemblages encountered that correspond to the transitional marginal environment (C4a).

From 7.8 m to 6.7 m, diversity and abundance variations are small, and the interval corresponds to the stable marginal environment (C4b). A noticeable barren sample was obtained from 7.4 m. This sample, similar to that at 11.0 m is within a pale regular crystalline laminated interval (Reeves, 2004). The same explanation for lack of coccoliths is thus accepted.

From 6.6 m to 6.3 m abundance and diversity fall drastically to reach those observed at the beginning of the subunit. Accordingly, sediment at 6.6 m is recognised as been deposited in a transitional marginal environment, whereas the following samples were deposited under confined conditions.

At 6.2 m, the coccoliths are moderately abundant and the assemblage consists exclusively of species from assemblages A and C. This level is correlated to the marginal stable environment. There are no coccoliths found above 6.2 m, in this unit.

- **Unit II**

Spanning from 6.1 m to 0.4 m, this unit corresponds to the Lake Carpentaria environment, but includes an episode from 4.7 m to 1.5 m characterised by a very low concentration of species from assemblage A. This assemblage consists of placolith-bearing opportunist species that are more resistant to dissolution because of the interlocking arrangement of their plates. A maximum of 20 individuals has been counted indicating a really small living community, and/or poor preservation conditions. Because of the way all samples were processed by the author, in a systematic order from the top to the bottom of the core, it is unlikely that these low concentrations are due to contamination. There is no reason for selective contamination as the samples from 0.4 m to 1.5 m and from 4.5 m to 6.2 m would also have been affected. Furthermore, the species present are variable in both quality and quantity.

- **Unit I**

This unit from 0.4 m to the top of the core corresponds to the highest diversity and abundance with up to 29 species determined per horizon, and over 3000 individuals recognised per sample. This unit represents the modern assemblages.

4.1.4 Summary of the palaeoenvironments of the Gulf of Carpentaria

Form 14.84 m to 14 m (Unit IV) the absence of coccoliths is due to non-marine conditions corresponding to the closure of both Torres Strait and the Arafura Sill, and the existence of Lake Carpentaria, or to poor preservation. The preservation of coccoliths from 13.9 m (Sub-unit IIIa) corresponds with the breaching of Arafura Sill, at least. There are no specific species from the Pacific Ocean; it is thus difficult to define when Torres Strait was submerged.

However, there is a significant increase in diversity and abundance of the coccolith assemblages above 11.5 m (Sub-unit IIIb), which could be interpreted as the breaching of Torres Strait. This explanation is supported by the dominance of *Gephyrocapsa oceanica.* This species is recognised as the typical dominant species in neritic warm, moderate to fertile water that contains a low diversity nannoflora (Okada and Honjo 1975; Cheng and Wang, 1997). In addition the assemblage during this episode is closely related to the modern assemblages, as observed by Q-mode cluster analysis (Figure 4.13).

At 9.40 m, the environmental conditions change significantly as shown by the coccolith record. The diversity falls to less than ten species and the abundance is about a tenth of those previously observed. The conditions continue to degrade up to 8.9 m where only three individuals representing opportunistic species are observed. These changes are so radical that they should be related to the closure of both sills, and to the subsequent change in the water composition away from open marine.

Above 8.8 m (Sub-unit IIIc) the re-colonisation by coccolithophorids of the area happened rapidly but not to the same extent previously recorded. Abundance and diversity are lower than in Sub-unit IIIb and quite similar to those of Sub-unit IIIa. The conditions are appropriate but not optimal for the development of the coccolithophorid community. These observations indicate connection to the open ocean over the Arafura Sill with Torres Strait being a land bridge. Above 6.6 m, increasing environmental stress led to a decrease in both diversity and abundance reflecting the closure of Arafura Sill.

The short-term re-colonisation of the Gulf of Carpentaria around 6.2 m indicates a temporary transgression of Arafura Sill.

Above 6.2 m (Unit III) there are no coccoliths (cf. Unit I) expressing non-marine conditions, and thus the existence of Lake Carpentaria. From 4.7 m to 1.5 m, depauperate coccolith assemblages were recovered. These may be related to a marginal marine influence and/or to a lower preservation rate, or higher dilution of the coccolith abundance by increasing proportion of clastic sediment.

4.2 Automated optical analysis, SYRACO

The sediment cores from the Gulf of Carpentaria were investigated using a semi-automatic coccolith recognition software SYRACO (SYstème Reconnaissance Automatique de COccolith) (Dolfus, 1997; Beaufort and Dollfus, 2004) on filter slides from all six cores. The sample description and filter slide preparation is presented in Chapter 2, Sections 2.2.4 and 2.5.2, respectively. This investigation was processed with high resolution on MD972131, at 1 cm increments where critical facies changes were recognised. Altogether more than 800 sediment-core samples were processed, and a piece of the resulting filter that holds the coccoliths was mounted in Canada balsam.

4.2.1 Why MD31?

Core MD31 was chosen for the high resolution automated optical investigation because it is the second longest core collected in the Gulf of Carpentaria, and the first one (MD32) was already optically studied in high resolution. The notion was to acquire high-resolution information on another core rather than reassessing the same one.

4.2.2 Automatic picture analysis: SYRACO

SYRACO, version 3.5 (called SYRACO in this study) is a semi-automatic coccolith recognition software based on hierarchical Artificial Neural Network (ANN) that directly processes images (64 x 64 pixels).

- Fields captured

The filter slides are placed on a Leica DMRBE optical microscope with an automatic mechanical stage, and linked to a computing system allowing the automatic capture of images. A 50 x lens and a standard digital camera (756 x 582 pixels) provide an image of coccoliths large enough for determination by a specialist and sufficiently small to allow short processing time by computer. For each slide (i.e. sample) a hundred fields (each 126 x 97 µm) are randomly captured under cross-polarised light. Under such lighting, coccoliths and all calcite fragments appear whitish on a dark background. From these

fields all objects are captured as a 64 x 64 pixel image. Objects correspond to groups of pixels with a grey level lower than average background grey level. The software that also controls displacement of the microscope stage and the focus allows the capture of 4.8 objects per second (Dollfus and Beaufort, 1999). These digital images are then rotated to bring their major axis to a preferred angle of 45° (normalisation) before presentation to the network (Beaufort and Dollfus, 2004).

All filter slides from core MD31 were processed, whereas for the five other cores, filter-slides with very low density (i.e. with no coccoliths on the first imaged field) were not processed further. Altogether, 6,370 fields were captured using this protocol, resulting in more than 2 million objects captured.

- Artificial Neural Network

The ANN is a powerful data-modelling tool that is able of capturing and representing complex input/output relationships. The first task is to acquire knowledge through learning (i.e. to recognize patterns in a data set). Once the ANN has been trained on samples of the data set, its second task is to make predictions by detecting similar patterns in future data. The ANN uses artificial intelligence (software that learns is artificial intelligence) to learn by past experience and compute whether a biometric sample and template are a match. Like any data-modelling tool, time consumption is an important consideration and SYRACO was configured to compromise between classification efficiency and computing time (Dollfus and Beaufort, 1999).

The SYRACO database 'Tropic3' was the more appropriate and thus used for the current study. This database of all input images used by the learning algorithm contains about 150 images for each eight species (*Emiliania huxleyi*, *Gephyrocapsa ericsonii*, *Gephyrocapsa oceanica*, *Florisphaera profundis*, *Helicosphaera* spp., *Rhabdosphaera clavigera*, *Umbilicosphaera sibogae* and *Umbellospaera* spp.) and about 2500 images of non-coccolith objects. The higher number of images for the latter group is due to the high shape variability of this class.

The specificity of SYRACO (v. 3.5) compared to previous versions is its double ANN: a main ANN that corresponds to the vision module; and the parallel ANN corresponding to the motor modules (Beaufort and Dollfus, 2004).

a) Main ANN

Each object previously captured is classified by SYRACO and copied to an output frame of 640 x 640 pixels dedicated to its given class. These frames can receive 10 rows of 10 objects (Figure 4.14). For each class, a new
frame is created every 100 objects.

Altogether 22,499 frames were created between the eight species recognised for this study. From these files, 9,959 correspond to the high-resolution investigation on core MD31. Half of these latter output frames (≈ 5,000) were subsequently crosschecked (Section 4.2.4) by the author to validate the use of SYRACO on the Gulf of Carpentaria samples. These frames could also be used for further morphometric studies (Beaufort, 1992).

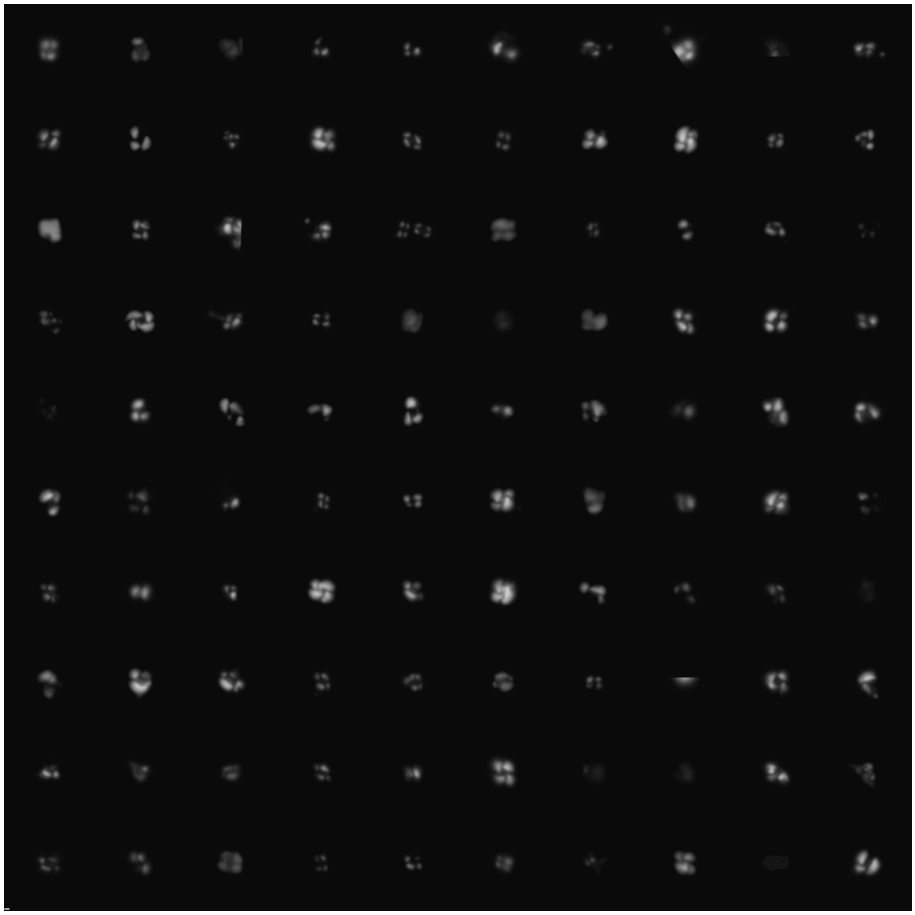

Figure 4.14: Output file from SYRACO of the *Emiliania huxleyi*
class after processing to the main ANN.

b) Parallel ANN

The aim of the parallel ANN is to transform an object (from the output frame of the main ANN) to create a new object that will be presented to the main ANN. This transformation could consist of translation, rotation, dilation, contrast and symmetry and is due to five motor modules (Figure 4.15). The motor modules learn how to transform objects for recognition by the vision module.

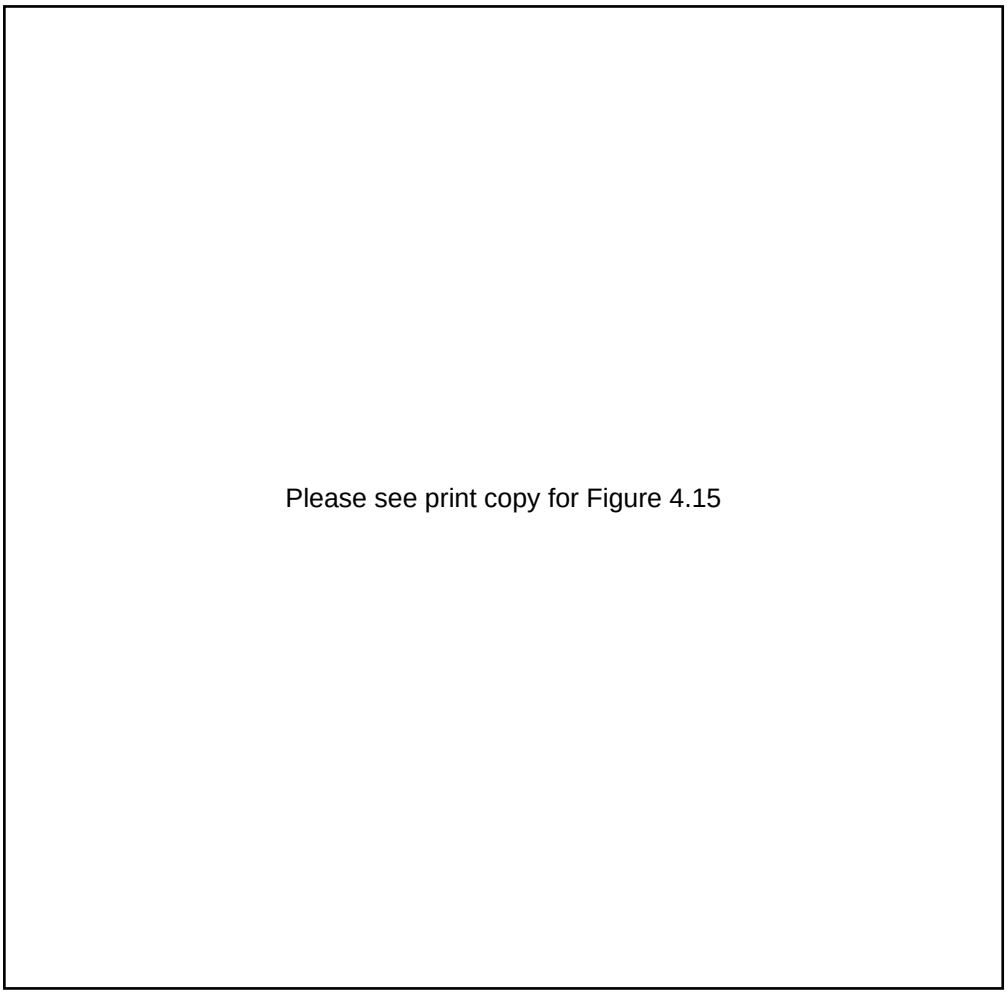

Figure 4.15: Schematic view of the complete ANN. Left panel
(pink) represents the vision module and right panels (orange) represent the motor modules. Arrows are connections between layers propagating information forward (blue) or backward (green) (from Beaufort and Dollfus, 2004).

The identity of each object is always the hypothesis to confirm or deny and determine the sequence of the actions to be processed. This sequence depends on the class being tested.

The main ANN thus perceives the same object in different positions to find the best match for this specimen with a 'learned' template. In fact, the motor and vision modules work in parallel and in synergy (back-propagation procedure). This principle is the strength of the new generation SYRACO, and the current mean accuracy of recognition for selected species of coccolithophorids is 91%. This value is significantly higher than the one obtained with previous version 2 of SYRACO (86%) that did not include motor modules (Beaufort and Dollfus, 2004).

SYRACO allows statistically sound results to be reached even in the common case of coccolith assemblages dominated by one or two species, and with higher reproducibility than human efforts for which taxonomy and counting biases generate errors. Because of the domination of *Gephyrocapsa* spp. in the Gulf of Carpentaria sediment, it is thus appropriate to use such a tool.

4.2.3 The automated investigation

The reprocessing of the 22,499 output files generated 10,091 new (reprocessed = automatically corrected) files for seven selected species: *Emiliania. huxleyi*, *Florisphaera profunda*, *Gephyrocapsa* spp., *Helicosphaera* spp., *Rhabdosphaera* spp., *Umbilicosphaera sibogae* and *Umbellosphaera tenius*, over the six cores. These files are used to plot, for all six cores from the Gulf of Carpentaria, the variation of coccolith abundance versus the depth in the core (Figure 4.16).

In these plots, placolith-bearing species (*E. huxleyi*, *Gephyrocapsa* spp. and *U. sibogae*) are yellow to red, *U. tenius* (umbelliform) is dark blue, and *F. profunda* (floriform) is dark green. All other species that belong to Young's (1994) miscellaneous group are blue (*Helicosphaera* spp. and *R. clavigera*).

The counts from SYRACO for each sample and for every species were multiplied by a coefficient (K) to obtain the number of individuals per gram of wet sediment. This coefficient is calculated as follow:

$$K = (Sf / So) / (W / D)$$

With K: coefficient to apply to the raw data;

Sf: filtration surface (42 mm effective from the 47 mm filter used, Sf = 1385.4 mm^2);

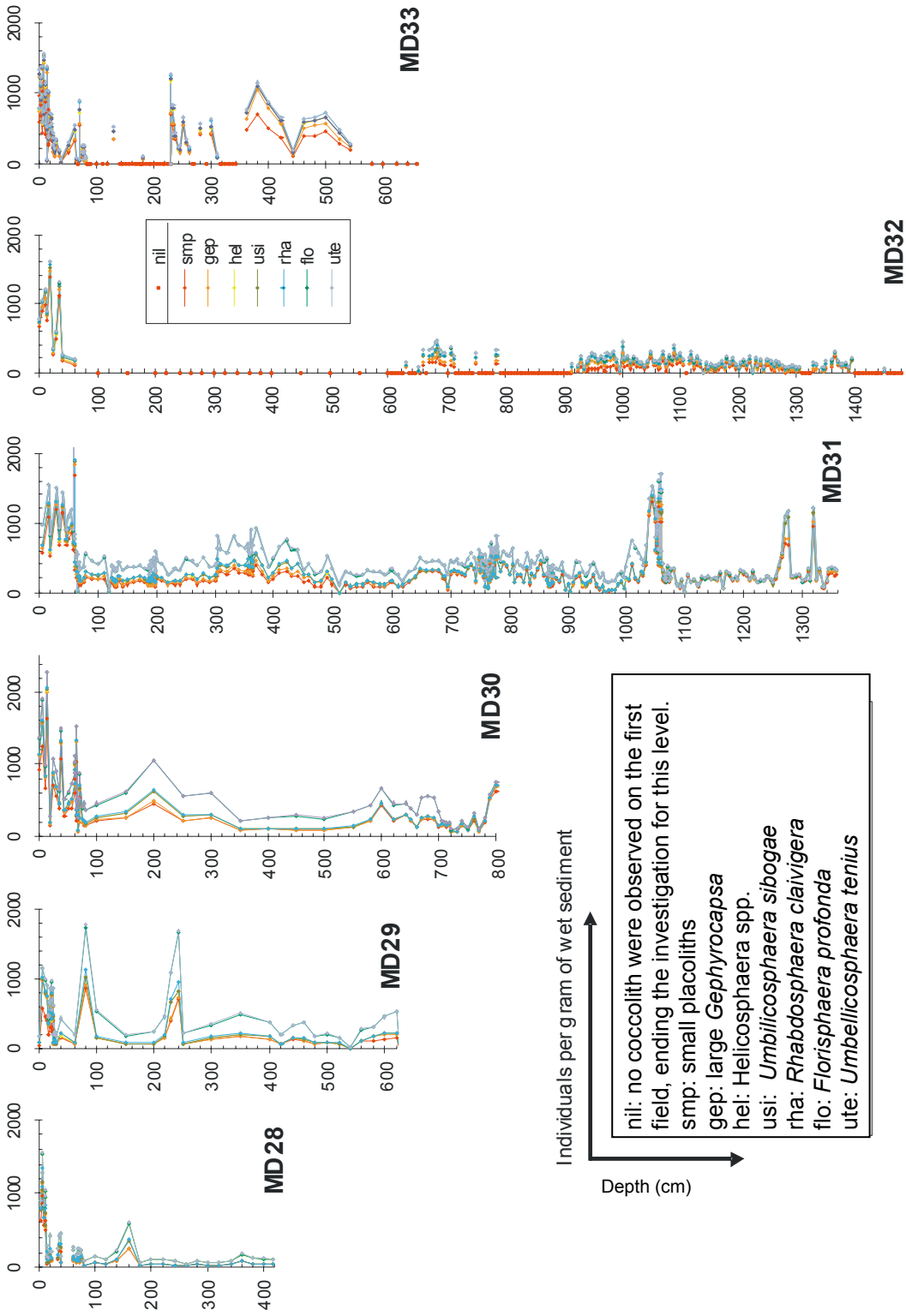

Figure 4.16: Coccolith distribution estimated and corrected by SYRACO versus depth in the core.

So surface of the observed fields (100 fields of 126 x 97 µm, So = 1222.4 mm^2);

W: weight sediment sample filtered

D: coefficient of dilution (20 ml drawn up from the 500 ml solution, Cd = 25)

Thus, $K = 28.34 / W$

This normalisation is crucial to be able to compare the results to other studies and to estimate the palaeoproductivity in the Gulf. These comparison and interpretation are discussed in Section4.6.

4.2.4 Validation of the reprocessing on core MD31 samples

As stipulated before (Section 4.2.2), the author examined the first-step output-frames from SYRACO to validate the second step (reprocessing) of this software. This validation consists of a basic counting of the number of coccoliths for each eight selected species, present on these first-step output-frames. The 5,000 selected first-step output-frames correspond to the high-resolution investigation on core MD31 from 5 to 60 cm and from 600 to 1050 cm depth. The comparison of this result with the results of the reprocessing of the same first-step output-frames is shown in Figure 4.17).
In these charts the red dotted line correspond to a 1/1 relation, meaning that both optical correction and automatic reprocessing gave the same value.

These charts show that significant variation in the automatic versus visual correction of the SYRACO analysis between species exists. Both over- and underestimation has been recognised in core MD31.

The disparity of the results shown in Figure 4.17 impedes correlation or a clear understanding of the SYRACO results at the species level. Therefore, the information on the global assemblage level was assessed. This result is more straightforward as shown in Figure 4.18. On this graph, the cumulative abundance of all coccolith species (except *Florisphaera profunda*) recognised and corrected by SYRACO is plotted versus those optically corrected.

Figure 4.18 shows the correlation between the optical investigation and automated optical analysis of coccolith distribution in core MD31 from the Gulf of Carpentaria, considering the species classified by SYRACO, without *Florisphaera profunda.*

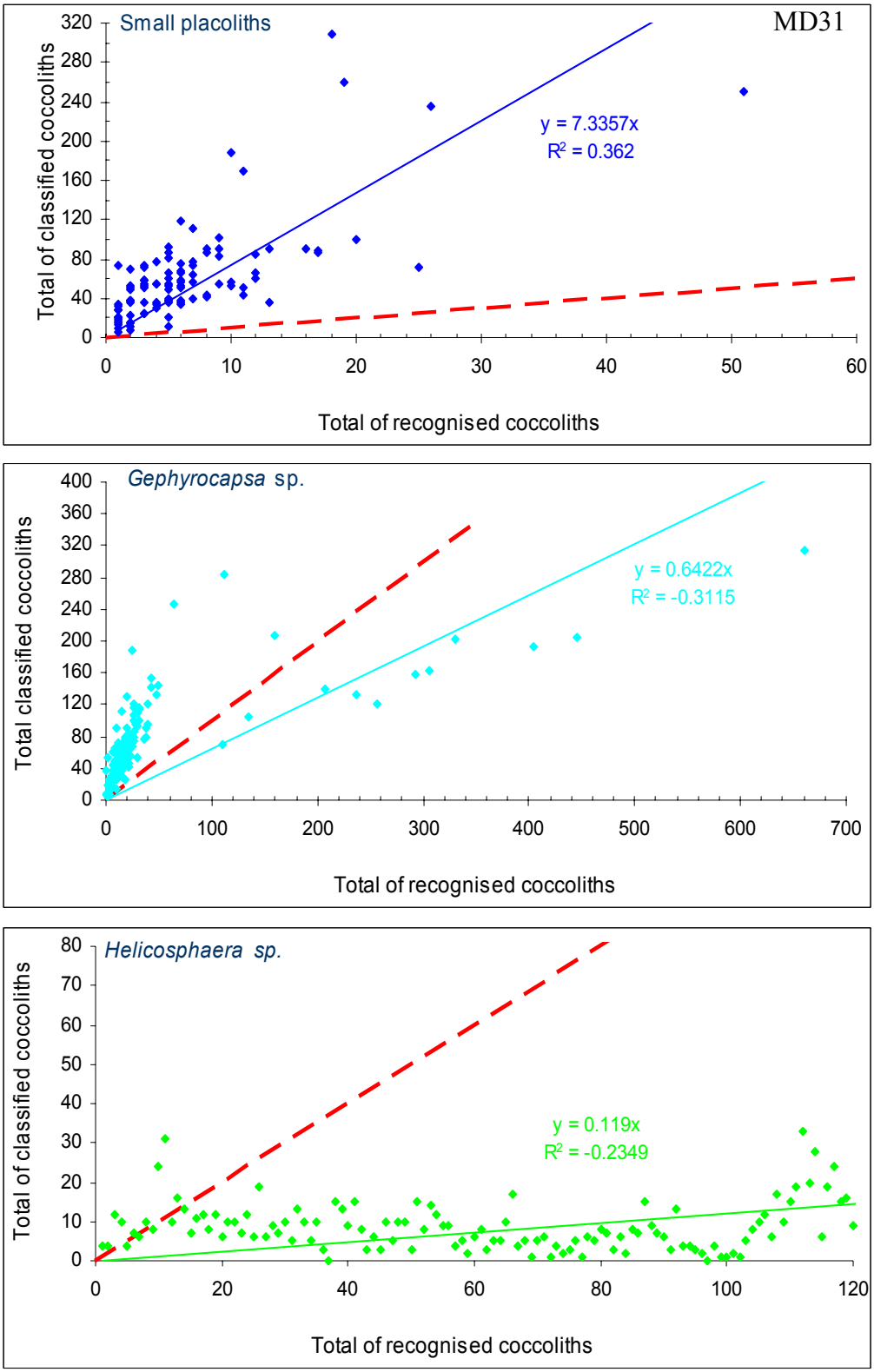

Figure 4.17: Comparison of optical and automatic corrections on MD31 samples. The values are in number of coccoliths per gram of sediment. The trendline equation and squared regression (R^2) value are also given for each population. The red dotted line corresponds to a 1/1 ratio.

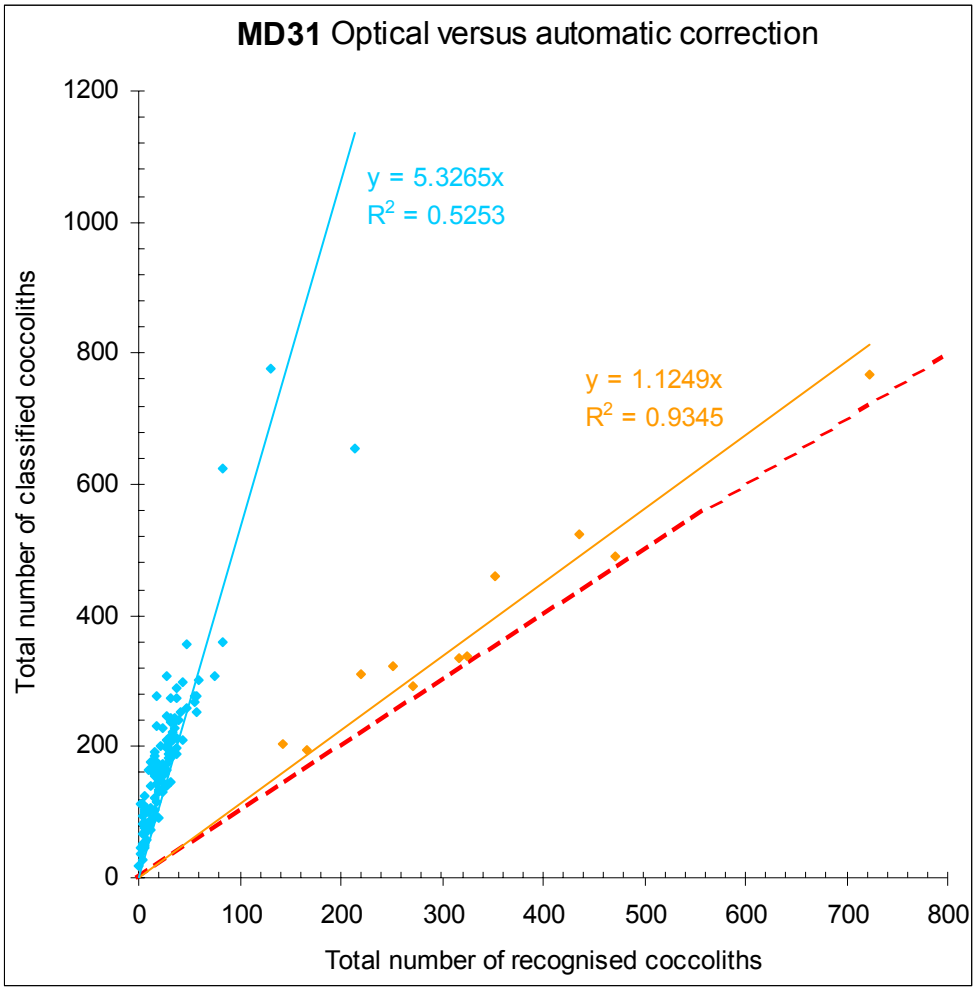

Figure 4.18: Comparison of optical and automatic corrections on MD31 for six selected species (*small placotihts, Gephyrocapsa* spp., *Helicosphaera* spp., *Rhabdosphaera clavigera*, *Umbilicosphaera sibogae* and *Umbellosphaera tenius*) in number of coccoliths per gram of sediment. Orange and blue symbols represent modern samples (5 to 60 cm) and older samples (600 to 1050 cm), respectively. The trendlines (orange, blue) equation and squared regressions (R^2) value for both modern and older assemblages are given, the red dotted line corresponds to a 1/1 ratio, and orange.

There is a strong correlation for the group of samples that corresponds to the modern assemblages (5 cm to 60 cm depth, orange diamonds) whereas there is much less correlation with older assemblages (600 to 1050 cm depth, blue diamonds in Figure 4.18). This depth-discrimination is probably due to a lower preservation of coccoliths in the older samples, which increases misclassification.

- *Florisphaera profunda*

Florisphaera profunda counts were not further considered because after checking the first-step output-frames of this class, the author realised that almost none (less than 1%) of the specimens classed in these frames were actually *F. profunda.* The alteration caused by sediment transport and/or diagenesis that affects the carbonated component of the sediment from the Gulf of Carpentaria (Preda and Cox, 2005), generates calcite fragments that SYRACO wrongly classified as *Florisphaera profunda.* The tendency for SYRACO to classify many invaders in this class is well known. Beaufort and Dollfus (2004) found up to 87% of invaders in measurements, but most of the invaders where removed after reprocessing the files. In the case of the sediment of the Gulf of Carpentaria the reprocessing cut by 70% the number of *F. profunda* found by SYRACO, which is consistent with the results of Beaufort and Dollfus (2004), but the resultant count is still very high and not realistic.

4.3 Comparison of both methods for MD32

As a high resolution optical investigation of MD32 was conducted, the results in terms of coccolith abundance and diversity is compared to SYRACO automatic counting of recognised species to validate the use of this software in all the cores. The comparison of these two methods is done only on the seven species for which SYRACO is trained (*Florisphaera profunda* was disregarded). The following graph (Figure 4.19) shows for each level the results of both techniques. For some levels, coccolith assemblages were not assessed optically, while other levels were not classified by SYRACO as shown in the following figure. The cumulative abundance of the six species recognised by SYRACO are represented on a weighted scale (1 to 6) for the optical investigation and in number of individuals per wet gram of sediment for the SYRACO investigation.

Figure 4.19 shows an unexpected good correlation between SYRACO and the optical investigation of core MD32. This result is probably due to the close relation existing between coccolith abundance and primary production (Beaufort et al., 1997; Sabine et al., 2002; Baumann et al., 2004). In fact, SYRACO misclassifies tiny calcite particles that are similar to coccoliths by their size and optical property (symmetry for example) under polarised light. These tiny calcite particles are likely to be of biogenic origin, representing fragments from larger organisms (mainly foraminifera) and thus indicating the productivity level present at the time of their deposition.

Due to the good correlation between SYRACO and optical analysis shown in Figure 4.19, the curve of the SYRACO investigation of all six cores (Figure 4.16) is used to interpret palaeoenvironments of the Gulf of Carpentaria. However, the levels with no coccoliths on the first field have to be interpreted with caution as they may just express lower abundance.

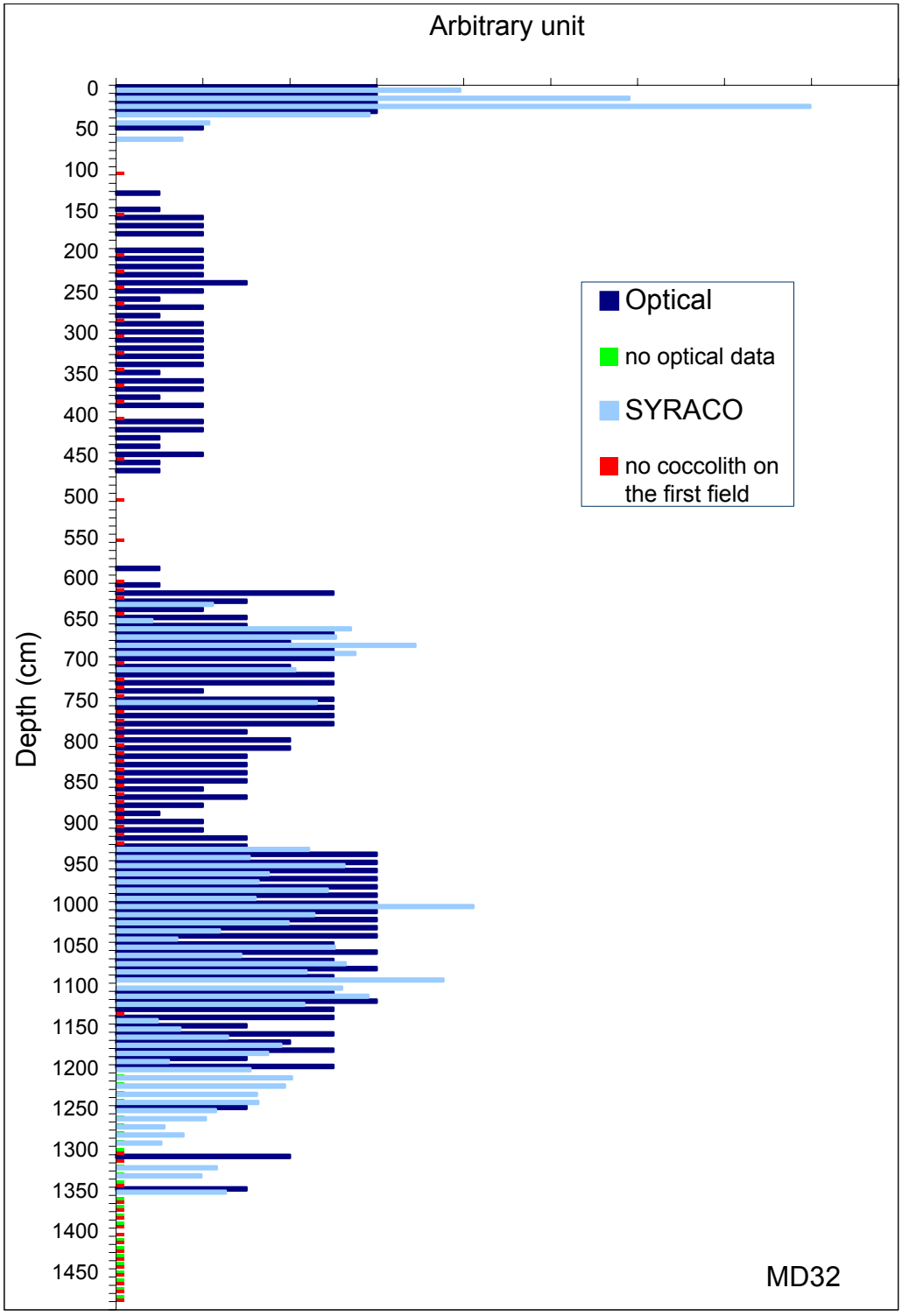

Figure 4.19: Comparison between SYRACO automated optical investigation and classic counting for core MD32 from the Gulf of Carpentaria.

4.4 Summary

In MD 32, microscopic observation of nannofossils allows the definition of four major environmental facies in the Gulf of Carpentaria cores, and a succession of different conditions ranging from open ocean to confined water are noted. These conditions correspond to the opening of one, two, or none of the sills, and the transitional periods whilst active channels sporadically connected Lake Carpentaria to the Indian Ocean. At least two major non-marine/marine cycles are recognised with suggested minor incursions of seawater during non-marine phases.

The optical investigation on MD32 provides a framework for interpreting the SYRACO analysis of all six cores collected in the Gulf of Carpentaria. Like the optical observation, the automated optical investigation shows a clear dominance of placolith-bearing coccoliths.

Chapter 5:

Synthesis and Conclusions

5.1 Introduction

This chapter provides an interpretation of the palaeoenvironments of the Gulf of Carpentaria over the last 180 ka by means of OSL dating (Chapter 3) and analysis of coccolith assemblage and abundance distributions (Chapter 4) within a series of marine sediment cores. The interpretations presented here integrate the results of this thesis as presented in Chapters 3 and 4, with the detailed sedimentological analysis by Reeves (2004, 2005 unpublished data) and physical data from the preliminary report on the Gulf of Carpentaria (Chivas et al., 2001). A comparison between the interpretation based on this integrated analysis, and those based on other palaeoenvironmental data, namely ostracods (Reeves, 2004), pollen (Chivas et al., 2001; van der Kaars unpublished data, 2002) and for the Late Quaternary foraminifers (Holt, 2005), is also undertaken to reconstruct more precisely the sequence of palaeoenvironmental successions recorded in the Gulf.

When viewed together, the compilation and interpretation of these data enable the development of a detailed spatial and temporal understanding of the palaeoenvironmental history of the Gulf of Carpentaria since MIS 6.6 (ca. 180 ka). These collated results are presented on a series of maps illustrating the discrete closure and breach sequences of the Arafura Sill and Torres Strait as related to Quaternary sea level fluctuations, and the corresponding alternations between the Gulf of Carpentaria and Lake Carpentaria.

5.2 Synthesis

The two following graphs summarise this study outcomes, and form the basis of interpretation and discussion. Figure 5.1 shows details of the correlation between the optical coccolith investigation of MD32 and a sea level curve, and Figure 5.2 correlates all six cores utilising results of the SYRACO analysis.

On the sea-level curve in Figure 5.1, where the red curve passes through the green shading it corresponds to times of activity of the palaeochannels incised in the Arafura Sill, i.e. when sea-level was lower than the Arafura Sill but a marine influence was still present in the Gulf of Carpentaria. The light blue shading signifies times when the sea was higher than the Arafura Sill, but lower than Torres Strait. And the dark blue shading corresponds to open marine conditions with both sills open. The section of the sea-level curve not shaded represents periods where there was no connection between Lake Carpentaria and the ocean. In Figure 5.1, the dashed lines connecting the relative sea-level curve to the cumulative abundance graph indicate boundaries between units and sub-units as described in Section 5.3. In the cumulative abundance graph on the upper portion of the figure only OSL dates are displayed (in red). The coccolith distribution shown in this graph has added data in the deeper section (from 13.9 m to 13.6 m, 13.3 m to 13.2 m, 13.0 m to 12.6 m, and 12.4 m to 12.1 m). A smear slide at 11 m was re-made, as the previous slide was composed entirely of gypsum, and is also included in this graph.

The older palaeoenvironments of cores MD28, MD29 and MD30 are not discussed in Section 5.3 because of the sparcity of the data available and the lack of dating older than 14.35 ± 0.09 ka, 9.81 ± 0.09 ka and 11.88 ± 0.17 ka, respectively. However the correlation of the younger intervals of these cores corresponding to unit I and late unit II is mentioned in Section 5.3.6 and an attempt to correlate the older levels of each three cores is performed in Figure 5.2. All dates in Figure 5.2 are shown in ka, radiocarbon dates are in pink, OSL dates in purple. Solid lines correlating units between all cores are supported by dates, whereas dashed lines are an attempt at correlation based only on SYRACO classification of coccoliths. The definition of the units in core MD32 is also based on the optical investigation, which is more precise.

Figure 5.1: Correlation between the nannofossil assemblage obtained by optical investigation of core MD32 from the Gulf of Carpentaria (Chapter 4, Section 4), and the sea level curve (red line) with associated confidence interval (pink lines) from Waelbroeck et al. (2002). Units (blue) and sub-units (green) are separated by blue and green dotted lines, respectively. Grey dotted lines represent noticeable events.

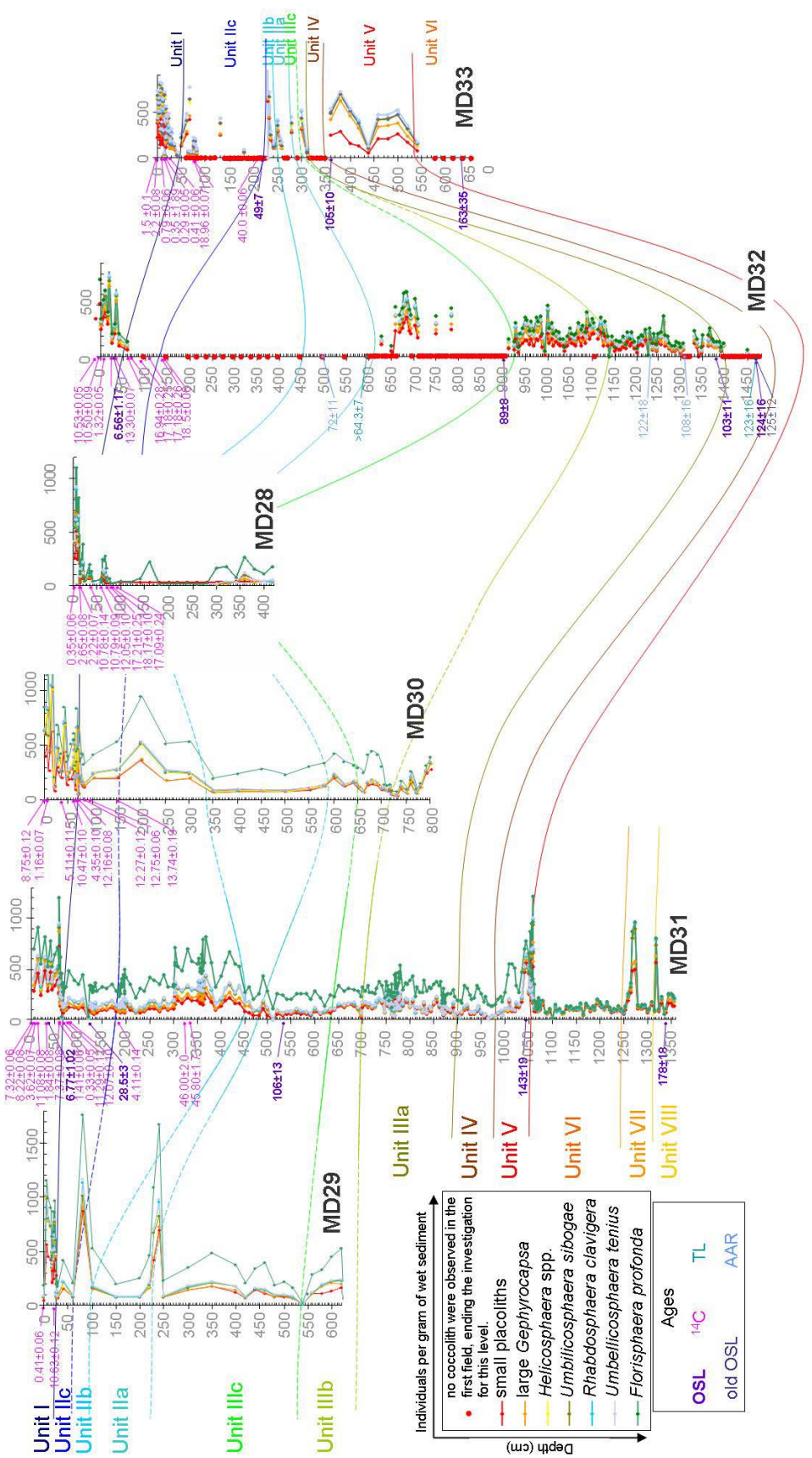

Figure 5.2: Correlation, on a west-east cross section, between all six cores collected in the Gulf of Carpentaria by the means of SYRACO results on the nannofossil assemblage distribution. Units are represented by dotted lines over the cores, plain line portions corresponding to interpretation supported with OSL, TL and ^{14}C dating.

5.3 Palaeoenvironments of the Gulf for the last 180 ka

Foraminifers were investigated by Holt (2005) for the top 1.5 metres for each of the six Gulf cores, and consequently her palaeoenvironmental reconstructions for this environmental proxy are limited to a relatively short interval in cores that are up to 14.8 metres in length. Pollen was also initially investigated for the top 1.5 metres at 5 cm increments for all six cores by van der Kaars (Chivas et al., 2001) who subsequently carried out a similar investigation on the whole length of core MD32 (van der Kaars, unpublished data 2002). The following comparison presented in this chapter consists primarily of a correlation between ostracodal (Reeves, 2004) and coccolith records. The major difference between ostracods and coccoliths lies in their dwelling habit; the former fauna are benthic (i.e. live on the sea floor) whereas the latter flora are planktonic (i.e. live in the upper parts of the water column). However, because the Gulf of Carpentaria is and was shallow over the Late Quaternary study period (Chapter 1, Section 1.2), both organisms were exposed to similar sub-aqueous conditions except during possible extended periods of stratification of the water column.

The different environments recorded by nanno- and microfossil assemblages, together with typical sedimentological features identified within the cores, can be logically interpreted in terms of connection to, or isolation from, the Indian and Pacific Oceans, thereby providing information about past sea-level fluctuations in the area. Three major environments have occurred in the Gulf of Carpentaria throughout the Quaternary, corresponding to the flooding of both (marine), one (restricted), or neither (lacustrine/exposed) of the sills forming the eastern and western oceanic boundaries, due to the difference in elevation between the sills. These major environmental changes are expressed in the floral and faunal records as distinct assemblages, which are indicative of marine environments ranging from open-marine to confined, or by the absence of signature marine communities, indicating non-marine episodes. Other assemblages typical of a more sporadic marine influence have been recorded in the Gulf cores analysed for this study. These communities probably correspond to periods when sea levels were lower than the Arafura Sill, but when active channels episodically delivered Indian Ocean water to the Gulf (confined environment). Jones and Torgersen, (1988) reported the existence of at least two former deep channels, incised to 62 m and 75 m below present sea level (bpsl), respectively, across the Arafura Sill. The sedimentary deposits forming the surface of the Arafura Sill are also thought to have fluctuated in elevation between 50 m to 60 m bpsl over the mid-late Quaternary (Jones and Torgersen, 1988).

In the following interpretation, AAR dates were not utilised because they are thought to be overestimated. Thus chronology is only based on OSL dates determined in this study (Chapter 3) together with ^{14}C (calibrated and conventional) and TL ages (Chivas et al., 2001; Price, personal communication, 2001).

5.3.1 Marine Isotope Stage 6

The oldest unit (unit VIII, Figure 5.2) collected from the Gulf of Carpentaria during this sampling campaign is briefly represented (from 13.6 m to 13.4 m) at the bottom of core MD31, located on the western margin of the basin. The base of this unit was OSL dated at **180 ± 18 ka,** an age that corresponds to MIS 6.6 (Figure 5.3).

Please see print copy for Figure 5.3

Figure 5.3: Palaeoenvironmental condition contemporaneous with unit VIII deposition or MIS 6.6. On this and the following maps, core(s) used for the palaeoenvironmental interpretation supported by dates are identified by dark red text, cores from which no sediment was recovered from that depth (i.e. the unit deposited at that time is not represented) are identified by light red text, and cores in which the unit is represented but this interpretation is not supported by dates are identified by pink text.

This unit consists of very dark grey sticky sediment with well-sorted rounded quartz and calcareous concretions that Reeves (2004) attributed to a marginal mudflat environment with possible fluvial input. Unit VIII has certainly been deposited when both the Arafura Sill and Torres Strait were sub-aerially exposed. However the presence of sparse coccoliths suggests a probable sporadic marine influence. This intermittent marine influence is considered to be related to the active operation of at least the deeper incised channel across the Arafura Sill and thus a sea level around 75 m bpsl (Jones and Torgersen, 1988).

Unit VII, (from 13.3 m to 12.6 m in core MD31, Figure 5.2) is characterised by highly fluctuating coccolith abundance (Figure 5.4). The almost complete disappearance of coccoliths around 13 m may be due to poor preservation in a high-energy environment rather than the existence of non-marine conditions, as suggested by the presence of larger marine shell fragments.

Please see print copy for Figure 5.4

Figure 5.4: Palaeoenvironmental condition contemporaneous with unit VII deposition or MIS 6.5

Organic matter content around this level is much lower than in previous deeper levels (Reeves, 2004), which supports the theory of low preservation potential. The dissolution of organic matter increases the partial pressure of carbon dioxide within the water column and prevents further dissolution of calcium carbonate. Water with low levels of organic matter has a lower preservation rate for organisms with calcium carbonate skeletons. The broken marine shells are also suggestive of deposition in a high-energy environment that is consistent with the position of core MD31 on a channel track.

In unit VII the abundant coccolith community is associated with planktonic and benthic foraminifers, with minor mica and pyrite framboidal aggregates in a silty-clay sediment (Reeves, 2004). The presence of in-situ marine flora and probably transported marine fauna, along with the non-marine fauna, indicates an increased marine influence. This is interpreted as the transgression prior to MIS 6.5, when rising sea levels activated the more deeply incised channel across the Arafura Sill, implying a global sea level of about 55 m bpsl.

The overlying unit VI (from 12.5 m to 10.7 m in core MD31, Figure 5.2) is barren of coccoliths and is interpreted as a drop in sea level below that necessary to allow exchange of sea-water from the Indian Ocean through the Arafura Sill incised channels into the Gulf of Carpentaria. This unit corresponds to MIS 6.4 to MIS 6 (Figure 5.5). It is characterised by a coarsening upward sequence that includes many fine dry silty laminae. The barren fine-grained horizons are interbedded with coarser intervals rich in marine and non-marine fossils (Reeves, 2004). These highly heterogeneous successions where fossil assemblages range from abundant and diversified to barren intervals imply repetitive and drastic changes to environmental conditions.

The presence of pteropods within the unit, which have aragonitic shells, is suggestive of excellent preservation conditions that are contradictory with the absence of coccoliths. When preservation conditions are sub-optimal, pteropods can nevertheless be preserved in mass transported sediments such as turbidites (Singh et al., 1998; Sabine et al., 2002). The presence of turbidite-type transport into the Gulf of Carpentaria seems less than probable due to the very slow slope of the basin. However mass transport sedimentation into this basin might be generated by major overwash events from the Indian Ocean. The recent tsunami (26/12/04) that affected the Indonesian area, proves that overwash events

related to extreme seismic activity can occur in the area, and can have considerable impact on the surrounding low-lands over large distances. Similarly, overwash events from extreme cyclone activity could also have considerable impact over lowland areas. The fact that both marine and non-marine fossils are found in abundance in the coarser laminae of this unit suggests that enhanced cyclonic activity generating both stormy marine conditions and high terrestrial rainfall/runoff seems a plausible explanation for the unusual characteristics of this unit. This model is consistent with a sea level around 80 m bpsl that is within the confidence interval of the sea level curve for MIS 6.3 (Figure 5.1), and with the open shallow marine pulses recognised between 11.8 m and 11.1 m depth in core MD31 by Reeves (2004).

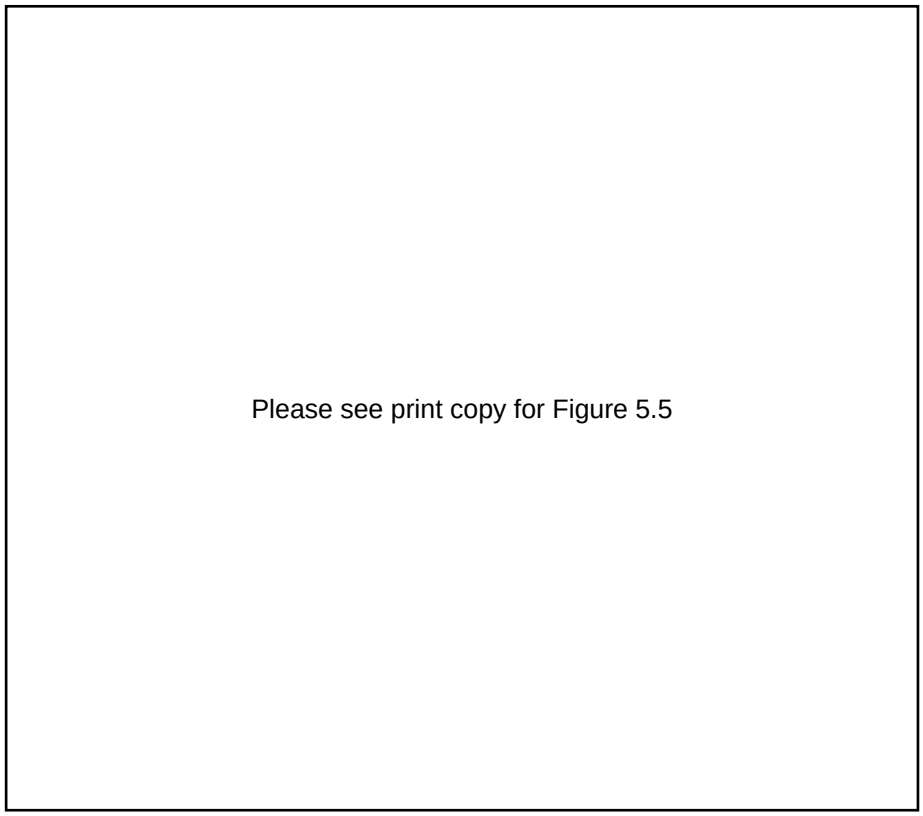

Figure 5.5: Palaeoenvironmental condition contemporaneous with unit VI deposition or MIS 6.

Another scenario is possible if considering that in anoxic sediments, sulfate reduction increases alkalinity, leading to calcium carbonate fossils being excellently preserved (Berger and Soutar, 1970; Diester-Haass et al., 1998). Singh et al. (2005) found that pteropod shells in sediments of regions with anoxic bottom conditions are generally well preserved. The rhythmicity between coarse macrofossil-rich horizons and silty-fine barren laminae would then correspond to periods of high productivity, ending by eutrophication

of the system, and alternating with unproductive and low energy episodes. In this model the high-energy high-production periods express enhanced cyclonic activity and/or monsoon intensification and important rainfall/runoff. During these periods the sediment of the Gulf would become anoxic with decreasing fresh-water input, as indicate y the presence of organic matter and pyrite. As low water inputs persisted, corresponding to dry conditions with low cyclonic and monsoonal activities, and probably associated with low winds, fine silty laminae were deposited/precipitated in the Gulf.

A probable combination of both scenarios occurs in the Gulf. Episodic input of Indian Ocean waters along with overwash contribution related to a period of enhanced cyclonic activity, associated with desiccation periods might explain the heterogeneity/rhythmicity of the signal in Unit VI.

Unit VI is also represented (from 6.6 to 5.5 m) in core MD33, which lies in a more central location within the Gulf of Carpentaria. In this core the unit lacks fossils but contains large concretions and a cemented horizon. In core MD33 there is no comparable sedimentary signature to the stormy overwash deposits found in core MD31; however the presence of the concretions clearly indicates an increase in aqueous carbonate content that could be related to post-storm overwash conditions. The substantial quantity of shelly matter delivered into the Gulf from overwash of shallow subaqueous and subaerial parts of the Arafura Sill (as indicated by the coarse fossil-rich strata), together with decaying organic matter, is likely to have increased the carbonate saturation of the water, resulting in production of carbonate concretions (Leeder, 1982). Unit VI was OSL dated at **163 ± 65 ka** in core MD33 and corresponds to MIS 6.3. This age correlates with the upward coarsening of the sediment profile toward the top of the same unit in core MD31 that suggests a transgressive episode, which is interpreted as the regression prior to MIS 6.2.

5.3.2 Marine Isotope Stage 5

Unit V is marked with abundant coccolith assemblages in core MD31 (from 10.6 m to 10.0 m, Figure 5.2) and core MD33 (from 5.4 m to 3.6 m, Figure 5.2). This unit begins with a shell lag layer in core MD31, which is consistent with typical transgressive sequences. In core MD31, the fossil assemblage shows evidence of reworking and the presence of broken shells and echinoid spines indicating a moderate-energy environment (Reeves, 2004). In core MD33, a diverse marine microfauna is present above 5.5 m. This

community has a sugary texture, which Reeves (2004) interpreted as being characteristic of transportation, but subsequent accumulation in a low-energy environment is also evident because of the presence of fragile organisms. All microfossil species present in core MD33 show evidence of reworking whereas only a few species from core MD31 display such features (Reeves, 2004). Because core MD33 is sourced from a deeper part of the Gulf than the more marginal core MD31 obtained from closer to the Arafura Sill (Figure 5.6), the evidence of marine assemblage reworking in core MD33 cannot be inferred to be the result of fluvial or palaeochannel activities. In spite of this, cyclonic activity, which is far more erratic, can produce such reworking regardless of distance to the shore in the relatively shallow waters of the Gulf. The reduction in the microfossil assemblage diversity observed by Reeves (2004) after 4.6 m in core MD33 may indicate the beginning of the regression post-MIS 5.5. The lack of coccoliths at 4.4 m deep is probably due to poor preservation due to a change in water quality as indicated by the simultaneous disappearance of pyrite and appearance of iron-oxide observed by Reeves (2004) in the sediment.

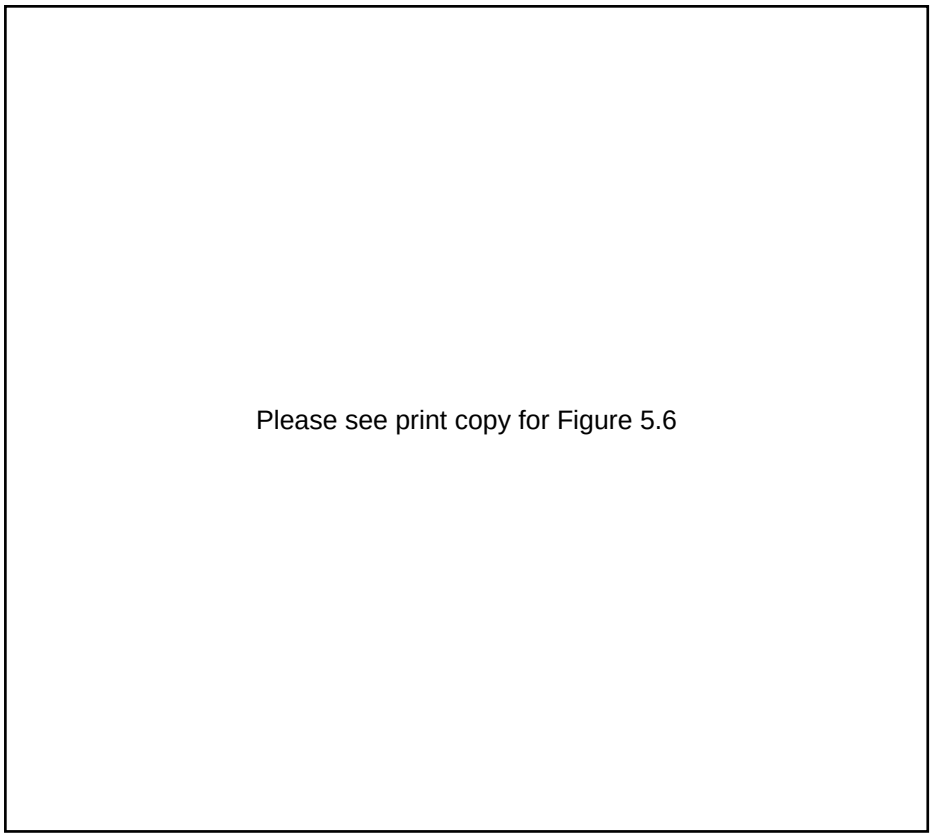

Figure 5.6: Palaeoenvironmental condition contemporaneous with unit V deposition or MIS 5.5.

The presence of a large variety of marine fauna together with an abundant marine flora in both cores record the breaching of at least the Arafura Sill, and probably Torres Strait. Unit V is thus interpreted as being deposited during MIS 5.5 (Figure 5.6). This interpretation is consistent with a sample near the base of this unit in core MD31 OSL dated at **143 ± 19 ka**, and a sample near the top o this unit in core MD33 OSL dated at **105 ± 10 ka**.

There is a large difference between the length representing unit V in the core logs of cores MD31 and MD33. The unit is longer in core MD33 than MD31, which may be due to the high energy level during the transgression from MIS 6 to MIS 5.5. Most of the sediment was probably washed through to the deepest centre of deposition (MD33).

Unit IV, which lies on top of unit V, is radically different with sparse marine flora and fauna. This unit is represented in core MD31 from 9.9 m to 8.9 m, in core MD33 from 3.5 m to 3.1 m and in core MD32 from 14.8 m to 14 m. In core MD32, this unit is barren of flora and fauna but is rich in quartz and returned OSL dates of **124 ± 16 ka** at the base and **103 ± 11 ka** at the top. These close ages imply a period of rapid deposition and/or mixing for this well sorted relatively coarse unit. The base of unit IV was previously OSL dated at **125 ± 12 ka** and TL dated at **123 ± 16 ka** (Chivas et al., 2001). Combined with the result of the present study, the pooled dates give a mean age of approximately 110 ka for unit IV that corresponds to MIS 5.4, an interpretation that is also supported by the sedimentological nature of unit IV. As suggested by Reeves (2004), the combination of the quartz variety and distribution, together with other mineral occurrences indicative of decreasing energy upwards through the sequence, may represent a prograding deltaic sequence deposited after a drier episode (Figure 5.7).

In core MD33, unit IV is briefly represented. The unit is barren of coccoliths or planktonic foraminifers, but includes some benthic microfauna characteristic of Lake Carpentaria assemblages, with all microfauna showing evidence of bleaching (Reeves, 2004). These selective preservation conditions, together with the lack of microfossils within unit IV in cores MD31 and MD32, suggest the probable existence of salinity stratification within the water column. Highly dissolving water (freshwater) at the top of the water column would prevent the development of a planktonic community or at least rapidly dissolve their skeletons after death, whereas less aggressive (more saline) underlying waters in the deeper part of the basin, allowed the development and partial preservation of a benthic

community. These considerations are suggestive of wetter conditions than present at 103 ka that corroborates well with increasing evidence from recent research indicating wetter conditions after about 100 ka in the southern hemisphere (Nanson et al., 2005; Baker et al., 2002).

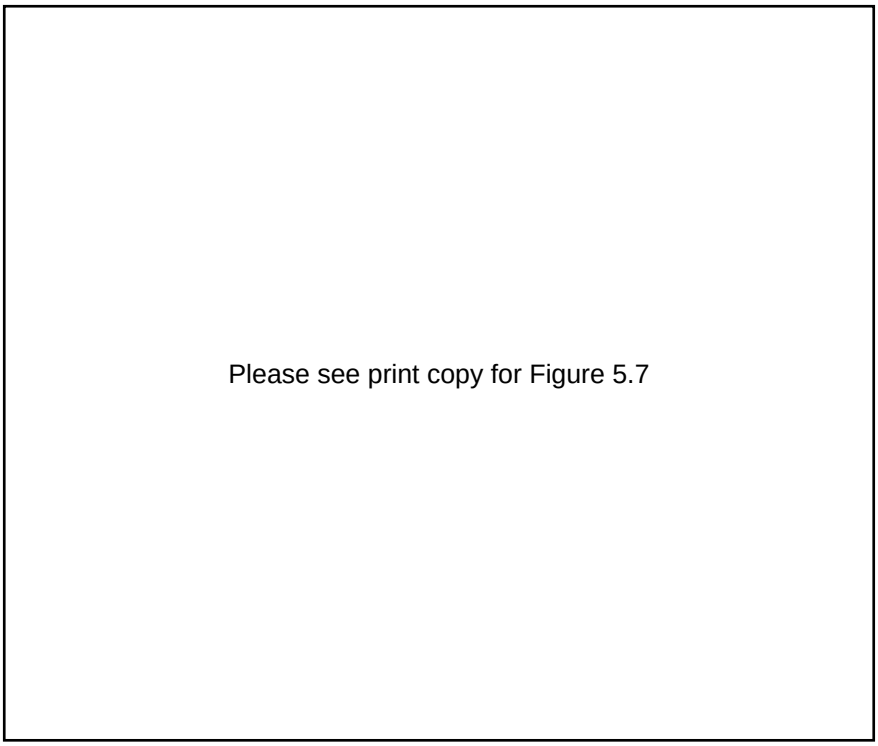

Figure 5.7: Palaeoenvironmental condition contemporaneous with unit IV deposition or MIS 5.4.

The lack of coccolith and planktonic microfauna within unit IV is probably due to poor preservation conditions related to salinity stratification rather than to the complete disconnection of the Gulf from marine influences. The marine water was probably diluted by monsoonal rainfall and runoff, with the top of the water column becoming highly dissolving for carbonates, whereas the stratification protected the bottom layer of water from such dilution, allowing the development of a benthic community. However, the low diversity of the benthic assemblage and the presence of a benthic microfossil assemblage characteristic of Lake Carpentaria, are suggestive of a restricted environment sensitive to the opening of the Arafura Sill and with a sea level close to the height of the sill. Unit IV is thus associated with MIS 5.4.

This reasoning is consistent with the longer sequence representing unit IV in core MD31 (1.4 m) compared to cores MD32 (0.8 m) or MD33 (0.4 m). When conditions are wetter, river discharge into the Gulf is increased and results in a net increase in sedimentation rates in the more landward parts of the basin. MD33 is the most centrally located core and thus the most distal to riverine influences. MD31 is a more landward core, and consequently accumulated a greater depth of fluvial origin sediment than the other cores during the same time intervals. Furthermore, the pollen record indicates an ephemeral brackish lake at the base of unit IV, becoming fresher toward the top of the unit together with wetter climatic conditions (van der Kaars, unpublished data 2002).

Unit III is represented in the 3 major cores from 8.8 m to 4.9 m in core MD31, from 3.0 m to 2.8 m in core MD33, and from 13.9 to 6.2m in core MD32. This unit is well represented in core MD32 (Chapter 4, Figure 4.11) where the high-diversity coccolith assemblage indicates marine influence and thus breaching of at least the Arafura Sill, and allows the definition of three sub-units. In core MD32, the moderate uneven coccolith abundance at the base of unit III (sub-unit IIIa from 13.9 m to 11.5 m), increases to a plateau with abundances similar to modern assemblages (sub-unit IIIb from 11.4 m to 9.4 m), then drastically falls to a few individuals to return later to moderate uneven levels (sub-unit IIIc from 9.3 m to 6.2 m).

Sub-unit IIIa corresponds to the transgression between MIS 5.4 and MIS 5.3 (Figure 5.8), while sub-unit IIIb is interpreted as the breaching of Torres Strait during early MIS 5.3.

The similarity between sub-unit IIIb and modern assemblages shown by the Q-mode cluster analysis (Chapter 4, Figure 4.13) supports this interpretation. The ensuing stability of coccolith diversity and abundance suggests stability in environmental conditions and is attributed to late MIS 5.3 (Figure 5.9). Sub-unit IIIa spans a longer core length but represents a shorter time period than sub-unit IIIb, and probably experienced higher sedimentation rate. The increase in sedimentation rate may be due to a boost of clastic input during the transitional transgression phase under wetter conditions, and is substantiated by the coarsening upwards of the sequence as described by Reeves (2004). Establishment of extensive mangroves along the coastal zone (van der Kaars, unpublished data 2002) also indicates a period of sea level rise, recorded from between

13.9 m to 12 m in core MD32 (sub-unit IIIa). The mangrove cover subsequently reduces and then disappears at a level of 9.6 m in core MD32 (sub-unit IIIc).

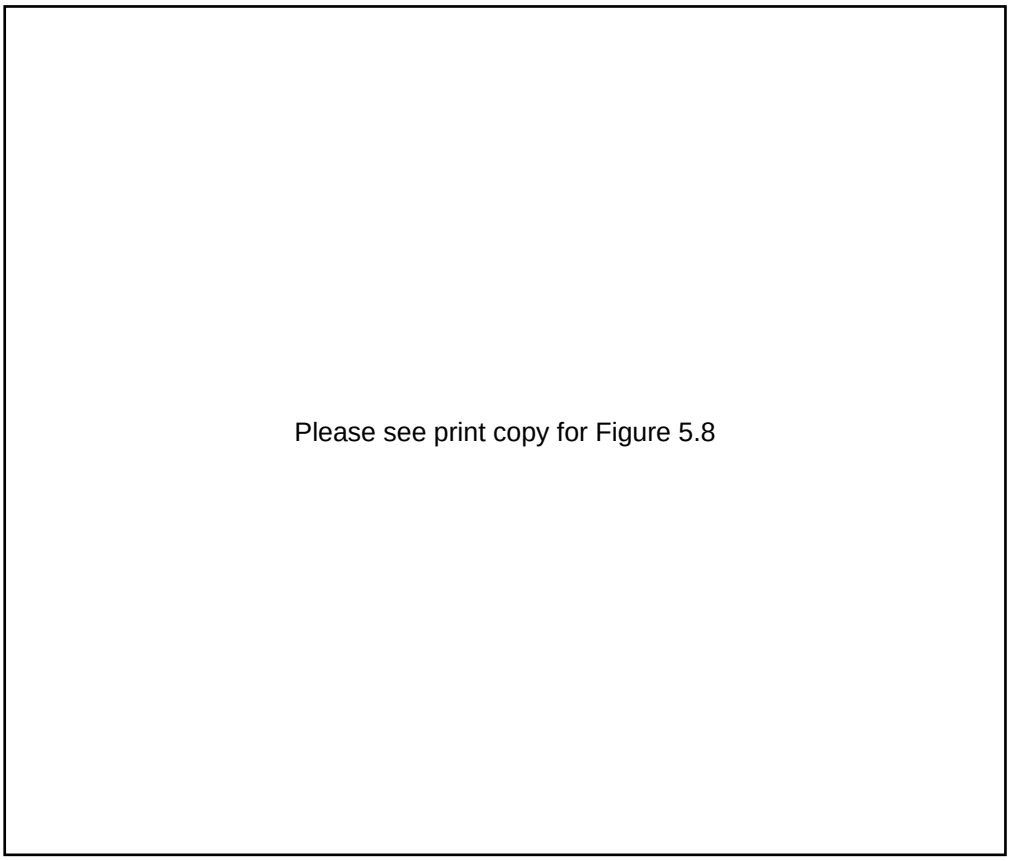

Figure 5.8: Palaeoenvironmental condition contemporaneous with unit IIIa deposition during MIS 5.4/5.3 transgression.

The three sub-units of unit III can be recognised in core MD31: sub-unit IIIa from 8.8 m to 7.0 m; sub-unit IIIb from 6.9 m to 6.5 m; and sub-unit IIIc from 6.4 m to 4.9 m. In core MD31, coccolith abundance varies in similar manner to core MD32, with high variability during the transgressive transition phase (sub-unit IIIa), then a stabilisation is observed (sub-unit IIIb) before a drastic fall in abundance. Sub-unit IIIc in core MD31 is characterised by the very low occurence of preserved coccoliths probably indicating a high dissolution rate. The presence of abundant quartz in this sub-unit indicative of enhanced fluvial activity and sediment delivery, together with the lack of microfauna from 5.8 m to 4.8 m in MD31 (Reeves, 2004), supports this interpretation. An increase in coccolith abundance at the very end of sub-unit IIIc (4.9 m) is also apparent.

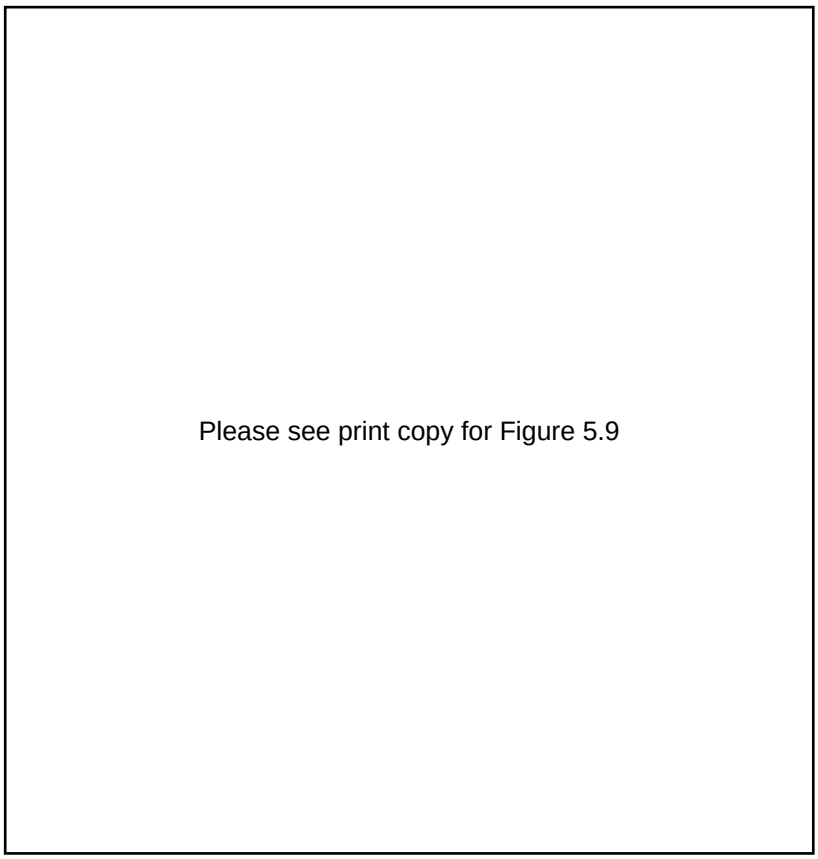

Figure 5.9: Palaeoenvironmental condition contemporaneous with unit IIIb deposition or MIS 5.3.

The record is less clear in core MD33 due to the sparsity of slides counted by SYRACO within this interval. Also, unit III is less well represented in this core than in cores MD31 and MD32, with only 30 cm (from 3.1 m to 2.8 m) of core log compared to 3.9 m in core MD31 and 7.7 m in core MD32. This difference can possibly be explained by a proximal-distal relationship as the modern sedimentation rate is lower in the depocentre of the Gulf. The large difference in the length of core log representing unit III between the eastern core and the two more western cores is probably due to the massive input of clastic fraction due to wetter conditions and the transgression phase, which had enough energy to encompass core MD31's location and to just reach the site of core MD32. Despite the relative proximity of cores MD33 and MD32, they belong to two unlike physical environments, core MD32 sits on a very low gradient plateau whereas MD33 is at the bottom of a steep depression. This characteristic together with the distance from the sediment source can possibly explain the significant difference between the sedimentation rates of these two sites. The lack of coccoliths in MD33 at 2.9 m must correspond to the very start of sub unit IIIc.

The drastic changes in the coccolith community, which almost entirely disappears at the beginning of sub-unit IIIc, OSL dated at **89 ± 8 ka**, is most likely related to the closure of both sills, and is interpreted as indicating MIS 5.2. The subsequent rapid re-establishment of the coccolith community is a result of the flooding of the Arafura Sill and is interpreted as evidence of MIS 5.1 (Figure 5.10).

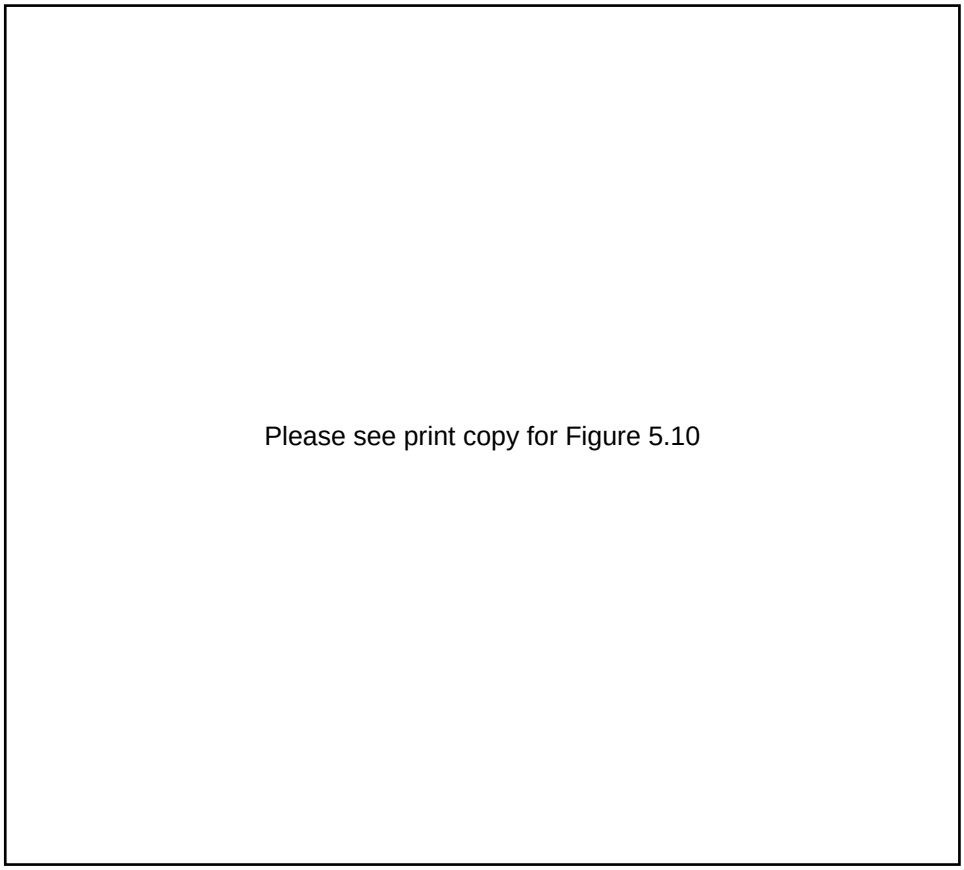

Figure 5.10: Palaeoenvironmental condition contemporaneous with unit IIIc deposition or MIS 5.1

Sub-unit IIIc was OSL dated at **106 ± 13 ka** in core MD31. This age seems too old for this unit and may again be the result of reworking of surficial sediment in core MD31 that sits near a palaeochannel. In fact, most of the cores collected in the Gulf that were intensively dated by ^{14}C show evidence of reworking (Appendices 7.1 to 7.6).However because it is the second date in core MD31 that seem to be overestimated, the suitability of the water correction applied to calculate the OSL dates (Chapter 3, Section 3.11.3) may be questioned. The water content for MD31-1040 and MD31-530 samples was valued at 40% of the modern water content. However, if only 20% of the modern water content is applied (i.e. 10.9 ± 0.8 wt% and 6.4 ± 0.2 wt%, respectively), MD31-1040 age changes

from 143 ± 19 ka to **126 ± 13 ka** and MD31-530 age changes from 106 ± 13 ka to **93.5 ± 7.3 ka**. These two ages appear more realistic and, because of the long pedogenic interval recognised in core MD31 from 17.8 m to 1.4 m, a severe correction to modern water content for OSL dating assumption is not inconsistent with stratigraphic evidence.

Coccolith abundance and diversity decline toward the end of sub-unit IIIc, corresponding to the marine regression and subsequent exposure of the Arafura Sill. At the very top of sub-unit IIIc, a diverse and abundant coccolith assemblage is encountered in core MD32 (6.2 m) and may correspond to a brief transgressive interval associated with the re-opening of the Arafura Sill, during the major regressive episode. This brief transgressive episode is also evident in core MD31 at 6 m and in core MD33 at 2.8 m.

Only rare ostracods and a few foraminifers were recognised in sub-unit IIIc in core MD32 (Reeves, 2004). This selective preservation may indicate high dissolution rates, with coccoliths being more resistant to dissolution than foraminifers or ostracods, or stratification of the water column during deposition of sub-unit IIIc. However, the preservation of a few planktonic foraminifers within this unit tends to confirm the stratification of the water column. The tropical climate in the Gulf of Carpentaria implies relatively warm temperatures all year long (Chapter 1, Section 1.2.2) and thus substantial evaporation that leads to hypersaline lakes. Thus the stratification would correspond to a top layer of good quality marine water allowing the development of planktonic populations whereas the hypersaline bottom part of the water column prevented the development of a healthy benthic community. The pyrite, organic material and gypsum lamination in core MD32 in the first part of sub-unit IIIc could be the result of temporary mixing of the water column bringing ‘aggressive’ fresher water to the bottom. This episodic freshwater input, probably produced by heavy monsoonal rainfall and runoff, would dissolve carbonate present and thus allow gypsum precipitation. In the modern Gulf of Carpentaria, the break-down of periods of temporary thermal vertical and/or latitudinal saline stratifications by a variety of processes such as cyclonic activity, tidal currents or internal waves, are well documented (Chapter 1, Section 1.2.3).

5.3.3 Marine Isotope Stage 4

In core MD32, Unit II is characterised by the lack of coccoliths from 6.1 m to 4.8 m (sub-unit IIa) and from 1.4 to 0.5 m (sub-unit IIc) expressing non-marine conditions, and thus the existence of Lake Carpentaria at two separate times. The first interval barren of

coccoliths, sub unit IIa, is interpreted as MIS 4 (Figure 5.11) whereas the second (sub unit IIc) corresponds to MIS 2.

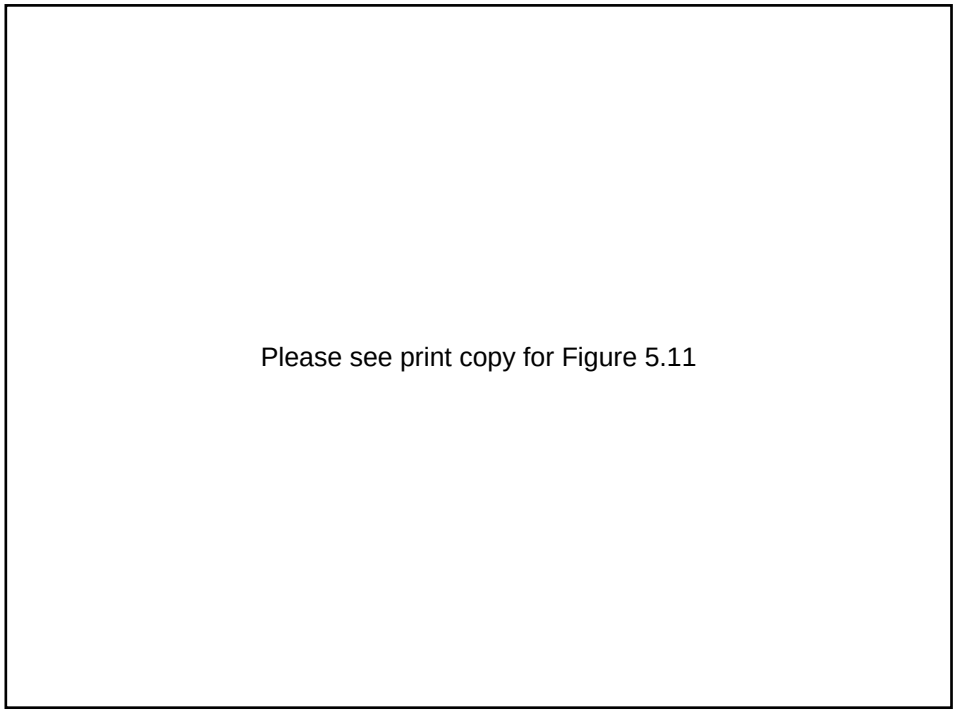

Figure 5.11: Palaeoenvironmental condition contemporaneous with unit IIa deposition or MIS 4. The lake shown on this graph might have been dry from time to time as expressed by pedogenic features.

In core MD32, sub-unit IIa was TL dated older than **64.3 ± 7 ka** (David Price, personal communication, 2001). Sub-unit IIa is represented in core MD31 from 4.8 m to 4.7 m and in core MD33 at 2.7 m. This sub-unit is briefly represented in core MD31 compared to the more eastern core MD32. In core MD31 sub-unit IIa is barren of micro- and nannofossils, which may indicate a period of non-deposition with probable pedogenesis, or be the result of a significant level of energy during the transgression prior to MIS 3 that washed eastward the sediment deposited during MIS 4. Whereas the concise representation of sub-unit IIa in core MD33, compared to the more western core MD32, is probably due to the isolation of the former from fluvial inputs.

In all three cores this sub-unit IIa is characterised by pedogenic features, and proves that for some times after the deposition of this unit, the Gulf was totally dry, the deepest part of the basin (MD33 site) being exposed.

5.3.4 Marine Isotope Stage 3

In core MD32, depauperate coccolith assemblages were recovered in sub-unit IIb from 4.7 m to 1.5 m. These may be related to a marginal marine influence and/or to a lower preservation rate, or higher dilution of the coccolith abundance by an important proportion of clastic sediment. Because of the very low abundance of coccoliths, the connection to the Indian Ocean seems weaker than during MIS 6.5 (Figure 5.2), possibly indicating partial infilling of the incised palaeochannels that delivered Indian oceanic waters to the Gulf. The activity of these palaeochannels incised in the Arafura Sill during MIS 3 was identified by Jones and Torgesen (1988). The environmental conditions of deposition of sub-unit IIb, reconstructed by means of coccolith assemblage distribution, correlates well with ostracod results from Reeves (2004). She recognised a switch from a brackish lake to more marine conditions at 4.7 m in MD32 that lasted up to 3.8 m. Sub-unit IIb also corresponds to the lowest unit obtained by Torgesen et al. (1985, 1988) who associated this unit with the sea-level high stands of MIS 3 (Figure 5.12).

The top of sub-unit IIb is OSL dated at **49.7 ± 4.9 ka** in core MD33 whereas the middle was carbon dated at **45.8± 1.7 ka** and **46± 2 ka**. However, the OSL date is probably more reliable, because the two ^{14}C dates are only conventional ages (i.e. no reservoir correction) and near the limit of applicability of carbon dating.

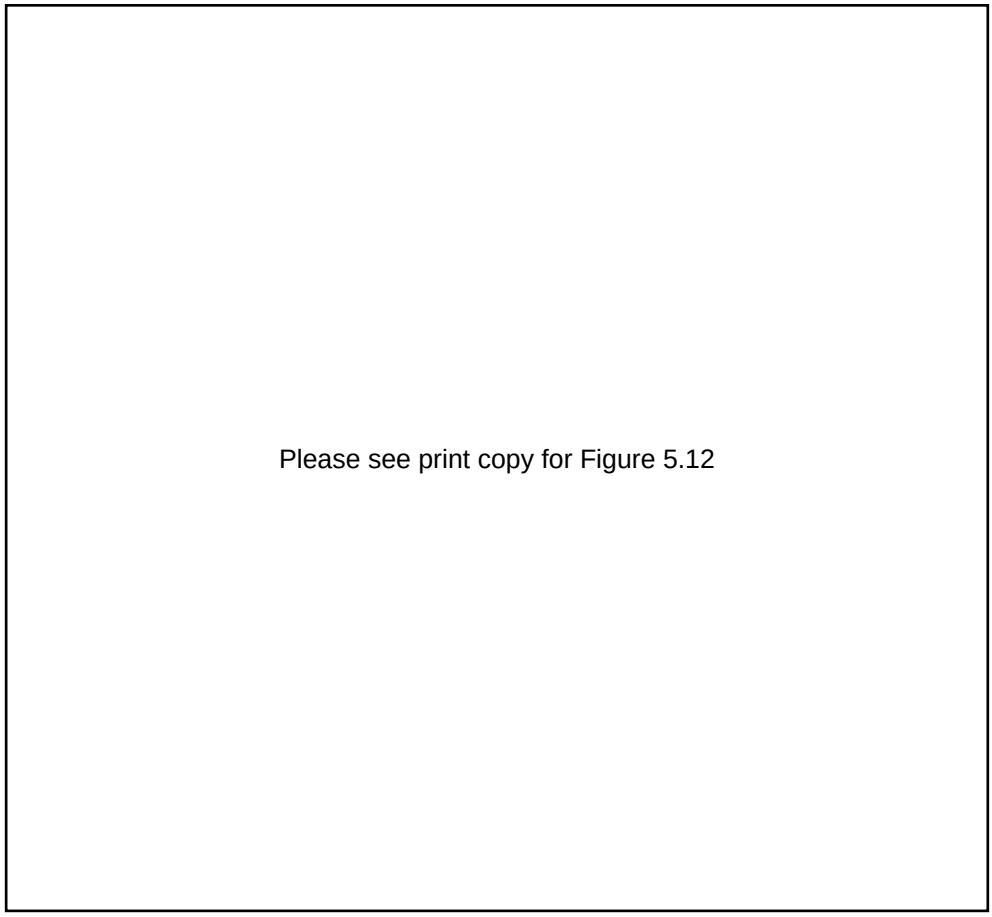

Figure 5.12: Palaeoenvironmental condition contemporaneous with unit IIb deposition or MIS 3.

Sub-unit IIb is represented in core MD31 from 4.6 m to 2 m, and in core MD33 between 2.6 m and 2.3 m, with moderate to high coccolith abundance indicating a significant marine influence. Reeves (2004) recognised common lacustrine and/or lagoonal benthic fauna from 4.4 m together with reworked marine benthic foraminifers from 4.1 m in core MD31 and marginal marine fauna including planktonic foraminifers from 2.5 m to 2.2 m in core MD33. Her notes indicate the onset of a marine-influenced environment 10 to 20 cm later than the coccolith data. The delay in the establishment of the marine influenced benthic community compared to the planktonic community expresses again a probable stratification of the water column.

The difference in the distribution of coccolith populations in sub-unit IIb observed between cores MD31, MD32 and MD33 indicates a sporadic marine influence. The marine water often reached through to core MD31 site but water levels fluctuated. More often, marine water reached the location of core MD32, but evaporated. Whereas a permanent water

body existed in the area of core MD33, thus the occasional marine water input allowed the development of a healthy coccolith community

5.3.5 Marine Isotope Stage 2

Sub-unit IIc, barren of coccoliths in core MD32 (1.4 m to 0.5 m), is represented in core MD31 by a very low abundance of coccoliths between 1.9 m and 0.7 m, the remains of a non-marine benthic population and shell fragments (Reeves, 2004; Holt, 2005). The presence of broken shells within sub-unit IIc in core MD31 (Reeves, 2004) indicates a lake margin environment and thus a larger lake than during MIS 4. This result suggests wetter conditions during MIS 2 than during MIS 4. Therefore, although the glacial periods are known to be times of cooler and drier conditions in northern Australia, the Last Glacial Maximum (LGM) is confirmed by this study to have been wetter than the previous glacial episode, such as has been previously recognised in the Gulf of Carpentaria region by Nanson et al. (in press). In core MD33 sub-unit IIc is represented from 2.2 m to 0.5 m. The lack of coccoliths from 2.2 m in core MD33 together with the shell layer at 2.1 m and the presence of carbonate concretions indicate a probable closure of the system. After a brief transgression that brought marine (but less saline) water to Lake Carpentaria, causing carbonate precipitation and during which a shell layer was deposited, the global sea-level regression caused by ice build-up leading into the LGM ended the connection between Lake Carpentaria and the Indian Ocean (Figure 5.13).

The few coccoliths observed in core MD33 during deposition of sub-unit IIc are interpreted as storm events (at 1.8 m and 1.3 m). This reasoning is also consistent with the presence of abundant shells in cores MD31, MD32 and MD33 that could have been redistributed and reworked by cyclonic activity. The presence of relatively abundant quartz sand particles at 130cm of core MD31 (Holt, 2005), where surrounding levels are mainly biogenic, also supports this hypothesis. Nonetheless, a high productivity episode could also explain such scattering of shells, with selective preservation of the thicker shells compared to coccoliths, and preservation of coccoliths only when the water column was carbonate saturated. The second interpretation explains altogether the preservation of shells, while there was little coccoliths and microfauna found, and also explains the presence of carbonate concretions.

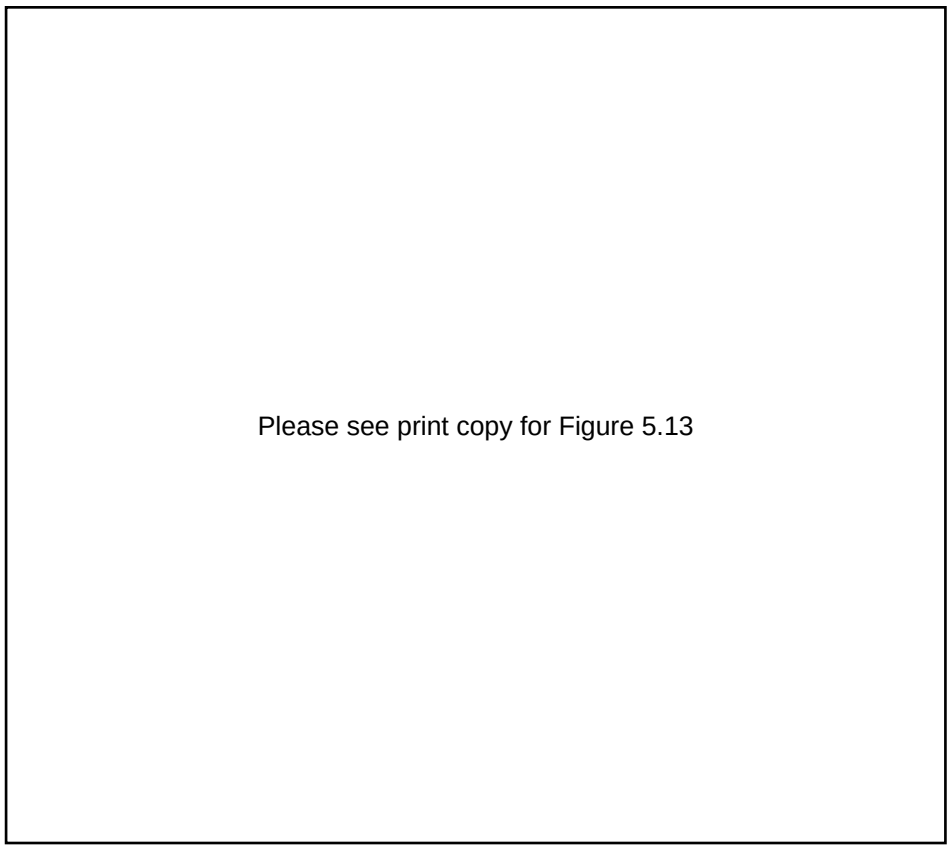

Figure 5.13: Palaeoenvironmental condition contemporaneous with unit IIc deposition or MIS 2

However the more constant presence of coccoliths in core MD33 from 0.8 m to 0.5 m corresponds to the establishment of a coccolith community in a restricted environment similar to sub-unit IIb. This episode is also recognised in core MD31 from 1.1 m to 0.7 m. Holt (2005) noted an increase in lake size from 0.85 m to 0.55 m in core MD33; from 0.95 to 0.65 m in core MD31, with a slight marine influence beginning at 85cm; and from 1.5 m (her maximal studied depth) to 0.4 m in core MD32. The expanded lake meant the edge of the lake was closer to the ocean, perhaps catching more marine waters from cyclones or other extreme events. The large lake may have also had some connection to the ocean at some stage via the outlet channels through the Arafura Sill.

The base of sub-unit IIc was carbon dated at **40 ± 1.7 ka** in core MD33 and OSL dated at **23 ± 1 ka** in MD31, whereas the top was carbon dated at **12.1 ± 0.1 ka** in core MD31, **14.3 ± 1.9 ka** in core MD32, and **17.6 ± 0.3 ka** and **19.0 ± 0.1 ka** in core MD33. These dates are consistent with the regression post MIS 3.

However the fact that a sample from MD31 at 1.8 m depth was also carbon dated at **4.13 ± 0.1 ka** together with several other dating inconsistencies in all the cores for the top marine unit I indicate reworking probably relate to cyclonic activity in the area. Reworking is more evident in core MD31 than in cores MD32 and MD33 probably because of the shallower position of this core, and possibly also due to its proximity to the palaeochannels.

Sub-unit IIc is represented by a long log interval in core MD33 that indicates a high-energy environment during the transgression prior to MIS I. The long length of the interval indicates the sediment that was previously deposited on the margins of Lake Carpentaria was washed out to the depocentre during the transgressive phase. This interpretation also correlates with the relatively thin intervals representing sub-unit IIc in cores MD31 and MD32.

5.3.6 Marine Isotope Stage 1

Unit I shows a high variability in coccolith abundance in all three cores, in which a similar coccolith community is observed. This high variability in coccolith abundance is more likely related to high variability of the preservation rate and thus of salinity. The salinity in this area is correlated with runoff magnitude, with freshwater being more aggressive to carbonates. Therefore, monsoon intensification, which is the main factor influencing terrestrial runoff and delivery of freshwater to the Gulf of Carpentaria, is probably recorded by these fluctuations in coccolith abundance.

Unit I was OSL dated at **6.77 ± 1.02 ka** in core MD31 at 0.30 m and at **6.56 ± 1.17 ka** in core MD32 at 0.38 m (Figure 5.14). This unit, which corresponds to the modern environment, was also abundantly carbon dated in all the cores (Chivas et al., 2001; Reeves, 2004) and gave an age for the most recent transition to marine of 12.2 ka to 10.5 ka (Holt, 2005). Because of the extensive dating and the clear change in the sediment coloration and consistency, unit I is easily identified in all six cores.

Coccolith assemblage investigation placed the lowest limit of unit I at 0.7 m in cores MD30 and MD31, 0.5 m in cores MD32 and MD33, and 0.25 m in cores MD28 and MD29. Foraminiferal assemblages (Holt, 2005) indicate a similar timing, although not exactly synchronous in all cores, for the first indication of marine conditions: at 0.7 m in MD30, 0.6 m in MD31, 0.35 m in MD32, 0.5 m in MD33, 0.6 m in MD28, and 0.25 m in MD29.

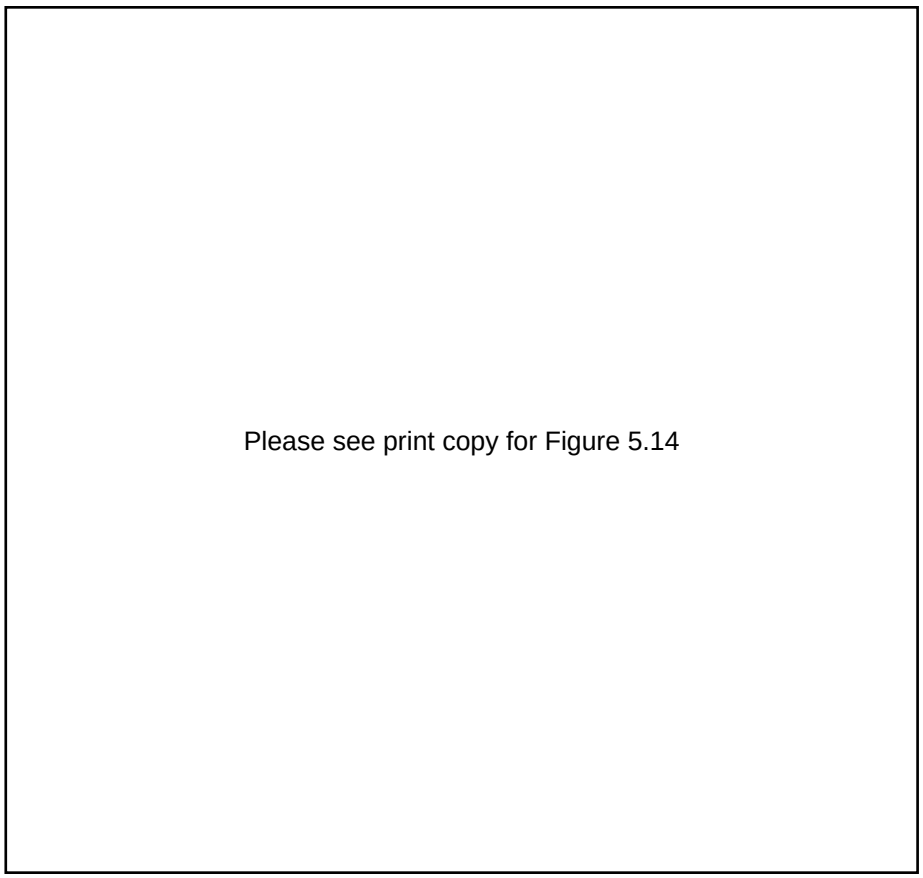

Figure 5.14: Palaeoenvironmental condition contemporaneous with unit I deposition or MIS 1

Even when fully marine conditions are well established in all core sites, there is still a substantial variability in coccolith abundance for all six cores. For example, in core MD28, coccoliths first occur at 0.75 m and continue until 0.6 m, then the interval is barren of coccoliths until a fluctuating population is established from 0.35 m to 0.15 m, when fully marine conditions occur. As sea-level rose to the level of the channels in the Arafura Sill, and continued to rise, the tidal channels created a lagoonal environment in the basin. Fluctuations in species abundance and diversity would occur as the channels temporarily closed and re-opened. Holt (2005) notes a similar variability in foraminiferal assemblages, with a the first incidence of marine influence in core MD28 seen as a lagoonal population at 0.6 m, becoming more open lagoonal toward 0.3 m, and a permanent connection to the sea established at 0.25 m, with fully marine conditions established at 0.15 m. On the other hand, this variability rapidly disappears in core MD29. This fact suggests that the variability is also related to the impact of river runoff, and thus monsoon intensity probably linked to ENSO, MD29 being less affected due to its location further off shore.

5.4 Conclusions

This thesis presents the longest dated interpretation of the palaeoenvironmental history of the Gulf of Carpentaria - spanning 180 ka to the late Holocene. The outcomes of this study can be summarised as follows:

- The OSL dating technique is applicable on sediment cores that have passed through a MSCL device including densitometry by gamma-ray attenuation.

- The importance of the water content history and water depth at the time of deposition for each sample from the Gulf of Carpentaria to be dated by OSL has been highlighted and accounted for.

- The assessment of the disequilibrium in the uranium and thorium decay chains due to the high variability in environmental conditions ranging from open marine to enclosed lacustrine was accomplished by α- and γ-spectrometry comparison, a new combination of techniques.

- The reliability of OSL dating for changing environments from open marine to enclosed lake, which has never been attempted before, was proven by this study.

- 12 dates were determined on quartz grains from the Gulf of Carpentaria sediment cores ranging from 7 ± 1 ka to 180 ± 18 ka. These dates correspond to various depths in the three major cores collected in the Gulf, principally at major unit boundaries.

- A high variability in the sedimentation rate was calculated in the Gulf of Carpentaria from a low of 4.1 $cm.ka^{-1}$ in the central area to 7.8 $cm.ka^{-1}$ on the western margin, and up to 14.2 $cm.ka^{-1}$ between these two locations. However this sedimentation rate is not linear and high variation exists for different periods at each location.

- Coccolith abundance in the Gulf is well correlated with the sea level curve of Waelbroeck et al. (2002) and can thus be use as a productivity proxy.

- SYRACO, a semi-automatic coccolith recognition software, was found to be applicable at the community level but not at the species level due to the malformed partially dissolved population recovered from the Gulf of Carpentaria cores.

- Eight distinct sedimentological units were described over the last 180 ka (since MIS 6.6) in the Gulf. They represent two major cycles (125 ka and 10 ka) with breaching of both Arafura Sill and Torres Strait, two minor cycles (from 104 ka to 80 ka) where Torres Strait was still a land bridge while the Arafura Sill was flooded, and several intervals (180 ka, 165 ka and 50 ka) during which incised channels in the Arafura Sill brought Indian ocean waters into the Gulf of Carpentaria. At three times Lake Carpentaria was completely isolated from both Pacific and Indian Oceans (145 ka, 65 ka and 25 ka), and was dominated by non-marine brackish conditions.

Further Research

- More dating is now necessary to elaborate further on the palaeohistory of the Gulf as described in this thesis, and to more precisely date the transgression and regression periods over both sills that are of major importance from a palaeoenvironmental and especially ethnological point of view.
- More terrestrial Quaternary studies on fluvial input, highlighting periods of high and low activity, would allow cross-checking of the variation observed in sedimentation rates within the Gulf of Carpentaria.
- A combination and comparison of the outcomes of this study with long-term Quaternary terrestrial and marine palaeoenvironmental investigations from northern Australia and the Indo-Pacific regions will allow its integration in a global context of palaeoclimatology and palaeoceanographic research.

References

References

Adamiec G. and Aitken M. J. (1998) Dose-rate conversion factors: update. *Ancient TL* **16**, 37-50.

Agersnap Larsen N., Bulur E., Bøtter-Jensen L. and McKeever S. W. S. (2000) Use of the LM-OSL technique for the detection of partial bleaching in quartz. *Radiation Measurements* **32**(5-6), 419-425.

Ahagon N., Tanaka Y. and Ujiie H. (1993) Florisphaera profunda, a possible nannoplankton indicator of late Quaternary changes in sea-water turbidity at the northwestern margin of the Pacific. *Marine Micropaleontology* **22**(3), 255-273.

Aitken M. J. (1985a) *Thermoluminescence Dating*, Academic Press, London.

Aitken M. J. (1985b) Thermoluminescence dating: Past progress and future trends. *Nuclear tracks and Radiation Measurements* **10**(1-2), 3-6.

Aitken M. J. and Smith B. W. (1988) Optical dating: Recuperation after bleaching. *Quaternary Science Reviews* **7**(3-4), 387-393.

Aitken M. J. (1990) Optical dating of sediments: Initial results from Oxford. *Archaeometry* **32**, 19-31.

Aitken M. J. (1992) Optical dating. *Quaternary Science Reviews* **11**(1-2), 127-131.

Aitken M. J. (1994) Optical dating: A non-specialist review. *Quaternary Geochronology* **13**, 503-508.

Aitken M. J. (1998) *An Introduction to Optical Dating: The Dating of Quaternary Sediments by the use of Photon-Stimulated Luminescence*, Oxford University Press, Oxford, New York.

Aizawa C., Oba T. and Okada H. (2004) Late Quaternary paleoceanography deduced from coccolith assemblages in a piston core recovered off the central Japan coast. *Marine Micropaleontology* **52**(1-4), 277-297.

Arkhangelsky A.D. (1912) Verkhnemelovyya otolozheniga vostoka evropeyskog Rossii (Upper Cretaceous deposits of east Europeen Russian). *Materialien zur Geologie Russlands* **25**, 1-631.

Baker P., Seltzer, G. and Fritz, S. (2002) Lake Titicaca Drilling 2001. *ICDP Newsletter* **4**, 6-8.

Balch W. M. (2004) Re-evaluation of the physdiological ecology of coccolithophores. In: *Coccolithophores, from Molecular Processes to Global Impact (ed* H.R. Thierstein and J.R. Young), pp. 165-190, Springer, Berlin.

Banerjee D., Bøtter-Jensen L. and Murray A. S. (2000) Retrospective dosimetry: estimation of the dose to quartz using the single-aliquot regenerative-dose protocol. *Applied Radiation and Isotopes* **52**(4), 831-844.

Banerjee D. (2001) Supralinearity and sensitivity changes in optically stimulated luminescence of annealed quartz. *Radiation Measurements* **33**(1), 47-57.

Banerjee D., Hildebrand A. N., Murray-Wallace C. V., Bourman R. P., Brooke B. P. and Blair M. (2003) New quartz SAR-OSL ages from the stranded beach dune sequence in south-east South Australia. *Quaternary Science Reviews* **22**(10-13), 1019-1025.

Baumann K.-H., Boëckel B. and Frenz M. (2004) Coccolith contribution to South Atlantic carbonate sedimentation. In: *Coccolithophores, from Molecular Processes to Global Impact (ed* H.R. Thierstein and J.R. Young), pp. 367-402, Springer, Berlin.

Baumann K.-H. and Freitag T. (2004) Pleistocene fluctuations in the northern Benguela Current system as revealed by coccolith assemblages. *Marine Micropaleontology* **52**(1-4), 195-215.

Beaufort L. (1992) Size variation in late Miocene reticulofenestra and implication for palaeoclimatic interpretation. *Mem. Sci. Geol.* **43**, 339-350.

Beaufort L., de Garidel-thoron T., Mix A. C. and Pisias N. G. (2001) Enso-like Forcing on Oceanic Primary Production During the Late Pleistocene. *Science* **293**, 2440-2444.

Beaufort L. and Dollfus D. (2004) Automatic recognition of coccoliths by dynamical neural networks. *Marine Micropaleontology* **51**(1-2), 57-73.

Bell W. T. and Zimmerman D. W. (1978) The effect of HF etching on the morphology of quartz inclusions for thermoluminescence dating. *Archaeometry* **20**, 63-65.

Berger G. W. and Luternauer J. J. (1987) Preliminary field work for thermoluminescence dating studies at the Fraser River delta, British Columbia. *Geological Survey of Canada Paper* **87-1A**, 901-904.

Berger G. W. and Huntley D. J. (1994) Tests for optically stimulated luminescence from tephra glass. *Quaternary Science Reviews* **13**(5-7), 509-511.

Berger G. W. (1995) Progress in Luminescence Dating Methods for Quaternary Sediments. In: *Dating Methods for Quaternary Deposits* (*ed* N.W. Rutter and N. Catto), pp. 81-104, Geological Association of Canada, ST John's, Newfoundland.

Berger W. H. and Soutar A. (1970) Preservation of plankton shells in an anaerobic basin off California. *Geol. Soc. Am. Bull* **81**, 275-282.

Biekart J. W. (1989) Coccolithophores in the Upper Quaternary of some Southeast Indonesian Basins. *Netherlands Journal of Sea Research* **24-4**, 523-530.

Billard C. and Inouye I. (2004) what is new in coccolithophore biology? In: *Coccolithophores, from Molecular Processes to Global Impact (ed* H.R. Thierstein and J.R. Young), pp. 1-29, Springer, Berlin.

Black M. (1963) The fine structure of the mineral parts of Coccolithophoridae. *Linnean Society, London Proc* **174**, 41-46.

Black M. (1965) Coccoliths. *Endeavour* **24**, 131-137.

Black M. (1972) *British lower Cretaceous Coccoliths*. Palaeontographical Society monographs, 142 , 34 plates pp, Palaeontographical Society, London.

Blackwell B. (1995) Electron spin resonances dating. In: *Dating Methods for Quaternary Deposits (ed* N.W. Rutter and N. Catto), pp., Geological Association of Canada, GEOtext2, ST John's, Newfoundland.

Boeckel B. and Baumann K.-H. (2004) Distribution of coccoliths in surface sediments of the south-eastern South Atlantic Ocean: ecology, preservation and carbonate contribution. *Marine Micropaleontology* **51**(3-4), 301-320.

Bøtter-Jensen L. and Duller G. A. T. (1992) A new system for measuring optically stimulated luminescence from quartz samples. *International Journal of Radiation Applications and Instrumentation. Part D. Nuclear Tracks and Radiation Measurements* **20**(4), 549-553.

Bøtter-Jensen L., Duller G. A. T. and Poolton N. R. J. (1994) Excitation and emission spectrometry of stimulated luminescence from quartz and feldspars. *Radiation Measurements* **23**(2-3), 613-616.

Bøtter-Jensen L., Agersnap Larsen N., Mejdahl V., Poolton N. R. J., Morris M. F. and McKeever S. W. S. (1995) Luminescence sensitivity changes in quartz as a result of annealing. *Radiation Measurements* **24**(4), 535-541.

Bøtter-Jensen L. (1997) Luminescence techniques: instrumentation and methods. *Radiation Measurements* **27**(5/6), 749-768.

Bøtter-Jensen L., Mejdahl V. and Murray A. S. (1999) New light on OSL. *Quaternary Science Reviews* **18**(2), 303-309.

Bøtter-Jensen L. (2000) Development of Optically Stimulated Luminescence Techniques using Natural Minerals and Ceramics, and their Application to Retrospective Dosimetry. *PhD thesis Thesis*, 186 pp, Faculty of Science, University of Copenhagen, Danemark.

Bøtter-Jensen L., Bulur E., Duller G. A. T. and Murray A. S. (2000) Advances in luminescence instrument systems. *Radiation Measurements* **32**(5-6), 523-528.

Bøtter-Jensen L., Andersen C. E., Duller G. A. T. and Murray A. S. (2003) Developments in radiation, stimulation and observation facilities in luminescence measurements. *Radiation Measurements* **37**(4-5), 535-541.

Boyle R. (1663) *Experiments and considerations upon colours with observations on a diamond that shines in the dark*. The Sources of Sciences, Woolf, H. and Shepard, W. K., New York and London, 1964.

Bowler J. M., Johnston H., Olley J. M., Prescott J. R., Roberts R. G., Shawcross W., Spooner N. A. (2003) New ages for human occupation and climatic change at Lake Mungo, Australia. *Nature* **421**, 837-840.

Braarud T., Gaarder K. R., Markali J. and Nordli E. (1952) Coccolithophorids studied in the electron microscope. *Nytt. Mag. Bott.* **1**, 129-134.

Bramlette M. N. and Riedel W. R. (1954) Stratigraphic value of Discoasters ans some other microfossils related to recent Coccolithophores. *Journal of Paleontology* **28**, 385-403.

Brander R. W., Kench P. S. and Hart D. (2004) Spatial and temporal variations in wave characteristics across a reef platform, Warraber Island, Torres Strait, Australia. *Marine Geology* **207**(1-4), 169-184.

Brownlee C. and Taylor A. (2004) Calcification in coccolithophores: A cellular perspective. In: *Coccolithophores, from Molecular Processes to Global Impact (ed* H.R. Thierstein and J.R. Young), pp. 31-49, Springer, Berlin.

Bulur E. (1996) An alternative technique for optically stimulated luminescence (OSL) experiment. *Radiation Measurements* **26**(5), 701-709.

Bulur E., Bøtter-Jensen L. and Murray A. S. (2000) Optically stimulated luminescence from quartz measured using the linear modulation technique. *Radiation Measurements* **32**(5-6), 407-411.

Bulur E., Duller G. A. T., Solongo S., Bøtter-Jensen L. and Murray A. S. (2002) LM-OSL from single grains of quartz: a preliminary study. *Radiation Measurements* **35**(1), 79-85.

Burns D. A. (1977) Phenotypes and dissolution morphotypes of the genus *Gephyrocapsa* Kamptner and *Emiliana huxleyi* (Lohmann). *New Zealand Journal of Geology and Geophysics* **20**(1), 143-155.

Chappell J., Rhodes E. G., Thom B. G. and Wallensky E. (1982) Hydro-isostasy and the sea-level isobase of 5500 B.P. in north Queensland, Australia. *Marine Geology* **49**(1-2), 81-90.

Chappell J. M. A. (1983) A revised sea-level record for the last 300,000 years from Papua New Guinea. *Search* **14**, 99-101.

Chappell J. M. A. and Shackleton N. J. (1986) Oxygen isotopes and sea level. *Nature* **324**(137-140).

Chappell J. M. A., Omura A., Ezat T., McCulloch M. T., Pandolfi J., Ota Y. and Pillans B. (1996) Reconciliation of late Quaternary sea levels derived from coral terraces at Huon Pensinsula with deep-sea oxygen isotope records. *Earth and Planetary Sciences Letters* **141**, 227-236.

Cheng X. and Wang P. (1997) Controlling factors of coccolith distribution in surface sediments of the China seas: marginal sea nannofossil assemblages revisited. *Marine Micropaleontology* **32**, 155-172.

Chivas A. R., Garcia A., van der Kaars S., Couapel M. J. J., Holt S., Reeves J. M., Wheeler D. J., Switzer A. D., Murray-Wallace C. V., Banerjee D., Price D. M., Wang S. X., Pearson G., Edgar N. T., Beaufort L., De Deckker P., Lawson E. and Cecil C. B. (2001) Sea-level and environmental changes since the last interglacial in the Gulf of Carpentaria, Australia: an overview. *Quaternary International* **83-85**, 19-46.

Christensen T. (1962) Alger. In: *Botanik II (ed* T.W. Bocher, M. Lange and T. Sorensen), Systematic Botanik, pp., Munksgaard, Copenhagen.

Church J. A. and Forbes A. M. G. (1981) Non linear model of the tides of the Gulf of Carpentaria. *Australian Journal of Marine and Freshwater Research* **32**, 685-697.

Church J. A. and Forbes A. M. G. (1983) Circulation in the Gulf of Carpentaria, I: Direct observations of currents in the southeast corner of the Gulf of Carpentaria. *Australian Journal of Marine and Freshwater Research* **34**, 1-10.

Clarke M. L., Rendell H. M. and Wintle A. G. (1999) Quality assurance in luminescence dating. *Geomorphology* **29**(1-2), 173-185.

CODENET (2002) Coccolithophorid evlotutionary biodiversity and ecology network. In. J.R. Young (Editor), pp., The Natural History Museum, London.

Conley S. M. (1979) Recent Coccolithophores from the Great Barrier Reef-Coral Sea region. *Micropaleontology* **25-1**, 20-43.

Cortés M. Y. (2000) Further evidence for the heterococcolith-holococcolith combination Calcidiscus leptoporus-Crystallolithus rigidicus. *Marine Micropaleontology* **39**, 35-37.

Cox M. E. and Preda M. (2003) Trace metal distribution and relation to marine sediment mineralogy, Gulf of Carpentaria, Northern Australia. *Marine Pollution Bulletin* **46**(12), 1623-1629.

Couapel M. J. J. and Bowles C. J. (2006) Impact of gamma densitometry on the luminescence signal of quartz grains. *Geo-Marine Letters* **26**, 1-5.

Cros L., Kleijne A., Zeltner A., Billard C. and Young J. R. (2000) New examples of holococcolith-heterococcolith combination coccospheres and their implications for coccolithophorid biology. *Marine Micropaleontology* **39**(1-4), 1-34.

Cutshall N. H., Larsen I. L. and Olsen C. R. (1983) *Nuclear Instruments and Methods* **206**, 309.

Daniels F., Boyd C. A. and Saunders D. F. (1953) Thermoluminescence as a research tool. *Science* **117**, 343-349.

De Deckker P., Chivas A. R., Shelley J. M. G. and Torgersen T. (1988) Ostracod shell chemistry: A new palaeoenvironmental indicator applied to a regressive/transgressive record from the Gulf of Carpentaria, Australia. *Palaeogeography, Palaeoclimatology, Palaeoecology* **66**(3-4), 231-241.

De Deckker P. and Corrège T. (1991) Late Pleistocene record of cyclic eolian activity from tropical Australia suggesting the Younger Dryas is not an unusual climatic event. *Geology* **19**, 602-605.

Deflandre G. and Fert C. (1954) Observations sur les coccolithophoridés actuels et fossiles en microscopie ordinaire et electronique. *Annales de Paléontologie* **40**, 115-176.

Diester-Haass L., Robert C. and Chamley H. (1998) *Paleoproductivity and climate variations during sapropel deposition in the eastern Mediterranean Sea*. Proceedings of the Ocean Drilling Program, Scientific Results, 160. 227-248 pp.

Ditlefsen C. and Huntley D. J. (1994) Optical excitation of trapped charges in quartz, potassium feldspars and mixed silicates: The dependence on photon energy. *Radiation Measurements* **23**, 675-682.

Dixon H. H. (1900) On the structure of coccospheres and the origin of coccoliths. *Proc. Royal Society, London* **66**, 305-315.

Dollfus D. (1997) Reconnaissance de formes naturelles par des réseaux de neurones artificiels: application au nannoplancton calcaire. *PhD Thesis Thesis*, 162 pp, Université d'Aix-Marseilles III, Marseilles.

Dollfus D. and Beaufort L. (1999) Fat neural network for recognition of position-normalised objects. *Neural Network* **12**, 553-560.

Doutch H. F. (1972) The paleogeography of the northern Australia and New Guinea and its relevance to the Torres Strait area. , , . In: *Bridge and Barrier, The Natural and Cultural History of Torres Strait (ed* D. Walker), pp. 1-10, Research School of Pacific Studies, Department of Biogeography and Geomorphology, The Australian National University, Canberra.

Duller G. A. T. (1991) Equivalent dose determination using single aliquots. *Nuclear tracks and Radiation Measurements* **18**, 371-378.

Duller G. A. T. (1994a) Luminescence dating of poorly bleached sediments from Scotland. *Quaternary Science Reviews* **13**(5-7), 521-524.

Duller G. A. T. (1994b) Luminescence dating of sediments using single aliquots: New procedures. *Quaternary Science Reviews* **13**(2), 149-156.

Duller G. A. T. (1996) Recent developments in luminescence dating of Quaternary sediments. *Progress in Physical Geography* **20**(2), 127-145.

Duller G. A. T., Bøtter-Jensen L. and Mejdahl V. (1999) An automated iterative procedure for determining palaeodoses using the SARA method. *Quaternary Science Reviews* **18**(2), 293-301.

Duller G. A. T. (2003) Distinguishing quartz and feldspar in single grain luminescence measurements. *Radiation Measurements* **37**(2), 161-165.

Edgar N. T., Cecil C. B., Mattick R. E., Chivas A. R., De Deckker P. and S. D. Y. (2003) A modern analogue for tectonic, eustatic, and climatic processes in cratonic basins: Gulf of Carpentaria, Northen Australia. In: *Climate Controls on Stratigraphy (ed* C.B. Cecil and N.T. Edgar), pp. 193-205, SEPM Special Publication.

Edvardsen B., Eikrem W., Green J. C., Andersen R. A., Moon-Van der Staay S. Y. and Medlin L. K. (2000) Phylogenetic reconstructions of the Haptophyta inferrred from 18S ribosomal DNA sequences and available morphological data. *Phycologia* **39**, 19-35.

Ehrenberg C. G. (1836) New microscopic characters of earthy and compact minerals. *Monatsberichte* Poggendorff's Annalen(**xxxix**), 101.

Ehrenberg C. G. (1854) *Mikrogeologie; Das Erden und Felsen schaffende Wirken des unsichtbar kleinen selbständigen Lebens auf des Erde*. 405p. pp, Leipzig.

Evans J. L. and Allan R. J. (1992) El Niño /Southern Oscillation modification to the structure of the monsoon and tropical cyclone activity in the Australasian region. *International Journal of Climatology* **12**, 611-623.

Feathers J. K. (2003) Single-grain OSL dating of sediments from the Southern High Plain, USA. *Quaternary Science Reviews* **22**, 1035-1042.

Flores J. A. and Sierro F. J. (1997) Revised technique for calculation of calcareous nannofossil accumulation rates. *Micropaleontology* 43(3), 321-324.

Flores J. A. and Sierro F. J., Francés G., Vázquez A., Zamarreño I. (1997) The last 100,000 years in the western Mediterranean: sea surface water and frontal dynamics as revealed by coccolithophores. *Marine Micropaleontology* **29**, 351-366.

Flores J. A., Marino M., Sierro F. J., Hodell D. A. and Charles C. D. (2003) Calcareous plankton dissolution pattern and coccolithophore assemblages during the last 600 kyr at ODP Site 1089 (Cape Basin, South Atlantic): paleoceanographic implications. *Palaeogeography, Palaeoclimatology, Palaeoecology* **196**(3-4), 409-426.

Folz E. and Mercier N. (1999a) A single-aliquot OSL protocol using bracketing regenerative doses to accurately determine equivalent doses in quartz. *Radiation Measurements* **30**(4), 477-485.

Folz E. and Mercier N. (1999b) Use of a new procedure to determine paleodose in the OSL dating of quartz: The MARA protocol. *Quaternary Science Reviews* **18**(6), 859-864.

Folz E. (2000) La luminescence stimulée optiquement du quartz: développements méthodologiques et applications à la datation de séquances du Pléistocène supérieur

du Nord-Ouest de la France. *PhD thesis Thesis*, 173 pp, Université Paris 7 - Denis Diderot, Paris, France.

Forbes A. M. G. and Church J. A. (1983) Circulation in the Gulf of Carpentaria II: residual currents and mean sea level. *Australian Journal of Marine and Freshwater Research* **34**, 11-22.

Forbes A. M. G. (1984) The contribution of local processes to the seasonal hydrology of the Gulf of Carpentaria. *Oceanographie tropicale* **19**(2), 151-167.

Forbes A.M.G., 1986 Oceanographie tropical, ORSTOM, 19(2):193-201. CSIRO Mar. Lab., P.O. Box 1538, Hobart, Tas. 7001, Australia. (1984) The contribution of local processes to seasonal hydrology of the Gulf of Carpentaria :. *Deep Sea Research Part B. Oceanographic Literature Review* **33**(3), 200.

Fuchs M. and Wagner G. A. (2003) Recognition of insufficient bleaching by small aliquots of quartz for reconstructing soil erosion in Greece. *Quaternary Science Reviews* **22**(10-13), 1161-1167.

Gaarder K.R. (1971). Comments on the distribution of coccolithophorids in the ocean. In: *The Micropaleontology of Oceans* (*eds* B.M. Funnell, W.R. Riedel) Cambridge University Press, Cambridge, pp. 97–103.

Galbraith R. F. (1988) Graphical display of estimates having differing standard errors. *Technometrics* **30**(3), 271-281.

Galbraith R. F. (1990) The radial plot: Graphical assessment of spread in ages. *International Journal of Radiation Applications and Instrumentation. Part D. Nuclear Tracks and Radiation Measurements* **17**(3), 207-214.

Galbraith R. F. and Laslett G. M. (1993) Statistical models for mixed fission track ages. *Nuclear tracks and Radiation Measurements* **21**, 459-470.

Galbraith R. F., Roberts R. G., Laslett G. M., Yoshida H. and Olley J. M. (1999) Optical dating of single and multiple grains of quartz from Jimnium rock shelter, northern Australia: Part I, experimental design and statistical models. *Archaeometry* **41**(2), 339-364.

Galbraith R. F., Roberts R. G. and Yoshida H. (2005) Error variation in OSL palaeodose estimates from single aliquots of quartz: a factorial experiment. *Radiation Measurements* **39**(3), 289-307.

Galloway R. B. (1996) Equivalent dose determination using only one sample: Alternative analysis of data obtained from infrared stimulation of feldspars. *Radiation Measurements* **26**(1), 103-106.

Gartner S. and Bukry D. (1969) Tertiary holococcoliths. *Journal of Paleontology* **43**, 1213-1221.

Gayral P. and Fresnel J. (1983) Description, sexualité et cycle de développements d'une nouvelle Coccolithophoracée (Prymnesiophyceae): *Pleurochrysis pseudoroscoffensis* sp. nov. *Protistologia* **19**, 245-261.

Geisen M., Young J. R., Probert I., Sáez A. G., Baumann K.-H., Sprengel C., Bollmann J., Cros L., de Vargas C. and Medlin L. K. (2004) Species level variation in coccolithophores. In: *Coccolithophores, from Molecular Processes to Global Impact (ed* H.R. Thierstein and J.R. Young), pp. 327-366, Springer, Berlin.

Geitzenauer K. R. (1969) Coccoliths as Late Quaternary paleoclimatic indicators in teh Subantartic Pacific Ocean. *Nature* **223**, 170-172.

Geotek® (2000) *Geotek MSCL Manual*, Geotek, Daventry, United Kingdom.

Godfrey-Smith D. I., Huntley D. J. and Chen W.-H. (1988) Optical dating studies of quartz and feldspar sediment extracts. *Quaternary Science Reviews* **7**(3-4), 373-380.

Godfrey-Smith D. I., McMullan W. G., Huntley D. J. and Thewalt M. L. W. (1989) Time-dependent recombination luminescence spectra arising from optical ejection of trapped charges in zircons. *Journal of Luminescence* **44**, 47-57.

Greeman D. J., Rose A. W. and Jester W. A. (1990) Form and behavior of radium, uranium and thorium in Central Pennsylvania soils derived from dolomite. *Geophysical Research Letters* **17**, 833-836.

Grim M. S. and Edgar N. T. (1998) Bathymetric map of the Gulf of Carpentaria and Arafura Sea, 1:2,500,000. In: Geologic Investigation Series, map I-2550. U.G. Survey (Editor), pp.

Grootes P. M., Stuiver M., White J. W. C., Johnsen S. and Jouzel J. (1993) Comparison of oxygen isotopes records from the GISP2 and GRIP Greenland ice cores. *Nature* **366**, 552-554.

Haddon A. C., Sollas W. J. and Cole G. A. J. (1894) On the geology of the Torres Straits. *Transactions of the Royal Irish Academy* **30**, 411-476.

Hagino K., Okada H. and Matsuoka H. (2000) Spatial dynamics of coccolithophore assemblages in the Equatorial Western-Central Pacific Ocean. *Marine Micropaleontology* **39**(1-4), 53-72.

Hallegraeff G. M. (1984) Coccolithophorids (Calcareous Nannoplankton) from Australian Waters. *Botanica Marina* **27**, 229-247.

Hallegraeff G. M. (2000) Marine phytoplankton communities in the Australian region: current status and futur threats. In: *State of the marine Environment Report for Australia (ed* L.P. Zann and P. Kailola), pp. 85-96, Department of the Environment, Sport and Territories, Ocean Rescue 2000 Program, Canberra.

Haq B. U. (1983) *Nannofossil biostratigraphy*. Benchmark Papers in Geology, 78. xiii, 386 pp, Hutchinson Ross, Stroudsburg, Pennysylvania.

Haq B. U. (1984) *Calcareous nannoplankton*. Benchmark Papers in Geology, 79. xiii, 338 pp, Hutchinson Ross, Stroudsburg, Pennysylvania.

Harris P. T. (1988) Sediments, bedforms and bedload transport pathways on the continental shelf adjacent to Torres Strait, Australia - Papua New Guinea. *Continental Shelf Research* **8**, 979-1003.

Harris P. T. (1994) Comparison of tropical, carbonate and temperate siliciclastic tidally dominated sedimentary deposits: Examples from the Australian continental shelf. *Australian Journal of Earth Sciences* **41**, 241-254.

Harris P. T. (2000) Marine geology and sedimentology of the Australian continental shelf. In: *State of the marine Environment Report for Australia (ed* L.P. Zann and P. Kailola), pp. 11-24, Department of the Environment, Sport and Territories, Ocean Rescue 2000 Program, Canberra.

Harrison S. P. (1993) Late Quaternary lake-level changes and climates of Australia. *Quaternary Science Reviews* **12**(4), 211-231.

Harrison S. P. and Dodson, J., (1993) Climates of Australia and New Guinea since 18,000 yr B.P. In: *Global Climates since the Last Glacial Maximum*(*eds* H.E. Jr.Wright et al.), pp. 265-293, University of Minnesota Press, Minneapolis.

Hay W. W. and Sandberg P. A. (1967) The Scanning Electron Microscope, a major breakthrough for micropaleontology. *Micropaleontology* **13**, 407-418.

Hemer M. A., Harris P. T., Coleman R. and Hunter J. (2004) Sediment Mobility due to currents and waves in the Torres Strait - Gulf of Papua region. *Continental Shelf Research* **24**(19), 2297-2316.

Hibbert D. J. (1976) The ultrastructure and taxonomy of the Chrysophyceae and Prymnesiophyceae (Haptophyceae): a survey with some new observations on the ultrastucture of the Chrysophyceae. *Botanical Journal of the Limn. Society* **72**, 55-80.

Hibbert D. J. (1980) Prymnesiophytes (= Haptophytes). In: *Phytoflagellates (ed* E.R. Cox), pp. 273-318, Elsevier, North Holland.

Hiramatsu C. and De Deckker P. (1997) The late Quaternary calcareous nannoplankton assemblages from three cores from the Tasman Sea. *Palaeogeography, Palaeoclimatology, Palaeoecology* **131**, 391-412.

Holligan P. M., Viollier M., Harbour D. S., Camus P. and Champagne-Philippe M. (1983) Satellite and ship studies of coccolithophore production along a continental shelf edge. *Nature* **304**, 339-342.

Holt S. (2005) Palaeoenvironments of the Gulf of Carpentaria from the Last Glacial Maximun to the Present, as determined by foraminiferal assemblages. *Submitted PhD thesis Thesis*, 204 pp. pp, University of Wollongong, Wollongong.

Honjo S. (1975) Dissolution of suspended coccoliths in the deep-sea water column and sedimentation of coccolith ooze. In: *Dissolution of deep sea carbonates (ed* W. Silter, W.B. A. and H.B. W.), Foraminiferal Research Special Publication, pp. 114-128, Cushman Found.

Honjo S. (1976) Coccoliths:Production, Transportation and sedimentation. *Marine Micropaleontology* **1**, 65-79.

Honjo S. (1977) Biogeography and provincialism of living coccolithophorids. In: *Oceanic Micropalaeontology (ed* A.T.S. Ramsey), pp. 951-972, Academic Press, London.

Hopley D. (1982) *The Geomorphology of the Great Barrier Reef: Quaternary Development of Coral Reefs*, Wiley, New York.

Houdan A., Billard C., Marie D., Not F., Sáez A. G., Young J. R. and Probert I. (2004) Flow cytometric analysis of relative ploidy levels in holococcolithophore-heterococcolithophore (Haptophyta) life cycles. *Systematics and Biodiversity* **1**(4), 453-465.

Houghton S. D. (1993) Recent coccolith sedimentation patterns and transport in the North Sea: implications for palaeoceanographic studies of marginal and continental shelf seas. In: *Applied Micropaleontology* (*ed* G. Jenkins), pp. 1-40, Springer, Berlin.

Hughen K. A., Baillie M. G. L., Bard E., Bayliss A., Beck J. W., Bertrand C., Blackwell P. G., Buck C. E., Burr G., Cutler K. B., Damon P. E., Edwards R. L., Fairbanks R. G., Friedrich M., Guilderson T. P., Kromer B., McCormac F. G., Manning S., Bronk Ramsey C., Reimer P. J., Reimer R. W., Remmele S., Southon J. R., Stuiver M., Talamo S., Taylor F. W., Van Der Plicht J. and Weyhenmeyer C. E. (2004) Marine04 Marine Radiocarbon Age Calibration, 0–26 cal kyr BP. *Radiocarbon* **46**, 1059-1086.

Hulburt E. M (1968) Phytoplankton observations in the western Caribbean Sea. *Bulletin Marine Science Gulf Caribb*. **18**, 388-399.

Huntley D. J., Godfrey-Smith D. I. and Thewalt M. L. W. (1985) Optical dating of sediments. *Nature* **313**(5998), 105-107.

Huntley D. J., Godfrey-Smith D. I. and Haskell E. H. (1991) Light-induced emission spectra from some quartz and feldspars. *International Journal of Radiation Applications and Instrumentation. Part D. Nuclear Tracks and Radiation Measurements* **18**(1-2), 127-131.

Huntley D. J., Hutton J. T. and Prescott J. R. (1993) The stranded beach-dune sequence of south-east South Australia: A test of thermoluminescence dating, 0-800 ka. *Quaternary Science Reviews* **12**(1), 1-20.

Huntley D. J., Short M. A. and Dunphy K. (1996) Deep traps in quartz and their use for optical dating. *Canadian Journal of Physics* **74**, 81-91.

Hutchinson G. E. (1967) *Introduction to Lake Biology and the Limnoplankton*. A Treatise on Limnology, 2, Wiley J. & Sons, New York.

Hütt G., Jaek I. and Tchonka J. (1988) Optical dating: K-feldspars optical response stimulation spectra. *Quaternary Science Reviews* **7**(3-4), 381-385.

Huxley T. H. (1858) *Deep-sea soundings in North Atlantic Ocean between Ireland ans Newfoundland*, Admirality, London.

Huxley T. H. (1868) On some organisms living at great depths in the North Atlantic Ocean. *Quaterly Journal of Microscopial Science* **8**, 203-212.

Imbrie J., Hays J. D., Martinson D. G., McIntyre A., Mix A. C., Morley J. J., Pisias N. G., Prell W. L. and Shackleton N. J. (1984) The orbital theory of Pleistocene climate: Support from a revised chronology of the marine $d^{18}O$ record. In: *Milankovitch and Climate (ed* Berger A. L. et al.), pp. 269-305, Riedel D.

Ivanovich M. and S. H. R. (1992) *Uranium series disequilibrium*. Applications to Earth, Marine and Environmental Sciences, 2nd edition. 910 pp, Clarenton Press, Oxford.

Jafar S. A. and Martini E. (1975) On the validity of the calcareous nannoplankton genus *Helicosphaera*. *Senckenbergiana lethaea* **56**(4/5). 381-397.

Jennings J. N. (1972) Some attributes of Torres Strait. In: *Bridge and Barrier, The Natural and Cultural History of Torres Strait (ed* D. Walker), pp. 29-38, Research School of Pacific Studies, Department of Biogeography and Geomorphology, The Australian National University, Canberra.

Jones B. G. and Facer R. A. (1982) CORRMAT/PROB, a program to create and test a correlation coefficient matrix from data with missing values *Computers and Geosciences* **8**(2), 191-198.

Jones M. R. (1986) Surficial sediment of the central Gulf of Carpentaria. In: Geological survey of Queensland, pp.

Jones M. R. (1987) Surficial sediments of the western Gulf of Carpentaria, Australia. *Australian Journal of Marine and Freshwater Research* **38**, 151-167.

Jones M. R. and Torgersen T. (1988) Late Quaternary evolution of Lake Carpentaria on the Australia-New Guinea continental shelf. *Australian Journal of Earth Sciences* **35**, 313-324.

Jordan R. W. and Green J. C. (1994) A check-list of the extant Hapophyta of the world. *Journal of Marine Biology Association U.K.* **74**, 149-174.

Jordan R. W. and Kleijne A. (1994) A classification system for living coccolithophhores. In: *Coccolithophores (ed* A. Winter and W.G. Siesser), pp. 83-105, Cambridge University Press, Cambridge.

Jordan R. W., Kleijne A., Heimdal B. R. and Green J. C. (1995) A glossary of the extant Haptophyta of the world. *Journal of Marine Biology Association U.K.* **75**, 769-814.

Jordan R. W. and Chamberlain A. H. L. (1997) Biodiversity among haptophyte algae. *Biodiversity and Conservation* **6**, 131-152.

Jordan R. W., Broerse A. T. C., Hagino K., Kinkel H., Sprengel C., Takahashi K. and Young J. R. (2000) Taxon lists for studies of modern nannoplankton. *Marine Micropaleontology* **39**(1-4), 309-314.

Jungner H. and Bøtter-Jensen L. (1994) Study of sensitivity change of OSL signals from quartz and feldspars as a function of preheat temperature. *Radiation Measurements* **23**(2-3), 621-624.

Kilham P. and Kilham S. S. (1980) The evolutionary ecology of phytoplankton. In: *The Physiological Ecology of Phytoplankton (ed* I. Morris), pp. 571-597, California University Press, Berkeley.

Kinkel H., baumann K.-H. and Capek M. (2000) Coccolithophores in the Equatorial Atlantic Ocean: response to seasonal and Late Quaternary surface water variability *Marine Micropaleontology* **39**, 87-112.

Klaveness D. and Paasche E. (1979) Physiology of coccolithophorids. In: *Biochemistry and Physiology of Protozoa, 2nd edition (ed* M. Levandovsky and S.H. Hunter), pp. 191-213, Academic Press, London.

Kleijne A., Kroon D. and Zevenboon W. (1989) Phytoplankton and Foraminiferal frequencies in Northern Indian ocean and Red Sea surface waters. *Netherlands Journal of Sea Research* **24-4**, 531-539.

Kleijne A. (1990) Distribution and malformation of extant calcareous nannoplankton in the Indonesian Seas. *Marine Micropaleontology* **16**, 293-316.

Kleijne A. (1992) Extant Rhabdosphaeraceae (coccolithophorids, class Prymnesiophyceae) from the Indian Ocean, Red Sea, Mediterranean Sea and North Atlantic Ocean. *Scripta Geologica* **100**, 1-63.

Kleijne A., Jordan R. W., Heimdal B. R., Samtleben C., Chamberlain A. H. L. and Cros L. (2001) Five new species of the coccolithophorid genus *Alisphaera* (Haptophyta) with notes on their distribution, coccolith structure and taxonomy. *Phycologia*, **40**(6)' 583-601.

Krbetschek M. R., Rieser U., Zoller L. and Heinicke J. (1994) Radioactive disequilibria in palaeodosimetric dating of sediments. *Radiation Measurements* **23**, 485-489.

Krbetschek M. R., Reiser U. and Soltz W. (1996) Feldspar dating: Applicability of different luminescence missions bands. In: 8th International Conference on Luminescence and Electron Spin Resonance Dating, pp. 140-142, Canberra, Australia.

Laguna R., Romo J., Read B. A. and Wahlund T. M. (2001) Induction of phases variation events in the life ofthe marine coccolithophorid *Emiliana huxleyi*. *Applied Environmental Microbiology* **67**, 3824-3831.

Lamothe M., Balescu S. and Auclair M. (1994) Natural IRSL intensities and apparent luminescence ages of single feldspar grains extracted from partially bleached sediments. *Radiation Measurements* **23**, 555-562.

Lang A. (1995) Die Infrarot-Stimulierte-Lumineszenz als Datierungsmethode für holozäne Lössderivate. *PhD thesis* Universität Heidelberg.

Lang A. (1996) Die Infrarot Stimulierte Lumineszenz als Datierungsmethode für holozäne Lössderivate. *PhD Thesis*, 134pp pp, Universität Heidelberg, Heidelberg.

Lang A., Lindauer S., Kuhn R. and Wagner G. A. (1996) Procedures used for optically and infrared stimulated luminescence dating from sediments in Heidelberg. *Ancient TL* **14**(3), 7-11.

Lang A. and Nolte S. (1999) The chronology of Holocene alluvial sediments from the Wettereau, Germany, provided by optical and ^{14}C dating. *The Holocene* **9**(2), 207-214.

Lawson E. M., Elliott G., Fallon J., Fink D., Hotchkis M. A. C., Hua Q., Jacobsen G. E., Lee P., Smith A. M., Tuniz C. and Zoppi U. (2000) AMS and ANTARES - The first 10 years. *Nuclear Instruments and Methods in Physics Research Section B: Beam Interactions with Materials and Atoms* **172**, 95-99.

Leeder M. R. (1982) *Sedimentology: Process and Product*, London.

Li S.-H. and Wintle A. G. (1992) Luminescence sensitivity change due to bleaching of sediments. *International Journal of Radiation Applications and Instrumentation. Part D. Nuclear Tracks and Radiation Measurements* **20**(4), 567-573.

Lohman H. (1902) Die Coccolithophoridae, eine Monographie der Coccolithen bidenden Flagellaten, zugleich ein Beitrag zur Kenntnis der Mittlemeerauftriebs. *Arch. Protistenk* **1**, 89-165.

Manton I. (1986) Functional parallels between calcified and uncalcified periplasts. In: *Biomineralisation in Lower Plants ans Animals (ed* B.S.C. Leadbeater and R. Riding), The Systematics Association, Special Volume, pp. 157-172, Clarendon Press, Oxford.

Markey B. G., Bøtter-Jensen L. and Duller G. A. T. (1997) A new flexible system for measuring thermally and optically stimulated luminescence. *Radiation Measurements* **27**(2), 83-89.

Martinez J. I., De Deckker P. and Chivas A. R. (1997) New estimates for salinity changes in the Western Pacific Warm Pool during the Last Glacial Maximum: Oxygen-isotope evidence. *Marine Micropaleontology* **32**(3-4), 311-340.

Martinson D. G., Pisias N. G., Hays J. D., Imbrie J., Moore Jr T. C. and Shackleton N. J. (1987) Age dating and the orbital theory of the ice ages: development of a high-resolution 0 to 300 000-year chronostratigraphy. *Quaternary Research* **27**(1), 1-29.

McCormac F. G., Hogg A. G., Blackwell P. G., Buck C. E., Higham T. F. G. and Reimer P. J. (2004) SHCal04 Southern Hemisphere Calibration, 0–11.0 cal kyr BP. *Radiocarbon* **46**, 1087-1092.

McCulloch M. T., De Deckker P. and Chivas A. R. (1989) Strontium isotope variations in single ostracod valves from the Gulf of Carpentaria, Australia: A palaeoenvironmental indicator. *Geochimica et Cosmochimica Acta* **53**(7), 1703-1710.

McIntyre A. (1967) Coccoliths as paleoclimatic indicators of Pleistocene Glaciations. *Science* **158**, 1314-1317.

McIntyre A. and Bé A. W. H. (1967) Modern Coccolithophoridae of the Atlantic Ocean-I, Placoliths and Cyrtoliths. *Deep-Sea Research* **14**, 561-597.

McIntyre A., Bé A. W. H. and Roche M. B. (1970) Modern Pacific Coccolithophorida: a palaeontological thermometer. *New York Academic Science Transcription, series 2* **32**, 720-731.

McIntyre A. and Mcintyre R. (1971) Coccolith concentrations and differential solution in ocenic sediments. In: *The Micropalaeontology of Oceans (ed* B.M. Funnell and W.R. Riedel), pp. 253-261, Cambridge University Press, Cambridge.

McIntyre A., Ruddiman W. F. and Jantzen R. (1972) Southward penetration ot the North Atlantic Polar Front: faunal and floral evidence of large-scale surface water mass movements over the last 225,000 years. *Deep-Sea Research* **19**, 61.

McKeever S. W. S., Agersnap Larsen N., Bøtter-Jensen L. and Mejdahl V. (1997) OSL sensitivity changes during single aliquot procedures: Computer simulations. *Radiation Measurements* **27**(2), 75-82.

McKeever S. W. S. and Chen R. (1997) Luminescence models. *Radiation Measurements* **27** (5-6), 625-661.

McKeever S. W. S. and Moscovitch M. (2003) Topics under Debate - On the advantages and disavantages of optically stimulated luminescence dosimetry and thermoluminescence dosimetry. *Radiation Protection Dosimetry* **104**, 263-270.

McMillan J. (1982) A Global Atlas of GEOS-3 Significant Wave height Data and Comparison of the Data with National Buoy Data (156882). *Technical report, NASA*, Wallops Flight Centre, Virginia.

Mejdahl V. (1979) Thermoluminescence dating: beta-dose attenuation in quartz grains. *Archaeometry* **21**(Part 1), 61-72.

Mejdahl V. (1988) The plateau method for dating partially bleached sediments by thermoluminescence. *Quaternary Science Reviews* **7**(3-4), 347-348.

Mejdahl V. and Christiansen H. H. (1994) Procedures used for luminescence dating of sediments. *Quaternary Science Reviews* **13**(5-7), 403-406.

Mejdahl V. and Bøtter-Jensen L. (1997) Experience with the SARA OSL method. *Radiation Measurements* **27**(2), 291-294.

Meteorology C. B. o. (2004) Climate averages map. http://www.bom.gov.au/climate/map/climate_avgs/clim_avgs1.shtml

Michel J. (1984) Redistribution of uranium and thorium series isotopes during isovolumetric weathering of granite. *Geochimica et Cosmochimica Acta* **48**, 1249-1255.

Milankovitch M. (1941) Canon of Insolation and the Ice-Age Problem. In: Royal Serbian Academy Special Publication 132, pp., Israel Program for Scientific Translations, Jerusalem, 1969.

Morrison R. J. and Delaney J. R. (1996) Marine pollution in the Arafura and Timor Seas. *Marine Pollution Bulletin* **32**(4), 327-334.

Munk W. H. and Riley G. (1952) Absorption of nutrients by aquatic plants. *Journal of Marine Research* **11**, 215-240.

Munro I. S. R. (1967) *Gulf of Carpentaria - Southern part, Depht contours*, Department of Harbour and Marine, Brisbane, Queensland.

Munro I. S. R. (1972) The fauna of the Gulf of Carpentaria: No.1. Introductin and station lists. In: Fisheries Notes Queensland (New Series), pp. 1-38.

Munro I. S. R. (1984) Atlas of operational, environmental, and biological data from the Gulf of Carpentaria prawn survey, 1963-65, Part 3. physical and chemical environment. In: Marine Laboratory Hobart Report, pp., CSIRO (Australia).

Murray-Wallace C. V., Banerjee D., Bourman R. P., Olley J. M. and Brooke B. P. (2002) Optically stimulated luminescence dating of Holocene relict foredunes, Guichen Bay, South Australia. *Quaternary Science Reviews* **21**(8-9), 1077-1086.

Murray A., Olley J. M. and Wallbrink P. J. (1991) *Radionuclides for analysis of sediment in water supply catchments*, CSIRO Division of Water Resources, Consultancy report, Canberra.

Murray A., Wohl E. and East J. (1992) Thermoluminescence and excess ^{226}Ra decay dating of late Quaternary fluvial sands. East Alligator River, Australia. *Quaternary Research* **37**, 29-41.

Murray A. S., Olley J. M. and Caitcheon G. G. (1995) Measurement of equivalent doses in quartz from contemporary water-lain sediments using optically stimulated luminescence. *Quaternary Science Reviews* **14**(4), 365-371.

Murray A. S. and Roberts R. G. (1997) Determining the burial time of single grains of quartz using optically stimulated luminescence. *Earth and Planetary Science Letters* **152**(1-4), 163-180.

Murray A. S., Roberts R. G. and Wintle A. G. (1997) Equivalent dose measurement using a single aliquot of quartz. *Radiation Measurements* **27**, 171-184.

Murray A. S. and Roberts R. G. (1998) Measurement of the equivalent dose in quartz using a regenerative-dose single-aliquot protocol. *Radiation Measurements* **29**(5), 503-515.

Murray A. S. and Wintle A. G. (1998) Factors controlling the shape of the OSL decay curve in quartz. *Radiation Measurements* **29**(1), 65-79.

Murray A. S. and Wintle A. G. (1999) Isothermal decay of optically stimulated luminescence in quartz. *Radiation Measurements* **30**(1), 119-125.

Murray A. S. and Olley J. M. (1999) Determining sedimentation rates using luminescence dating. *Geo Research Forum* **5**, 121-144.

Murray A. S. and Wintle A. G. (2000a) Application of the single-aliquot regenerative-dose protocol to the 375[deg]C quartz TL signal. *Radiation Measurements* **32**(5-6), 579-583.

Murray A. S. and Wintle A. G. (2000b) Luminescence dating of quartz using an improved single-aliquot regenerative-dose protocol. *Radiation Measurements* **32**(1), 57-73.

Murray A. S. and Olley J. M. (2002) Precision and accuracy in the optically stimulated luminescence dating of sedimentary quartz: a status review. *Geochronometria* **21**, 1-16.

Murray A. S. and Wintle A. G. (2003) The single aliquot regenerative dose protocol: potential for improvements in reliability. *Radiation Measurements* **37**(4-5), 377-381.

Murray J. (1876) Preliminary report. *Proc. Royal Society, London* **24**(471-544).

Murray J. and Renard A. F. (1891) Report on deep-sea deposits based on the specimens collected during the voyage of H. M. S. Challenger during years 1872 to 1876. In: *Report on the Scientific Results of the Voyage of H. M. S. Challenger During Years 1872 -76, part 3, Deep-sea Deposits (ed*, pp. 257-258, pl.x.i, H.M. Stationary Office, London.

Murray J. and Blackman V. H. (1898) On the nature of coccospheres and rhabdospheres. *Philosophical Transaction Royal Society London, Serie B* **190**, 427-441.

Nakada M. and Lambeck K. (1989) Late Pleistocene and Holocene sea-level change in the Australian region and mantle rheology. *Geophysical Journal* **96**, 497-517.

Nambi K. S. V.; Aitken M. J. (1986) Annual dose conversion factors for TL and ESR dating. *Archaeometry* **28***,* 202-205.

Nanson G. C., Jones B. G., Price D. M. and Pietsch T.J. (2005) Rivers turned to rock: Late Quaternary alluvial induration influencing the behaviour and morphology of an anabranching river in the Australian monsoon tropics. *Geomorphology* **70**, 398-420.

Nathan R. P., Thomas P. J., Jain M., Murray A. S. and Rhodes E. J. (2003) Environmental dose rate heterogeneity of beta radiation and its implications for luminescence dating: Monte Carlo modelling and experimental validation. *Radiation Measurements* **37**(4-5), 305-313.

Nicholls N. and Wong K. K. (1990) Dependence of rainfall variability on mean rainfall, latitude and the Southern Oscillation. *Journal of Climate* **3**, 163-170.

Nishida S. (1979) Atlas of Pacific Nannoplankton. *Micropalaeontology Society, Osaka, Special Paper* **3**.

Nix H. A. and Kalma J. D. (1972) Climate as a dominant control in the biogeography of northern Australia and New Guinea. In: *Bridge and Barrier: the Natural and Cultural History of Torres Strait (ed* D. Walker), pp. 61-91, Department of Biogeography and Geomorphology Australian National University, Canberra.

NOAA (2005) El Niño Theme page.
http://www.pmel.noaa.gov/tao/elnino/nino-home.html

Noël M.-H., Kawashi M. and Inouye I. (2004) Induced dimorphic life cycle of a coccolithophorid, Calyptroshaera spaeroidae (Prymnesiophyceae, Haptophyta). *Journal of Phycology* **40**(1), 112-129.

Norman M. D. and De Deckker P. (1990) Trace metals in lacustrine and marine sediments: A case study from the Gulf of Carpentaria, northern Australia. *Chemical Geology* **82**, 299-318.

Okada H. and Honjo S. (1973) The distribution of oceanic coccolithiophorids in the Pacific. *Deap-sea Research* **20**, 355-374.

Okada H. and Honjo S. (1975) Distribution of Coccolithophores in Marginal Seas along the Western Pacific Ocean and in the Red Sea. *Marine Biology* **31**, 271-285.

Okada H. and McIntyre A. (1979) Seasonal Distribution of Modern Coccolithophores in the Western North Atlantic Ocean. *Marine Biology* **54**, 319-328.

Okada H. (1983) Modern nannofossil assemblages in sediments of coastal and marginal seas along the western pacific ocean. *Ultrecht Micropaleontological Bulletins* **30**, 171-187.

Okada H. (1992) Use of microbeads to estimate the absolute abundance of nannofossils. *INA News 1* **14**, 96-97.

Okada H. and Wells P. (1997). Late Quaternary nannofossil indicators of climate change in two deep-sea cores associated with the Leeuwin Current off Western Australia. *Palaeogeography. Palaeoclimatology. Palaeoecology*. **131**, 413–432

Okada H. (2000) Neogene and Quaternary calcareous nannofossils from the Blake Ridge, Sites 994, 995, and 997. *Proceedings of the Ocean Drilling Program, Scientific Results* **164**, 331-341.

Olley J. M., Murray A. and Roberts R. G. (1996) The effect of disequilibria in the uranium and thorium decay chains on burial dose rates in fluvial sediments. *Quaternary Geochronology* **15**, 751-760.

Olley J. M., Roberts R. G. and Murray A. S. (1997) Disequilibria in the uranium decay series in sedimentary deposits at Allen's cave, Nullarbor Plain, Australia: Implications for dose rate determinations. *Radiation Measurements* **27**(2), 433-443.

Olley J. M., Caitcheon G. G. and Murray A. S. (1998) The distribution of apparent dose as determined by optically stimulated luminescence in small aliquots of fluvial quartz: implications for dating young sediments. *Quaternary Geochronology* **17**(11), 1033-1040.

Olley J. M., Caitcheon G. G. and Roberts R. G. (1999) The origin of dose distributions in fluvial sediments, and the prospect of dating single grains from fluvial deposits using optically stimulated luminescence. *Radiation Measurements* **30**, 207-217.

Olley J. M., De Deckker P., Roberts R. G., Fifield L. K., Yoshida H. and Hancock G. (2004a) Optical dating of deep-sea sediments using single grains of quartz: a comparison with radiocarbon. *Sedimentary Geology* **169**(3-4), 175-189.

Olley J. M., Pietsch T. and Roberts R. G. (2004b) Optical dating of Holocene sediments from a variety of geomorphic settings using single grains of quartz. *Geomorphology* **60**(3-4), 337-358.

Ostenfeld C. H. (1899) Uber coccosphaera und einige neue Tintinniden im Plankton des nordlichen Atlantischen Oceans. *Zool. Anz* **22**, 433-439.

Ostenfeld C. H. (1900) Uber coccospharea. *Zool. Anz* **23**, 198-200.

Paasche E. (1962) Coccolith formation. *Nature* **193**, 1094-1095.

Parke M., Manton I. and Clarke B. (1955) Studies on marine flagellates.II. Three new species of *Chrysochromulina*. *Journal of Marine Biology Association U.K.* **35**, 387-414.

Parke M. and Adams I. (1960) The motile *Crystallolthus haylinus* (Garder and Markali) and the non-motile phases in the life history of *Coccolithus pelagicus* (Wallich) Schiller. *Marine Biology Association United Kingdom Journal* **39**, 263-274.

Passmore V. L., Williamson P. E., Gray A. R. G. and Wellman P. (1993) The Bamaga Basin - a new exploration target. In: Second Papua New Guinea Petroleum Convention. G.J. Carman and Z. Carman (Editors), pp. 233-240, Port Moresby.

Phipps C. V. G. (1966) Gulf of Carpentaria (Northern Australia). In: *The Encyclopedia of Oceanography (ed* R.W. Fairbridge), pp. 316-424, Reinhold, New York.

Phipps C. V. G. (1970) Dating of eustatic events from cores taken in the Gulf of Carpentaria and samples from the New South Wales continental shelf. *Australian Journal Science* **32**, 329-331.

Phipps C. V. G. (1980) The Carpentaria plains. In: *The Geology and Geophysics of Northeastern Australia (ed* R.A. Henderson and P.J. Stephenson), pp. 382-386,388-390, Geological Society of Australia, Queensland Division.

Pittock A. B. (1975) Climatic change and the patterns of variation in Australian rainfall. *Search* **6**, 498-504.

Pittock A. B. (1978) Patterns of variability in relation to the general circulation. In: *Climatic Change and Variability: A Southern Perspective (ed* A.B. Pittock, L.A. Frakes, D. Jenssen, J.A. Peterson and J.W. Zillman), pp., Cambridge University Press, Cambridge.

Poiner I. R. and Peterken C. (2000) Seagrass. In: *State of the marine Environment Report for Australia (ed* L.P. Zann and P. Kailola), pp. 107-117, Department of the Environment, Sport and Territories, Ocean Rescue 2000 Program, Canberra.

Poolton N. R. J., Bøtter-Jensen L. and Rink W. J. (1995) An optically stimulated luminescence study of flint related to radiation dosimetry. *Radiation Measurements* **24**, 551-556.

Prasad S. (2000) HF treatment for the isolation of fine grain quartz luminescence dating. *Ancient TL* **18**(1), 15-17.

Prasad S. and Gupta S. K. (1999) Luminescence dating of a 54 m long core from Nal region, western India - implications. *Quaternary Science Reviews* **18**(13), 1495-1505.

Preda M. and Cox M. E. (2005) Chemical and mineralogical composition of marine sediments, and relation to their source and transport, Gulf of Carpentaria, Northern Australia. *Journal of Marine Systems* **53**(1-4), 169-186.

Prescott J. R. and Stephan L. G. (1982) The contribution of cosmic radiation to the environmental dose for thermoluminescence dating. Latitude, altitude and depth dependences. *PACT* **6**, 17-25.

Prescott J. R. and Hutton J. T. (1988) Cosmic ray and gamma ray dosimetry for TL and ESR. *International Journal of Radiation Applications and Instrumentation. Part D. Nuclear Tracks and Radiation Measurements* **14**(1-2), 223-227.

Prescott J. R. and Hutton J. T. (1994) Cosmic ray contributions to dose rates for luminescence and ESR dating: Large depths and long-term time variations. *Radiation Measurements* **23**(2-3), 497-500.

Prescott J. R. and Robertson G. B. (1997) Sediment dating: a review. *Radiation Measurements* **27**(5-6), 893-922.

Rasmusson E. M. and Carpenter T. (1982) Variations in tropical sea surface temperature and surface wind fields associated with the Southern Oscillation. *Monthly Weather Review* **110**, 354-384.

Readhead M. L. (1987) Thermoluminescence dose rate dataand dating equations for the case of disequilibrium in the decay series. *Nuclear tracks and Radiation Measurements* **13**, 197-207.

Rees-Jones J., Hall S. J. B. and Rink W. J. (1997) A laboratory inter-comparison of quartz optically stimulated luminescence (OSL) results. *Quaternary Science Reviews* **16**(3-5), 275-280.

Reeves J. M. (2004) The use of ostracoda in the palaeoenvironmental reconstruction of the Gulf of Carpentaria, Australia, from the last interglacial to present. *PhD thesis Thesis*, 466 pp, University of Wollongong, Wollongong.

Regnauld H., Mauz B. and Morzadec-Kerfourn M. T. (2003) The last interglacial shoreline in northern Brittany, western France. *Marine Geology* **194**(1-2), 65-77.

Reid F. M. H. (1980) Coccolithophorids from the North Pacific central gyre with notes on their vertical and seasonal distribution. *Micropalaeontology* **26**, 151-176.

Reimer P. J., Baillie M. G. L., Bard E., Bayliss A., Beck J. W., Bertrand C., Blackwell P. G., Buck C. E., Burr G., Cutler K. B., Damon P. E., Edwards R. L., Fairbanks R. G., Friedrich M., Guilderson T. P., Hughen K. A., Kromer B., McCormac F. G., Manning S., Bronk Ramsey C., Reimer R. W., Remmele S., Southon J. R., Stuiver M., Talamo S., Taylor F. W., Van Der Plicht J. and Weyhenmeyer C. E. (2004) IntCal04 Terrestrial Radiocarbon Age Calibration, 0–26 cal kyr BP. *Radiocarbon* **46**, 1029-1058.

Reimer P. R. and Reimer R. (2005) Marine Reservoir Correction Database. In, pp.

Rendell H. M., Webster S. E. and Sheffer N. L. (1994) Underwater bleaching of signals from sediment grains: new experimental data. *Quaternary Science Reviews* **13**(5-7), 433-435.

Rhodes E. J. (1988) Methodological considerations in the optical dating of quartz. *Quaternary Science Reviews* **7**(3-4), 395-400.

Rhodes E. J. (1990) Optical dating of quartz from sediments. *Unpublished PhD thesis Thesis*, Oxford University, Oxford.

Rhodes E. J. and Pownall L. (1994) Zeroing of the OSL signal in quartz from young glaciofluvial sediments. *Radiation Measurements* **23**(2-3), 581-585.

Ridd P., Sandstrom M. W. and Wolanski E. (1988) Outwelling from tropical tidal salt flats. *Estuarine, Coastal and Shelf Science* **26**(3), 243-253.

Rieser U., Lang A., Wagner G. A., Krbetschek M. R. and Stolz W. (1997) Luminescence dating in archaeology: recent developments. In: Proceedings of the 4th International Conference on Optics within Life Sciences 1996, pp., Springer, Berlin.

Roberts H. M. and Wintle A. G. (2001) Equivalent dose determinations for polymineralic fine-grains using the SAR protocol: application to a Holocene sequence of the Chinese Loess Plateau. *Quaternary Science Reviews* **20**(5-9), 859-863.

Roberts R. G. (1991) Thermoluminescence dating. *PhD thesis Thesis*, 349-384. pp, University of Wollongong, Wollongong.

Roberts R. G., Spooner N. A. and Questiaux D. G. (1994) Palaeodose underestimates caused by extended-duration preheats in the optical dating of quartz. *Radiation Measurements* **23**(2-3), 647-653.

Roberts R. G., Walsh G., Murray A., Olley J., Jones R., Morwood M., Tuniz C., Lawson E., Macphail M., Bowdery D., Naumann I. (1997) Luminescence dating of rock art and past environments using mud-wasp nests in northern Australia. *Nature* **387**, 696–699.

Roberts R. G., Bird M., Olley J. M., Galbraith R. F., Lawson E., Laslett G. M., Yoshida H., Jones R., Fullagar R., Jacobsen G. and Hua Q. (1998a) Optical and radiocarbon dating at Jimnium rock shelter in northern Australia. *Nature* **393**, 358-362.

Roberts R. G., Yoshida H. and Galbraith R. (1998b) Single-aliquot and single-grain optical dating confirm thermoluminescence ages estimates at Malakunanja II rock shelter in northern Australia. *Ancient TL* **16**(1), 19-24.

Roberts R. G., Galbraith R. F., Olley J. M., Yoshida H. and Laslett G. M. (1999) Optical dating of single and multiple grains of quartz from Jimnium rock shelter, northern Ausralia: Part II, results and implications. *Archaeometry* **41**(2), 365-395.

Roberts R. G., Galbraith R. F., Yoshida H., Laslett G. M. and Olley J. M. (2000) Distinguishing dose populations in sediment mixtures: a test of single-grain optical dating procedures using mixtures of laboratory-dosed quartz. *Radiation Measurements* **32**(5-6), 459-465.

Roth P. H. and Berger W. H. (1975) Distribution and dissolution of coccoliths in the south and central pacific. In: *Dissolution of deep sea carbonates (ed* W. Silter, W.B. A. and H.B. W.), Foraminiferal Research Special Publication, pp. 87-113, Cushman Found.

Roth P. H. and Coulborne W. T. (1982) Floral and solution patterns of coccoliths in surface sedimnets of the North Pacific. *Marine Micropaleontology* **7**, 1-52.

Ruddiman W. F. and McIntyre A. (1976) Northeast Atlantic paleoclimatic changes over the past 600,000 years. *Geol Soc American Mem.* **145**, 111-112.

Sabine C. L., Key R. M., Feely R. A. and Greeley D. (2002) Inorganic carbon in the Indian Ocean: distribution and dissolution processes. *Global Biogeochemical Cycles* **16**(4), 1067.

Sáez A. G., Probert I., Young J. R., Edvardsen B., Eikrem W. and Medlin L. K. (2004) A review of the phylogeny of Haptophyta. In: *Coccolithophores, from Molecular Processes to Global Impact (ed* H.R. Thierstein and J.R. Young), pp. 251-269.

Sáez A. G., Lozano E. (2005) Cryptic species: as we discover more examples of species that are morphologically indistinguishable, we need to ask why and how they exist. *Nature* **433**, 111.

Sato T., Yuguchi S., Takayama T. and Kameo K. (2004) Drastic change in the geographical distribution of the cold-water nannofossil Coccolithus pelagicus (Wallich) Schiller at 2.74 Ma in the late Pliocene, with special reference to glaciation in the Arctic Ocean. *Marine Micropaleontology* **52**(1-4), 181-193.

Schiebel R., Zeltner A., Treppke U. F., Waniek J. J., Bollmann J., Rixen T. and Hemleben C. (2004) Distribution of diatoms, coccolithophores and planktic foraminifers along a trophic gradient during SW monsoon in the Arabian Sea. *Marine Micropaleontology* **51**(3-4), 345-371.

Schiller J. (1913) Vorlaufige Ergebnisse der Phytoplankton-Utersuchungen auf den Fahrten SMS Najade in der Adria 1911-12. Die Coccolithophoriden. *SitzBerg. K. Akad. Wiss. (Wien), MAth.-Naturw. Kl., Abt.1* **122**, 597-617.

Schiller J. (1930) Coccolithineae. In: *Rabenhorst's Kryptogamen-Flora (ed* L. Rabenhorst), pp. 89-263, Akadamie Verlagsgesellschaft, Leipzig.

Schmidt R. R. 1978. Calcareous Nannofossils. *Utrecht Micropaleontological Bulletins* **17**, 241-265.

Shackleton N. J. and Opdyke N. D. (1973) Oxygen isotope and paleomagnetic stratigraphy of equatorial Pacific core V28-238; oxygen isotope temperatures and ice volumes on a 10^5 and 10^6 year scale. *Quaternary Research* **3**, 39-55.

Shackleton N. J. (1977) The oxygen isotope stratigraphic record of the Late Pleistocene. *Philosophical Transaction Royal Society London* **Series B 280**, 169-182.

Shackleton N. J., Imbrie J. and Hall M. A. (1983) Oxygen and carbon isotope record of East Pacific core V19-30: implications for deep water in the late Pleistocene North Atlantic. *Earth and Planetary Science Letters* **65**, 233-244.

Shackleton N. J. (1987) Oxygen isotopes, ice volume and sea-level. *Quaternary Science Reviews* **6**, 183-190.

Shulmeister J., Shane P., Lian O. B., Okuda M., Carter J. A., Harper M., Dickinson W., Augustinus P., Heijnis H. (2001) A long late-Quaternary record from Lake Poukawa, Hawke's Bay, New Zealand. *Palaeogeography, Palaeoclimatology, Palaeoecology* **176**, 81-107.

Sikes C. S., Roer R. D. and Wilbur K. M. (1980) Photosynthesis and coccolith formation: Inorganic carbon sources and net inorganic reaction of deposition. *Limnology and Oceanography* **25**, 248-261.

Simmonds I. and Hope P. (1997) Persistence characteristics of Australian rainfall anomalies. *International Journal of Climatology* **17**(6), 597-613.

Singh A. D., Schiebel R. and Nisha N. R. (1998) Occurrence of pteropods in a deep eastern Arabian Sea core: Neotectonic implications. *Current Science* **78**(9), 1142-1144.

Singh A. D., Nisha N. R. and Joydas T. V. (2005) Distribution patterns of Recent pteropods in surface sediments of the western continental shelf of India *Journal of Micropalaeontology* **24**(1), 39-54.

Smart J. (1977) Late Quaternary sea-level changes, Gulf of Carpentaria, Australia. *Geology* **5**, 755-759.

Smith B. W., Aitken M. J., Rhodes E. G., Robinson P. and Geldard D. M. (1986) Optical dating: Methodological aspects. *Radiation Protection Dosimetry* **17**, 229-233.

Smith M. A., Prescott J. R. and Head M. J. (1997) Comparison of ^{14}C and luminescence chronologies at Puritjarra rock shelter, central Australia. *Quaternary Science Reviews* **16**(3-5), 299-320.

Somers I. F. and Long B. G. (1994) Note on the sediments and hydrology of the Gulf of Carpentaria, Australia. *Australian Journal of Marine and Freshwater Research* **45**, 283-291.

Sorby H. C. (1861) On the organic origin of the so-called 'Crystalloid' of the chalk. *Annals and Magazine of Natural history, serie 3* **8**, 193-200.

Spooner N. A. and Questiaux D. G. (1990) Optical dating - Achenheim beyond the Eemian using green/infrared stimulation. In: Long and Short Range Limits in Luminescence Dating, pp. 97-103, Research Laboratory for Archaeology and History of Art, Oxford, Oxford, April 1989.

Spooner N. A. (1994) On the optical dating signal from quartz. *Radiation Measurements* **23**(2-3), 593-600.

Stokes S. (1994) The timing of OSL sensitivity changes in a natural quartz. *Radiation Measurements* **23**(2-3), 601-605.

Stokes S., Colls A. E. L., Fattahi M. and Rich J. (2000) Investigations of the performance of quartz single aliquot DE determination procedures. *Radiation Measurements* **32**(5-6), 585-594.

Stokes S., Bray H. E. and Blum M. D. (2001) Optical resetting in large drainage basins: tests of zeroing assumptions using single-aliquot procedures. *Quaternary Science Reviews* **20**(5-9), 879-885.

Stokes S., Hetzel R., Bailey R. M. and Mingxin T. (2003a) Combined IRSL-OSL single aliquot regeneration (SAR) equivalent dose (De) estimates from source proximal Chinese loess. *Quaternary Science Reviews* **22**(10-13), 975-983.

Stokes S., Ingram S., Aitken M. J., Sirocko F., Anderson R. and Leuschner D. (2003b) Alternative chronologies for Late Quaternary (Last Interglacial-Holocene) deep sea sediments via optical dating of silt-sized quartz. *Quaternary Science Reviews* **22**(8-9), 925-941.

Stuiver M. and Polach H. A. (1977) Discussion: Reporting of ^{14}C data. *Radiocarbon* **19**(3), 355-363.

Stuiver M. and Reimer P. J. (1993) Extended ^{14}C database and revised CALIB radiocarbon calibration program. *Radiocarbon* **35**, 215-230.

Stuiver M., Reimer P. J., Bard E., Beck J. W., Burr G. S., Hughen K. A., Kromer B., McCormac G., Van Der Plicht J. and Spurk M. (1998) INTCAL98 radiocarbon age calibration, 24,000-0 cal BP. *Radiocarbon* **40**(3), 1041-1083.

Stuiver M., Reimer P. J. and Reimer R. (2005) CALIB Radiocarbon Calibration, version 5.0. http://calib.qub.ac.uk/calib/

Suppiah R. (1993) ENSO phenomenon and the 30-50 day variability in the Australian summer monsoon rainfall. *International Journal of Climatology* **13**, 837-851.

Suppiah R. (2004) Trends in the southern oscillation phenomenon and Australian rainfall and changes in their relationship. *International Journal of Climatology* **24**(3), 269-290.

Sym S. and Kawashi M. (2000) Ultrastructure of Calyptrospharea radiata, sp. nov. (Prymnesiophyceae, Haptophyta). *Eur. Jour. Phycol* **35**, 283-293.

Takahashi K. (1994) Coccolithophorid biocenesis: production and fluxes to the deep sea. In: *The Haptophyte Algae (ed* J.C. Green and B.S.C. Leadbeater), pp., Clarendon Press, Oxford.

Takahashi K. and Okada H. (2000a) Environmental control on the biogeography of modern coccolithophores in the southeastern Indian Ocean offshore of Western Australia. *Marine Micropaleontology* **39**(1-4), 73-86.

Takahashi K. and Okada H. (2000b) The paleoceanography for the last 30,000 years in the southeastern Indian Ocean by means of calcareous nannofossils. *Marine Micropaleontology* **40**(1-2), 83-103.

Takahashi K. and Okada H. (2001) Paleoceanography for the last 195,000 years in the Solomon Sea (ODP Site 1109) by means of calcareous nannofossils. *Marine Micropaleontology* **42**(1-2), 45-59.

Tanaka Y. (1991) Calcareous nannoplankton thanatocoenoses incsurface sediments from seas around Japan. *Sci. Rep. Tohoku University. 2nd Ser., Geol.* **61**, 127-198.

Tanaka Y. (1997) Sedimentary processes from the shelf edge to the Okinawa Trough in the East China Sea based on the coccolith assemblages. *Journal Sedimentol. Soc. Japan* **44**, 33-41.

Tappan H. (1980) Chapter 9: Haptophyta, coccolithophores and other calcareous nannoplankton. In: *The paleobiology of plant protists (ed*, pp. 679-803, W. H. Freeman, San Francisco.

Thierstein H. R., Cortès M. Y. and T. Haidar A. T. (2004) Plankton community time -scale: When models confront evidence. In: *Coccolithophores, from Molecular Processes to Global Impact (ed* H.R. Thierstein and J.R. Young), 455479, pp., Springrer, Berlin.

Thierstein H. R. and Young J. R. (2004) *Coccolithophores: From Molecular processes to Global Impact*, Springer, Berlin.

Thomas P. J., Murray A. S. and Sandgren P. (2003) Age limit and age underestimation using different OSL signals from lacustrine quartz and polymineral fine grains. *Quaternary Science Reviews* **22**(10-13), 1139-1143.

Thompson C. W. (1874) *The Depths of the Sea*, Macmillan & Co., London.

Tija H. D. (1966) Arafura Sea. In: *The Encyclopedia of Oceanography (ed* R.W. Fairbridge), pp. 44-47, Reinhold, New York.

Tizard T. H., Moseley H. N., Buchahan J. V. and Murray A. S. (1885) Narrative of the cruise of H.M.S. Challenger. In: *Report of the Sciewntific Results of the Voyage of the H.M.S. Challenger during the Years 1873-75 (ed*, pp., Neil & Co., Edinburgh.

Torgersen T., Hutchinson M. F., Searle D. E. and Nix H. A. (1983) General bathymetry of the Gulf of Carpentaria and the Quaternary physiography of Lake Carpentaria. *Palaeogeography, Palaeoclimatology, Palaeoecology* **41**(3-4), 207-225.

Torgersen T., Jones M. R., W. S. A., Searle D. E. and Ullman W. J. (1985) Late Quaternary hydrological changes in the Gulf of Carpentaria. *Nature* **313**, 785-787.

Torgersen T., Luly J., De Deckker P., Jones M. R., Searle D. E., Chivas A. R. and Ullman W. J. (1988) Late Quaternary environments of the Carpentaria Basin, Australia. *Palaeogeography, Palaeoclimatology, Palaeoecology* **67**(3-4), 245-261.

Turney C. S. M., Bird M. I., Fifield L. K., Roberts R. G., Smith M. A., Dortch C. E., Grün R., Lawson E., Ayliffe L. K., Miller G. H., Dortch J. and Cresswell R. G. (2001) Early human occupation at Devil's Lair, southwestern Australia 50,000 years ago. *Quaternary Research* **55**(1), 3-13.

Vartanian E., Guibert P., Roque C., Bechtel F. and Schvoerer M. (2000) Changes in OSL properties of quartz by preheating: an interpretation. *Radiation Measurements* **32**(5-6), 647-652.

Waelbroek C., Labeyrie L., Michel E., Duplessy J. C., McManus J. F., Lambeck K., Balbon E. and Labracherie M. (2002) Sea-level and deep water temperature changes derived from benthic foraminifera isotopic records. *Quaternary Science Reviews* **21**, 295-305.

Wallich G. C. (1861) Remarks on some novel phases of organic life, and on the boring powers of minute Annelids, at great depths in the sea. *Annals and Magazine of Natural history, serie 3* **8**, 52-58.

Wallich G. C. (1875) On the true nature of the so-called *Bathybius* and its alleged function in the nutrtion of the Protozoa. *Annals and Magazine of Natural history, serie 4* **16**, 322-339.

Wallich G. C. (1877) Observations on the coccosphere. *Annals and Magazine of Natural history, serie 4* **19**, 342-350.

Wallinga J., Murray A. S., Duller G. A. T. and Tornqvist T. E. (2001) Testing optically stimulated luminescence dating of sand-sized quartz and feldspar from fluvial deposits. *Earth and Planetary Science Letters* **193**(3-4), 617-630.

Wallinga J., Murray A. and Bøtter-Jensen L. (2002) Measurement of the dose in quartz in the presence of feldspar contamination. *Radiation Protection Dosimetry* **101**, 367-370.

Walsby A. F. and Reynolds C. S. (1980) Sinking and floating. In: *The Physiological Ecology of Phytoplankton (ed* I. Morris), pp. 1-625, California Press, Berkely.

Watabe N. and Wilbur K. M. (1966) Effects of temperature on growth, calcification, and coccolith form in *Coccolithus huxleyi* (Coccolihtineae). *Limnology and Oceanography* **11**, 567-575.

Weber Van Bosse A. (1901) Etudes sur les algues de l'archipel malaysien. III. Note préliminaire sur les résultats algologiques de l'expédition du Siboga. *Ann. Jard. Bot. Buitenz., 17: Série 2* **2**, 126-141.

Wilkinson A. J. (1997) Theoretical simulation of preheat-OSL cycles. *Radiation Measurements* **27**(3), 489-497.

Willmott W. F., Palfreyman W. D., Trail D. S. and Whitaker W. G. (1969) The igneous rocks of Torres Strait Queensland and Papua. *Bureau of Mineral Resources, Australia* **Records 1969/119**, (unpublished).

Winter A., Jordan R. W. and Roth P. H. (1994) Biogeography of living coccolithophores in ocean waters. In: *Coccolithophores (ed* A. Winter and W.G. Siesser), pp. 161-177, Cambridge University Press, Cambridge.

Winter A. and Siesser W. G. (1994a) Atlas of living coccolithophores. In: *Coccolithophores (ed* A. Winter and W.G. Siesser), pp. 107-159, Cambridge University Press, Cambridge.

Winter A. and Siesser W. G. (1994b) *Coccolithophores*. ix, 242 pp, Cambridge University Press, Cambridge.

Wintle A. G. and Huntley D. J. (1979) Thermoluminescence dating of a deep-sea sediment core. *Nature* **279**, 710-712.

Wintle A. G. (1981) Thermoluminescence dating of late Devensian loesses in southern England. *Nature* **289**, 479-480.

Wintle A. G. and Huntley D. J. (1980) Thermoluminescence dating of ocean sediments. *Canadian Journal of Earth Sciences* **17**, 348-360.

Wintle A. G. (1997) Luminescence dating: laboratory procedures and protocols. *Radiation Measurements* **27**(5-6), 769-817.

Wintle A. G. and Murray A. S. (1997) The relationship between quartz thermoluminescence, photo-transferred thermoluminescence and optically stimulated luminescence. *Radiation Measurements* **27**, 611-624.

Wintle A. G. and Murray A. S. (1998) Towards the development of a preheat procedure for OSL dating of quartz. *Radiation Measurements* **29**(1), 81-94.

Wintle A. G. and Murray A. S. (1999) Luminescence sensitivity changes in quartz. *Radiation Measurements* **30**, 107-118.

Wolanski E., Ridd P. and Inoue M. (1988) Currents through Torres Strait. *Journal of Physical Oceanography* **18**, 1535-1545.

Wolanski E. and Ridd P. (1990) Mixing and trapping in Australian tropical coastal waters. In: *Residual Currents and Long-term Transport (ed* R.T. Chang), pp. 165-183, Coastal and Estuarine Studies.

Wolanski E. (1993) Water circulation in the Gulf of Carpentaria. *Journal of Marine Systems* **4**(5), 401-420.

Wolanski E., Norro A. and King B. (1995) Water circulation in the Gulf of Papua. *Continental Shelf Research* **15**(2-3), 185-212.

Woodroffe C. D., Kennedy D. M., Hopley D., Rasmussen C. E. and Smithers S. G. (2000) Holocene reef growth in Torres Strait. *Marine Geology* **170**(3-4), 331-346.

Woodroffe C. D. and Chappell J. (1993) Holocene emergence and evolution of the McArthur River Delta, southwestern Gulf of Carpentaria, Australia. *Sedimentary Geology* **83**(3-4), 303-317.

Yan X.-H., Ho C.-R., Zheng Q. and Klemas V. (1992) Temperature and size variabilities of the Western Pacific warm pool. *Science* **258**, 1643-1645.

Yokoyama Y., Purcell A., Lambeck K. and Johnston P. (2001) Shore-line reconstruction around Australia during the Last Glacial Maximum and Late Glacial Stage. *Quaternary International* **83-85**, 9-18.

Yoshida H., Roberts R. G. and Olley J. M. (2003) Progress towards single-grain optical dating of fossil mud-wasp nests and associated rock art in northern Australia. *Quaternary Science Reviews* **22**(10-13), 1273-1278.

Young J. R. (1994) Functions of coccoliths. In: *Coccolithophores (ed* A. Winter and W.G. Siesser), pp., Cambridge University press, Cambridge.

Young J. R., Bergen J. A., Bown P. R., A Burnett J. A., Fiorentino A., W Jordan R. W., Kleijne A., van Niel B. E., Ton Romein A. J. and K. v. S. (1997) Guidelines for Coccolith and Calcareous Nannofossil Terminology. *Paleontology* **40-4**, 875-912.

Young J. R. and Bown P. R. (1997) Higher classification of calcareous nannofossils. *Journal of Nannoplankton Research: Proposals for a revised classification system for a calcareous nannoplankton* **19-1**, 15-20.

Young J. R. (2002) *Images provisionally selected for inclusion in the guide to calcareous nannopankton taxonomy.* The Natural History Museum, London. http://www.nhm.ac.uk/hosted_sites/ina/CODENET/GuideImages/index.htm

Ziveri P., Baumann K.-H., Boëckel B., Bollmann J. and Young J. R. (2004) Biogeography of selected Holocene coccoliths in the Atlantic Ocean. In: *Coccolithophores, from Molecular Processes to Global Impact (ed* H.R. Thierstein and J.R. Young), pp. 403-428, Springer, Berlin.

Appendices

Appendix 1.1: ^{14}C AMS Calibrated dates

Conventional radiocarbon ages were corrected for isotopic fractionation and rounded according to Stuiver and Polach (1977). Calibrated ^{14}C ages were calculated with CALIB 5 (based on Stuiver and Reimer, 1993) for samples younger than 26 ka (Stuiver et al., 2005).

Calibration of the marine samples (bold blue font) was performed using the Marine04.14C calibration dataset (Hughen et al., 2004) that incorporates a time-dependent global ocean reservoir correction of about 400 years, and applying a reservoir correction of 52 ± 31 that is regarded as the average for northeast Australian waters (Reimer and Reimer, 2005). The Southern-Hemisphere calibration dataset SHCal04.14C (McCormac et al., 2004), which is limited to 0-11 ka BP, was applied to young lacustrine samples (green italic). The IntCalo4.14C calibration dataset (Reimer et al., 2004) was used for all other lacustrine samples (orange) and no reservoir correction was applied. All calibrated ages were rounded according to Stuiver et al. (1998).

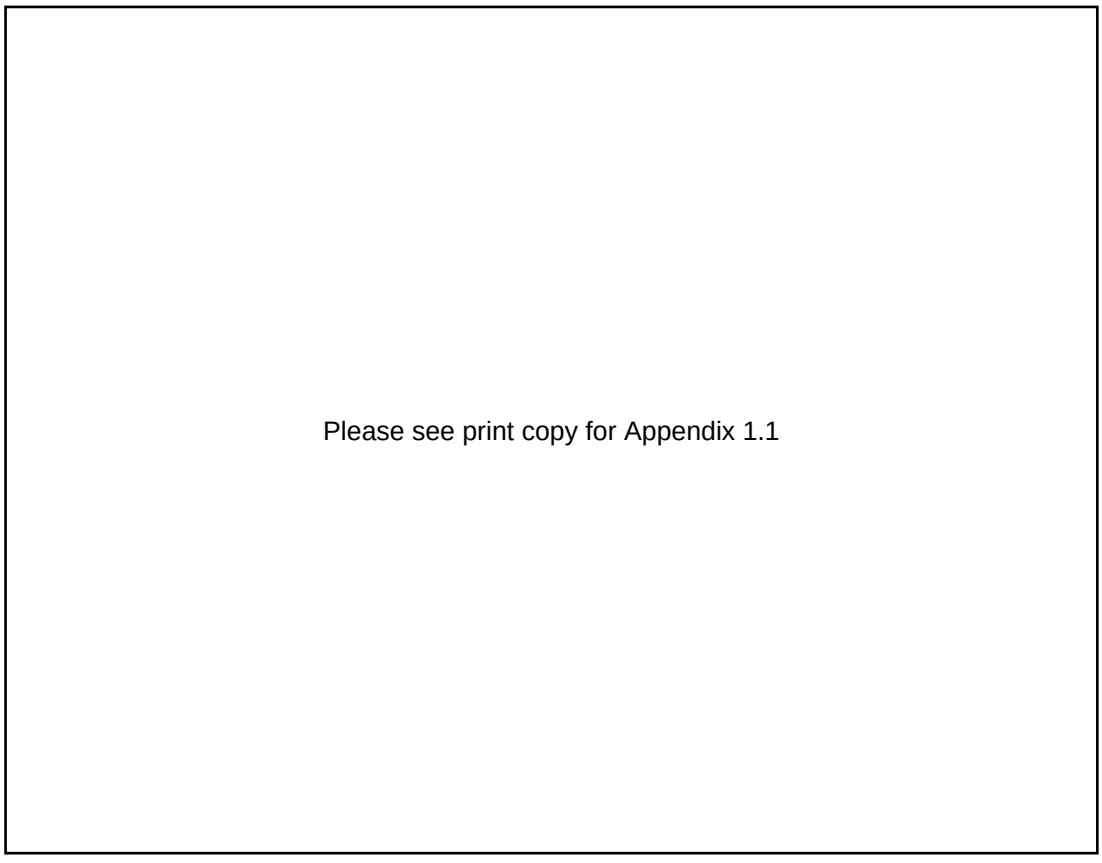

Appendix 1.2: Amino Acid Racemisation (AAR), thermoluminescence (TL), ^{14}C and Optically Stimulated Luminescence (OSL) dates

The following table presents all dates that were determined by ^{14}C (blue), AAR (pink), TL (green) and OSL (red), prior to this study on cores MD-31, MD-32 and MD-33,. All samples are labelled referring to the younger depth of the interval they were collected from in the core. Most of the dating analyses were performed on 1 cm-thick core-segments, but in core MD32 at 500 cm, 581 cm and 1238 cm depth levels the dates were performed on 2, 3 and 2 cm-thick core-segments, respectively (Chivas et al., 2001).

Core MD31

Depth (cm)	a BP	±	Method
0	7320	60	^{14}C Calibrated
0	8220	80	^{14}C Calibrated
5	3620	70	^{14}C Calibrated
10	11080	80	^{14}C Calibrated
30	1840	80	^{14}C Calibrated
55	7370	80	^{14}C Calibrated
55	1410	60	^{14}C Calibrated
60	330	50	^{14}C Calibrated
65	11290	120	^{14}C Calibrated
70	12070	100	^{14}C Calibrated
180	4110	140	^{14}C Calibrated
320	46000	2000	^{14}C Conventional
330	45800	1700	^{14}C Conventional

Core MD33

Depth (cm)	a BP	±	Method
0	1500	110	^{14}C Calibrated
0	2200	80	^{14}C Calibrated
10	790	60	^{14}C Calibrated
20	350	180	^{14}C Calibrated
20	290	50	^{14}C Calibrated
30	410	60	^{14}C Calibrated
77	18960	70	^{14}C Calibrated
77	17620	250	^{14}C Calibrated
210	40000	60	^{14}C Conventional

Core MD32

Depth (cm)	a BP	±	Method
0	10530	50	^{14}C Calibrated
10	10500	90	^{14}C Calibrated
20	1320	50	^{14}C Calibrated
35	12150	100	^{14}C Calibrated
40	13300	70	^{14}C Calibrated
70	14270	190	^{14}C Calibrated
75	17280	240	^{14}C Calibrated
100	16940	280	^{14}C Calibrated
120	17180	250	^{14}C Calibrated
145	17180	260	^{14}C Calibrated
150	18750	80	^{14}C Calibrated
500	72000	11000	AAR
581	>64300	7000	TL
1238	122000	18000	AAR
1318	108000	16000	AAR
1482	123000	16000	TL
1482	125000	120000	OSL

Appendix 2.1: MD31 data used for the OSL sample selection

(from Chivas et al., 2001)

Please see print copy for Appendix 2.1

Appendix 2.2: MD32 data used for the OSL sample selection

(from Chivas et al., 2001)

Please see print copy for Appendix 2.2

Appendix 2.3: MD33 data used for the OSL sample selection

(from Chivas et al., 2001)

Please see print copy for Appendix 2.3

Appendix 3

Please see print copy for Appendix 3

Appendix 4:

Please see print copy for Appendix 4

Appendix 5.1: Impact of incorrect water content on the D_R estimation

Three samples from the Gulf of Carpentaria MD31-30, MD32-629 and MD33-629 representing the maximum (71.6%), average (40.3%) and minimum (14%) modern water content found in the sediment levels chosen for OSL dating, were selected to determine the impact of an uncorrected estimation of the water content on the D_R estimation, For these samples, the water correction factors (WCF) for cosmic, β and γ doses are calculated for ten different water contents ranging from 150% to 50% of the modern water content (MWC). The deviation of these former WCF from the modern WCF is presented for each of the 3 samples as a function of the water content used for the calculation in percent of the MWC, in Table 1:

Table 1: Percent of variation in the WCF compared to the modern WCF. The water content is given in percent of the MWC that is 71.6%, 40.3% and 14% for MD31-30, MD32-629 and MD33-629, respectively.

Water	**150%**	**140%**	**130%**	**120%**	**110%**	**90%**	**80%**	**70%**	**60%**	**50%**
Sample	WCF deviation from modern WCF									
Moisture correction factor for cosmic dose										
MD31-30	-19%	-15%	-12%	-8%	-4%	5%	10%	16%	22%	30%
MD32-629	-14%	-11%	-9%	-6%	-3%	3%	7%	11%	15%	19%
MD33-629	-7%	-5%	-4%	-3%	-1%	1%	3%	4%	6%	8%
Moisture correction factor for β dose										
MD31-30	-18%	-15%	-12%	-8%	-4%	5%	10%	16%	22%	29%
MD32-629	-14%	-11%	-9%	-6%	-3%	3%	7%	10%	14%	19%
MD33-629	-6%	-5%	-4%	-3%	-1%	1%	3%	4%	6%	7%
Moisture correction factor for γ dose										
MD31-30	-19%	-16%	-12%	-9%	-5%	5%	10%	17%	23%	31%
MD32-629	-14%	-12%	-9%	-6%	-3%	3%	7%	11%	15%	20%
MD33-629	-7%	-6%	-4%	-3%	-1%	2%	3%	5%	6%	8%

The error on the WCF increases with increasing change in water content from the MWC and with the increasing value of this latter. The error on the WCF varies with the absolute water content of the sediment. This error increases more for each 10% increment from the MWC

when this latter is high. The WCF are used at the end of the D_R estimation to convert the dry D_{Rc}, $D_{R\beta}$ and $D_{R\gamma}$ in wet rate. Thus these coefficients are critical, the age being directly affected by their values. Table 1 shows that a 50% overestimation of the water content can produce an underestimation on the D_R of at least 7%, 19% and 29%, for a MWC of 71.6%, 40.3% and 14%, respectively. Whereas a 50% underestimation of the water content result in a 6%, 14% and 18% overestimation on the D_R for a MWC of 71.6%, 40.3% and 14%, accordingly.

In the case of marine/lacustrine sediment core, it could be assumed that the MWC corresponds to the saturation level of the sediment. Thus the error could only be an overestimation of the water content at the time of deposition. An overestimation of the water content will produce an underestimation of the D_R and thus an overestimation of the age of the sediment. The variation of D_R values for each of the 3 samples as a function of the water content (in percent of the MWC) used for the calculation is given in Table 2, together with their consequent ages.

Table 2: The D_R (blue, in $Gy.ka^{-1}$) and age (orange, in ka) variation as a function of the overestimation of the water content. The water content is given in percent of the MWC that is 71.6%, 40.3% and 14% for MD31-30, MD32-629 and MD33-629, respectively.

Water	**100% MWC**		90% MWC		80% MWC		70% MWC		60% MWC		50% MWC	
($Gy.ka^{-1}$)	D_R	*se*	D_R	*se*	D_R	*se*	D_R	*se*	D_R	*se*	D_R	*se*
MD31-30	**0.660**	**0.091**	0.690	0.091	0.723	0.091	0.761	0.091	0.801	0.091	0.848	0.091
MD32-629	**1.548**	**0.078**	1.599	0.079	1.653	0.080	1.712	0.081	1.775	0.082	1.842	0.083
MD33-629	**0.957**	**0.066**	0.957	0.065	0.984	0.065	0.999	0.065	1.013	0.065	1.028	0.065
(ka)	Age	*se*	Age	*se*	Age	*se*	Age	*se*	Age	*se*	Age	*se*
MD31-30	**6.7**	**1.0**	6.4	0.9	6.1	0.8	5.8	0.8	5.5	0.7	5.2	0.6
MD32-629	**140.6**	**8.7**	136.1	8.3	131.7	7.9	127.1	7.5	122.7	7.1	118.2	6.7
MD33-629	**156.9**	**17.9**	156.9	17.8	152.6	17.2	150.4	16.8	148.2	16.5	146.0	16.2

Table 2 shows that for a 50% overestimation of the water content, the age variations for MD31-30, MD32-629 and MD33-629 are 1.5, 22.4 and 10.9 ka, respectively. Thus the

overestimation of the age for the sample with an average content of water (MD32-629, 40.3%) is the largest. This was expected because:

-high water content usually corresponds to young samples and even if the age variation is a high proportion of the overestimated age, it is small, in absolute terms.

-low water content usually corresponds to drier samples. They could be old, but as the age variation is a low proportion of the overestimated age, the variation also remains small, in absolute terms.

To conclude, it is clear that the water content history of samples dated by OSL technique is essential to obtain an accurate age. For a water content of 40 wt % of dry sediment, the under-/over-estimation of the age of the sample could be as high as 14 or 19 percent, respectively.

Appendix 5.2: Density of the overlying sediment for each OSL sample

Density values were compiled from the geophysical data collected by the Multi-Sensor-Core-Logger onboard the *Marion Dufresne*. The density of the entire sediment column above the sample level is used to calculate the depth density (Chapter 3, Section 3.9.5) overlying the sample. These densities correspond to the average of the density estimated for each centimetre of sediment above the sample.

	Density ($g.cm^{-3}$)	
	at the sample level	of the sediment column above this level
MD31-30	1.40	1.33
MD31-120	1.68	1.46
MD31-530	1.66	1.63
MD31-902	1.52	1.61
MD31-1040	1.53	1.60
MD31-1340	1.61	1.59
MD32-38	1.33	1.32
MD32-629	1.66	1.51
MD32-921	1.53	1.54
MD32-1397	1.92	1.57
MD33-220	1.62	1.53
MD33-360	1.64	1.56
MD33-629	1.99	1.63

Appendix 6.1: Protocols for α-spectrometric analysis of Uranium and Thorium

Both of the following charts were modified from ANSTO, Environment Division Protocols. The pre-treatment step (grey) was not processed on the samples from the Gulf of Carpentaria. For each analysis, a tracer was added prior to dissolution, ^{236}U and ^{229}Th for the uranium and thorium analysis, respectively.

(a) Uranium analysis flow chart

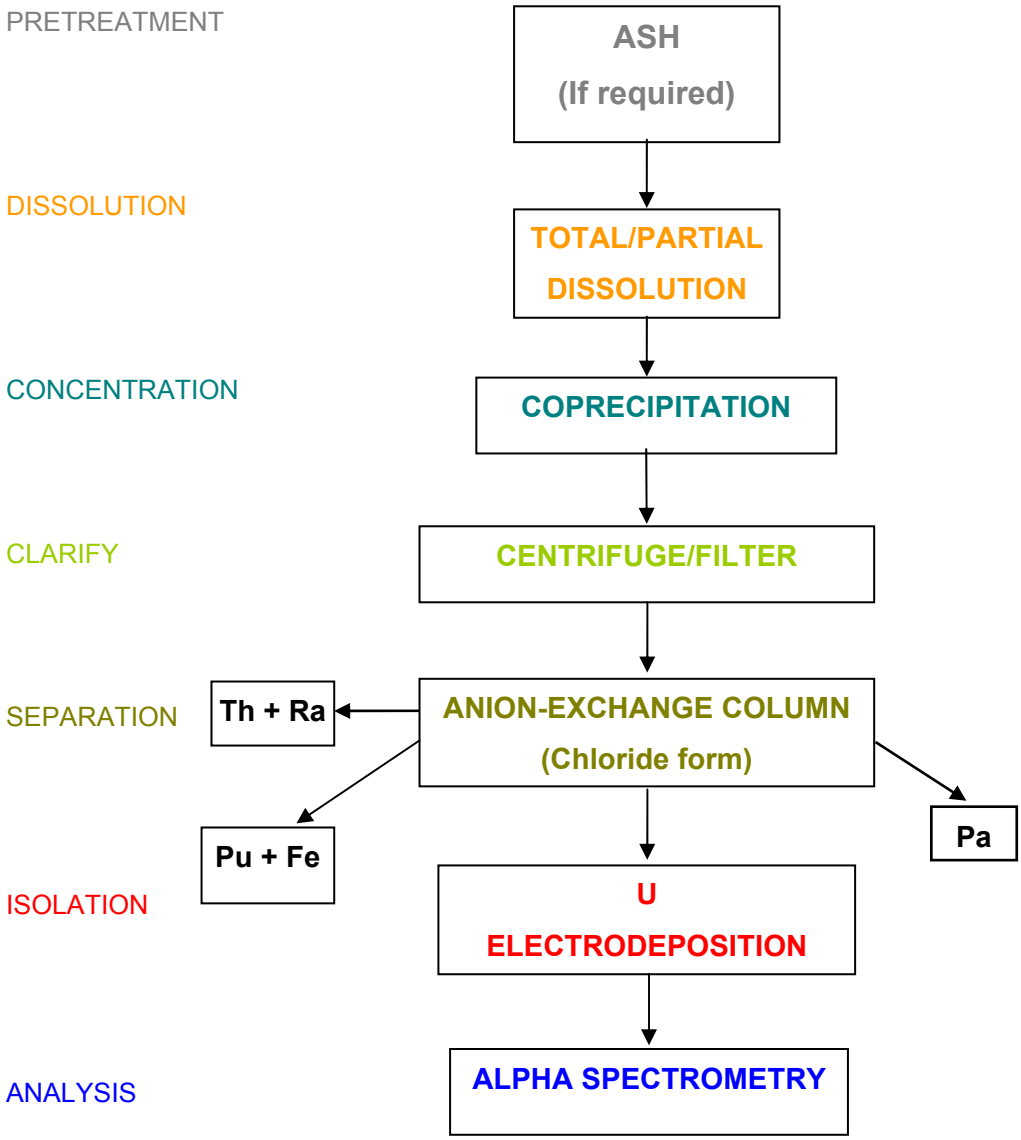

(b) Thorium analysis flow chart

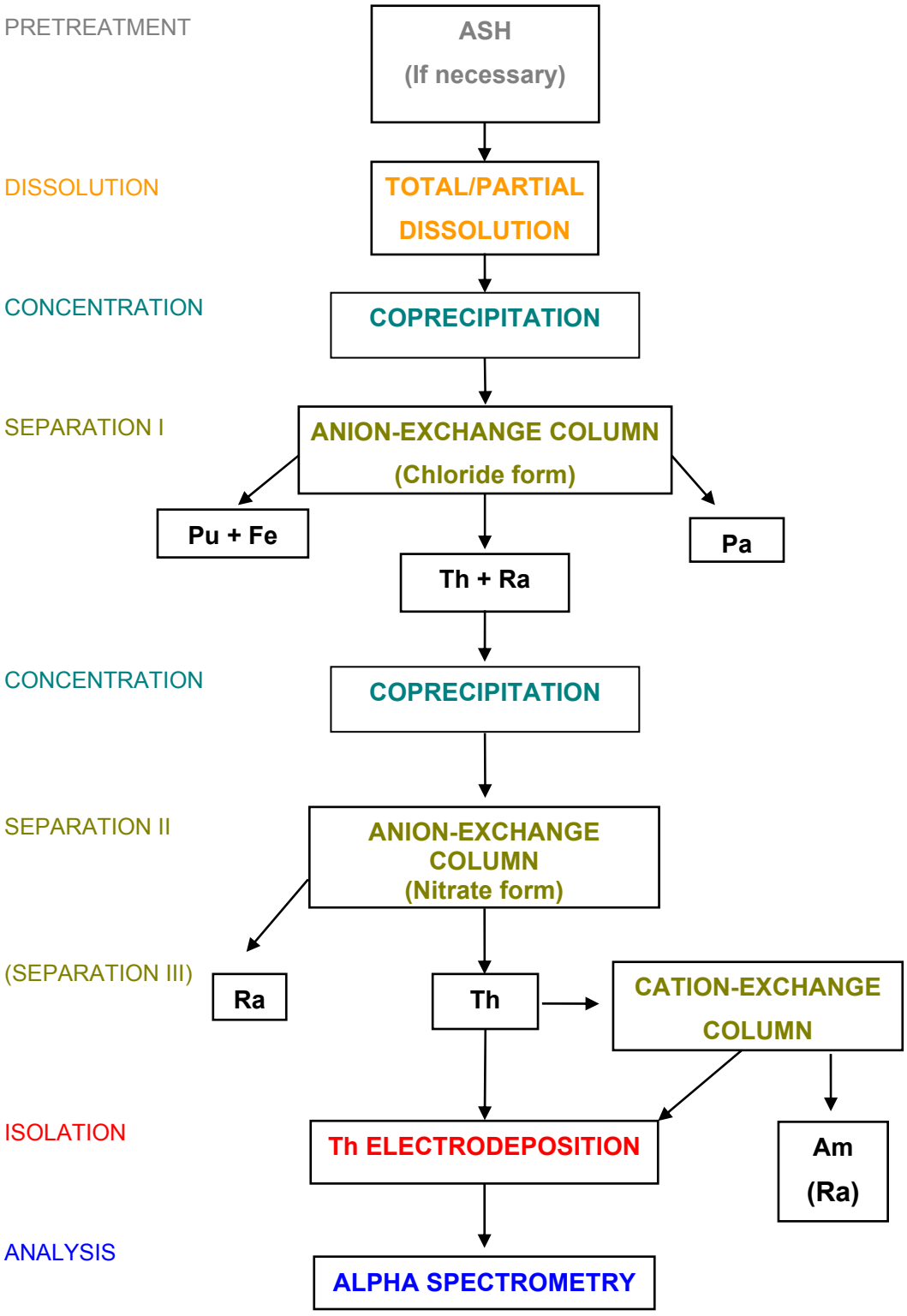

Appendix 6.2: Results of α-spectrometry analysis for several elements of the ^{238}U (a) and ^{232}Th (b) decay chains

(a)

		^{238}U chain							
Sample	ANSTO ID	U-238 Bq.kg^{-1}	error Bq.kg^{-1}	U-234 Bq.kg^{-1}	error Bq.kg^{-1}	Th-230 Bq.kg^{-1}	error Bq.kg^{-1}	**U-234 / U-238**	**Th-230 / U-234**
MD31-30	C926	18.2	0.6	20.8	0.7	17.1	0.7	**1.14±0.05**	**0.82±0.04**
MD31-120	C927	15.7	0.5	18.4	0.6	28.0	1.5	**1.17±0.05**	**1.52±0.10**
MD31-530	C928	16.1	0.6	18.5	0.7	26.2	2.1	**1.15±0.06**	**1.42±0.13**
MD31-530	C928(2)	18.7	0.6	22.0	0.7			**1.18±0.05**	**1.19±0.10**
MD31-530	C928(3)	17.8	1.1	22.6	1.3			**1.27±0.11**	**1.16±0.11**
MD31-902	C929	23.7	1.1	28.0	1.3	23.4	1.9	**1.18±0.08**	**0.84±0.08**
MD31-1040	C930	12.8	0.6	16.2	0.7	17.9	0.9	**1.27±0.08**	**1.10±0.07**
MD31-1040	C930(2)	14.0	1.0	16.3	1.1			**1.16±0.11**	**1.10±0.09**
MD32-38	C456	21.8	0.7	26.9	0.8	20.7	1.8	**1.23±0.05**	**0.77±0.07**
MD32-38	C456(2)	21.1	1.0	24.2	1.1	17.4	1.2	**1.15±0.08**	**0.72±0.06**
MD32-629	C457	23.7	0.9	27.7	1.0	23.5	2.8	**1.17±0.06**	**0.85±0.11**
MD32-629	C457(rep)					28.2	1.3		**1.02±0.06**
MD32-921	C458	93.6	2.4	101.5	2.6	92.5	4.4	**1.08±0.04**	**0.91±0.05**
MD32-1397	C925	17.9	0.6	19.8	0.6	20.9	0.7	**1.11±0.05**	**1.06±0.05**
MD33-220	C459	13.9	0.5	15.5	0.5	31.3	1.3	**1.12±0.05**	**2.02±0.11**
MD33-360	C460	21.2	0.6	22.2	0.6	17.2	1.2	**1.05±0.04**	**0.77±0.06**
MD33-629	C461	16.0	0.5	16.3	0.5	18.4	0.7	**1.02±0.04**	**1.13±0.06**

(b)

		^{232}Th chain				
Sample	ANSTO ID	Th-232 Bq.kg^{-1}	*error* Bq.kg^{-1}	Th-228 Bq.kg^{-1}	*error* Bq.kg^{-1}	**Th-228 / Th-232**
MD31-30	C926	16.5	0.7	17.1	0.7	**1.04±0.06**
MD31-120	C927	27.1	1.4	27.3	1.5	**1.01±0.08**
MD31-530	C928	23.6	1.9	30.7	2.3	**1.30±0.14**
MD31-902	C929	21.3	1.8	29.7	2.4	**1.39±0.16**
MD31-1040	C930	23.8	1.0	27.3	1.2	**1.15±0.07**
MD32-38	C456	21.3	1.8	17.9	1.6	**0.84±0.10**
MD32-38	C456(2)	21.0	1.3	21.4	1.4	**1.02±0.09**
MD32-629	C457	26.1	3.0	29.5	3.4	**1.13±0.18**
MD32-629	C457(rep)	31.1	1.4	40.7	1.8	**1.31±0.08**
MD32-921	C458	21.3	1.3	30.8	1.8	**1.45±0.12**
MD32-1397	C925	16.4	0.6	16.2	0.6	**0.99±0.05**
MD33-220	C459	27.0	1.1	32.5	1.3	**1.20±0.07**
MD33-360	C460	21.2	1.4	26.2	1.7	**1.24±0.11**
MD33-629	C461	8.6	0.4	9.5	0.5	**1.11±0.08**

Results from the ANSTO □-spectrometry analyses with their discrepancy from equilibrium (relative to the closest measured parent) shown in bold print. The shading of this latter indicates the level of discrepancy; white if smaller than 20%; light blue if between 20% and 50% and dark blue for larger than 50%.

Appendix 6.3: Characteristics of the γ-ray spectrometer

A Compton suppression gamma-ray spectrometer, comprising an N-type high-purity germanium detector (HPGe) surrounded by a 75 mm-thick sodium iodide annulus and 75x75 mm sodium iodide "plug" was utilised in this study. The general arrangement is illustrated (not to scale).

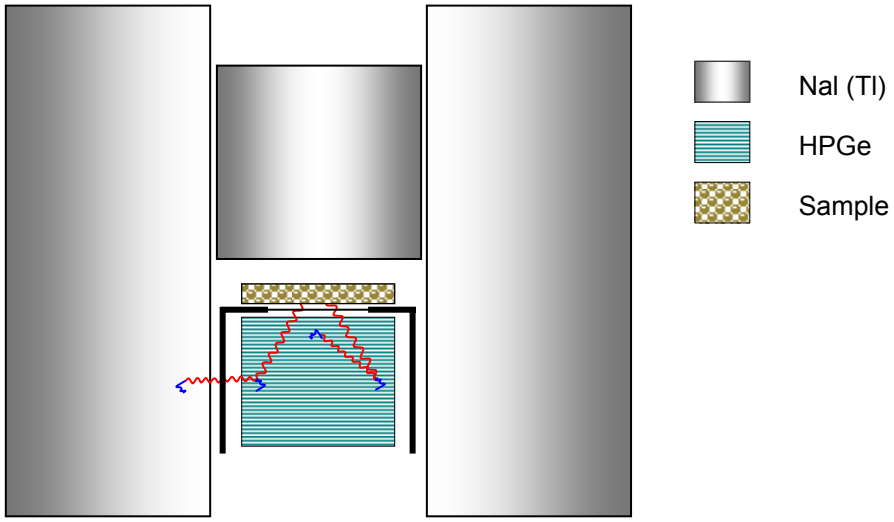

HPGe detector Specification

Manufacturer:	Canberra Industries
Geometry:	Reverse electrode closed-end coaxial
Diameter:	60.8 mm
Length:	63.5 mm
End cap to crystal:	5 mm
End cap window :	Carbon composite
Resolution:	2.03 keV @ 1332 keV
	1.09 keV @ 122 keV
Relative efficiency:	50.1%

Self-absorption correction

Self-absorption corrections were calculated by measuring the transmission of a point ^{226}Ra source through each sample (Cutshall et al., 1983).

Appendix 6.4: Results of γ-spectrometry analysis for several elements of the ^{238}U (a) and ^{232}Th (b) decay chains

(a)

		^{238}U chain							
		^{238}U	error	^{226}Ra	error	^{210}Pb	error	$\frac{^{226}Ra}{^{238}U}$	$\frac{^{210}Pb}{^{226}Ra}$
Sample	ANSTO ID	Bq.kg^{-1}	Bq.kg^{-1}	Bq.kg^{-1}	Bq.kg^{-1}	Bq.kg^{-1}	Bq.kg^{-1}		
MD31-30	C926	73.7	10.1	19.7	2.0	18.6	8.6	**0.27±0.05**	**0.94±0.45**
MD31-120	C927	53.0	14.1	33.6	0.7	26.0	4.9	**0.63±0.17**	**0.78±0.15**
MD31-530	C928	63.9	5.4	34.1	0.6	32.7	4.6	**0.53±0.05**	**0.96±0.14**
MD31-902	C929	49.1	9.3	36.8	1.0	33.2	8.2	**0.75±0.14**	**0.90±0.22**
MD31-1040	C930	45.8	6.9	30.7	1.2	32.8	5.9	**0.67±0.10**	**1.07±0.20**
MD32-38	C456	45.9	15.2	24.2	2.2	19.6	11.9	**0.53±0.18**	**0.81±0.50**
MD32-629	C457	55.3	12.3	36.6	0.8	36.5	5.3	**0.66±0.15**	**1.00±0.15**
MD32-921	C458	111.8	25.2	103.4	1.6	93.9	8.8	**0.93±0.21**	**0.91±0.09**
MD32-1397	C925	46.0	15.1	34.9	1.0	26.9	6.5	**0.76±0.25**	**0.77±0.19**
MD33-220	C459	39.8	24.5	28.8	1.4	26.7	8.5	**0.72±0.45**	**0.93±0.30**
MD33-360	C460	51.1	10.8	36.9	1.5	19.6	8.5	**0.72±0.16**	**0.53±0.23**
MD33-629	C461	23.6	6.0	26.3	0.7	25.4	3.7	**1.11±0.28**	**0.97±0.14**

(b)

		^{232}Th chain				
		^{228}Th	error	^{228}Ra	error	$\frac{^{228}Ra}{^{228}Th}$
Sample	ANSTO ID	Bq.kg^{-1}	Bq.kg^{-1}	Bq.kg^{-1}	Bq.kg^{-1}	
MD31-30	C926	15.3	6.0	36.5	3.9	**2.39±0.97**
MD31-120	C927	43.1	2.6	46.6	2.1	**1.08±0.08**
MD31-530	C928	44.2	3.2	47.8	2.0	**1.08±0.09**
MD31-902	C929	53.4	3.8	60.6	3.1	**1.14±0.09**
MD31-1040	C930	43.8	2.8	48.3	2.3	**1.10±0.09**
MD32-38	C456	20.6	10.4	37.8	6.5	**1.84±0.98**
MD32-629	C457	56.3	3.6	54.7	2.4	**0.97±0.08**
MD32-921	C458	47.1	5.0	47.5	3.4	**1.01±0.13**
MD32-1397	C925	35.2	3.0	37.6	2.5	**1.07±0.12**
MD33-220	C459	46.9	5.7	48.4	4.0	**1.03±0.15**
MD33-360	C460	38.6	6.3	44.5	4.2	**1.15±0.22**
MD33-629	C461	13.6	2.6	18.9	1.6	**1.39±0.29**

Results from the ANSTO □-spectrometry analyses with their discrepancy from equilibrium (relative to the closest measured parent) shown in bold print. The shading of this latter indicates the level of discrepancy; white if smaller than 20%; light blue if between 20% and 50% and dark blue for larger than 50%.

Appendix 6.5: Comparison between α-spectrometry leaching versus total-digestion analyses results for (a) uranium and (b) thorium isotopes

(a)	Leach (L)		Total (T)		T-L/ T	Leach (L)		Total (T)		T-L/ T
	^{238}U	error	^{238}U	error		^{234}U	error	^{234}U	error	
MD32-629	23.7	0.9	30.5	1.3	**22±5%**	27.7	1	32.8	1.3	**16±5%**
MD33-360	21.2	0.6	38.1	1.2	**44±4%**	22.2	0.6	37.3	1.2	**40±4%**
MD33-629(1)	16	0.5	23.6	0.8	**32±4%**	16.3	0.5	22.8	0.8	**29±4%**
MD33-629(2)			24.1	0.7	**34±4%**			24.4	0.7	**33±4%**
Certified (C)	64.7		64.7			69		69		
Measured (M)	52.6	4.7	58.2	2.7	**10±9%**	51.3	4.6	63.7	2.9	**19±9%**
C-M/M	19%		10%			26%		8%		
Blank			0.4	0.1				4	0.4	

(b)	Leach (L)		Total (T)		T-L/T	Leach (L)		Total (T)		T-L/T	Leach (L)		Total (T)		T-L/T
	^{228}Th	error	^{228}Th	error		^{230}Th	error	^{230}Th	error		^{232}Th	error	^{232}Th	error	
MD32-629	29.5	3.4	53.8	2.5	**45±8%**	23.5	2.8	42.9	2.1	**45±8%**	26.1	3	56.3	2.5	**54±7%**
MD33-360	26.2	1.7	38.8	1.5	**32±6%**	17.2	1.2	44.9	1.6	**62±5%**	21.2	1.4	40.5	1.5	**48±5%**
MD33-629	9.5	0.5	18.5	0.8	**49±5%**	18.4	0.7	32.8	1.3	**44±5%**	8.6	0.4	17.9	0.8	**52±6%**
Certified (C)	64		64			88		88			72.4		72.4		
Measured (M)	65.1	6.1	71.9	4	**9±10%**	79.6	7.3	122.7	5.6	**35±8%**	57.5	5.5	81.1	4.2	**29±9%**
C-M/M	-2%		-12%			10%		-39%			21%		-12%		
Blank			4	0.9				2	0.7				0.2	0.2	

Results (Bq.kg^{-1}) from the ANSTO □-spectrometry analyses after both leaching and total dissolution with their relative discrepancy from equilibrium shown in bold print. The light blue shading fields correspond to Certified samples that were processed in the same batch as the Gulf of Carpentaria samples. The dark blue shading fields correspond to the error (in percent) on the Certified values estimation.

Appendix 6.6: Leaching α–spectrometry analysis results versus γ-spectrometry analysis results

Sample	α-spectrometry U-238 Bq.kg^{-1}	error Bq.kg^{-1}	γ-spectrometry U-238 Bq.kg^{-1}	error Bq.kg^{-1}	**α leach-γ** γ	α-spectrometry Th-228 Bq.kg^{-1}	error Bq.kg^{-1}	γ-spectrometry Th-228 Bq.kg^{-1}	error Bq.kg^{-1}	**α leach-γ** γ
MD31-30	18.2	0.6	73.7	10.1	**-75±17%**	17.1	0.7	15.3	6.0	**12±39%**
MD31-120	15.7	0.5	53.0	14.1	**-70±32%**	27.3	1.5	43.1	2.6	**-37±7%**
MD31-530	16.1	0.6	63.9	5.4	**-75±11%**	30.7	2.3	44.2	3.2	**-31±9%**
MD31-530	18.7	0.6			**-71±10%**					
MD31-530	17.8	1.1			**-72±10%**					
MD31-902	23.7	1.1	49.1	9.3	**-52±21%**	29.7	2.4	53.4	3.8	**-44±9%**
MD31-1040	12.8	0.6	45.8	6.9	**-72±19%**	27.3	1.2	43.8	2.8	**-38±7%**
MD31-1040	14.0	1.0			**-69±19%**					
MD32-38	21.8	0.7	45.9	15.2	**-53±37%**	17.9	1.6	20.6	10.4	**-13±51%**
MD32-38	21.1	1.0			**-54±38%**	21.4	1.4			**4±51%**
MD32-629	23.7	0.9	55.3	12.3	**-57±26%**	29.5	3.4	56.3	3.6	**-48±9%**
MD32-629						40.7	1.8			**-28±7%**
MD32-921	93.6	2.4	111.8	25.2	**-16±23%**	30.8	1.8	47.1	5.0	**-35±12%**
MD32-1397	17.9	0.6	46.0	15.1	**-61±38%**	16.2	0.6	35.2	3.0	**-54±10%**
MD33-220	13.9	0.5	39.8	24.5	**-65±73%**	32.5	1.3	46.9	5.7	**-31±13%**
MD33-360	21.2	0.6	51.1	10.8	**-59±24%**	26.2	1.7	38.6	6.3	**-32±18%**
MD33-629	16.0	0.5	23.6	6.0	**-32±27%**	9.5	0.5	13.6	2.6	**-30±20%**

The discrepancy between □- and □-spectrometry analyses results is shown in bold print. The shading indicates the level of discrepancy: white if less than 20%; light blue if between 20% and 50% and dark blue for greater than 50%.

Appendix 7.1: Sedimentary log of core MD28

(from Reeves, 2004)

Please see print copy for Appendix 7.1

Appendix 7.2: Sedimentary log of core MD29

(from Reeves, 2004)

Please see print copy for Appendix 7.2

Appendix 7.3: Sedimentary log of core MD30

(from Reeves, 2004)

Please see print copy for Appendix 7.3

Appendix 7.4: Sedimentary log of core MD31

(from Reeves, 2004)

Please see print copy for Appendix 7.4

Appendix 7.5: Sedimentary log of core MD32

(from Reeves, 2004)

Please see print copy for Appendix 7.5

Appendix 7.6: Sedimentary log of core MD33

(from Reeves, 2004)

Please see print copy for Appendix 7.6

Appendix 8: Taxonomic list of coccoliths found in core MD32 from the Gulf of Carpentaria

All species recognised in the gulf are heterococcoliths, which Braarud et al. (1955) have defined as built up of distinct crystal units of variable shape and size (Jordan et al., 1995). The following taxonomy list is based on the recent review of the phylogeny of the Haptophyta in the light of DNA analyses (Sáez and al., 2004). All the species investigated by Sáez et al. are underlined. The other species were classified according to more classic morphological variation by extrapolation of previous taxonomy (Jordan and Green, 1994; Jordan and Kleijne, 1994; Jordan et al., 1995, 2000; Young and Bown, 1997; Young et al., 1997; Edvardsen et al., 2000; Kleijne, 2001; Bilard and Inouye, 2004).

Kingdom: Protista, Haeckel, 1866

Division: Haptophyta, Hibbert, 1976

Class: Prymnesiophyceae, Hibbert, 1976

Cells have a smooth flagella (i.e. no hairs) and may possess a fully developed or reduced haptonema. Cells covered with organic and/or calcite scales.

Order: Isochrysidales, Pasher, 1910 ex Edvardsen and Eikrem(1996)

Family: Noëlaerhabdaceae, Jerkovic, 1970

Cell covered by overlapping placoliths. Placolith has no taxonomic inference, but is used to describe a shirt-stud-shaped or double-shielded heterococcolith (Lohman, 1902). Placoliths are characterized by a reticulum or grill covering the proximal part of the central area opening.

Genus: *Emiliana*, Hay and Mohler, 1967

Coccoliths with "I" or "T" elements in distal shield.

E. huxleyi, (Lohman, 1902) Hay and Mohler, 1967

T-shaped elements in both shields

E. corona, (Okada and McIntyre, 1977) Jordan and Young 1990

Genus: *Gephyrocapsa*, Kamptner, 1943

G. oceanica, Kamptner, 1943

G. ericsonii, McIntyre and Bé, 1967

Family: Coccolithaceae, Poche, 1913

Cell covered by overlapping placoliths. Each placolith consists of two shields of sub-horizontal elements and a connecting tube.

Genus: *Coccolithus,* Schwarz, 1894

C. pelagicus, (Wallich, 1877) Schiller, 1930

Family: Calcidiscaceae, Young and Bown

Genus: *Oolithitus,* Reinhart, in Cohen and Reinhart, 1968

O. fragilis, (Lohman, 1912) Martini and Müller, 1972

Genus: *Calcidiscus,* Kamptner, 1950

C. leptoporus, Loeblich and Tappan, 1978

Genus: *Umbilicosphaera,* Lohman, 1902

U. sibogae, (Weber-Van Bosse, 1901) Gaarder, 1970

U. foliosa, (Kamptner, 1963) Okada and McIntyre, 1977

U. hulburtiana, Gaarder, 1970

U. anulus, Lecal, 1967

Family: Reticulosphaeraceae, Cavalier-Smith, 1996

A heterococcolith with two sub-horizontal shields connected by a central tube (= placolith) and possessing a reticulum or grill, which is formed at the base of the tube and covers the central area (Jordan et al., 1995).

Genus: *Reticulosphaera,* Grell, 1990

R. parvula, Okada and McIntyre, 1989

R. sessilis, Lohman, 1912

R. minutula, (Gartner, 1967) Haq and Berggren 1978

Family: Rhabdosphaeraceae, Haeckel, 1866

A heterococcolith which consists of a bi-cyclic sub-horizontal rim and a central area with one to three concentric cycles of elements. The central area may bear a distal protrusion process (Schmidt, 1870; Kleijne, 1992).

Genus: *Rhabdosphaera*, Lohman, 1902

R. clavigera, Murray and Blackman, 1898

Family: Helicosphaeraceae, Black, 1971, emend. Jafar and Martini, 1975

An elliptical heterococcolith composed of an outer cycle of elements (the flange) arranged around a filled central tube. The central area may be closed or perforated by two pore

slits. with a lamella which partially spans the short axis of the central area. The portion of the flange that becomes separated from the proximal part is referred to as the wing. This is best seen in proximal views of the coccoliths of Helicosphaera (Jafar and Martini, 1975).

Genus: *Helicosphaera*, Kamptner, 1954

H. carterii, (Wallich, 1877) *Kamptner, 1954*

H. hyalina, (Gaarder, 1970) Jordan and Young, 1990

H. wallichii, Theodoridis, 1984

H. pavimentum, (Okada and McIntyre, 1977)

Family: Pontosphaeraceae, Lemmermann, 1908

Cell completely or mostly covered by discoliths. Discoliths are elliptical heterococcoliths perforated by roundish pores (Huxley, 1868). Rim may be present as a low thick or high thin wall. Lopadoliths, if present, are situated equatorially and are vase-shaped. Each is a hollow structure with ornamentations on the wall and perforations on the proximal surface.

Genus: *Pontosphaera*, Lohman 1902

Pontosphaera discorpa (Schiller, 1925)

Family: Syracosphaeraceae Lemmermann, 1908

Cell completely or mostly covered by caneoliths. Irrespective of shape, the two coccolith types have a distal arrangement of wall elements, each joined at their bases by lamellae (lamellae are absent in one genus). In trough-shaped coccoliths and rhombolith-like caneoliths, these lamellae are arranged across the short axis of the coccolith, whereas in most caneoliths they are radial. Only in caneoliths do the lamellae converge in the central area to form an overlapping random arrangement of elements or an organised central structure. This central structure may or may not produce a distally protruding central spine.

Genus: *Syracosphaera,* Lohman, 1902

S. pulchra, Lohman, 1902

S. lamina, Lecal-Schlasuder, 1951

S. ossa, (Lecal, 1966) Loeblich and Tappan, 1968

S. nana, (Kamptner, 1941) Okada and McIntyre, 1977

Order: incertae sedis

Family: Braarudosphaeraceae, Deflandres 1947, 1952

Cells covered by twelve pentaliths to form a regular dodecahedron. The pentalith is generally constructed of five crystals, each radiating from a central point. The lack of test perforations may suggest that the coccosphere is really a resting stage or cyst (Tappan, 1980).

Genus: *Braarudosphaera*, Deflandres, 1947

B. bigelowii, (Gran and Braarud, 1935) Deflandres 1947

Family: Calcioseleniaceae, Kampter 1937

Spindle-shaped cell covered by scapholiths. Placoliths (rhombolith). Scapholiths are diamond-shaped and composed of upright wall elements. Each wall element is associated.

Genus: *Calsisolenia*, Gran, 1912

C. murrayi, Gran 1912

Family: Ceratolithaceae, Norris, 1965

A horseshoe shape coccolith, which may extend past the protoplast. It is composed of two arms of unequal length, with each arm possessing a rodded and smooth keel on its upper and lower portion, respectively (Tappan, 1980).

Genus: *Ceratolithus*, Kamptner 1950

C. cristatus, Kamptner 1950

Appendix 9: Coccolith counting sheets of MD32, weighted value

1 = 1; 2 = 2 to 10; 3 = 11 to 50; 4 = 51 to 100, 5 = 101 to 500 and 6 = over 500 individuals

Depth in core (cm)	*Emiliania huxleyi*	*Gephyrocapsa omega*	*Gephyrocapsa ericsonii*	*Gephyrocapsa oceanica*	*Gephyrocapsa (small)*	*Reticulofenestra parvula*	*Syracosphaera pulchra*	*Reticulofenestra sessilis*	*Helicosphaera carterii*	*Gephyrocapsa (large)*	*Umbilicosphaera hulburtiana*	*Umbilicosphaera sibogae*	*Umbilicosphaera foliosa*	*Syracosphaera nana*	*Pseudoemiliania lacunosa*	*Syracosphaera lamina*	*Helicosphaera hyalina*	*Syracosphaera anthos*	*Discosphaera tubifera*	*Calcidiscus leptoporus*	*Reticulosphaera minuta*	*Rhabdosphaera clavigera*	*Calciosolenia murrayi*	*Anoplosolenia brasiliensis*	*Ophiolithotus fragilis*	*Braarudosphaera bigelowii*	*Helicosphaera wallichi*	*Ceratolithus cristatus*	*Florisphaera profunda*	*Umbilicosphaera anulus*	*Helicosphaera sp.*	*Emiliania corona*	*Umbellosphaera tenuis*	*Pontosphaera discopora*
0	5	4	3	6	5	5	3	3	2	3	2	2	3	1	2	3	2	2	2	2	2	2	2	2				1	1				1	2
10	5	5	3	6	5	5	3	2	3	3	2	2	3	2	2	3	3	3	2	2	2	2	3		1	1	1		1	1			1	2
20	5	4	3	6	4	5	3	3	2	3		3	3	2	3	3	2	3	3	1	2	3	2				1		1				1	3
30	4	3	3	4	4	3	2	3	1	2	2	2	2		2	3		2		1		1						1					
40																																		
50				2															?															
60																																		
70																																		
80	?										?																		?					
90																																		
100																																		
110																																		
120									?																									
130	1																																	
140																																		
150	1							1																						?				
160	1	1																																
170	1	1			1						?																							
180		1			1			1						?																				
190																																		
200	2	2		2	?																													
210	1	1																																
220	2	2			1																													
230	1	1																																
240	2	1			1																													
250	1									1																								
260	1				?																									?				
270		2																																
280		1																																
290		2					?																							?				
300		1			1																												?	
310	1	1		1				1																										
320	1	1		1																														
330		1			1			1																										
340	1	1					?																											
350		1																																
360	1	1	?																															
370	1	2																																
380		1																																
390	1	1																																
400																																		
410	1	1		1			?																											
420	1				1			1																										
430	1							1																										
440	1																																	
450	1	1	1	1	1																													
460	1	1					?																											
470	1																																	
480																																		
490																																		
500																																		
510																																		
520																																		
530																																		
540																																		
550																																		
560																																		
570																																		
580																																		
590				1																														
600																																		
610				1																														
620	2	3	3	3	2		1		1												2												1	2
630	2	2	1	2	2		1		1																									
640	1	1							1																									
650	1	2		1	2				1			1								?	1									1			1	
660	2	2		2	2				2	2	2	2									2													
670	3	2	3	3	1		1		2	2		3									1									1			2	1
680	3	2		1	1	2	?		1	3	?	3																					2	
690	3	3	2	2	2	2	1		2	1	2	2																		1			2	1
700	3	3	2	2	3		1		2	3	1	2																						
710	2	2	2	1	2	2	2		2	2		1					1			1	1											1	2	

Depth in core (cm)	*Emiliania huxleyi*	*Gephyrocapsa ornega*	*Gephyrocapsa ericsonii*	*Gephyrocapsa oceanica*	*Gephyrocapsa (small)*	*Reticulofenestra parvula*	*Syracosphaera pulchra*	*Reticulofenestra sessilis*	*Helicosphaera carteri*	*Gephyrocapsa (large)*	*Umbilicosphaera hulburtiana*	*Umbilicosphaera sibogae*	*Umbilicosphaera foliosa*	*Syracosphaera nana*	*Pseudoemiliania lacunosa*	*Syracosphaera lamina*	*Helicosphaera hyalina*	*Syracosphaera anthos*	*Discosphaera tubifera*	*Calciodiscus leptoporus*	*Reticulosphaera minuta*	*Rhabdosphaera clavigera*	*Calciosolenia murrayi*	*Anoplosolenia brasiliensis*	*Ooithotus fragilis*	*Braarudosphaera bigelowii*	*Helicosphaera wallichii*	*Ceratolithus cristatus*	*Florisphaera profunda*	*Umbilicosphaera anulus*	*Helicosphaera sp.*	*Emiliania corona*	*Umbellosphaera tenius*	*Pontosphaera discopora*
720	2	3		3	2	2	2		2	3	1	1				1			2	?			?									?	1	1	1
730	3	3	2	3	3	2	2		2	1		1				1			1				1									?		2	1
740				2																															
750	3	3	2	3	1	?			1	2	2	2									?											2	2	2
760	3	3	2	2	3	2	2		2	2	1	2				1																1	2	1
770	3	3	2	3	2	2	1		2	2	1	1				1					1											2	?	
780	3	3	2	3	1		?		3	2	1										1											2	2	1
790	2	2		1	1				2	2		1																					1	
800	2	2		1			1		2	2		1				1							2									1	2	1
810	2	2	1	2	2			1	2	1		1						1	1	2			1	?											
820	1		1	2	1		1	1	2	1	1						1	1															1	
830	3		1	1	2		2	2	2		1	1								1			?										1	
840	1	2	1	2	2	2	1	3	2			1						?																
850	2	2			2	2	1	3	2	1	?	1						1																
860	1			1		2	2	2	1		1							1	1				1	?									1	
870	1	2	1	1	1	1		1	1	1	1	1	2	1		1																		
880				1		1		2	1		1					1	1				1													
890	1							1														1												
900	1		1		1	1		1														1												
910	1	1		1		1		2	1																									
920	2	2		2	1	2	1	2	1									1																
930	2	2	1	2	1	2	1	1	1														?											
940	4	4	3	5	4	4	3	4	3									1				2							2				1	
950	4	5	4	5	2		2		2							1						4	4				1		2					
960	4	4	3	5	4	5	2	4	2			1				2		1	?	1	2	?							1				1	
970	4	4	3	5	4	4	2	4	2		1	?						2		1	3								2	2			1	
980	4	4	3	6	4	4	2	4	2		2	1			2				1	1	3													
990	3	4	3	5	5	4	2	3	2		2	1			2		1			1	3									1			1	?
1000	4	4	4	6	4	4	2	2	2		1	1			2			1			2									1			1	1
1010	4	3	4	5	5	3	3	4	2			2			2	1	2				2	1							2					1
1020	4	3	4	5	6	3	2	3	2		?	2				1	1					2						1	1					
1030	4	3	3	4	6	3	2	2	2		2	1			2	2	2	1			3	1							1					
1040	4	2	3	5	6	3	2	2	1		1	1			2	2	2	2														1		
1050	3	2	1	4	5	2	2	3	2		1	1	1	2	2	2	2	2		1										1		1		
1060	4	2	2	4	4	3	2	2	2	3		1	2	1	2	3	2	2		1	1	1								1			1	
1070	3	3	2	3	4	3	3	2	1		1	2	2	1	3	2	2	2			1									1		?		
1080	3	3	3	4	4	3	2	3	2	2	2	1		1	3	1	1	2	2													2		
1090	2	2	2	3	3	2	2	2	1	2	2	2	2		3	2	2	2	1	1		1										1		
1100	3	3	3	4	4	3	2	2	2	2	2	3	2	2	2	2		2				1							2					
1110	3	3	2	3	4	3	2	3	1	3	1	2	2	1	3	2	2	2	2	1		1												
1120	3	3	2	4	4	3	3	3	2	3	2	3	2		3	2	2	1	?									1						
1130	2	3	2	3	3	3	2	2		2	1	2	1		3	2	1	2	2		1							1	2	1	2			
1140	3	3	1	3	4	3	2	2			1	2	2		2	1	1	2											2				1	
1150	2	2		2	2	2	2	1	?						2			2	1										1	1		1		
1160	3	2	1	2	4	3	2	2	1	1					1	1	1	3	?	1												1		
1170	3	2	1	2	3	3	2	2	1				1		1	2	1	2	1										1					
1180	3	2	2	2	3	2	2	2	1	2	1				1	1	1	2		1								1	1					
1190	2	2	1	2	2	2	1	1	1		2				1	2	1	2	?		1								2			1		
1200	3	3	2	3	4	3	2	2	1		2				1	2	2	2											2					
1210	3	2	2	3	3	3					?	3		3																				
1220	4	3	4	2	3	3	1	2	2		2	2		3				2					2									1		
1230	3	1	3	3	2	4	2	1	1		2	3		3	2			3	2		2											1		1
1240	4	3	3	3	3	3	2			2		2		2	2	2		2			2												1	
1250	2	1	1	2	2		1			1	1			1	1																			
1260	3	3	3		3	3		3						2				1	1									1				?		
1270	4	2	3	3	3	3	2	3			2	3		2	2							2	2						1					
1280	4	3	3	3	3	3		3	2					3	1													1						
1290	4	3	4	4	3	4	3	2			2	2		3	2			2					3					1	1					
1300	3	3	3	3	3	3	1	3	2		2			2				2														3		
1310	3	1	1	2	3	2	1	2	1		2				2														1			1	1	
1320	2			3	3		2		1			2																					2	
1330	3	3	3	2	3	3		3				1		2				2																
1340																																		
1350	3	2	1	2	1	1	2	2	1	1	2				2		1	1											2	?			1	
1360	4	2	4	3	4	4	2	3			1	3		3	1								2						?					
1370	2	3	3	3	2	2	1	2						1		2		2																
1380	3	1	3	2	3	3	2							2				1																
1390	2			1	2	1		1				2			1																			
1400																																		
1410																																		
1420																																		
1430																																		
1440																																		
1450																																		
1460																																		
1470																																		
1480																																		